UNIVERSITY OF KWAZULU-NATAL
INYUVESI YAKWAZULU-NATALI

An assessment of gold nanoclusters in the delivery of therapeutic siRNA to breast cancer cells *in vitro*

By

Jananee Padayachee

213519464

Submitted in fulfilment of the academic requirements for the degree of Doctor of Science in the School of Life Sciences, University of KwaZulu-Natal, Durban

Supervisor: Prof M. Singh

Signed:_____ Date:___22/01/2024

Abstract

Strategies that inhibit the expression of aberrant genes have potential in the treatment of triple-negative breast cancer (TNBC), a highly heterogeneous subtype of breast cancer that lacks targeted treatments. Small interfering RNA (siRNA)-mediated knockdown of the inflammatory cytokine tumour necrosis factor-alpha (TNF-α) and the oncogene *c-MYC* has emerged as a potential novel TNBC therapy. siRNA, however, requires a vector to ensure safe and successful delivery into the target cells. Gold nanoclusters (AuNC) are novel ultrasmall nanoparticles (NPs) that have been widely investigated as imaging agents due to their unique optical properties, and have recently gained attention as vectors for gene delivery. This study aimed to synthesize and functionalize AuNC and investigate their potential as vectors for the delivery of siRNA in selected breast cancer cell lines.

AuNC were synthesized through glutathione reduction of chloroauric acid and functionalized with chitosan and polyethylene glycol in weight ratios of 1% and 2%. The synthesized AuNC and its functionalized counterpart (FAuNC) were characterized using UV-visible and Fourier transform infrared (FTIR) spectroscopy, nanoparticle tracking analysis (NTA), and transmission electron microscopy (TEM). Interactions between the FAuNC and siRNA were investigated using the gel retardation, ethidium bromide intercalation, and nuclease protection assays. *In vitro* studies were conducted in three cell lines, the hormone receptor positive MCF-7, TNBC MDA-MB-231, and non-cancer HEK293. Cytotoxicity and cellular uptake of the FAuNC were evaluated using the 3-(4,5-dimethylthiazol-2-yl)-2,5-diphenyl tetrazolium bromide (MTT) cytotoxicity assay and fluorescence microscopy, respectively. The *in vitro* effects of anti-TNF-α siRNA delivery were investigated using flow cytometry to determine the effects on the apoptosis and oxidative stress levels, and cell cycle distribution in treated cells. Knockdown efficiency was evaluated *in vitro* using anti-*c-MYC* siRNA, targeting the upregulated *MYC* oncogene, in MCF-7 cells. Reverse transcription-quantitative polymerase chain reaction (RT-qPCR) and the enzyme-linked immunosorbent assay (ELISA) were conducted to assess gene knockdown at the mRNA and protein levels, respectively.

UV spectroscopy and TEM confirmed the synthesis of nanoclusters less than 2 nm in diameter. NTA analysis showed all FAuNC to display appropriate hydrodynamic diameters for cellular uptake and good colloidal stability. All FAuNC were capable of effectively binding and condensing siRNA, and providing protection from complete degradation by RNase A. The MTT cytotoxicity assay showed all FAuNC to be well-tolerated in all cell lines. Cellular uptake

studies indicated successful interactions between FAuNC and cells, suggesting successful uptake. Flow cytometry assays showed delivery of anti-*TNF-α* siRNA to have little effect on the growth of HEK293 and MCF-7 cells; however, delivery in MDA-MB-231 cells was observed to lead to slight increases in apoptosis and oxidative stress levels, and slight shifts in cell cycle distribution. Based on these results, the AuCS-2% PEG were chosen as vectors for gene silencing studies. From qPCR and ELISA, the AuCS-2% PEG did not induce significant knockdown of the *c-MYC* gene. Overall, the FAuNC synthesized in this study showed favourable physicochemical characteristics and low cytotoxicity in vitro, but the results obtained warrant further optimization of the PEGylated FAuNC should they be considered for delivery of siRNA.

Keywords: Gold nanoclusters; breast cancer; gene silencing; TNF-α; *c-MYC*; cytotoxicity

Preface

The experimental work described in this dissertation was carried out in the Discipline of Biochemistry, School of Life Sciences, University of KwaZulu-Natal, Durban under the supervision of Prof Moganavelli Singh.

These studies represent original work by the author and have not otherwise been submitted in any form for any degree or diploma to any tertiary institution. Where use has been made of the work of others it is duly acknowledged in the text.

Declaration – Plagiarism

I, Jananee Padayachee, declare that:

1. The research reported in this thesis, except where otherwise indicated, is my original research.

2. This thesis has not been submitted for any degree or examination at any other university.

3. This thesis does not contain other persons' data, pictures, graphs, or other information, unless specifically acknowledged as being sourced from other persons.

4. This thesis does not contain other persons' writing unless specifically acknowledged as being sourced from other researchers. Where other written sources have been quoted then:

    a. their words have been re-written, but the general information attributed to them has been referenced.

    b. where their exact words have been used, then their writing has been placed in italics and inside quotation marks and referenced.

5. This thesis does not contain text, graphics or tables copied and pasted from the Internet, unless specifically acknowledged, and the source being detailed in the thesis and in the References sections.

Signed: 

Date: 22/01/2024

Declaration 2 - Publications

Details of contribution to publications and presentations that form part and include research presented in this thesis. My role in the publication is indicated.

Publication: This publication is part of Chapter two.

Padayachee J. and Singh, M. (2020). Therapeutic applications of CRISPR/Cas9 in breast cancer and delivery potential of gold nanomaterials. *Nanobiomedicine*. 7, 1-15. doi:10.1177/1849543520983196

J Padayachee designed the review, collected, analysed the data, and wrote the first draft of the paper. M Singh reviewed and edited the manuscript.

[redacted]

22/01/2024

Jananee Padayachee **Date**

Declaration Publications FHDR 22/05/08 Approved

Acknowledgements

I would like to acknowledge the following:

- My supervisor, Prof. M. Singh, for her guidance.
- My parents, for their unending support.
- The National Research Foundation (NRF), for providing financial support.
- Drs A. Daniels and S. Habib, for their assistance with the gene expression assays.
- Dr Kolawole Olofinsan and Kerisha Ramessar, for their help with the RT-qPCR machine.
- Colleagues at the Non-viral Gene and Drug Delivery Lab, for their companionship.

Table of Contents

Abstract ii
Preface iv
Declaration – Plagiarism v
Declaration 2 - Publications vi
Acknowledgements vii
List of Figures xii
List of Tables xv
List of Abbreviations xvi
CHAPTER 1 INTRODUCTION 1
1.1. Background of study 1
1.2. Aims and objectives 3
1.3. Novelty of study 4
1.4. Overview of thesis 4
CHAPTER 2 LITERATURE REVIEW 5
2.1. Breast cancer 5
2.1.1. Subtypes of breast carcinoma 5
2.1.2. Triple Negative Breast Cancer 6
2.1.3. Subtypes of TNBC 7
2.1.4. Current treatment of TNBC 8
2.2. Tumour necrosis factor alpha 8
2.2.1. Inflammation and cancer 8
2.2.2. Tumour necrosis factor alpha (TNF-α) 10
2.2.3. TNF-α structure 11
2.2.4. TNF-α's functions in inflammation 12
2.2.5. TNF receptors 13
2.2.6. TNF- α signalling pathways 14
2.2.6.1. TNFR1 signalling 15
2.2.6.2. TNFR2 signalling 16
2.2.7. TNF-α in anti-cancer studies 16
2.2.8. TNF-α in promoting cancer 17
2.2.9. Role of TNF-α in BC 18
2.2.9.1. Luminal BCs 19
2.2.9.2. TNBC 20

2.3. The *c-MYC* oncogene 22
2.3.1. *c-MYC* gene structure 22
2.3.2. c-MYC protein structure 23
2.3.3. c-MYC as a transcription factor 24
2.3.4. Activation of *c-MYC* 26
2.3.5. *c-MYC* dysregulation in BC 28
2.4. RNA interference 29
2.4.1. Mechanism of siRNA 30
2.4.2. RNAi-mediated knockdown of *TNF-α* and *c-MYC* 32
2.4.3. Challenges to siRNA therapy 33
2.4.3.1. Off-target effects 33
2.4.3.2. Barriers to siRNA delivery 34
2.5. Vectors for siRNA delivery 35
2.5.1. Viral vectors 35
2.5.2. Non-viral vectors 35
2.5.2.1. Lipid nanoparticles 35
2.5.2.2. Polymeric nanoparticles 36
2.5.2.3. Gold nanoparticles 37
2.6. Gold nanoclusters 37
2.6.1. Optical characteristics of AuNC 38
2.6.2. Synthesis of AuNC 40
2.6.2.1. Bottom-up methods 41
2.6.2.2. Top-down methods 42
2.6.3. Cytotoxicity and clearance of AuNC 42
2.6.4. AuNC as nucleic acid delivery agents 44
2.7. Overcoming barriers to transfection 44
2.7.1. Avoiding removal from circulation 44
2.7.1.1. PEGylation 46
2.7.2. Cellular uptake 47
2.7.3. Endosomal escape 49
CHAPTER 3 MATERIALS AND METHODS 52
3.1. Materials 52
3.1.1. Synthesis and functionalisation 52
3.1.2. siRNA duplexes 52
3.1.3. Binding studies 52

3.1.4. *In vitro* cell culture studies 53
3.1.5. Gene knockdown 53
3.2. Methods 54
3.2.1. Synthesis and functionalisation of nanoclusters 54
3.2.1.1. Synthesis of AuNC 54
3.2.1.2. Functionalisation of AuNC 54
3.2.1.3. Preparation of nanocomplexes 54
3.2.2. Characterisation of nanoclusters and nanocomplexes 55
3.2.3. Binding studies 56
3.2.3.1. Band shift assay 56
3.2.3.2. Ethidium Bromide (EtBr) intercalation assay 56
3.2.3.3. Nuclease protection assay 57
3.2.4. *In vitro* cell culture maintenance 57
3.2.5. Cell viability studies 57
3.2.5.1. MTT cytotoxicity assay 57
3.2.5.2. Apoptosis assay 58
3.2.6. Cellular uptake studies 58
3.2.7. Flow cytometry studies 58
3.2.7.1. Caspase 3/7 analysis 59
3.2.7.2. Cell cycle analysis 59
3.2.7.3. Oxidative stress analysis 59
3.2.8. Analysis of gene knockdown 59
3.2.8.1. Analysing knockdown at the mRNA level 60
3.2.8.1.1. RNA extraction 60
3.2.8.1.2. cDNA synthesis 60
3.2.8.1.3. RT-qPCR 61
3.2.8.2. Analysing knockdown at the protein level 62
3.2.8.2.1. Protein extraction 62
3.2.8.2.2. BCA assay 62
3.2.8.2.3. Enzyme-linked Immunosorbent Assay (ELISA) 62
3.2.9. Statistical analysis 63
CHAPTER 4 RESULTS AND DISCUSSION 64
4.1. Synthesis and functionalisation of AuNPs 64
4.2. Physicochemical characterisation of AuNC 66
4.2.1. Optical characterisation 66

4.2.2. FTIR analysis 69
4.2.3. Sizing and zeta potential 70
4.2.3.1. TEM 70
4.2.3.2. NTA sizing and zeta potential 72
4.3. Binding studies 75
4.3.1. Band shift assay 75
4.3.2. Ethidium bromide (EtBr) intercalation assay 78
4.3.3. Nuclease protection assay 81
4.4. *In vitro* cell culture assays 83
4.4.1. MTT cytotoxicity assay 83
4.4.2. Ethidium bromide/acridine orange apoptosis assay 86
4.4.3. Cellular uptake 88
4.4.4. Flow cytometry studies 94
4.4.4.1. Caspase 3/7 Activity 94
4.4.4.2. Oxidative stress 97
4.4.4.3. Cell cycle 100
4.4.5. Gene knockdown studies 103
CHAPTER 5 CONCLUSION AND FUTURE STUDIES 109
5.1. Conclusion 109
5.2. Future Studies 110
BIBLIOGRAPHY 112
APPENDIX 167
Appendix A: Published paper 167
Appendix B: Similarity report 168

List of Figures

Figure 2.1: Characteristics of the five intrinsic molecular subtypes of BC and their corresponding IHC subtypes (information adapted from Dai *et al*., 2015 and Perou *et al*., 2000). 6
Figure 2.2: Chronic inflammation promotes cancer development and spread through the intrinsic or extrinsic pathway. Both pathways lead to the accumulation of inflammatory mediators and immune cells within the tissue, which may promote transformation. 9
Figure 2.3: The structure of the 233 AA tmTNF-α monomer. TACE cleaves within the extracellular domain to release the 157 AA sTNF-α (adapted from Horiuchi *et al*., 2010). 11
Figure 2.4: The diverse roles of NF-κB signalling in immune cells and its gene targets that regulate the inflammation process (Liu *et al*., 2017). 14
Figure 2.5: The signalling pathways activated by TNF-α through TNFR1. Complex I, which promotes the expression of genes associated with the inflammation process, is initially formed following binding. The cell death-signalling complexes IIa, IIb, and IIc form subsequently and are regulated by the gene products of complex I (Kalliolias & Ivashkiv, 2016). 15
Figure 2.6: TNFR2 is generally associated with the transduction of proliferation, differentiation, and survival signals through NF-κB, AKT, and MAPK pathways (Kalliolias & Ivashkiv, 2016). 16
Figure 2.7: TNF-α involvement in BC. A) High levels of TNF-α have been observed in the tissue and sera of BC patients, B) Elevated TNF-α levels have been observed in tumour tissue due to production by various cells in the TME, C) TNF-α has been implicated in every step of carcinogenesis, promoting tumour growth and spread, and drug resistance (Cruceriu *et al*., 2020). 19
Figure 2.8: The structure of the *c-MYC* gene on chromosome 8 (Carabet *et al*., 2018). 23
Figure 2.9: The structure of the c-MYC protein containing six conserved MBs (Duffy *et al*., 2021). 23
Figure 2.10: The cellular pathways regulated by c-MYC, including the factors that are upregulated (up arrow) or downregulated (down arrow) by c-MYC (adapted from Kress *et al*., 2015). 25
Figure 2.11: Dysregulated *c-MYC* expression induces transformation by upregulating cell proliferation and survival pathways (green section), while preventing cell death or protective processes (red area) (Dhanasekaran *et al*., 2021). 26
Figure 2.12: Schematic representation of a typical 21 nt siRNA molecule, consisting of a 19bp duplex region and 2bp 3'-OH overhangs. The antisense strand (3' > 5') acts as the guide sequence. 30
Figure 2.13: The siRNA-mediated RNAi process, leading to sequence-specific degradation of complementary mRNA. 31
Figure 2.14: siRNA may induce on- or off-target effects. On-target effects result from complete binding of the guide strand to the complementary target mRNA. Off-target effects are most often mediated by the miRNA-like effect, where the seed sequence at the 5' end of the siRNA binds to the 3' UTR of unintended mRNA (Québatte and Dehio, 2017). 34
Figure 2.15: NCs display a similar electronic structure to atoms. (A) The energy band structure of AuNP is continuous, as the high density of atoms leads to overlap of the valence and conduction bands. (B) AuNC display quantum confinement effects, where electrons are

confined to discrete bands – a similar electronic structure to that of atoms (C) (Liu & Corma, 2018). 39
Figure 2.16: AuNC fluorescence is dependent on the (A) size and (B) ligand. A) Smaller AuNC clusters emit shorter wavelengths of light, as shown by pepsin-Au_{25}, Au_{13}, and Au_8 and Au_5 clusters emitting red, green, and blue light, respectively (Kawasaki *et al*., 2011); B) Different emissions by AuNC coated with a) PEI, b) and c) mercaptoundecanoic acid, and d) dihydrogen lipoic acid (Lin *et al*., 2010). 40
Figure 2.17: Comparison of the structures of conventional AuNC and Au(0)Au(I)-thiolate AuNC. Conventional AuNC, which display poor QY, are coated with short Au(I)-thiolate complexes, while highly-luminescent Au(0)Au(I)-thiolate AuNC are coated with longer Au(I)-thiolate complexes (Luo *et al*., 2012). 42
Figure 2.18: The process of opsonisation, which leads to phagocytosis of the vector (Hillaireau & Couvreur, 2009) 45
Figure 2.19: PEG assumes a (a) mushroom conformation at low grafting densities and (b) a brush conformation at high grafting densities (Fam *et al*., 2020).....47
Figure 2.20: The various endocytic pathways facilitating entry into cells (Chou *et al.*, 2011). 48
Figure 2.21: The suggested mechanism of the proton sponge effect whereby polymers with high buffering capacities are able to rupture the endosome. (1) The polymer enters the cell by endocytosis, (2) The polymer binds the protons pumped into the endosome, leading to the influx of Cl^-, (3) This leads to the inflow of water, swelling the endosome and causing it to burst (Vermeulen *et al*., 2018). 50
Figure 4.1: Scheme showing synthesis of AuNC through GSH-induced reduction of $HAuCl_4$. 64
Figure 4.2: Scheme showing synthesis of AuCS nanoconjugates. 65
Figure 4.3: Scheme showing synthesis of PEGylated chitosan functionalised AuNC. 66
Figure 4.4: UV-vis spectra of AuNC and FAuNC. Inset shows the shoulder peak present at ~390 nm in the spectrum of the AuNC. 66
Figure 4.5: Comparison of the AuNC and FAuNC solutions under (top) visible light and (bottom) UV light (λ = 366 nm). (A) ddH_20 (B) AuNC (C) AuCS (D) AuCS-1% PEG (E) AuCS-2% PEG....68
Figure 4.6: FTIR spectra of AuNC and FAuNC with major peaks labelled. A) AuNC, B) AuCS, C) AuCS-1% PEG, and D) AuCS-2% PEG. 69
Figure 4.7: TEM images of AuNC and FAuNC. A) AuNC, B) AuCS, inset shows organisation of AuNC in circular AuCS nanogels, C) AuCS-1% PEG, and D) AuCS-2% PEG. Scale bars represent 20 nm on all figures except B), where the scale bar represents 100 nm. .71
Figure 4.8: Band shift assay results for A) AuCS, B) AuCS-1% PEG, and C) AuCS-2% PEG run on a 2% agarose gel. Lane 1 contains uncomplexed siRNA, lanes 2-8 contain increasing siRNA:FAuNC weight ratios. Endpoints are indicated by arrows. 76
Figure 4.9: EtBr intercalation assays for A) AuCS, B) AuCS-1% PEG, and C) AuCS-2% PEG. Points of inflection are indicated by arrows. 78
Figure 4.10: RNase protection assay for FAuNC nanocomplexes. +) Positive control of untreated siRNA; -) negative control of RNase-treated siRNA; lanes 1, 2, and 3 contain the sub-optimal, optimal, and supra-optimal ratios, respectively, of the indicated FAuNC. 81

Figure 4.11: MTT assay results in the A) HEK293, B) MCF-7, and C) MDA-MB-231 cell lines. *p<0.05 was considered statistically significant between nanocomplex ratios; #p<0.05, ##p<0.01 were considered statistically significant vs. the control. 84
Figure 4.12: Dual EtBr/AO assay in MDA-MB-231 treated with B) free siRNA, C) LF3K, D) AuCS, E) AuCS-1% PEG, and F) AuCS-2% PEG complexes. A) represents the untreated control. The scale bar represents 200 μm for all images. L = live cells, EA = early apoptosis, LA = late apoptosis. 87
Figure 4.13: Cellular uptake of FAuNC and LF3K complexed with BLOCK-iT™ fluorescent siRNA in HEK293 cells. Images were taken on a fluorescence microscope. The scale bar represents 200 μm for all images. 89
Figure 4.14: Cellular uptake of FAuNC and LF3K complexed with BLOCK-iT™ fluorescent siRNA in MCF-7 cells. Images were taken on a fluorescence microscope. The scale bar represents 200 μm for all images. 90
Figure 4.15: Cellular uptake of FAuNC and LF3K complexed with BLOCK-iT™ fluorescent siRNA in MDA-MB-231 cells. Images were taken on a fluorescence microscope. The scale bar represents 200 μm for all images except AuCS; scale bar represents 100 μm for AuCS. 91
Figure 4.16: Graphical representation of the apoptotic profiles following *TNF-α* knockdown in A) HEK293, B) MCF-7, and C) MDA-MB-231 cells. Control = cell-only control; siRNA only = anti-*TNF-α* siRNA only; LF3K = Lipofectamine 3000. 95
Figure 4.17: Graphical representation of the ROS levels following TNF-α knockdown in A) HEK293, B) MCF-7, and C) MDA-MB-231 cells. Control = cell-only control; siRNA only = anti-*TNF-α* siRNA only; LF3K = Lipofectamine 3000. 98
Figure 4.18: Graphical representation of the cell cycle distribution following *TNF-α* knockdown in A) HEK293, B) MCF-7, and C) MDA-MB-231 cells. Control = cell-only control; siRNA only = anti-*TNF-α* siRNA only; LF3K = Lipofectamine 3000. 101
Figure 4.19: Gene knockdown studies in MCF-7 cells, showing the relative (A) gene and (B) protein expression of *c-MYC* following treatment with naked siRNA and LF3K and AuCS-2% PEG complexes. Data are presented as means ± SD (n=2). 104

List of Tables

Table 2.1: Proposed subtypes for classification of TNBC tumours.....7
Table 2.2: The processes during inflammation that TNF-α has been implicated in.....12
Table 2.3: The potential pro-tumourogenic effects of chronic, low-level TNF-α production.18
Table 2.4: Characteristics of commonly used viral vectors for siRNA delivery. 35
Table 3.1: Sequences of non-targeted siRNA and individual siRNA duplexes in the SMARTpool mixture 52
Table 3.2: Quantities of LF3K and siRNA used for transfection in various plate formats 55
Table 3.3: Reaction conditions for cDNA synthesis using isolated RNA 61
Table 3.4: Components of PrimePCR™ assays and their final concentrations.....61
Table 3.5: PrimePCR™ Assay cycling conditions. 61
Table 4.1: Average sizes of the plain and functionalised AuNC obtained using TEM.....71
Table 4.2: Sizes and zeta potentials of AuNC and FAuNC as determined using NTA.....73
Table 4.3: The sub-optimal, optimal, and supra-optimal siRNA:FAuNC (***ww***) ratios determined using the band shift assay 76
Table 4.4: The siRNA:FAuNC (**ww**) ratios and decays in fluorescence observed at the point of inflection for all nanocomplexes in the EtBr intercalation assay 79
Table 4.5: Apoptotic indices in the MDA-MB-231 cell line following treatment with FAuNC complexes 88
Table 4.6: The fluorescent profiles of live, apoptotic, and necrotic cells determined by the Muse® Caspase-3/7 kit.....94

List of Abbreviations

AA	Amino acid
AAV	Adeno-associated viruses
AIE	Aggregation-induced emission
AR	Androgen receptor
BC	Breast carcinoma
bHLHZ	Basic helix-loop-helix leucine zipper
bp	Base pair
BSA	Bovine serum albumin
CRD	Coding region instability determinant
CRDBP	Coding region determinant binding protein
CS	Chitosan
CTD	C-terminal domain
DBD	DNA-binding domain
DD	Death domain
DISC	Death-induced signalling complex
DMSO	Dimethyl sulfoxide
DNA	Deoxyribonucleic acid
dsDNA	Double-stranded deoxyribonucleic acid
dsRNA	Double-stranded ribonucleic acid
E-box	Enhancer box
ECM	Extracellular matrix
ELISA	Enzyme linked immunosorbant assay
EMEM	Eagle's minimum essential medium
EMT	Epithelial-to-mesenchymal transition
ER	Oestrogen receptor
EtBr	Ethidium bromide
FBS	Foetal bovine serum
FTIR	Fourier transform infrared spectroscopy
GEP	Gene expression pattern
GSH	Glutathione
HBS	HEPES buffered saline
HPV	Human Papilloma virus

ICP	Inductively coupled plasma spectroscopy
IDC-NST	Invasive ductal carcinoma of no special type
IHC	Immunohistochemistry
LF3K	Lipofectamine 3000
LSPR	Localised surface plasmon resonance
MAX	MYC-associated factor X
MB	Myc box
miRNA	Micro ribonucleic acid
mRNA	Messenger ribonucleic acid
MTT	3-(4,5-dimethylthiazol-2-yl)-2,5-diphenyltetrazolium bromide
MW	Molecular weight
NK	Natural killer cells
NLS	Nuclear localisation signal
NO	Nitric oxide
NP	Nanoparticles
nt	Nucleotide
NTA	Nanoparticle tracking analysis
NTA	Nanoparticle tracking analysis
NTD	N-terminal domain
PARP	Polyadenosine diphosphate-ribose polymerase
PBS	Phosphate buffered saline
pCR	Pathological complete response
PEG	Poly(ethylene glycol)
PEI	Polyethyleneimine
PLL	Poly-L-lysine
PR	Progesterone receptor
QY	Quantum yield
RISC	RNA-induced silencing complex
RLC	RISC-loading complex
RNA	Ribonucleic acid
RNAi	RNA interference
ROS	Reactive oxygen species
RT-qPCR	Reverse transcription quantitative polymerase chain reaction

SDS	Sodium dodecyl sulphate
ssDNA	Single-stranded deoxyribonucleic acid
SSO	Single-stranded oligonucleotide
ssRNA	Single-stranded ribonucleic acid
sTNF-α	Soluble TNF-α
TACE	TNF converting enzyme
TAD	Transactivation domain
TAM	Tumour-associated macrophages
TCR	T-cell receptor
T_{eff}	Effector T-cell
TEM	Transmission Electron Microscopy
THD	TNF homology domain
TME	Tumour microenvironment
tmTNF-α	Transmembrane TNF-α
TNBC	Triple negative breast cancer
TNF	Tumour necrosis factor
TNFR	Tumour necrosis factor receptor
TNFSF	Tumour necrosis factor superfamily
TNF-α	Tumour necrosis factor alpha
TNF-β	Tumour necrosis factor beta
TRADD	TNFR1-associated death domain
TRAIL	TNF-related apoptosis-inducing ligand
TRBP	Trans-activation response RNA-binding protein
T_{reg}	Regulatory T-cell
TRID	TNFR1 internalisation domain
TSG	Tumour suppressor gene
UV	Ultraviolet
vdW	van der Waals forces

CHAPTER 1
INTRODUCTION

1.1. Background of study

The earliest known description of breast cancer (BC) occurs in the Edwin Smith papyrus, a medical treatise dating to 1600 BC, although thought to be a copy of an older manuscript dating to 3000 – 2500 BC (Ades *et al*., 2017). Today, it is the most common form of cancer diagnosed in women globally and in South Africa, and the second-most common cause of cancer deaths among South African women (Bray *et al*., 2018; Made *et al*., 2017; National Cancer Registry, 2020). BCs are clinically characterized by the presence of hormone receptors for oestrogen and progesterone, and the human epidermal growth factor receptor 2 (HER2). Approximately 15-21% of cases in South Africa are diagnosed as triple negative breast cancer (TNBC), a subtype characterised by the absence of these receptors (Cubasch *et al*., 2013, 2018; Langenhoven *et al*., 2016; McCormack *et al*., 2013; Nel *et al*., 2022). TNBC displays poorer clinical outcomes compared to other BC subtypes. This is partly due to their inherently aggressive nature, forming large tumours with increased proliferation, and a high likelihood of short-term recurrence and metastasis (Gupta *et al*., 2020; Malorni *et al*., 2012; Srivastava *et al*., 2022). Moreover, TNBC patients do not benefit from the targeted therapies that have significantly improved the survival rates of hormone and HER2 receptor-positive BCs, such as tamoxifen and trastuzumab (Chang *et al*., 2019; Patel *et al*., 2020; Quirke, 2017). Chemotherapy remains the only choice of systemic treatment, but is associated with side effects and often ineffective at preventing relapse and metastasis (Gupta *et al*., 2020). There is thus a need to develop treatments that target specific molecular targets in TNBC.

The involvement of inflammation in carcinogenesis was first suggested by Rudolf Virchow in 1863, when he identified leukocytes within tumour tissues (Balkwill & Mantovani, 2001). The relationship between inflammation and cancer development and progression has been the subject of much research. The tumour necrosis factor alpha (TNF-α) is a pleiotropic cytokine with a central role in the inflammation process (Li *et al*., 2023). While originally defined according to its role as an anticancer agent, it has since been shown to display both anti- and pro-tumour effects depending on the context and physiological concentration (Carswell *et al.*, 1975; Montfort *et al*., 2019). Low TNF-α levels present in the inflammatory tumour microenvironment have been implicated in promoting the development, growth, and spread of several cancers, including TNBC (Cruceriu *et al*., 2020; Montfort *et al*., 2019). TNF-α has been

shown to contribute to the aggressiveness of TNBC, by activating growth-promoting pathways that induce invasion and metastasis, and the generation of cancer stem cells that promote relapse (Mercogliano *et al*., 2020). The cytokine thus presents a novel target for the treatment of TNBC.

In addition to factors in the tumour microenvironment, transformation is driven by the activation of growth-promoting genes called oncogenes. The *c-MYC* oncogene is perhaps the most widely studied oncogene. *c-MYC* encodes a transcription factor that is suggested to act on 10 – 15% of all genes in the human genome (Dang *et al*., 2006). It plays a central role in driving cell growth in response to mitogenic signals by upregulating pathways involved in cell cycle progression, metabolism, protein synthesis, and angiogenesis; and down-regulating genes involved in cell adhesion (Dang *et al*., 2006; Miller *et al*., 2012). As such, its dysregulation is closely related with carcinogenesis, and it is estimated that over 70% of cancers show dysregulated *c-MYC* expression (Madden *et al*., 2021). *c-MYC* overexpression in BC, driven by dysregulated signalling or mutations, is associated with increased cancer growth, risk of recurrence, and the development of drug resistance (Xu *et al*., 2010). Aberrant *c-MYC* expression is also more prevalent in TNBC than luminal and HER2+ BCs (Horiuchi *et al*., 2012); where it contributes to genome instability, drug resistance, and enrichment of cancer stem cells, leading to a poorer prognosis (Lee *et al*., 2017; Yang *et al*., 2017a).

The adverse effects of TNF-α expression may be inhibited at the protein level, using anti-TNF-α antibodies, or at the mRNA level, using gene silencing processes. Similarly, *c-MYC* expression can also be silenced. One such gene silencing process is RNA interference (RNAi), a sequence-specific post-transcriptional process that naturally functions to regulate gene expression and defend against viral infection (Cooper *et al*., 2019). RNAi is activated by small, non-coding double-stranded RNA molecules, especially small interfering RNA (siRNA), which induce cleavage of complementary mRNA via assembly with a protein complex called the RNA-induced silencing complex (Dana *et al*., 2017). siRNAs are highly effective at mediating gene knockdown; however, the delivery of naked siRNA faces several drawbacks. Naked siRNA is highly susceptible to nuclease degradation and removal from circulation, and the large size and anionic charge of the molecule inhibits cellular uptake (Babu *et al*., 2016). Much research has focussed on the development of suitable vectors that can protect siRNA and deliver it to the cytoplasm of target cells, where it can mediate gene silencing.

Nanoparticles (NPs) present a promising solution to the problems associated with siRNA delivery. These non-viral systems generally have simple and tunable synthesis methods, and a

large surface area for functionalization with polymers to improve efficacy and biocompatibility (Mirza & Karim, 2021). Organic NPs composed of lipids have thus far shown the most promise for siRNA delivery, with the first approved siRNA drug being a liposomal formulation (Urits *et al*., 2020; Zhang *et al*., 2021b). Inorganic metallic NPs, particularly those synthesised from gold have also been widely studied as delivery vehicles. These NP display tunable physical characteristics and unique properties not present in organic NP, such as magnetism, fluorescence, and photothermal properties, that enhance their therapeutic potential (Anselmo and Mitragotri, 2015; Huang *et al*., 2020). Gold nanoclusters (AuNC) are small nanomaterials, typically displaying sizes smaller than 2 nm in diameter (Cheng *et al*., 2022). Their unique physicochemical and optical qualities have facilitated their use in theranostics as bioimaging agents, photothermal therapy agents, and gene and drug delivery vehicles (van de Looij *et al*., 2022). This study thus focussed on the development of coated AuNC carriers for siRNA delivery to breast cancer cell lines.

1.2. Aims and objectives

The aim of this study was to develop and characterise AuNC vectors functionalised with chitosan and polyethylene glycol and evaluate their potential as siRNA delivery vectors in breast cancer models.

The objectives of the study were:

- To synthesise small AuNC and functionalise them with the cationic polymer chitosan and the steric stabiliser PEG_{2000} in two weight ratios of 1% and 2%.
- To characterise the plain and functionalised AuNC (FAuNC) using UV-Vis spectroscopy, TEM, NTA, and FTIR to determine their physical and chemical characteristics.
- To investigate the siRNA-binding capabilities of the FAuNC using the band shift, ethidium bromide, and RNase protection assays.
- To evaluate the cytotoxicity of the FAuNC vectors *in vitro* using the MTT assay.
- To determine the *in vitro* effects of delivery of FAuNC complexed with anti-*TNF-α* siRNA on apoptosis levels, oxidative stress levels, and cell cycle distribution using flow cytometry assays.
- To evaluate the ability of the FAuNC vectors to induce knockdown at the mRNA and protein levels using RT-qPCR and ELISA, respectively.

1.3. Novelty of study

Several studies have shown peptide- and PEI-capped AuNC to be capable of effectively delivering plasmid DNA and siRNA *in vitro* (Lei *et al*., 2017; Sun *et al*., 2018; Tao *et al*., 2013). Chitosan-coated AuNC, in contrast, have been investigated as agents for cell imaging, biosensing, chemodynamic and antimicrobial therapy (Girija *et al*., 2019; Mi *et al*., 2022; Xie *et al*., 2019; Zhu *et al*., 2022), but have not yet been exploited as gene delivery vectors. This study further investigates the effects of PEGylation at two weight ratios on the FAuNC characteristics and efficiency. The addition of PEG to the polymer-coated AuNC for gene delivery is a novel formulation and yet to be fully explored.

1.4. Overview of thesis

The thesis comprises the following chapters:

Chapter one introduces the challenges faced in TNBC and siRNA therapy that the study aims to address. The aims and objectives and novelty of the study are also outlined.

Chapter two provides a review of the literature relevant to the study. Firstly, TNBC and the challenges faced in treating it are described. The role of TNF-α and *c-MYC* in carcinogenesis, and the potential of siRNA in silencing these genes for cancer therapy is discussed. Vectors for siRNA delivery are highlighted, with specific focus given to AuNC, their synthesis methods, and potential as delivery vectors. Lastly, barriers faced in transfection and methods of overcoming them are discussed.

Chapter three details the methodologies used in the study. The synthesis, functionalisation, and characterisation techniques are described. siRNA binding assays and *in vitro* cytotoxicity, uptake, and transfection methods are outlined. Lastly, the protocols for the gene expression assays conducted in the MCF-7 cell line are provided.

Chapter four provides the results obtained, and includes an interpretation of the results and discussion of their significance.

Chapter five concludes the study. The success of the study in achieving the aims and objectives set out in the introduction is assessed and recommendations for future studies are made.

CHAPTER 2
LITERATURE REVIEW

Part of this chapter has been published in:

Padayachee J. and Singh, M. (2020). Therapeutic applications of CRISPR/Cas9 in breast cancer and delivery potential of gold nanomaterials. *Nanobiomedicine*. 7, 1-15. doi:10.1177/1849543520983196.

2.1. Breast cancer

Breast cancers (BC) are a group of cancers arising from cells of the mammary gland (Makki, 2015). They can be broadly classified as sarcomas or carcinomas, depending on the type of cells they develop from. Breast sarcomas, arising from the mesenchymal tissue, are a rare group of cancers estimated to account for less than 1% of all breast cancers (Li *et al*., 2016). Most BC are carcinomas that occur in cells of the terminal duct-lobular unit responsible for milk production (Feng *et al*., 2018; Figueroa *et al*., 2014). BC are themselves highly heterogenous and can be divided into several subtypes based on their histological and molecular characteristics, with varying treatment options and clinical outcomes.

2.1.1. Subtypes of breast carcinoma

Histological classification of BC is based on analysis of cytological characteristics, such as cell shape; nuclear shape, organisation, and density; cell growth patterns; and presence of certain IHC markers (Araújo *et al*., 2017; Dieci *et al*., 2014; Weigelt *et al*., 2010a). The World Health Organisation officially recognises 21 histological subtypes of BC (Kaur *et al*., 2019). The majority of BCs are invasive ductal carcinomas of no special type (IDC-NST), meaning they show no defining characteristics that facilitate their classification as 'special types' of BC (Badowska-Kozakiewicz *et al*., 2017; Natal *et al*., 2019). These subtypes differ in their prognoses, clinical behaviour, and epidemiology (Ntekim *et al*., 2019); however, the prognostic value of histological classification is currently limited by the classification of most BCs as IDC-NST (Rakha *et al*., 2010).

The molecular characteristics of BC can be evaluated using immunohistochemistry (IHC), which involves detection of cell surface or intracellular proteins, or through microarray analysis of the gene expression patterns (GEP) of different tumours (Fragomeni *et al*., 2018). IHC commonly analyses the progesterone (PR), oestrogen (ER), and HER2 receptors; and Ki-67

proteins. Ki-67 is a nuclear protein expressed in all stages of the cell cycle except the quiescent stage G0, and is used as a measure of cell proliferation and tumour aggressiveness (Zhu *et al*., 2020). Based on the expression of these markers, BCs can be classified into four groups: luminal A and B, HER2+, and triple negative (TNBC) (Figure 2.1). These subtypes were investigated in more detail by Perou *et al*., (2000) and Sørlie *et al*., (2001), who used microarray analysis to classify BC into five intrinsic molecular subtypes based on expression of genes such as oestrogen receptor 1 (*ESR1*) and *HER2*. These subtypes are identified by PAM50, a clinical test that analyses the expression of 50 genes using quantitative PCR (qPCR) to subtype biopsies (Malhotra *et al*., 2010). The characteristics of the intrinsic subtypes, and the IHC subtypes they correspond to, are shown in Figure 2.1.

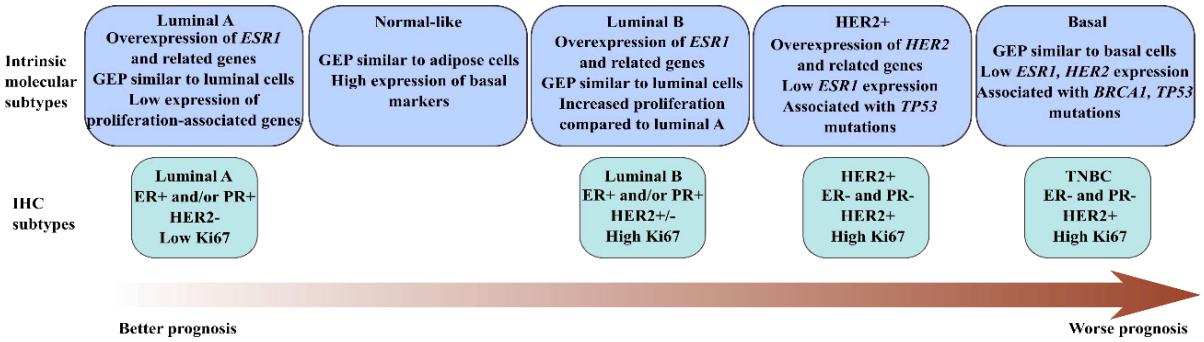

Figure 2.1: Characteristics of the five intrinsic molecular subtypes of BC and their corresponding IHC subtypes (information adapted from Dai *et al*., 2015 and Perou *et al*., 2000).

While GEP analysis may provide more information on therapeutic targets or recurrence risk, its price limits its use in the clinical setting, and IHC is thus often used to approximate the intrinsic subtype. The intrinsic subtypes also require refinement. Normal-like GEPs have been suggested to result from sample contamination with normal breast tissue (Weigelt *et al*., 2010b); and do not take into account the diverse molecular heterogeneity of TNBC.

2.1.2. Triple Negative Breast Cancer

TNBC is estimated to account for 15-20% of BC cases globally, and disproportionately affects certain ethnicities, such as Hispanic, and black American and British women (Bowen *et al*., 2008; Clarke *et al*., 2012; Lara-Medina *et al*., 2011). Studies in various South African populations have observed incidence rates of 15.2 - 21.7% (Cubasch *et al*., 2013, 2018; Langenhoven *et al*., 2016; McCormack *et al*., 2013). TNBC refers to a broad category of BCs lacking hormone and HER2 receptor overexpression. It generally displays an aggressive nature and a high rate of cellular proliferation, indicated by high Ki-67 levels and nuclear grade

(Nishimura & Arima, 2008). Compared to other BCs, TNBC is associated with younger ages at presentation (Bauer *et al*., 2007); and with an increased risk of relapse and a shorter time to local and distant recurrence (Asano *et al*., 2017; Dent *et al*., 2007). The risk of metastasis is similarly high, with TNBC often spreading to the brain and lungs (Gerratana *et al*., 2015; Molnár *et al*., 2017). Despite advances in cancer therapy, TNBC remains difficult to treat due to the lack of targeted therapies, as well as its poorly characterised molecular heterogeneity.

2.1.3. Subtypes of TNBC

The majority of TNBCs belong to the basal subtype; however, studies have identified all intrinsic subtypes within TNBC, necessitating the identification of TNBC-specific GEPs (Burstein *et al*., 2015; Lehmann *et al*., 2011, 2016). Several classifications have been proposed, commonly based on immune activity within the tumour and the presence of markers such as androgen receptors (AR) (Table 2.1). These subtypes have varying treatment options, for example, AR+ TNBCs may be treated using antiandrogens, while immunotherapy may be an option for treating immune active subtypes.

Table 2.1: Proposed subtypes for classification of TNBC tumours.

Study	Basis of subtyping	Proposed subtypes
Barton *et al*., (2015)	Presence of AR for therapy	AR+ Quadruple negative breast cancers
Burstein *et al*., (2015)	GEP, particularly of immunoregulatory genes	Luminal androgen receptor Mesenchymal Basal-like immune suppressed Basal-like immune active
Lehmann *et al*., (2016)	GEP	Luminal androgen receptor Mesenchymal Basal-like 1 Basal-like 2
Jézéquel *et al*., (2019)	GEP and histological analysis, particularly of immunoregulatory genes and cells	Molecular apocrine Basal-like pro-tumorigenic immune response Basal-like adaptive immune response
Prado-Vázquez *et al*., (2019)	GEP of cellular and immune genes	Luminal androgen receptor Basal Claudin-high Claudin-low

2.1.4. Current treatment of TNBC

Conventional therapies for TNBC include surgery, radiotherapy, and chemotherapy. Despite its poor prognosis, TNBC generally responds well to chemotherapy and displays higher rates of pathological complete responses (pCR) compared to other BC subtypes (Carey *et al*., 2007; Rouzier *et al*., 2005). Patients who achieve pCR have significantly improved survival compared to those with residual disease (Biswas *et al*., 2017). This phenomenon of chemosensitivity coupled with poor outcomes, known as the triple negative paradox, occurs due to the high relapse rate in patients who do not achieve a pCR (Carey *et al*., 2007; Chernikova *et al*., 2019; Hu *et al*., 2017). Radiotherapy and chemotherapy are also associated with potentially serious side effects, such as cardiac toxicity and the risk of secondary cancers (Stewart *et al*., 2019).

Several novel treatments have been recently approved for metastatic and *BRCA*-deficient TNBCs. These include the antibody-drug conjugate sacituzumab govitecan, which targets the Trop-2 protein overexpressed in TNBC (Bardia *et al*., 2019; Zong & Pegram, 2021); polyadenosine diphosphate-ribose polymerase (PARP) inhibitors, which repress the activity of the PARP 1 and 2 enzymes involved in DNA repair and replication and are thus synthetically lethal with *BRCA* mutations (Helleday, 2011; McCann & Hurvitz, 2018); and antibodies targeting the immune checkpoint protein programmed death ligand-1(PD-L1) on cancer cells, which binds the programmed death protein-1 (PD-1) on T-cells to prevent immune attack (Thomas *et al*., 2021). Among the novel factors being explored as targets for BC therapy are the pro-inflammatory cytokines, particularly the tumour necrosis factor alpha (TNF-α).

2.2. Tumour necrosis factor alpha

2.2.1. Inflammation and cancer

Inflammation plays a significant role in tumour development, growth, and spread. Acute inflammation is a defence mechanism initiated in response to infection or injury, and involves the recruitment of leukocytes to the wounded tissue. These leukocytes combat infection and release growth factors and cytokines to stimulate proliferation and repair of the damaged tissue (Freire & Van Dyke, 2013; Todoric *et al*., 2016). The process is highly regulated, with leukocytes leaving the tissue or undergoing apoptosis when homeostasis is restored and inflammation resolves (Burman *et al*., 2005). The persistence of this process leads to chronic inflammation, which is associated with the development of diseases, such as cardiovascular

diseases, allergies, and cancer. Chronic inflammation is linked to cancer through two pathways: the extrinsic and intrinsic pathways (Figure 2.2).

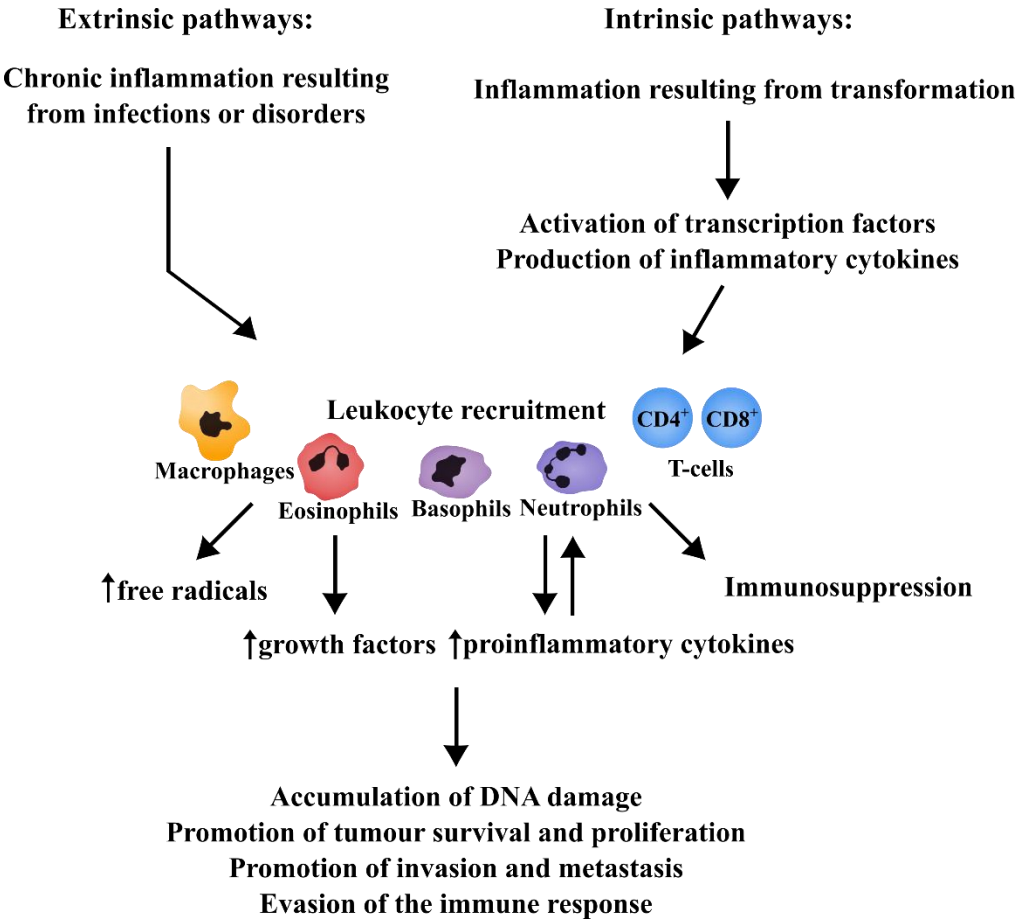

Figure 2.2: Chronic inflammation promotes cancer development and spread through the intrinsic or extrinsic pathway. Both pathways lead to the accumulation of inflammatory mediators and immune cells within the tissue, which may promote transformation.

The extrinsic pathway involves chronic inflammation resulting from infections, autoimmune disorders, or lifestyle factors such as smoking, which lead to the persistence of inflammatory cells within the tissue. Chronic inflammation is thus a predisposing factor to multiple cancers, including BC (Todoric *et al.*, 2016). However, inflammatory cells are present in most solid tumours, including those not preceded by chronic inflammation (Wang & Karin, 2015). Their recruitment occurs in response to cancer-intrinsic factors, such as hypoxia and necrosis within the tumour, and production of pro-inflammatory cytokines by tumour cells (Grivennikov *et al.*, 2010; Gun *et al.*, 2019). While the anti-tumour activity of cytotoxic natural killer (NK) and T cells recruited by this tumour-induced inflammation may initially inhibit growth, it also selects for cancer cells that can avoid immune detection (Gonzalez *et al.*, 2018). Macrophages are differentiated into pro-tumourogenic subtypes, termed tumour-associated macrophages

(TAM), that aid in promoting cancer growth and spread (Noy & Pollard, 2014). The tumour thus establishes an inflammatory microenvironment that promotes malignancy while providing protection from immune attack (Hanahan & Coussens, 2012).

The induction and termination of the inflammation process is mediated by cytokines. These proteins, secreted by immune cells, astrocytes, and glial cells, form complex networks that regulate tissue development, immune responses, and cell signalling (Kim *et al*., 2016; Stenken & Poschenrieder, 2015). Their role in inflammation may be categorised as either pro- or anti-inflammatory, although many cytokines are pleiotropic (Prieto & Cotman, 2017). The TNF superfamily (TNFSF) of cytokines comprises 29 receptors and 19 ligands with diverse roles in controlling apoptosis, proliferation, and cellular differentiation (Dostert *et al*., 2019). Notably, most members of this superfamily are synthesised as transmembrane proteins, which can be cleaved to form active soluble counterparts (Croft & Siegel, 2017). TNF-α, the founding member of the superfamily, remains widely studied due to its involvement in the development and progression of multiple autoimmune disorders and diseases such as cancer.

2.2.2. Tumour necrosis factor alpha (TNF-α)

The identification of TNF-α followed more than a century of research into reports of cancer remission in patients suffering from concurrent bacterial infections. This phenomenon was investigated in large-scale experiments by surgeon William Coley, who injected cancer patients with a mixture of heat-killed *Streptococcus pyogenes* and *Serratia marcescens*, called Coley's mixed toxins (Felgner *et al*., 2016). He reported remissions in multiple patients with inoperable sarcomas; however, the toxins fell out of use in favour of chemotherapy and radiotherapy (Coley, 1898; Kienle, 2012). The mechanism by which Coley's toxins worked nevertheless became the subject of much research, ultimately leading to the identification of "tumour necrosis factor", a serum component released in response to endotoxins and thought to be responsible for tumour death (Carswell *et al*., 1975). This factor was renamed TNF-α, to reflect its sequence homology to lymphotoxin, later renamed TNF-β (Aggarwal *et al*., 2012; Pennica *et al*., 1984). Studies later revealed the pleiotropic effects of TNF-α. It was shown to be the same protein as cachectin, responsible for cachexia, or wasting (Beutler *et al*., 1985a), while its role in inflammation was shown by Dinarello *et al*., (1986) and Beutler *et al*., (1985b), who reported TNF-α to be pyrogenic and responsible for septic shock, respectively.

2.2.3. TNF-α structure

The *TNF-α* gene is located within the major histocompatibility complex III region on chromosome 6, and is predominantly transcribed in activated macrophages, NK cells, and T-cells of the immune system (El-Tahan *et al*., 2016; Tian *et al*., 2014). It is synthesised as a type II transmembrane protein (tmTNF-α) that mediates cell-to-cell communication through direct contact, and controls the local inflammation process (Mitoma *et al*., 2018). The tmTNF-α is 26 kDa, with 233 amino acid (AA) monomers, each comprising a 30 AA intracellular N-terminal domain (NTD), a transmembrane region of 26 AA, and an 177 AA extracellular C-terminal domain (CTD) (Figure 2.3) (Horiuchi *et al*., 2010; Tang *et al*., 1996). The CTD contains the "TNF homology domain" (THD) characteristic of TNFSF ligands, which mediates homotrimer formation and receptor binding (Lang *et al*., 2016).

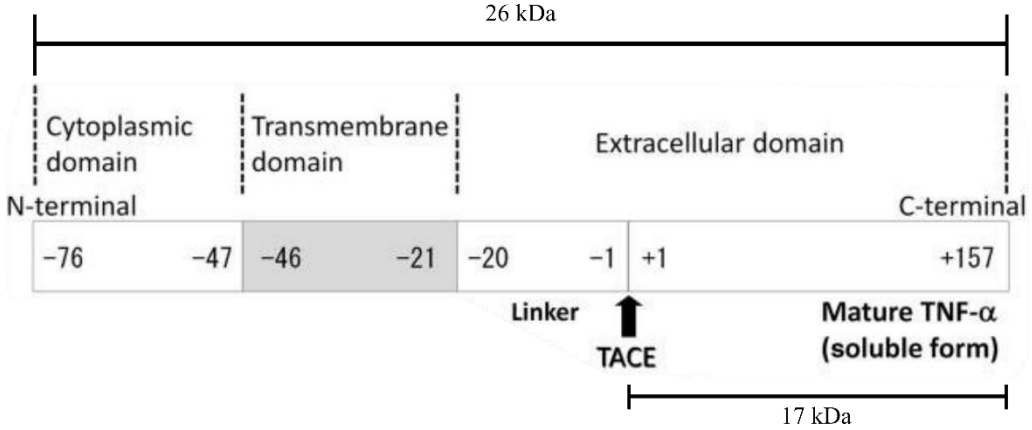

Figure 2.3: The structure of the 233 AA tmTNF-α monomer. TACE cleaves within the extracellular domain to release the 157 AA sTNF-α (adapted from Horiuchi *et al*., 2010).

The NTD contains a nuclear localisation signal (NLS) and is implicated in mediating reverse signalling. It has been observed to influence the expression of cytokines interleukins 12 and 1 beta (Domonkos *et al*., 2001; Friedmann *et al*., 2006). The generation of soluble TNF-α (sTNF-α) initially identified by Carswell *et al*., (1975) is mediated by metalloproteases that cleave within the extracellular domain to release sTNF-α from the cell membrane. sTNF-α is composed of ~17 kDa 157 AA monomers carrying the THD (Figure 2.3) (Bahia & Silakari, 2010). Cleavage is most commonly carried out by the TNF converting enzyme (TACE), also called a disintegrin and metalloproteinase 17 (ADAM17) (Briot *et al*., 2008; Hikita *et al*., 2009). The remaining tmTNF-α protein is further processed to remove the transmembrane domain (Friedmann *et al*., 2006). The NTD may then translocate to the nucleus to mediate gene expression.

2.2.4. TNF-α's functions in inflammation

TNF-α is the first cytokine produced during inflammation and mediates several aspects of the process (Table 2.2). It displays pro- and anti-inflammatory functions, stimulating the destructive initial stages of inflammation and subsequent processes that heal the injured tissue and restore homeostasis. It has been implicated in degradation of the extracellular matrix (ECM), and the promotion of epithelial-to-mesenchymal transition (EMT), which are important in wound healing (Marconi *et al*., 2021).

Table 2.2: The processes during inflammation that TNF-α has been implicated in.

	Mechanism	References
Facilitates leukocyte entry into the injured tissue	Promotes vasodilation Induces ECM and glycocalyx degradation Downregulates adherence junctional proteins	(Chappell *et al*., 2009; Hofmann *et al*., 2002; Mark *et al*., 2001)
Facilitates leukocyte-endothelial cell interactions	Upregulates leukocyte adhesion molecules	(Chandrasekharan *et al*., 2007; Ríos-Navarro *et al*., 2015)
Prevents the spread of infection	Induces fever Induces blood coagulation Stimulates ROS and NO production by macrophages	(Blaser *et al*., 2016; Kirchhofer *et al*., 1994; Page *et al*., 2018; Steinman, 2010)
Stimulates the immune response	Recruits leukocytes Activates dendritic cell and macrophages Promotes cytotoxic T_{eff} differentiation and proliferation	(Parameswaran & Patial, 2010; Trevejo *et al*., 2001; Ye *et al*., 2018)
Suppresses the immune response	Inactivates or kills T_{effs} Stimulates T_{regs} and myeloid-derived suppressor cells Regulates PD-L1 expression	(Ou *et al*., 2012; Salomon *et al*., 2018; Yee *et al*., 2017)
Stimulates wound healing	Promotes angiogenesis Promotes EMT Activates mesenchymal stem cells	(Broekman *et al*., 2016; Fajardo *et al*., 1992; Heo *et al*., 2011; Yan *et al*., 2010)

TNF-α regulates the immune response at the site of inflammation by activating various immune cells and directing effector T-cell (T_{eff}) differentiation into both cytotoxic CD4+ T_{effs} and immunosuppressive regulatory T-cells (T_{regs}). It has also been implicated in the regulation of PD-L1, an immune checkpoint protein that binds to its cognate receptor PD-1 on immune cells to facilitate self-tolerance. This prevents autoimmune attack; and promotes cytotoxic T_{eff} apoptosis and exhaustion, and T_{reg} development (Francisco *et al*., 2009; Qin *et al*., 2019). These diverse functions are mediated through binding of tmTNF-α and sTNF-α to their cognate TNF receptors (TNFRs), the type I transmembrane TNFR1 and TNFR2.

2.2.5. TNF receptors

TNFRs can be broadly divided into three groups based on their intracellular signalling domains: death receptors contain death domains (DD) that can signal both apoptotic and non-apoptotic pathways; costimulatory receptors; and decoy receptors without signalling domains that act as competitors for ligand binding (Antunes *et al*., 2012; Lang *et al*., 2016). TNFR1 and TNFR2 bear only 25.53% sequence identity to each other, most of which occurs in the extracellular domain (Uversky *et al*., 2017). The intracellular signalling domains differ significantly, contributing to the pleiotropic, and sometimes opposing, functions displayed by TNF-α. Both receptors may also exist in a soluble form, either through cleavage by TACE or exocytosis of the membrane-bound receptor (Puimège *et al*., 2014). These function as decoy receptors that bind circulating TNF-α to inactivate it, thus regulating immune responses, or stabilising its homotrimeric structure to promote activity (Aderka *et al*., 1992; Xanthoulea *et al*., 2004).

TNFR1 is a 60 kDa protein belonging to the death receptor class of TNFRs (Tian *et al*., 2014). However, it is a pleiotropic receptor that may activate apoptotic/necrotic or inflammatory pathways following binding to either sTNF-α or mTNF-α, with the latter pathways being most common (Lewis *et al*., 2012). TNFR1 is constitutively expressed at a low level on most nucleated cells (Hijdra *et al*., 2012). The intracellular region contains a TNFR1 internalisation domain (TRID) that mediates receptor endocytosis and the DD, which facilitates interactions with other DD-containing proteins (Jiang *et al*., 2017; Schneider-Brachert *et al*., 2004).

The 80 kDa TNFR2, in contrast, lacks a DD (Hong *et al*., 2019). It is thus generally associated with the promotion of cell growth; however, TNFR2 may induce apoptosis independently or through crosstalk with TNFR1 (Depuydt *et al*., 2005; Ruder *et al*., 2019). TNFR2 displays inducible expression limited to certain neuronal and endothelial cells, and immune cells (Medler & Wajant, 2019; Torrey *et al*., 2019). Unlike TNFR1, sTNF-α/TNFR2 complexes are highly unstable, and signalling is only activated by mTNF-α (Grell *et al*., 1995; Krippner-Heidenreich *et al*., 2002). TNFR2 has instead been suggested to increase local sTNF-α concentrations through rapid binding and release of the ligand, ultimately promoting sTNF-α binding by TNFR1 (Tartaglia *et al*., 1993).

2.2.6. TNF- α signalling pathways

The major pro-survival pathways signalled by TNFR1 and TNFR2 are the nuclear factor κB (NF-κB) and mitogen-activated kinase (MAPK) pathways. The NF-κB family includes the p50, p52, RelA, RelB, and c-Rel proteins, which form hetero- or homodimers for transcription. These dimers are located in the cytoplasm, bound by inhibitor of κB (IκB) proteins that inhibit their activity by preventing translocation to the nucleus (Hayden & Ghosh, 2008). They may be activated by the canonical or non-canonical pathway. The canonical pathway involves degradation of the IκBα, which frees the NF-κB proteins for activity (Atretkhany *et al*., 2020). The non-canonical pathway, in contrast, involves processing of the p100/RelB dimer into active p52/RelB for transcription (Sun, 2011). The MAPK pathway includes activation of p38 kinases, c-Jun N-terminal kinases (JNKs), or extracellular signal-regulated kinases (ERKs) (Soares-Silva *et al*., 2016). These pathways drive the expression of genes associated with cell survival, migration, differentiation, and inflammation, such as anti-apoptotic genes, cytokines such as TNF-α and ILs, and adhesion molecules (Figure 2.4) (Kang *et al*., 2019; Soares-Silva *et al*., 2016). However, the JNK pathway may also inactivate anti-apoptotic proteins and mediate pro-apoptotic signals. Cell death may be signalled through apoptosis, a controlled process mediated by caspases leading to phagocytosis by macrophages; or necroptosis, which leads to cell rupture and potentially promotes inflammation due to the release of intracellular components (Kalliolias & Ivashkiv, 2016). The pathways activated and their outcomes vary for different cell types (Gustin *et al*., 2004; Sedger & McDermott, 2014).

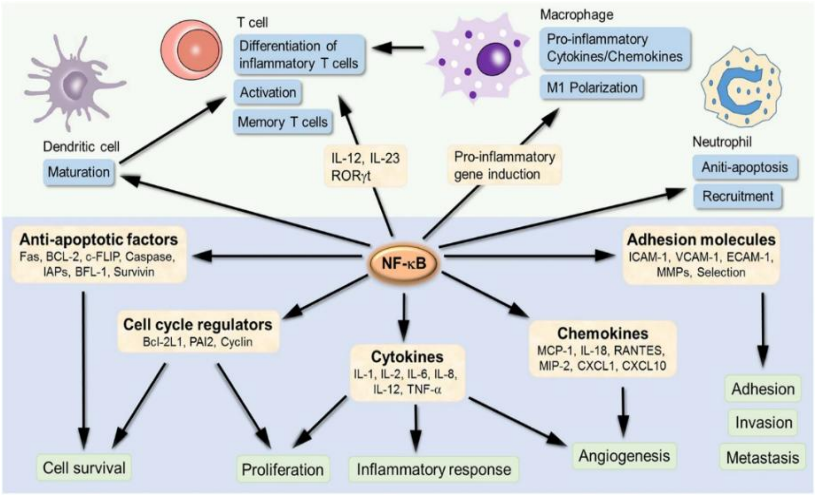

Figure 2.4: The diverse roles of NF-κB signalling in immune cells and its gene targets that regulate the inflammation process (Liu *et al*., 2017).

2.2.6.1. TNFR1 signalling

The opposing functions of TNFR1 are mediated through the formation of different signalling complexes following TNF-α binding: complex I activates transcription, while complexes IIa, IIb, and IIc signal cell death (Figure 2.5). Complex I is formed at the cell membrane immediately following ligand binding. TNFR1-associated death domain (TRADD) binds TNFR1 at the DD and promotes interactions with receptor interacting protein kinase-1 (RIP1), although RIP1 may bind TNFR1 in the absence of TRADD (Hsu *et al*., 1996; Pobezinskaya *et al*., 2008). The complex activates the p38 and JNK MAPK pathways through phosphorylation of MAPK kinases; and the canonical NF-κB pathway through phosphorylation of IκBα, triggering its ubiquination and degradation (Fechtner *et al*., 2017; Fischer *et al*., 2020). The NF-κB dimers may then translocate to the nucleus and drive transcription. Complex II is formed transiently, and, within 30 minutes of ligand binding, TNFRI undergoes endocytosis (Schütze *et al*., 1999). Modifications to TNFR1, such as depalmitoylation and ubiquitination, and the TRID promote its internalisation (Fritsch *et al*., 2014; Zingler *et al*., 2019). Complexes IIa and b induce apoptosis through the death-induced signalling complex (DISC) triggering the caspase cascade, while complex IIc induces necroptosis. Necroptosis generally promotes local inflammation; however, TNF-α-induced necroptosis may instead terminate the inflammation process by repressing TNF-α signalling (Kearney *et al*., 2015).

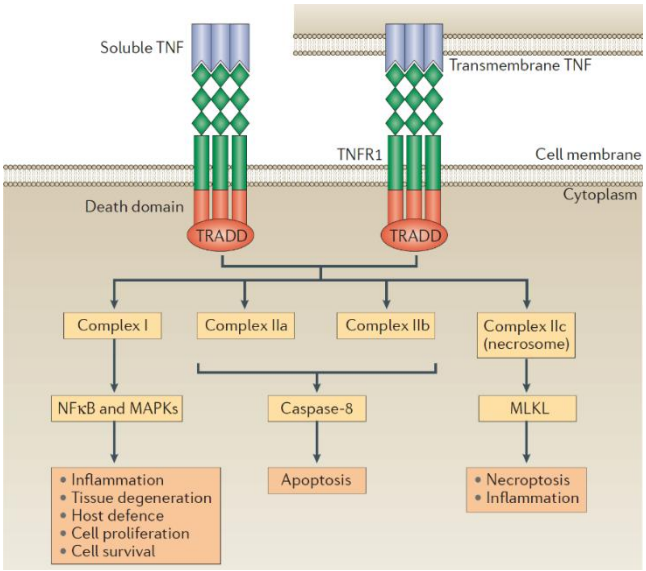

Figure 2.5: The signalling pathways activated by TNF-α through TNFR1. Complex I, which promotes the expression of genes associated with the inflammation process, is initially formed following binding. The cell death-signalling complexes IIa, IIb, and IIc form subsequently and are regulated by the gene products of complex I (Kalliolias & Ivashkiv, 2016).

2.2.6.2. TNFR2 signalling

The signalling pathways of TNFR2 are less well characterised due to its limited expression (Ji *et al*., 2012). tmTNF-α binding activates the transduction of several growth-promoting pathways (Figure 2.6). TNFR2 is most often associated with the non-canonical NF-κB pathway, although it may induce canonical NF-κB shortly after ligand binding (Borghi *et al*., 2018; Fotin-Mleczek *et al*., 2002; Rauert *et al*., 2010). TNFR2 may also induce long term NF-κB activation via the PI3K/Akt pathway, in contrast to TNFR1 which transiently activates NF-κB (Fischer *et al*., 2011; Marchetti *et al*., 2004).

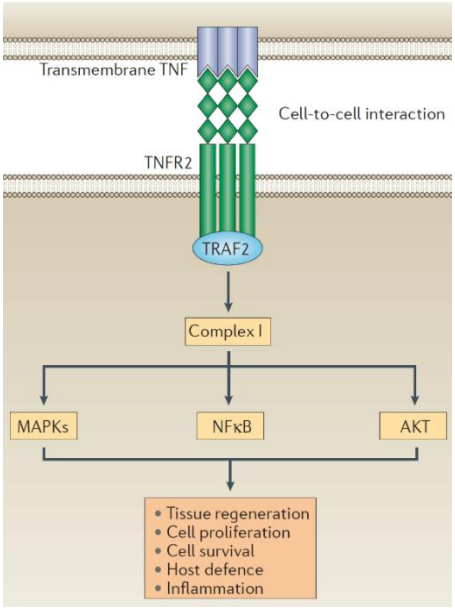

Figure 2.6: TNFR2 is generally associated with the transduction of proliferation, differentiation, and survival signals through NF-κB, AKT, and MAPK pathways (Kalliolias & Ivashkiv, 2016).

Crosstalk between TNFR1 and TNFR2 plays an important role in determining the fate of cells that co-express the receptors. Multiple studies have observed enhanced TNFR1 signalling in the presence of TNFR2 (Cabal-Hierro *et al*., 2014; Fotin-Mleczek *et al*., 2002; Rodríguez *et al*., 2011; Ruspi *et al*., 2014). TNFR2 has also been observed to induce apoptosis independently of TNFR1. The mechanisms by which it does so are unknown, but may involve JNK signalling (Inoue *et al*., 2015; Ji *et al*., 2012; Otano *et al*., 2020; Ramesh & Reeves, 2003).

2.2.7. TNF-α in anti-cancer studies

Studies have investigated TNF-α's potential as an anticancer therapeutic. Its cytotoxic action was reported to be cancer-specific (Carswell *et al*., 1975; Dealtry *et al*., 1987; Motoo *et al*., 1986), with *in vivo* studies reporting tumour regression after treatment with TNF-α alone and

in conjunction with interferons and other chemotherapeutic agents (Asher *et al*., 1987; Balkwill *et al*., 1986; Brouckaert *et al*., 1986; Haranaka *et al*., 1984). Despite the promise shown in animal studies, clinical trials reported very low response rates and adverse side effects, such as fevers, hepatotoxicity, and low blood pressure, in response to systemic TNF-α administration (Roberts *et al*., 2011). Isolated limp perfusion delivery of TNF-α and the drug melphalan is currently used for local control of advanced sarcomas (Smith *et al*., 2018). However, systemic delivery continues to be hindered by severe toxicity.

TNF-α treatment is thought to kill cancer cells indirectly, by damaging the tumour vasculature or by inciting an immune response, rather than directly through apoptosis induction (Shen *et al*., 2018). High doses of TNF-α have been observed to selectively disrupt adhesion proteins in melanoma models and endothelial cell lines, inducing apoptosis and vascular leakage (Menon *et al*., 2006; Rüegg *et al.*, 1998). This effect of increasing vascular permeability contributes to TNF-α's synergy with other therapeutic agents. TNF-α has also been shown to enhance the cytotoxic activity of NK cells, and may promote recruitment and differentiation of immune cells with anti-cancer activity (Josephs *et al*., 2018; Mocellin *et al*., 2003). Drugs that inhibit transcription may also synergise with TNF-α, as they promote TNF-α-induced apoptosis (Demidenko & Blagosklonny, 2004).

2.2.8. TNF-α in promoting cancer

While it was being investigated as an anti-cancer agent, studies showed an apparently paradoxical ability of TNF-α to promote tumour growth. Early studies in mice models reported that TNF-α promotes angiogenesis (Leibovich *et al*., 1987), tumour cell adhesion (Malik *et al*., 1989), and metastasis (Malik *et al*., 1990; Orosz *et al*., 1993). Evidence for a direct link between TNF-α and tumourigenesis was provided by Moore *et al*., (1999), who showed that TNF-α-deficient mice developed fewer skin tumours than normal mice following carcinogen exposure. Increased TNF-α levels have been observed in various cancer tissues and cell lines, either due to secretion by infiltrating immune cells, or cancer cells themselves (Egberts *et al*., 2008; Scheff *et al*., 2017; Shang *et al*., 2017; Szlosarek *et al*., 2006; Zins *et al*., 2007). This expression by malignant cells may result from secreted TNF-α forming an autocrine loop stimulating its own release, TNF-α-induced stabilisation of *TNF-α* mRNA, or mutations that promote *TNF-α* expression (Li *et al*., 2015a; Nabors *et al*., 2003; Szlosarek *et al*., 2006; Zins *et al*., 2007). Many processes induced by TNF-α through NF-κB during inflammation can also promote transformation and metastasis (Table 2.3), although it may also promote cancer through

inflammation-independent mechanisms (Li *et al*., 2009). Thus, the chronic production of low levels of TNF-α observed in cancers may promote tumour growth and spread, in contrast to the high concentrations required for effective tumour necrosis in therapy (Montfort *et al*., 2019).

Table 2.3: The potential pro-tumourogenic effects of chronic, low-level TNF-α production.

Functions of TNF-α in inflammation	Pro-tumourogenic effects	References
Stimulates release of cytokines and chemokines, including itself	Recruitment of TAM Increased NF-κB signalling	(Azenshtein *et al*., 2002; Son *et al*., 2013)
Upregulates adhesion molecules	Promotes metastasis	(Jassam *et al*., 2016; Liang *et al*., 2007)
Degrades the ECM	Promotes angiogenesis and invasion	(Azenshtein *et al*., 2002; Quintero-Fabián *et al*., 2019)
Induces EMT	Promotes invasion and metastasis	(Ieda *et al*., 2019; Li *et al*., 2012a)
Generates ROS and NO	Induces DNA damage	(Westbrook *et al*., 2012; Yan *et al*., 2006)
Upregulates pro-angiogenesis factors	Promotes tumour growth and spread	(Lai *et al*., 2016; Leek *et al*., 1998; Tanaka *et al*., 2018)
Promotes proliferation of T_{regs}	Suppresses the immune response against the tumour	(Chang *et al*., 2015)
Upregulates PD-L1	Suppresses the immune response against the tumour	(Li *et al*., 2018a; Lim *et al*., 2016; Wang *et al*., 2017)

2.2.9. Role of TNF-α in BC

TNF-α is involved in the regulation of multiple processes within the mammary glands, including differentiation of the tissue during puberty, pregnancy, and lactation (Ip *et al*., 1992; Lee *et al*., 2000; Shea-Eaton *et al*., 2001). It has also been implicated in the development and spread of BC (Figure 2.7). High levels of TNF-α and its receptors have been observed in the BC tumour microenvironment (TME), with early studies showing secretion by infiltrating macrophages (Leek *et al*., 1998; Miles *et al*., 1994). Clinically, these elevated levels have been associated with a higher risk of relapse and metastasis (Cui *et al*., 2008; García-Tuñón *et al*., 2006; Soria *et al*., 2011). Studies have also shown TNF-α to induce EMT in normal mammary cell lines, which may promote tumour invasion (Chua *et al*., 2007; Li *et al*., 2012a). Its role in the development and progression of the different BC subtypes has been the subject of much research.

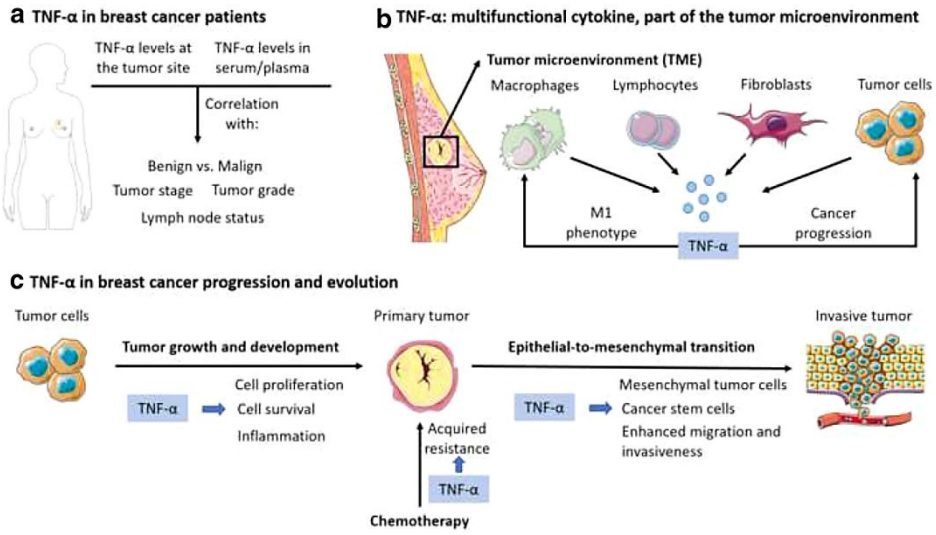

Figure 2.7: TNF-α involvement in BC. A) High levels of TNF-α have been observed in the tissue and sera of BC patients, B) Elevated TNF-α levels have been observed in tumour tissue due to production by various cells in the TME, C) TNF-α has been implicated in every step of carcinogenesis, promoting tumour growth and spread, and drug resistance (Cruceriu *et al*., 2020).

2.2.9.1. Luminal BCs

Luminal BCs are driven by the activity of the two ER, ERα and ERβ, and/or PR, which function as transcription factors (TF) (Gao *et al*., 2002). TNF-α upregulates enzymes involved in oestrogen synthesis, and has thus been implicated in the development and progression of ER+ BC (To *et al*., 2013). NF-κB and ER may display negative crosstalk termed "transrepression", where each pathway represses the other; however, TNF-α-induced NF-κB and ER have also been shown to promote each other's activity and synergistically upregulate survival genes (Frasor *et al*., 2009). ERα may also upregulate TNF-α expression in response to estradiol stimulation by directly binding its promoter (To *et al*., 2014). Increased TNF-α expression has, in contrast, been associated with decreased PR expression, and has thus been suggested to downregulate PR and increase the aggression of luminal BC (Kamali-Sarvestani *et al*., 2005).

Conflicting results have been reported regarding the involvement of TNF-α in luminal cell lines. Hamaguchi *et al*., (2011) observed low levels of secreted TNF-α in MCF-7 and ZR-75-1 cells, while To *et al*., (2014) reported high sTNF-α in MCF-7 and ZR-75-1 compared to T47D and MDA-MD-361 cells. TNF-α treatment has been observed to inhibit growth and induce apoptosis of MCF-7 and T47D through various mechanisms, such as upregulation of tumour suppressor genes (TSGs), and growth factor and cell cycle inhibitors; or by activating apoptotic caspase- and JNK-dependent pathways (Donato & Klostergaard, 2004; Jeoung *et al*., 1995; Pirianov & Colston, 2001; Pusztai *et al*., 1993; Rozen *et al*., 1998; Sgagias *et al*., 1991).

However, TNF-α treatment of MCF-7 has also been observed to promote migration and metastasis (Weitzenfeld *et al*., 2013; Wolczyk *et al*., 2016); and upregulate anti-apoptotic proteins (Wang *et al*., 2012). T47D cells have shown resistance to TNF-α-induced cytotoxicity, and mitogenic and proliferative effects in response to TNF-α treatment (Pirianov & Colston, 2001; Rivas *et al*., 2008; Rubio *et al*., 2006). Meng *et al*., (2001) further showed T47D cells to secrete TNF-α, inhibiting differentiation of fibroblasts into mature adipocytes. These fibroblasts form a dense layer around breast tumours that provides structural support for its growth. These discrepancies may result from differences in gene expression in cell lines from different laboratories. Burow *et al*., (1998) demonstrated that the levels of anti-apoptotic genes, TNFR1, and ceramide differed in three MCF-7 variants from different laboratories, ultimately influencing their sensitivity to TNF-α-induced apoptosis.

TNF-α has furthermore been associated with the development of drug resistance in *in vitro* and *in vivo* MCF-7 models, by downregulating ER expression (Gunnarsdóttir *et al*., 2020); or upregulating efflux proteins (Alamolhodaei *et al*., 2020). It has also been shown to promote EMT in non-invasive MCF-7 cells and BC cell stemness (Dong *et al*., 2007; Liu *et al*., 2020a; Storci *et al*., 2010). These BC stem cells display self-renewal capabilities and resistance to chemo- and radiotherapies, and promote tumour relapse and metastasis (Liu *et al*., 2020a).

2.2.9.2. TNBC

The paradoxical effects of TNF-α have been shown by Qiao *et al*., (2016), who reported TNF-α to both induce apoptosis in BT549 cells and activate c-Jun signalling of anti-apoptotic genes and genes associated with cell invasion. Weichhaus *et al*., (2011) observed an increase in the proportion of MDA-MB-231 cells in the sub-G1 phase following TNF-α treatment, which was suggested to indicate apoptosis induction, although no impact on proliferation was observed following treatment. In contrast, several studies have reported resistance to sTNF-α-induced cytotoxicity, NF-κB activation, and increased proliferation in TNBC cell lines in response to TNF-α treatment (Cai *et al*., 2017; Geng *et al*., 2013; Mueller *et al*., 1996; Yan *et al*., 2009).

Increased TNF-α production has been reported in TNBC cell lines and tumour samples (Gong *et al*., 2019; Hamaguchi *et al*., 2011; To *et al*., 2014; Yu *et al*., 2013). The cytokine has been shown to induce EMT in BT549 and Hs578T cells, and upregulate the PI3K/Akt and MAPK/ERK pathways (Qiao *et al*., 2015). These growth-promoting pathways have been observed to be increased in TNBC and basal BCs compared to other BC subtypes (Hoeflich *et*

al., 2009; Umemura *et al*., 2007). Lee *et al*., (2019a) found that TNF-α upregulates A20, a ubiquitin-editing enzyme, in TNBC cell lines, leading to increased expression of inflammatory and anti-apoptotic pathways, ultimately protecting TNBC cells from TNF-α-induced cytotoxicity and promoting EMT, metastasis, and BC stem cells. TNF-α may also contribute to treatment failure by promoting drug resistance (Liu *et al*., 2020c); or angiogenesis in response to taxane treatment (Harris *et al*., 2018). Lim *et al.*, (2016) also implicated TNF-α in stabilising PD-1/PD-L1 interactions by inhibiting degradation of PD-L1, thus suppressing the immune response against the tumour.

TNF-α has further been implicated in facilitating metastasis. Li *et al*., (2015) reported metastasis in TNBC patients to be associated with -308 G>A SNP that increases TNF-α expression. TNF-α stimulation has been reported to increase expression of pro-metastatic cytokines, and promote migration and invasion of TNBC-stroma models (Liubomirski *et al*., 2019). Geng *et al*., (2013) found TNF-α to induce aggregation of and upregulate the E-selectin ligand CD44V4 in MDA-MB-231 cells. These characteristics facilitate interactions between cancer cells and the surrounding inflamed endothelium, and ultimately promote extravasation into the bloodstream and metastasis. Cell-secreted TNF-α has also been suggested to induce expression of transforming growth factor-beta 2 in astrocytes, promoting metastasis of TNBC cells to the brain (Gong *et al*., 2019).

Studies have shown the therapeutic potential of TNF-α targeting in TNBC using antibodies. Hamaguchi *et al*., (2011) reported treatment with an anti-TNF-α antibody to suppress *in vitro* migration and invasion, and *in vivo* metastasis of MDA-MB-231 cells. MDA-MB-231 have also been found to display significantly higher levels of tmTNF-α, which has been implicated in mediating resistance to sTNF-α through reverse signals that activate NF-κB (Yan *et al*., 2009; Yu *et al*., 2013). Antibody targeting of tmTNF-α further induced tumour apoptosis in MDA-MB-231 xenografts (Yu *et al*., 2013). Tumour-targeted nanobodies have also inhibited MDA-MB-231 migration and metastasis *in vitro* and *in vivo* (Ji *et al*., 2017, 2020). However, antibody targeting may be inhibited by high levels of sTNF in the serum and tumour microenvironment, which may bind the antibody and prevent it from reaching the tumour (Yu *et al*., 2013). The use of anti-TNF-α antibodies is further inhibited by the risk of side effects, such as potential infections (Lee *et al*., 2014). Targeting *TNF-α* gene expression may thus provide more effective inhibition. This may be achieved through the gene silencing process of RNA interference (RNAi).

2.3. The *c-MYC* oncogene

The development of cancer is multi-step process, involving multiple mutations in different pathways controlling cell growth. Genes that promote transformation after gain-of-function mutations are broadly classified as oncogenes (Zhu *et al*., 2015). Perhaps the most well-known oncogene is *c-MYC*, identified in the 1970s following research into oncogenic animal retroviruses. This research began in the early 1900s, with reports that certain chicken cancers were transmissible via cell-free filtrates (Ellermann & Bang, 1909; Fujinami & Inamoto, 1914; Rous, 1911; Rous & Murphy, 1914). Despite scepticism, these results were corroborated by substantial research in the following decades that linked viral infection to mammalian cancers (Javier & Butel, 2008). In the 1960s and 70s, several avian retroviruses with oncogenic activity were isolated and found to carry an oncogene termed *v-MYC* (Conacci-Sorrell *et al*., 2014). The cellular homologue *c-MYC* was subsequently identified and characterised (Sheiness & Bishop, 1979; Vennstrom *et al*., 1982). The association between dysregulated *c-MYC* and human cancers was shortly revealed by studies that reported *c-MYC* amplification in leukaemia and colon cancer cell lines (Alitalo *et al*., 1983; Collins & Groudine, 1982); and gene translocation in Burkitt's lymphoma cells (Dalla-Favera *et al*., 1982).

The similarity of the c-MYC protein to known TFs and the identification of specific c-MYC DNA binding sequences within promoter regions led to its classification as a TF (Halazonetis & Kandil, 1991; Kerkhoff *et al*., 1991). Several gene pathways, including those involved in proliferation, cell cycle progression, and apoptosis, have since been identified as targets of c-MYC regulation (Madden *et al*., 2021).

2.3.1. *c-MYC* gene structure

The structure of the untransformed human *c-MYC* oncogene was first described by Battey *et al*., (1983). Located on the long arm of chromosome 8, at locus 8q24.21, it consists of three exons and two introns (Figure 2.8) (Carabet *et al*., 2018; Chen *et al*., 2014). Exon 1 contains regulatory elements, while exons 2 and 3 encode the protein sequence (Kubickova *et al*., 2023). Transcription may begin from one of four promoters, designated P0, P1, P2, and P3; however, the majority of transcripts (75 – 90%) originate from P2 (Wierstra & Alves, 2008). Additionally, the locus contains two regulatory elements upstream of P1 and P2: the far upstream sequence element, and the guanine-rich nuclease hypersensitivity element III 1, which assume conformations that promote or repress *c-MYC* transcription (Carabet *et al*., 2018; Chen *et al*., 2014).

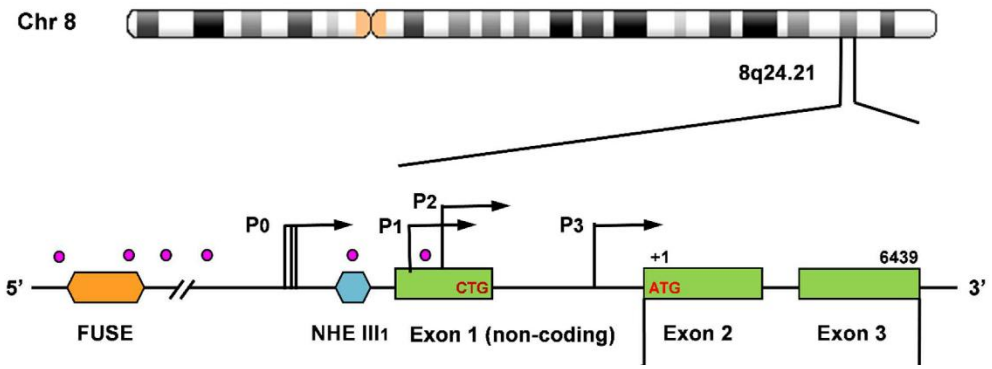

Figure 2.8: The structure of the *c-MYC* gene on chromosome 8 (Carabet *et al*., 2018).

2.3.2. c-MYC protein structure

Translation of the *c-MYC* mRNA may produce two full-length protein products depending on the site of initiation. p67 is produced through translation from the CUG codon at the end of exon 1, while translation of p64 is initiated at the AUG at the start of exon 2 (Blackwood *et al*., 1994). Both proteins thus share the same sequence containing an N-terminal transactivation domain (TAD), a central region, and a C-terminal DNA-binding domain (DBD), with p67 being slightly longer at the N-terminal (453 vs 439 AA). The p64 protein is, however, considered to be the predominant *c-MYC* product responsible for its oncogenic activity (Ji *et al*., 2016). Its structure is shown in Figure 2.9.

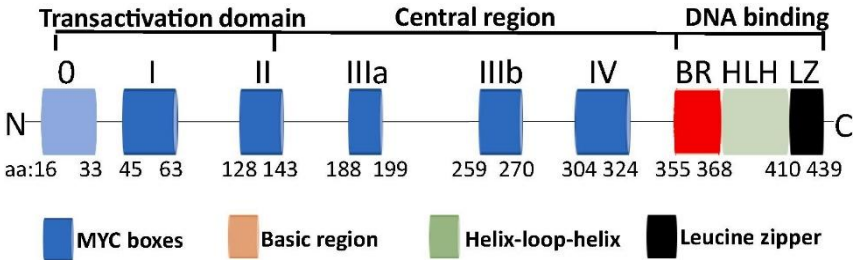

Figure 2.9: The structure of the c-MYC protein containing six conserved MBs (Duffy *et al*., 2021).

The c-MYC protein contains 6 highly conserved regions called Myc boxes (MB), which mediate protein-protein interactions and protein stability. Three - MB0, MBI, and MBII – are located in the TAD. The MB0 and MBII boxes are required for transactivation, by mediating interactions with transcription elongation factors and histone acetyltransferases (Kalkat *et al*., 2018; Zhang *et al*., 2017). MBI contains the phosphodegron – residues that promote ubiquitination and degradation once phosphorylated - as well as residues that stabilise the protein upon phosphorylation (Arthur *et al*., 2023; Llombart & Mansour, 2022). The region

between MBI and MBII additionally contains motifs that bind the TATA binding protein, which is required for transcription initiation (Beaulieu *et al*., 2020; Wei *et al*., 2019)

The MBIIIA, MBIIIb, and MBIV boxes are located in the central region. MBIIIa and MBIIIb regulate transcription. MBIIIa represses transcription through recruitment of histone deacetylases to the promoters of target genes (Kurland & Tansey, 2008); and may inhibit transcription of proapoptotic genes (Herbst *et al*., 2005). MBIIIb facilitates interactions with the chromatin cofactor WDR5, allowing binding of c-MYC to the DNA (Thomas *et al*., 2019). MBIIIb also contains a 10 AA sequence that mediates c-MYC degradation independently of ubiquitination (Gregory & Hann, 2000). The final MB, MBIV, modulates DNA binding activity and interaction with transcription regulators (Cowling *et al*., 2006; Thomas *et al*., 2016). The central region also contains two nuclear localisation signals (NLS) that facilitate nuclear entry (Dang & Lee, 1988; Llombart & Mansour, 2022).

The CTD is the most widely studied component of c-MYC due to the presence of the DBD. This domain is composed of a basic helix-loop-helix leucine zipper (bHLHZ) motif that facilitates heterodimerisation with the MYC-associated factor X (MAX), which also contains a bHLHZ motif (Blackwood & Eisenman, 1991; Yamashita *et al*., 2020). Homo- or heterodimerisation is a prerequisite for DNA binding by bHLH family TFs (Littlewood & Evan, 2023). The canonical enhancer box (E-box) sequence recognised by the MYC/MAX dimer is 5′-CACGTG-3′; however, non-canonical sequences may also be bound when c-MYC is overexpressed (Allevato *et al*., 2017).

Several small proteins may also be produced from the *c-MYC* gene. The mrtl and MycHex1 proteins are encoded by sequences upstream of and within exon 1, respectively. These proteins have possible roles in translational regulation of c-MYC expression and DNA replication (Jang *et al*., 2023; Ji *et al*., 2016). The c-MYC S protein has been implicated in regulating the transcriptional activity of the p64 and p67, and may be capable of regulating cell proliferation (Spotts *et al*., 1997; Xiao *et al*., 1998).

2.3.3. c-MYC as a transcription factor

c-MYC's mechanism of action is contested: differing models propose it to either regulate the expression of specific genes, or to non-specifically amplify the expression of all active genes (Caforio *et al*., 2018). *c-MYC* transcription is induced by developmental signals or growth factor stimulation (Miller *et al*., 2012). Following translation, the protein binds the

constitutively expressed MAX to form the MYC/MAX heterodimer, which binds the canonical E-box. X-ray studies have shown heterodimerisation specificity to be controlled by two AA in the bHLHZ domain, with sequence-specific DNA binding being mediated by three AA in the basic regions of MYC and MAX that interact with four nucleotides within the E-box (Allevato *et al*., 2017; Nair & Burley, 2003). Notably, the chromatin must be open in order for MYC/MAX to bind, as evidenced by the presence of histone modifications associated with active chromatin (Nie *et al*., 2012; See *et al*., 2022).

Following DNA binding, the complex recruits cofactors that facilitate transactivation or repression. Some cofactors promote transcription initiation; for example, histone acetyltransferases GCN5 and TIP6, and ATPases open the chromatin; while the transcription initiation factor TFIIIb activates RNA pol III (Hann, 2014). Associations with the positive transcription elongation factor P-TEFb promote transcription elongation, or release paused RNA pol II (Eberhardy & Farnham, 2002; Rahl & Young, 2014). Interactions with E3 ubiquitin ligases, kinases, and acetyltransferases may introduce post-translational modifications that improve c-MYC stability (Faiola *et al*., 2005; Hann, 2014; Su *et al*., 2018). Conversely, transcription may be repressed through interactions with histone methyltransferases and deacetylases (Kurland & Tansey, 2008; Tu *et al*., 2018). Repression of growth arrest is also mediated through binding and inhibition of the Myc-interacting zinc finger protein 1 Miz-1, a protein that regulates cell cycle progression in response to antimitogenic signals (Scafuro *et al*., 2021; Tu *et al*., 2018; Wiese *et al*., 2013). Through these numerous interactions, c-MYC regulates the expression of hundreds of genes to ultimately promote cell growth (Figure 2.10).

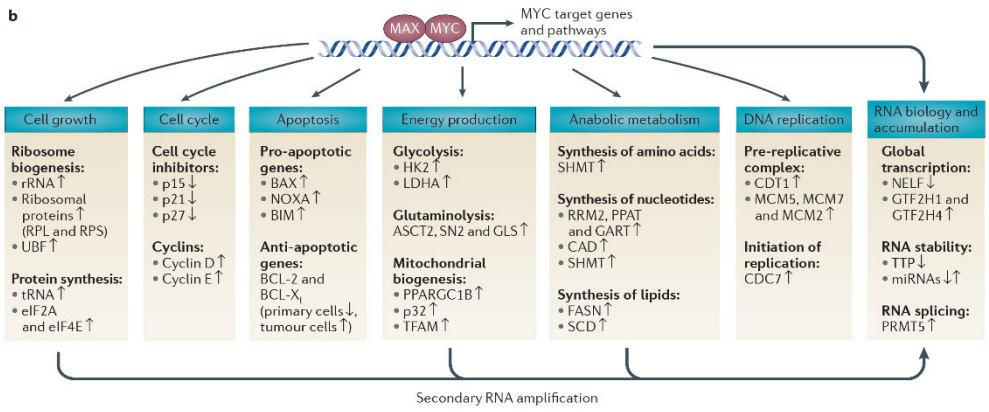

Figure 2.10: The cellular pathways regulated by c-MYC, including the factors that are upregulated (up arrow) or downregulated (down arrow) by c-MYC (adapted from Kress *et al*., 2015).

2.3.4. Activation of *c-MYC*

In normal cells, *c-MYC* expression is highly regulated by TFs, epigenetic factors, miRNAs, and post-translational modifications (Ahmadi *et al*., 2021). Expression is low in quiescent cells, increases during mitosis, and returns to basal levels thereafter (Elbadawy *et al*., 2019). *c-MYC* activation is most commonly the result of mutations that lead to dysregulated expression, rather than the result of coding sequence mutations producing an oncogenic protein (Das *et al*., 2023). Activation leads to accumulation of c-MYC in canonical promoter and enhancer regions, and increased binding to non-canonical E-boxes; inducing continuous activation of growth-promoting pathways (Allevato *et al*., 2017; Lin *et al*., 2012). Dysregulated *c-MYC* contributes to all the hallmarks of cancer, directing cell proliferation and spread, metabolic reprogramming, and genetic instability, while blocking immune detection and cell death mechanisms (Figure 2.11). The alterations which lead to increased c-MYC activity are described below.

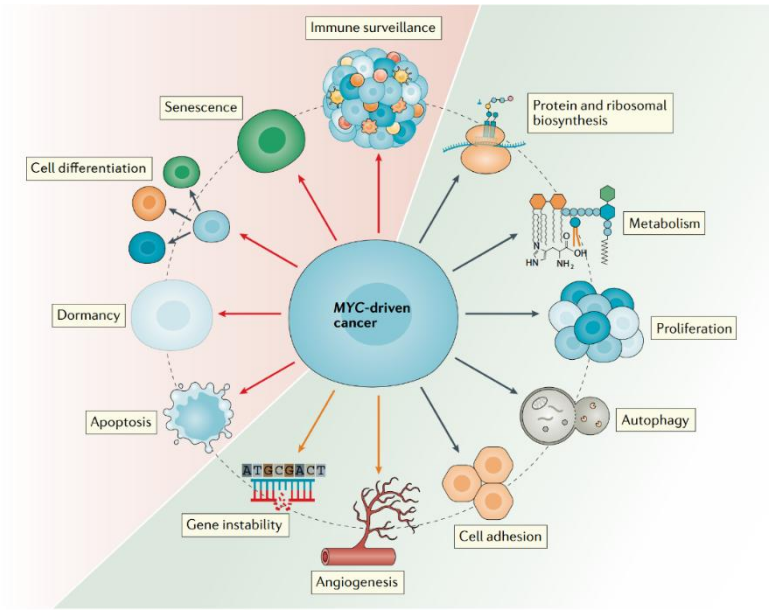

Figure 2.11: Dysregulated *c-MYC* expression induces transformation by upregulating cell proliferation and survival pathways (green section), while preventing cell death or protective processes (red area) (Dhanasekaran *et al*., 2021).

Several different types of alterations may lead to an increase in *c-MYC* transcription. *c-MYC* amplification, or an increase in the gene copy number, is commonly observed in epithelial tumours, and may correlate with tumour aggression (Ilic *et al*., 2011; Reyes-González & Vivas-Mejía, 2021; Schaub *et al*., 2018). Translocation may remove the *c-MYC* gene from the control of its tightly-regulated promoter and place it under the control of highly-expressed promoters with super-enhancer elements. This was first described in Burkitt's lymphoma, where

translocation moves *c-MYC* near immunoglobin gene super-enhancers on chromosomes 2, 22, or 14; and is also common in other haematological cancers such as multiple myeloma (Mikulasova *et al*., 2020; Schick *et al*., 2017). Alternatively, the *c-MYC* promoter or enhancer regions may themselves be activated by SNPs that promote TF interactions (Pomerantz *et al*., 2009; Sur *et al*., 2012); amplification (Zhang *et al*., 2016b); or epigenetic modifications such as hypomethylation (Shi *et al*., 2013; Urbanek-Olejnik *et al*., 2018).

c-MYC transcription may also increase in response to external factors, such as dysregulation of the signalling pathways that control its expression. Aberrant expression of the Wnt/β-catenin, PI3K/AKT, or oestrogen signalling pathways may upregulate *c-MYC* expression (Kalkat *et al*., 2017; Rennoll & Yochum, 2015). Retroviral insertion may disrupt endogenous promoters or lead to the production of viral oncoproteins, as observed in infection by the Human Papilloma Virus (HPV). The main integration site of HPV is within the *c-MYC* locus, leading to dysregulated *c-MYC* expression and ultimately cervical cancer growth (Pal & Kundu, 2020).

Mutations can also stabilise the normally unstable *c-MYC* mRNA and protein, leading to high expression in the absence of increased transcription. The half-life of *c-MYC* mRNA (30 – 60 min) may be improved through the binding of the coding region determinant binding protein (CRDBP) to a coding region instability determinant (CRD) in the mRNA, thus preventing endonucleolytic cleavage (Lemm & Ross, 2002; Yu *et al*., 2020). CRDBP expression is normally low or absent in adult tissues; however, overexpression leads to increased *c-MYC* mRNA stability and transactivation (Fakhraldeen *et al*., 2015; Tomita *et al*., 2019). The stability of the c-MYC protein, with a half-life of 20 – 30 min, may be increased through suppression of factors that target it for degradation or upregulation of proteins that inhibit degradation (Choi *et al*., 2010; Gu *et al*., 2017; Li *et al*., 2014). Although relatively rare, point mutations impacting c-MYC stability have been described in lymphomas. These inhibit c-MYC transcription of pro-apoptotic pathways, or proteolysis (Chakraborty *et al*., 2015; Hemann *et al*., 2005). However, it has been suggested that most point mutations improve cancer patient outcomes, by attenuating oncogenic *c-MYC* activity (Xu-Monette *et al*., 2016).

It is worth noting that *c-MYC* also promotes the transcription of pro-apoptotic genes. This functions as a protective mechanism against the transformative effects *c-MYC* overexpression (McMahon, 2014). Thus, tumourogenesis driven by *c-MYC* dysregulation can only occur in conjunction with TSG loss and the activation of other oncogenes (Gabay *et al*., 2014).

2.3.5. *c-MYC* dysregulation in BC

c-MYC is estimated to be aberrantly expressed in 30 - 50% of BC cases, where it has been associated with increased tumour size and aggression, and poorer prognoses (Fallah *et al.*, 2017; Qu *et al*., 2017). The effects of its overexpression vary among the different BC subtypes.

c-MYC overexpression in luminal BCs may be driven by oestrogen, which binds enhancer elements upstream of *c-MYC* to induce its transcription, and stabilises the protein (Rehman *et al*., 2022; Rodrik *et al*., 2006; Wang *et al*., 2011a). The importance of *c-MYC* in ER+ BC was shown by reports that it regulates 50% of the genes activated by oestrogen in MCF-7 cells (Musgrove *et al*., 2008). High *c-MYC* in luminal BCs has been associated with increased activity of proteins involved in translation and protein synthesis (Green *et al*., 2016). This activity is suggested to contribute to the development of endocrine resistance, as *c-MYC* overexpression allows cancer cells to avoid the growth-inhibitory effects of endocrine therapies (Saatci *et al*., 2021). Studies have also identified *c-MYC* gene signatures predictive of outcomes in tamoxifen-treated BC patients: Musgrove *et al*., (2008) identified a gene expression signature associated with cell growth; and Miller *et al*., (2011) reported a signature activated in the low oestrogen conditions induced by endocrine therapy. *c-MYC* may further promote the survival of endocrine-resistant cancer cells by altering their metabolism, increasing their uptake of glutamine and glucose while allowing them to survive glucose deprivation (Shajahan-Haq *et al*., 2014).

c-MYC amplification and expression has been observed to be increased in TNBC compared to other BC subtypes, where it simulates the response to oestrogen in the absence of oestrogen stimulation (Alles *et al*., 2009; Katsuta *et al*., 2019; Tang *et al*., 2022). Aberrant *c-MYC* is therefore considered to be a major driver of TNBC development and aggression. High *c-MYC* has been correlated with increased activity of cell cycle proteins (Green *et al*., 2016); improved immune evasion (Zimmerli *et al*., 2022); and increased glucose metabolism (Shen *et al*., 2015). *c-MYC* further contributes to TNBC recurrence and metastasis by promoting enrichment of drug-resistant cancer stem cells, through activation of the MAPK pathway and induction of the hypoxia inducible factor-1 (Gupta *et al*., 2017; Lee *et al*., 2017; Yang *et al*., 2017a). Yin *et al*., (2017) further showed *c-MYC* to differentially regulate stem cell and EMT changes in different TNBC cell lines depending on the tumour biology. Studies have also reported an association between *c-MYC* overexpression, *BRCA1* deficiency, and TNBC (Grushko *et al*., 2004; Ren *et al*., 2013). *BRCA1* is a TSG that normally regulates *c-MYC* expression, and is suggested to be

downregulated in approximately 50% of TNBC (Choi *et al*., 2023; Wang *et al*., 1998). Annunziato *et al*., (2019) reported *c-MYC* to drive the growth of *BRCA1*-deficient TNBCs by destabilising the genome, causing the loss of TSGs and amplification of oncogenes.

The suitability of *c-MYC* as a therapeutic target is demonstrated by the phenomenon of oncogene addiction, whereby cancers become dependent on a particular oncogene despite the accumulation of additional mutations that drive malignancy (Pagliarini *et al*., 2015). However, several characteristics of c-MYC make it difficult to target. The protein has an intrinsically disordered structure lacking motifs that can be targeted by typical small molecule drugs, and its nuclear location means therapeutics must cross both the cell and nuclear membranes to affect inhibition (Madden *et al*., 2021). Several small molecule drugs have nevertheless been developed that target *c-MYC* either indirectly by preventing its transcription and reducing protein stability, and directly by inhibiting MYC/MAX dimerization or transcription (Chen *et al*., 2018; Massó-Vallés & Soucek, 2020; Poole *et al*., 2018). The difficulties faced in developing c-MYC inhibitors has driven research into inhibitors of *c-MYC* gene activity. Similar to TNF-α, this may be achieved using RNAi techniques.

2.4. RNA interference

RNAi is a sequence-specific gene silencing process in eukaryotes that regulates gene expression at the post-transcriptional level (Kim & Rossi, 2008). Its discovery followed observations of gene silencing in eukaryotes induced by gene and antisense ssRNA transfection. Early experiments in plants, insects, and fungi, for example, reported knockdown following transfection with both sense and antisense genes (Napoli *et al*., 1990; Pal-Bhadra *et al*., 1997; Romano & Macino, 1992; Rothstein *et al*., 1987). This phenomenon was exploited to study gene function in the nematode *Caenorhabditis elegans* by transfecting embryos with antisense ssRNA, which was thought to bind its complementary mRNA and prevent translation (Lin *et al*., 1995; Powell-Coffman *et al*., 1996; Rao & Sockanathan, 2005). However, studies also reported the puzzling observation that sense RNA could similarly induce gene silencing (Guo & Kemphues, 1995; Lin *et al*., 1995). This phenomenon was termed RNA interference by Rocheleau *et al*., (1997), to differentiate it from antisense RNA-induced silencing. These observations were explained by Fire *et al*., (1998), who suggested that the ssRNA used for knockdown might contain small amounts of dsRNA due to the infidelity of the bacteriophage RNA polymerases used to produce the ssRNA. They further showed that dsRNA induced greater silencing of the *unc-22* gene in *C. elegans* than either sense or antisense strand,

identifying dsRNA as the trigger for RNAi. Later studies identified the RNAi machinery and elucidated its mechanism (Setten *et al*., 2019).

RNAi is mediated by several classes of small, non-coding dsRNAs produced from cleavage of longer dsRNA molecules. These include microRNAs (miRNA), small interfering RNAs (siRNA), and PIWI-interacting RNAs (piRNA). Of these molecules, siRNA have been widely investigated for cancer therapy. They are small molecules, ranging from 21-25 nt in length, with 2 nt overhangs at the 3'-hydroxyl ends and 5'-phosphates (Olina *et al*., 2018). For therapeutic use, siRNA are chemically synthesised to lengths between 15 and 30 nt, as dsRNA molecules smaller than 15 nt do not induce RNAi while those longer than 30 nt trigger an immune response (Alshaer *et al*., 2021; Sajid *et al*., 2020). Conventional siRNA range from 21 to 23 nt (including the overhangs), with the antisense strand, or guide strand, bearing complementarity to the target mRNA (Figure 2.12); however, longer siRNA of 25-30 nt have been observed to show greater efficiency (Kim *et al*., 2005; Lam *et al*., 2015).

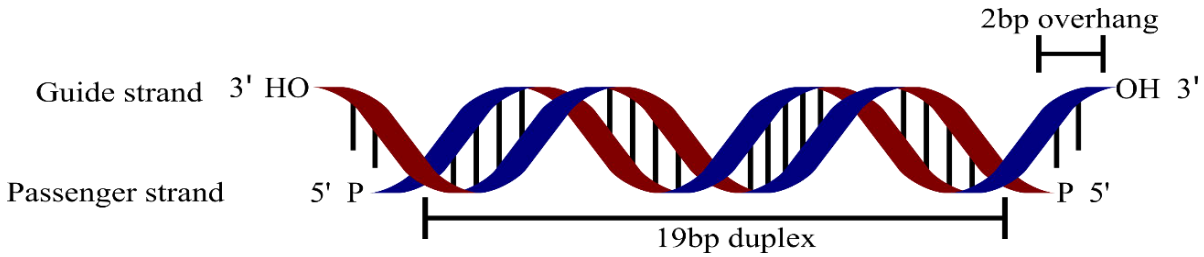

Figure 2.12: Schematic representation of a typical 21 nt siRNA molecule, consisting of a 19bp duplex region and 2bp 3'-OH overhangs. The antisense strand (3' > 5') acts as the guide sequence.

2.4.1. Mechanism of siRNA

RNAi-induced gene silencing is mediated by a multiprotein complex called the RNA-induced silencing complex (RISC). The core of the RISC consists of the endonuclease Argonaute-2 (Ago-2), which is directed by the guide strand of the siRNA to cleave complementary mRNA. Ago-2 consists of four domains: the N-terminal (N), PAZ, MID, and PIWI domains. PAZ and MID mediate binding to the 3' and 5' ends of the guide strand of the siRNA, respectively; the N domain mediates siRNA unwinding and target binding; and PIWI domain cleaves RNA (Kwak & Tomari, 2012; Müller *et al*., 2020). Multiple additional proteins and chaperone proteins have been reported to be involved in RISC assembly; however, the complete makeup

of the mammalian RISC remains unknown (Naruse *et al*., 2018; Yi, 2018). The RISC is assembled and activated in a two-stage process (Figure 2.13).

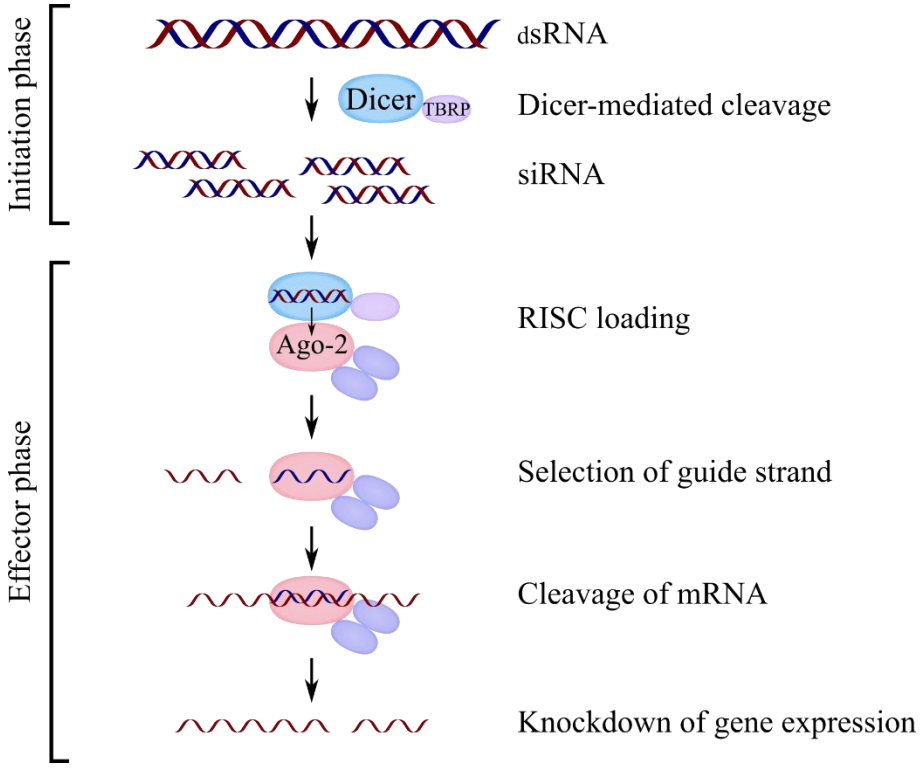

Figure 2.13: The siRNA-mediated RNAi process, leading to sequence-specific degradation of complementary mRNA.

In the initiation phase, foreign or endogenous dsRNA molecules are cleaved into smaller siRNA by the RNase III enzyme dicer (Olina *et al*., 2018; Smalheiser, 2012). Mammalian genomes encode one dicer isoform, which processes dsRNA into approximately 20-23 nt siRNA (Svobodova *et al*., 2016). Following cleavage, the siRNA are released and subsequently rebound by the helicase domain of dicer (Noland *et al*., 2011). Dicer is aided by the trans-activation response RNA-binding protein (TRBP), which enhances dsRNA cleavage and facilitates sensing of the asymmetry of the siRNA molecule (Chakravarthy *et al*., 2010; Lee *et al*., 2013; Noland *et al*., 2011). This allows dicer to select the most appropriate siRNA to load into the RISC in phase two. Conventional chemically synthesised siRNA bypass this cleavage process, but may still be bound by the dicer helicase domain (Noland *et al*., 2011; Sakurai *et al*., 2011). Longer 25-30 nt siRNA, however, still require processing by dicer into smaller molecules before entering the second phase (Kim *et al*., 2005; Lam *et al*., 2015).

The effector phase involves assembly of the RISC and knockdown of gene expression. The first step in RISC assembly is mediated by TRBP, which recruits Ago-2 to the dicer-siRNA complex to form the RISC-loading complex (RLC) and mediates transfer of the siRNA from dicer to Ago-2 (Chendrimada *et al*., 2005; Wang *et al*., 2009). The guide strand is then selected to direct knockdown. This selection process relies on the asymmetry of the siRNA molecule: the strand with the less thermodynamically stable 5' end is chosen, and the complementary passenger strand is cleaved by Ago-2 (Matranga *et al*., 2005). The siRNA duplex is subsequently unwound by the Ago-2 N-terminal and the passenger strand is discarded (Kwak & Tomari, 2012). The activated RISC is thus formed and is directed to the complementary target mRNA by the guide strand. Ago-2 then cleaves the mRNA between the 10^{th} and 11^{th} nucleotide from the 5' end, preventing translation and silencing gene expression.

2.4.2. RNAi-mediated knockdown of *TNF-α* and *c-MYC*

TNF-α has been targeted for knockout using siRNA, miRNA, and short hairpin RNA (shRNA), an artificial RNA molecule with a hairpin structure that also mediates RNAi. Knockout has allowed for both investigations into its role in physiological processes, such as sleep regulation (Taishi *et al*., 2007); and investigations of its potential as a therapeutic target in various diseases and disorders in which inflammation plays a key role. These include rheumatoid arthritis (Lee *et al*., 2014); pain (Ogawa *et al*., 2014; Wang *et al*., 2015); chronic obstructive pulmonary disease (Lokras *et al.*, 2021); and some cancers, such as oral squamous cell carcinoma (Iulia Irimie *et al*., 2015) and TNBC.

RNAi-mediated *TNF-α* knockdown in TNBC cell lines has been shown to inhibit growth and promote chemosensitivity. Pileczki *et al*., (2012) reported siRNA-mediated knockdown in Hs578T to inhibit cell growth and induce apoptosis. *TNF-α* knockdown has also been reported to synergise with knockdown of mutant p53 in Hs578T (Pileczki *et al.*, 2016). shRNA knockdown of tmTNF-α in MDA-MB-231 has been observed to inhibit cell growth and spread, and restore chemosensitivity to doxorubicin (Zhang *et al*., 2018c). Studies have also targeted dysregulated miRNA that normally function to regulate cytokine production. The miRNA miR-509 has been suggested to indirectly regulate TNF-α secretion by Hs578T and MDA-MB-231 cells, and has been reported to be downregulated in BC, particularly in TNBC and in brain metastases (Xing *et al*., 2015; Zhang *et al*., 2016a). Overexpression of miR-509 was observed to suppress TNF-α secretion, thus reducing the incidence of brain metastases in *in vivo* models.

The prevalence of *c-MYC* dysregulation in BC has also made it a popular target for RNAi therapies targeting both HR+ and TNBC. *c-MYC* knockdown has been shown to inhibit cancer cell growth and motility, and sensitise cells to cell death processes. Studies have indirectly targeted *c-MYC* by inhibiting upstream and downstream factors regulating *c-MYC* expression (Liu *et al*., 2014; Zhang *et al*., 2021a). Direct knockdown using siRNA and shRNA has also been reported *in vitro* in MCF-7 and MDA-MB-231 cell lines and in *in vivo* BC models (Daniels & Singh, 2019; Imani *et al*., 2018; Li *et al*., 2017b; Tangudu *et al*., 2015; Yang *et al*., 2016). Initial studies by Wang *et al*., (2005) reported *c-MYC* knockdown to inhibit the growth of HR+ MCF-7 cells and BC tumours *in vivo*. Treated cells further showed reduced transforming abilities, as evidence by their reduced colony-forming abilities in a soft agar assay, and increased sensitivity to apoptosis in response to nutrient depletion. Habib *et al.*, (2021) observed knockdown to reduce MCF-7 cell viability through apoptosis induction and inhibit cell motility in a wound healing assay. Dual delivery of anti-*c-MYC* and anti-*STAT3* siRNA has also been shown to reduce the colony-forming abilities of MDA-MB-231 cells (Bjorge *et al*., 2017).

2.4.3. Challenges to siRNA therapy

2.4.3.1. Off-target effects

siRNA were initially thought to be highly specific; however, they may induce off-target effects that reduce silencing efficiency and cause unwanted toxicity. siRNA can tolerate mismatches (Angart *et al.*, 2013); or bind unintended targets through the miRNA-like effect, where the seed region mediates binding to the 3' untranslated region (UTR) of unintended mRNA, similar to the targeting mechanism utilised by miRNA (Figure 2.14) (Jackson *et al*., 2006; Kamola *et al*., 2015). This effect notably allows siRNA to silence multiple genes, as the seed sequence is not specific (Québatte & Dehio, 2017). High concentrations of exogenous siRNA, which saturate the RNAi machinery, may also induce off-target effects by interfering with cellular gene regulation by endogenous miRNA (Grimm, 2011).

Off-target activity may be reduced through chemical modification of the seed sequence to destabilise seed-mediated binding; by lowering siRNA concentration; or by pooling multiple siRNA that target different regions of the same mRNA but individually display different off-

targets. This dilutes the off-target effects of the individual siRNA without interfering with on-target activity (Lam *et al*., 2015; Neumeier & Meister, 2021).

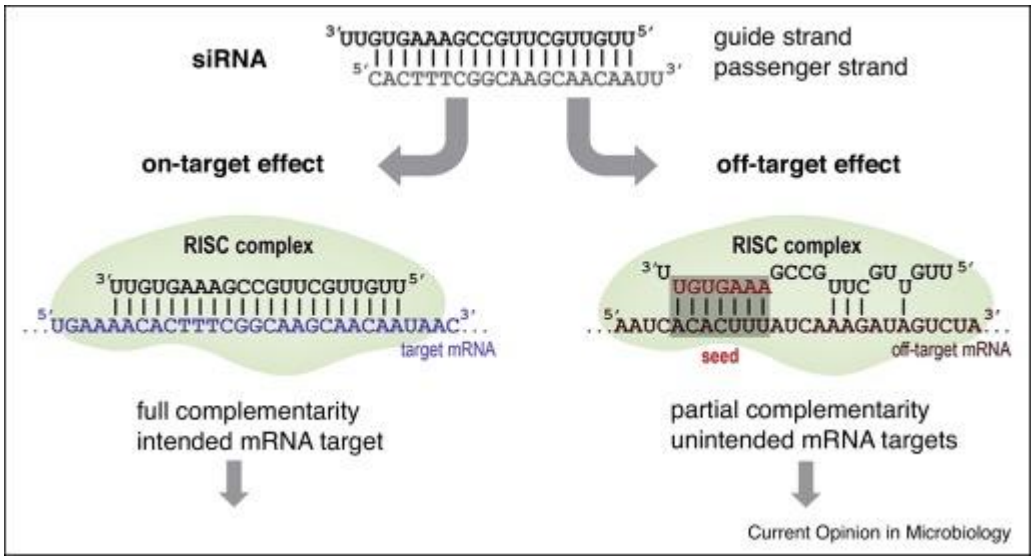

Figure 2.14: siRNA may induce on- or off-target effects. On-target effects result from complete binding of the guide strand to the complementary target mRNA. Off-target effects are most often mediated by the miRNA-like effect, where the seed sequence at the 5' end of the siRNA binds to the 3' UTR of unintended mRNA (Québatte and Dehio, 2017).

2.4.3.2. Barriers to siRNA delivery

The therapeutic efficacy of siRNA is dependent on its ability to reach the cytoplasm of the target cells with minimal biodegradation. However, systemic and local delivery of siRNA faces several challenges. Naked siRNA is highly susceptible to nuclease degradation and clearance by the mononuclear phagocytic system (MPS), and its small size predisposes it to removal by the kidneys (Sajid *et al*., 2020). siRNA has thus been observed to display a very short half-life in systemic circulation, ranging from minutes to half an hour (Huang *et al*., 2016). siRNA may also induce an immune response by activating toll-like receptors in a sequence-specific manner, or by stimulating cytoplasmic RNA sensor proteins that normally protect cells from viral RNA invasion (Meng & Lu, 2017). Cellular uptake is further inhibited by the large molecular weight, and anionic and hydrophilic nature of the oligonucleotide; and the inability of siRNA to escape the endosome into the cytoplasm where it mediates gene silencing (Tambe *et al*., 2016).

Some of these challenges, such as siRNA's poor stability in circulation and immune induction, may be reduced through chemical modification of the siRNA molecule. Chemically-modified siRNA may still, however, face difficulties remaining in circulation (Sarisozen *et al*., 2015). Alternatively, siRNA may be conjugated with delivery vectors, which protection from degradation, extend circulation time, and enhance cellular uptake.

2.5. Vectors for siRNA delivery

The ideal vector for siRNA delivery should be able to overcome the barriers to transfection faced by naked siRNA i.e., they should be able to evade circulating serum nucleases and MPS cells; avoid renal clearance; promote cellular uptake by the target cells; and enhance endosomal escape. They should also be non-toxic, biodegradable to prevent toxic accumulation, and non-immunogenic (Singh *et al*., 2018a). Vectors used for siRNA delivery are broadly categorised as viral and non-viral. Viral vectors show efficient transfection but are limited by their potential toxicity. Much research has thus focussed on developing non-viral vectors for efficient and safe siRNA delivery.

2.5.1. Viral vectors

Viral vectors have had their pathogenic genes removed, and retain only the genes required for cell entry and transgene expression (Lentz *et al*., 2012). Among the most commonly used viral vectors are those developed using adenoviruses; adeno-associated viruses (AAVs); retroviruses; and lentiviruses, a subclass of retrovirus. Their properties are shown in Table 2.4 (Herrera-Carrillo *et al*., 2017; Marquez *et al*., 2018; Ricobaraza *et al*., 2020).

Table 2.4: Characteristics of commonly used viral vectors for siRNA delivery.

	Adenoviruses	**AAV**	**Retroviruses**	**Lentiviruses**
Genome	dsRNA	ssDNA	ssRNA	ssRNA
Packaging capacity	Max 37 kbp in "gutless" vectors with all viral genes removed	4.7 kbp	8 kbp	8 kbp
Applicable cell types	Dividing and non-dividing cells	Dividing and non-dividing cells	Dividing cells only	Dividing and non-dividing cells
Advantages	High transfection efficiency; low risk of integration	Low pathogenicity	Low immunogenicity	Modifiable tropism; low immunogenicity
Drawbacks	Highly immunogenic	Difficult production; helper virus required for replication	Risk of insertional mutagenesis	Risk of insertional mutagenesis

2.5.2. Non-viral vectors

2.5.2.1. Lipid nanoparticles

Lipid-based systems facilitate delivery of hydrophobic, hydrophilic, and lipophilic drugs, and allow for controlled and sustained drug release (Ghasemiyeh & Mohammadi-Samani, 2018).

The lipid components are biocompatible and biodegradable, and can be easily modified to display stabilising and targeting compounds (García-Pinel *et al*., 2019). These advantageous characteristics have led to their extensive use as delivery vectors.

Liposomes are currently the most widely studied lipid NPs. Conventional liposomes are composed of membrane phospholipids with hydrophobic fatty acid tails bonded to a hydrophilic phosphate-containing head group; however, their neutral charge inhibits interactions with charged compounds (Barba *et al*., 2019). The inclusion of cationic lipids with amine-containing head groups promotes interactions with negative cell membrane components and drugs (Zhi *et al*., 2013). Helper lipids such as cholesterol are also included to improve stability (Cheng & Lee, 2016).

2.5.2.2. Polymeric nanoparticles

Cationic polymers have seen extensive use as vectors on their own and as coatings on inorganic nanoparticles to confer a positive charge that promotes nucleic acid binding and cellular uptake. These polymers bear positive charges due to the presence of primary, secondary, tertiary and/or quarternary amines in their structure (Eliyahu *et al*., 2005). Polymeric nanoparticles can be cheaply synthesised and easily scaled up for industrial production, although some polymers are limited by a low transfection efficiency and/or high cytotoxicity (Shi *et al*., 2017). Cationic polymers used for gene delivery are broadly categorised as natural or synthetic. The most popular synthetic polymer, polyethyleneimine (PEI), displays a high transfection efficiency and charge density (Hajifathaliha *et al*., 2020). Unmodified PEI is, however, limited by its cytotoxicity, as it is non-biodegradable and the high charge density disrupts cell membranes (Taranejoo *et al*., 2016).

Many natural polymers, such as polysaccharides and polypeptides, are biodegradable and biocompatible. However, they are limited by their potential immunogenicity and variable synthesis, as it may be difficult to achieve consistent breakdown of compounds to produce uniform batches (Chocholata *et al*., 2019; Raveendran *et al*., 2017). The most widely used natural polymer, chitosan (CS), is non-toxic, non-immunogenic, and biodegradable by chitonase enzymes (Mukhopadhyay *et al*., 2015). It is composed of repeating N-acetyl-D-glucosamine and D-glucosamine units linked by β-(1-4)-glycosidic bonds, obtained through deacetylation of chitin. The primary amine groups of the D-glucosamine units are protonated at weakly acidic and neutral pH, giving CS a positive charge that facilitates complex formation

(Dadou *et al*., 2017). While CS is popular, its use is limited by its low transfection efficiency and low charge density at physiological pH, which reduces stability and promotes aggregation (Sami El-banna *et al*., 2019).

2.5.2.3. Gold nanoparticles

Gold nanoparticles (AuNP) display many unique optical and physiochemical properties that facilitate their use as imaging agents, biosensors, and vectors. Among their attractive properties are their small size, and facile synthesis and functionalisation. Their highly tunable synthesis allows for modification of NP size and shape to optimise characteristics for therapy. Moreover, the ability of gold nanomaterials to convert absorbed light energy into heat following irradiation with near infrared light, leading to thermal ablation of surrounding tumour tissue, permits their use as photothermal therapy agents (Moon *et al*., 2018). AuNP of varying shapes and sizes have shown potential for cancer therapy.

Spherical gold nanoparticles (AuNP) are among the most popular NP for gene and drug delivery. Their unique optical properties include their localised surface plasmon resonance (LSPR), the phenomenon where free electrons on the NP surface collectively oscillate in response to light exposure. The electrons absorb and scatter light energy, facilitating the use of AuNP as imaging agents (Singh *et al*., 2018b). AuNP are most commonly synthesised using the citrate reduction method, in which chloroauric acid ($HAuCl_4$) is reduced by trisodium citrate, to produce citrate-capped AuNP of 10–20 nm in diameter and with a net negative charge (Elahi *et al*., 2018; Turkevich *et al*., 1951). This method can be easily modified by varying the ratios of reagents to produce AuNP of 15 - 150 nm in diameter (Frens, 1973).

2.6. Gold nanoclusters

Nanoparticles are generally defined as having a core diameter of greater than 3 nm, with particles smaller than 3 nm termed nanoclusters (Yau *et al*., 2013). These ultrasmall NP are composed of only a few to hundreds of atoms. This small size imparts them with characteristics unique from conventional metal NPs; most notably, NC display unique optical properties, such as strong photoluminescence, that facilitate their use as imaging agents (Kaur *et al*., 2018). Compared to conventional fluorophores such as dyes and quantum dots containing heavy metals, NC display good photostability, resistance to photobleaching, low toxicity, tunable emission wavelengths, and a large Stokes shift reducing crosstalk between the emission and

excitation wavelengths (Gao *et al*., 2017; Li *et al*., 2017a; Yang *et al*., 2020). A variety of metals have been used to synthesise NC, including noble and transition metals. Gold nanoclusters (AuNC) are among the most widely studied.

2.6.1. Optical characteristics of AuNC

AuNC are differentiated from AuNP by their lack of LSPR and strong fluorescence, and have thus been widely studied as sensors and cellular imaging agents (Liu *et al*., 2010; Selvaprakash & Chen, 2014; Zhang *et al*., 2015a, 2013). These different optical properties result from differences in their electronic structures, and have been explained using the free electron model (Figure 2.15). This model states that the valence electrons in metals are delocalised and can move freely due to inner electrons shielding their interaction with the nucleus (Zheng *et al*., 2007). The LSPR effect is strongly dependent on NP size and free electron density (Nan *et al*., 2018). AuNP contain a high density of electrons, leading to the overlap of the valence band, containing the outermost electrons, with the conduction band, the empty energy band into which electrons move when they are excited (Figure 2.15A). As a result, the free valence electrons are able to occupy the conduction band, and collectively oscillate in response to light energy to produce the LSPR effect (Zhang & Wang, 2014). These optical properties disappear as NP size decreases to approximately 2 nm – the critical size at which AuNP become AuNC and begin to display molecular-like properties (Jin, 2010). At this small size and atom number, AuNC display fewer free electrons and an electronic structure similar to that of atoms, where electrons are confined to discrete energy levels rather than occupying a continuous band of energy levels as for NP (Figure 2.15B) (Huang *et al*., 2018; Zheng *et al*., 2004). The free electrons in AuNC are thus unable to collectively oscillate to produce LSPR (Díez & Ras, 2010). Fluorescence instead results from the movement of single electrons from the highest occupied molecular orbital (HOMO) to the lowest unoccupied molecular orbital (LUMO) – called the HOMO-LUMO transition (Huang *et al*., 2018; Qian *et al*., 2012).

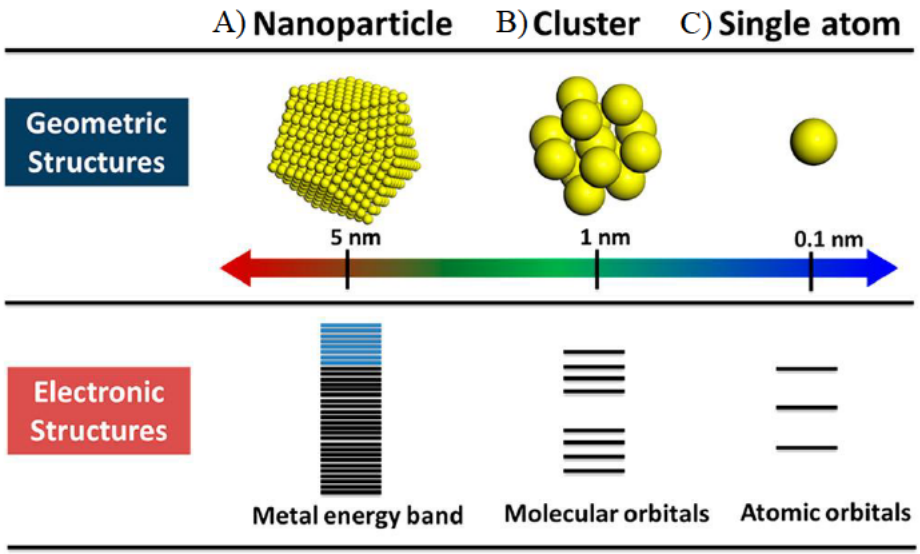

Figure 2.15: NCs display a similar electronic structure to atoms. (A) The energy band structure of AuNP is continuous, as the high density of atoms leads to overlap of the valence and conduction bands. (B) AuNC display quantum confinement effects, where electrons are confined to discrete bands – a similar electronic structure to that of atoms (C) (Liu & Corma, 2018).

The optical properties of AuNC are highly dependent on the cluster size and capping ligand. Alteration of these factors allows for the synthesis of AuNC that emit light at various wavelengths in the visible and near-infrared regions upon excitation. Size-dependent fluorescence, shown in Figure 2.16A, has been explained using the spherical jellium model, which describes the movement of free electrons around atomic clusters. The model predicts that the transition energy required for an electron to move between energy levels decreases as cluster size increases; thus, larger NC cluster sizes emit less light energy and longer wavelengths than smaller NCs (Kawasaki *et al*., 2011; Zheng *et al*., 2004). The importance of the ligand in promoting fluorescence has been shown by Londoño-Larrea *et al*., (2017), who observed that addition of various ligands to non-luminescent naked AuNC produced luminescence. Multiple studies have also reported differing emission wavelengths or intensities for AuNC synthesised with different capping agents or ratios of capping agent (Lin *et al*., 2010, 2018; Liu *et al*., 2013a, 2016) (Figure 2.16B). Wu and Jin, (2010) found that the presence of electron rich atoms or groups, such as COOH or NH_2, in ligands can enhance fluorescence, as these groups can donate delocalised electrons to the metal core either directly or via gold-sulphur bonds - a phenomenon termed ligand-to-metal charge transfer or ligand-to-metal−metal charge transfer, which includes interactions between Au atoms. Encapsulation of AuNC by bulky or large compounds may also enhance fluorescence intensity by restricting the movement of capping ligands and preventing excited electrons from returning to the ground

state by non-radioactive decay, which releases less energy than radioactive decay (Goswami *et al.*, 2016; Pyo *et al.*, 2015).

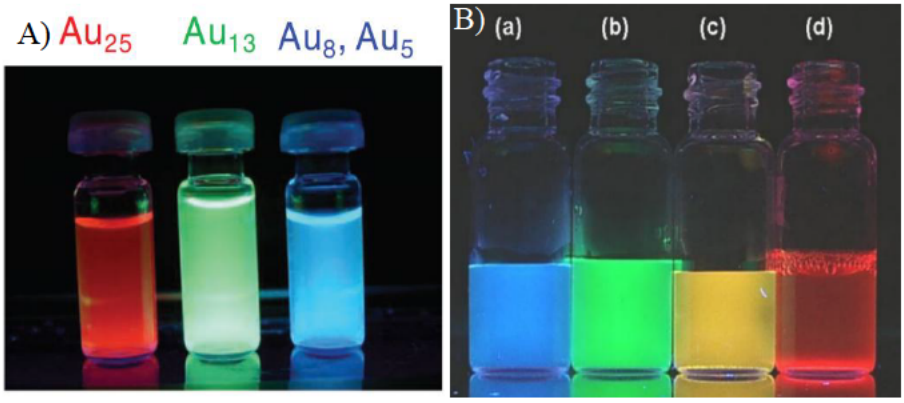

Figure 2.16: AuNC fluorescence is dependent on the (A) size and (B) ligand. A) Smaller AuNC clusters emit shorter wavelengths of light, as shown by pepsin-Au_{25}, Au_{13}, and Au_8 and Au_5 clusters emitting red, green, and blue light, respectively (Kawasaki *et al.*, 2011); B) Different emissions by AuNC coated with a) PEI, b) and c) mercaptoundecanoic acid, and d) dihydrogen lipoic acid (Lin *et al.*, 2010).

2.6.2. Synthesis of AuNC

The dependence of AuNC luminescence on the ligand and core size necessitates highly controlled synthesis procedures. Synthesis methods can be broadly grouped into top-down methods, which decompose AuNP into AuNC, and bottom-up methods, which reduce gold ions through various mechanisms to produce AuNC (Zheng *et al.*, 2017). In addition to strongly influencing luminescence, capping ligands are required to stabilise AuNC and prevent aggregation into AuNP (Zheng *et al.*, 2017). Compounds containing thiol, amine, or carboxyl functional groups, or nucleotides are often used due to their ability to bind gold (Bano *et al.*, 2015; Halawa *et al.*, 2018; Kennedy *et al.*, 2012).

Both large ligands, such as proteins and polymers that act as templates for AuNC formation, and small molecules, such as peptides that form monolayers coating the AuNC surface, have been used. Thiol-containing compounds are popular capping ligands due to the strong bond formed between sulphur and gold, and thiol-AuNC are often denoted Au_nSR_m, where n and m represent the number of gold atoms and thiol ligands, respectively (Jin, 2010). The reduced form of glutathione (GSH), a tripeptide antioxidant naturally present in the cytoplasm, is commonly used to produce biocompatible and easily-functionalised AuNC (Ding *et al.*, 2014). GSH monolayer coatings are thought to control AuNC size during synthesis, as the bulky nature of the ligand prevents the core size from becoming too large, and protect AuNC from serum protein adsorption and clearance by the liver (Schaaff *et al.*, 1998; Zhou *et al.*, 2011).

2.6.2.1. Bottom-up methods

Bottom-up methods involve reduction of Au(III) ions in chloroauric acid ($HAuCl_4$) to Au(0) in the presence of a capping ligands. Reduction of $HAuCl_4$ has been achieved through irradiation with UV light (Li *et al*., 2013; Zhang *et al*., 2012a); treatment with electric currents (Santiago González *et al*., 2010); and *in vivo* in cancer cells (Wang *et al*., 2013). However, methods which utilise chemical reducing agents are the most common. Chemicals such as sodium borohydride ($NaBH_4$) or citrate are often used; however, green methods which do not require additional reducing agents have been developed.

Early methods for the synthesis of thiol-protected AuNC utilised reducing agents such as $NaBH_4$ and modified the Brust-Schiffrin method originally developed for AuNP synthesis (Halawa *et al*., 2018; Jin, 2010). The original two-phase system uses phase-exchange agents to transfer $AuCl_4^-$ from aqueous $HAuCl_4$ to an organic solvent, where the Au(III) ions are initially reduced by thiols to form Au(I)-thiolate complexes that are subsequently reduced by $NaBH_4$ to Au(0) (Booth *et al*., 2017; Chen *et al*., 2020). However, these AuNC displayed low quantum yields (QY) – a measure of how efficiently absorbed light is emitted - due to the presence of poorly luminescent short Au(I)-thiolate motifs on the AuNC surface (Luo *et al*., 2012).

To overcome the issue of poor luminescence, Luo *et al*., (2012) exploited the phenomenon of Aggregation Induced Emission (AIE), where non-luminescent Au(I)-thiolate complexes become luminescent upon aggregation. Using GSH as both the reducing and capping agent, AuNC with a core-shell Au(0)@Au(I)−thiolate structure were synthesised. AuNC synthesis was proposed to occur in three stages. Initially, Au(III) ions are reduced to Au(I) by GSH. These Au(I) may then react with the thiol group in GSH to form Au(I)-thiolate complexes or may form non-thiolate complexes through interactions with the carboxyl group of GSH or Cl^- ions. In the second stage, heating of the solution to 70 °C selectively reduces Au(I)-non-thiolate complexes to Au(0), which bind Au(I)-thiolate complexes. The resulting Au(0)-on-Au(I)-thiolate complexes finally undergo controlled aggregation to form Au(0)@Au(I)−thiolate NC composed of an Au(0) core capped with shell of highly luminescent Au(I)-thiolate oligomers. In contrast to earlier methods, the AIE method is eco-friendly, requires no additional reducing agents, and produces biocompatible AuNCs with a relatively high QY, facilitating their use as probes (Figure 2.17) (Luo *et al*., 2012).

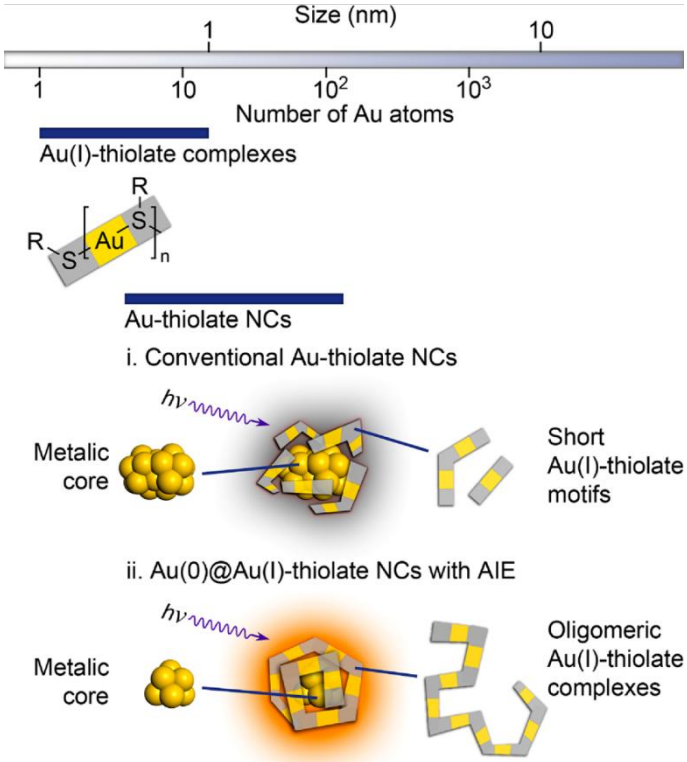

Figure 2.17: Comparison of the structures of conventional AuNC and Au(0)Au(I)-thiolate AuNC. Conventional AuNC, which display poor QY, are coated with short Au(I)-thiolate complexes, while highly-luminescent Au(0)Au(I)-thiolate AuNC are coated with longer Au(I)-thiolate complexes (Luo *et al*., 2012).

2.6.2.2. Top-down methods

Top-down methods include chemical etching, which uses excess ligand to reduce the size of larger AuNP into AuNC by removing gold atoms from the NP core. Various ligands have shown use as etchants, including thiol-containing compounds (Muhammed *et al*., 2008, 2010); and polymers (Duan & Nie, 2007). Muhammed *et al*., (2008) proposed two possible mechanisms for the etching process following etching of mercaptosuccinic acid-capped AuNP with GSH to produce AuNC. The GSH was suggested to interact with surface gold atoms to form Au(I)-thiolate complexes, thus reducing the size of the AuNP into AuNC. Alternatively, the Au(I)-thiolate complexes may interact with each other to form AuNC.

2.6.3. Cytotoxicity and clearance of AuNC

NP vectors should ideally display low toxicity and efficient clearance from the body. Gold is inert and gold nanomaterials are thus generally considered to be biocompatible. However, contradictory results have been obtained regarding their safety. As with the luminescence

abilities, the potential adverse effects of AuNC administration have been observed to be influenced by their core size and capping ligand.

AuNC coated with bovine serum albumin (BSA), GSH, and various other peptides and polymers have been widely reported to be non-toxic in both cancerous and normal cell lines (Duan *et al*., 2018; Escudero-Francos *et al*., 2017; Li *et al*., 2018b; Tay *et al*., 2014; Zhao *et al*., 2014). However, size-dependent cytotoxicity has been reported by Pan *et al*., (2007) and Tsoli *et al*., (2005), who observed cytotoxicity of 1.4 nm AuNC due to their ability to bind the major groove of DNA. BSA- and GSH-AuNC have been reported to induce adverse immune responses, and kidney and liver damage *in vivo* in mice; however, this damage was recoverable for mice treated with GSH-AuNC (Zhang *et al*., 2012b). Several studies have also reported that AuNC can induce ROS generation, although conflicting results have been obtained regarding the toxicity of the increased ROS. Tay *et al*., (2014) suggested that increased ROS in non-cancerous colon NCM460 cells following treatment with mercaptopropionic acid (MPA)-capped AuNC promoted proliferation by upregulating growth promoting pathways. In contrast, AuNC-induced ROS generation has been reported to induce dose- and time-dependent toxicity in normal and cancer cell lines (Dong *et al*., 2015; Yang *et al*., 2014b; Zhao *et al*., 2014). These contradictory results may result from differences in cell types, AuNC characteristics, and study design and dosage.

NP clearance from circulation is mediated by the kidneys, which removes those smaller than <5 nm, and the liver and spleen, which clears larger particles (Blanco *et al*., 2015). However, this is not always observed experimentally. BSA- and TPPMS-AuNC, for example, have been found to accumulate primarily in the liver; while GSH- and tiopronin-AuNC are primarily taken up by the kidneys (Escudero-Francos *et al*., 2017; Huo *et al*., 2017; Semmler-Behnke *et al*., 2008; Zhang *et al*., 2012b). These differences may result from ligand-specific interactions with the organs, or differences in plasma stability: GSH has been suggested to resist protein interactions, and GSH-AuNC may thus be more protected against aggregation induced by opsonisation (Zhou *et al.*, 2011). However, the long-term toxicity of GSH-AuNC may still be of concern despite their renal clearance. Zhang *et al*., (2015b) reported efficient renal clearance of GSH-AuNC within 30 days in mice; however, AuNC were observed to be stored and slowly released by muscle tissue, leading to a resurgence of AuNC in the blood that induced slight toxicity.

2.6.4. AuNC as nucleic acid delivery agents

The delivery of nucleic acids requires the vector to bear a net positive charge, which facilitates interactions with anionic phosphate groups on the nucleic acid backbone. This may be achieved by synthesising AuNC with cationic ligands. For example, AuNC capped with the positive oligopeptides have been shown capable of assembling with DNA and RNA (Wang *et al*., 2019); and of delivering siRNA for the knockdown of nerve growth factors in pancreatic cancer (Lei *et al*., 2017). Plasmid delivery has also been achieved using AuNC synthesised using PEI (Tao *et al.,* 2013); and PEI functionalised with sulfhydryl groups (PEI-SH) that allow for binding to the AuNC (Sun *et al*., 2018). Alternatively, AuNC may be synthesised with anionic capping agents, such as GSH, and thereafter coated with cationic polymers to facilitate their use as vectors.

2.7. Overcoming barriers to transfection

Vectors face several barriers to transfection following systemic administration. These include, removal from circulation by the MPS, degradation by circulating nucleases, efficient uptake by the target cells, and escape from the endosome. Viral vectors display high transfection efficiencies in part because they have evolved mechanisms of overcoming these barriers. Non-viral vectors are unable to overcome these barriers themselves as viral vectors can, and thus require functionalisation with various ligands that aid in circumventing them.

2.7.1. Avoiding removal from circulation

To increase their uptake by the target tissue and ensure therapeutically active concentrations, NC vectors should ideally display a long circulation half-life (Jokerst *et al*., 2011; Prencipe *et al*., 2009). However, while in the bloodstream, NC face removal by the MPS and conditions that may destabilise them. Circulating nucleases and proteases can degrade the therapeutic payload, and serum components, including proteins and other biomolecules such as lipids, may interact with the NC surface to form a coating called the corona (Corbo *et al*., 2016). A large portion of the corona is composed of plasma proteins called opsonins, including complement proteins, immunoglobins, and coagulation factors, that facilitate recognition and phagocytosis by macrophages (Figure 2.18) (Zanganeh *et al*., 2016). This process – called opsonisation – is vital for recognising and removing pathogens from the bloodstream; however, it may also significantly reduce the circulation times of vectors. NP with cationic or hydrophobic surfaces

have been observed to interact strongly with opsonins, leading to rapid elimination from circulation (Furtado *et al*., 2018; Ogawara *et al*., 2001).

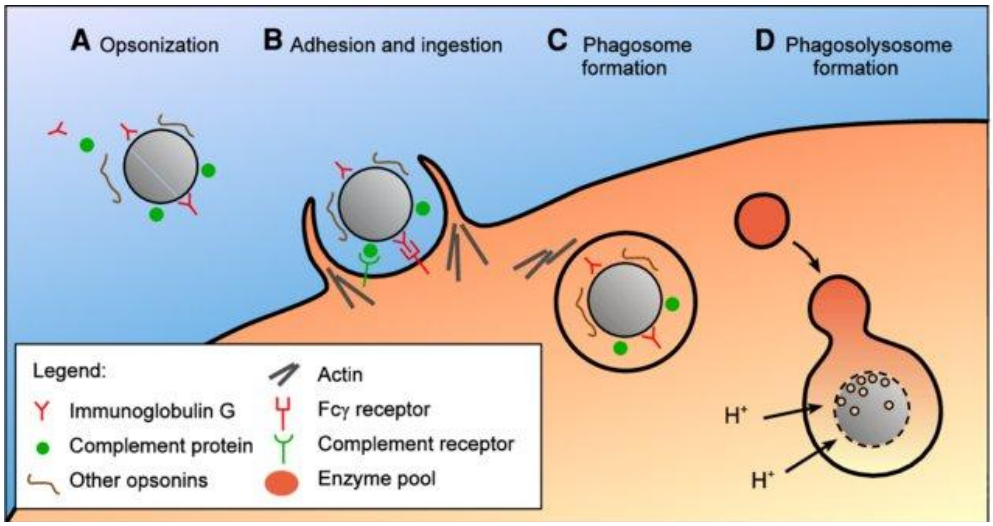

Figure 2.18: The process of opsonisation, which leads to phagocytosis of the vector (Hillaireau & Couvreur, 2009)

In addition to opsonisation, vectors may also aggregate due to protein adsorption or reduced stability in the bloodstream, leading to their removal from circulation. The stability of charged NP is dependent on electrostatic repulsion mediated by the EDL, which prevent attractive van der Waals (vdW) forces from inducing aggregation. However, in high ionic strength solutions such as blood, the EDL is neutralised, leading to increased vdW interactions and aggregation (Muraleetharan *et al*., 2019).

As-synthesised AuNC zwitterionic and GSH-AuNC have been reported to display low circulation half-lives, ranging from 1.2 to 6.5 min (Le Guével *et al*., 2018; Zhou *et al*., 2012). This may potentially be due to rapid uptake by tissue and efficient renal clearance rather than opsonisation, as the resistance of some AuNC, particularly GSH-AuNC, to serum protein adsorption has been reported (Porret *et al*., 2020; Zhou *et al*., 2011). Opsonisation and aggregation may, however, still present an issue to cationic polymer-encapsulated AuNC due to their larger size and attractive charge. For example, Duan *et al*., (2018) attributed the significant liver uptake of CS-AuNC to clearance by the MPS. The addition of poly(ethylene glycol) (PEG) polymers to the surface of vectors is the most common means of preventing opsonisation and aggregation, and improving circulation time.

2.7.1.1. PEGylation

PEG is a neutral, hydrophilic polymer composed of varying numbers of repeating ethylene glycol units. Several mechanisms have been proposed to explain PEG's ability to prevent opsonisation and aggregation. These include a reduction in the surface charge and hydrophobicity upon PEGylation, thus reducing the attraction between opsonins and the NP surface (Howard *et al.*, 2008). The long PEG chains may also sterically hinder NP-NP and NP-protein interactions, or trap water molecules to create a hydration layer that inhibits interactions (van Vlerken *et al*., 2007). The most widely-accepted theory states that the PEG chains assume an open and extended conformation in solution. When serum components attempt to bind the NP, they compress the PEG chains and force them into a higher energy conformation that repels the interaction (Jeon *et al*., 1991). By maintaining the stability of the vector during circulation, PEG prevents removal by the MPS and increases circulation time. For small AuNC, PEGylation may also increase circulation time by reducing renal clearance. This ultimately promotes tumour targeting via the enhanced permeability and retention (EPR) effect – where vectors accumulate in tumours due to their leaky vasculature. This principle has been shown by Liu *et al*., (2013b), who observed a significantly longer circulation half-life for PEG-AuNC (56.1 min) than GSH-AuNC (5.4 min), leading to a higher tumour-targeting efficiency.

Higher MW PEG chains with longer lengths have been observed to provide greater protection against opsonisation (Cui *et al*., 2015; Fang *et al*., 2006). Lower MW PEG chains with shorter lengths are effective at very high grafting densities (Yang *et al*., 2014a). PEG chains assume different conformations depending on the grafting density (Figure 2.19). At lower grafting densities, the chains display a "mushroom" conformation, as they have space to coil, while at higher grafting densities, a "brush" conformation is assumed where the PEG chains are unable to coil and instead extend outwards from the vector surface. Generally, higher densities with the brush conformation improve circulation times, as there is less space between the PEG chains for protein binding (Shalgunov *et al*., 2017; Yang *et al*., 2014a). However, the optimal grafting density may differ for different PEG MW and different serum proteins (Gref *et al*., 2000).

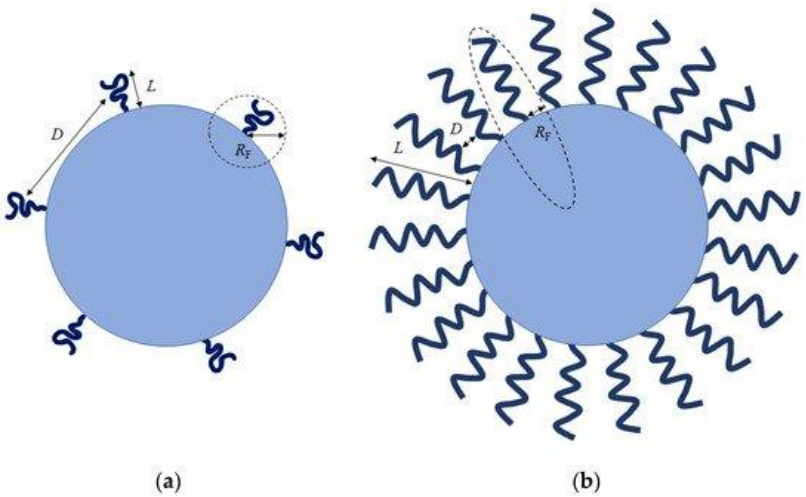

Figure 2.19: PEG assumes a (a) mushroom conformation at low grafting densities and (b) a brush conformation at high grafting densities (Fam *et al*., 2020).

While PEGylation can significantly improve circulation times, it has also been observed to reduce the efficiency of delivery (Mishra *et al*., 2004). This phenomenon is known as the PEG dilemma, where the features of PEG that prevent opsonisation and aggregation also reduce cellular uptake by inhibiting interactions with cell membranes and interfering with endosomal escape (Fang *et al*., 2017; Hatakeyama *et al*., 2013). Optimisation of the PEG grafting density and MW is thus required to ensure protection while also allowing efficient uptake. Moreover, studies have suggested that exposure to PEGylated NPs may lead to the generation of anti-PEG antibodies that may reduce the efficacy of PEGylated therapeutics, as they are recognised and cleared by the MPS (Moreno *et al*., 2019; Thi *et al*., 2020). Several strategies to overcome these issue have been investigated, such as acid-labile PEG polymers that are removed from the vector in the acidic TME, thus avoiding the PEG dilemma; and alternative natural and synthetic polymers with lower immunogenicity to avoid adverse immunogenic reactions (Fang *et al*., 2017; Thi *et al*., 2020). Nevertheless, PEG remains widely used as a steric stabiliser.

2.7.2. Cellular uptake

The physical characteristics of the NP, such as size, shape, surface charge, and capping ligand, influence interactions with the cell membrane and determine the mechanism of cellular uptake. The cell membrane is a phospholipid bilayer, which contains other lipids such as cholesterol in addition to phospholipids, and membrane proteins (Cooper, 2000). The external domains of some lipids and most proteins are modified through the addition of anionic oligosaccharides or glycans, forming glycolipids and glycoproteins (Cruz-Chu *et al*., 2014; Möckl, 2020). These

glycosylated regions, together with free glycans, form a negatively-charged carbohydrate coating around the bilayer called the glycocalyx (Möckl, 2020). Particles that cannot diffuse through the lipid bilayer may instead be taken up by various endocytic pathways, in which the membrane invaginates to form a vesicle called an endosome (Figure 2.20). The choice of pathway is dependent on both the vector's characteristics and the cell type.

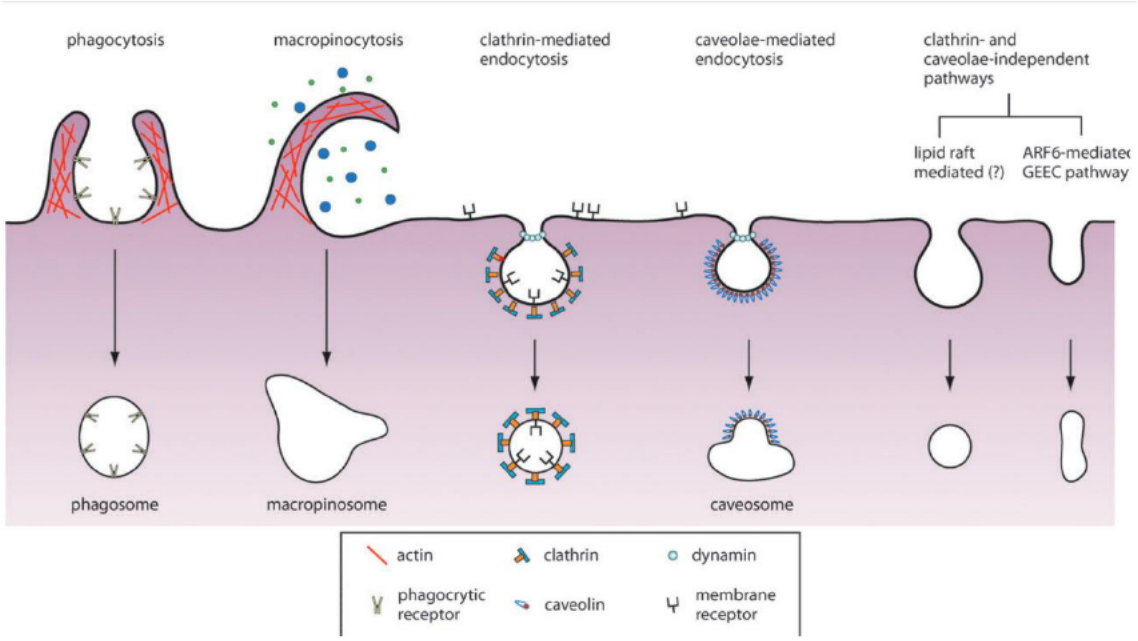

Figure 2.20: The various endocytic pathways facilitating entry into cells (Chou *et al.*, 2011).

The net surface charge of non-malignant cells is neutral or slightly positive due to the presence of zwitterionic phospholipids; however, cancer cells display a net negative charge due to enrichment with anionic phospholipids, increased glycosylation, and secretion of lactate anions produced by the malignant cells' abnormal metabolism (Chandra *et al.*, 2013; Kang *et al.*, 2018; Le *et al.*, 2019). NP with cationic surface charges thus generally show faster or increased uptake compared to anionic and neutral NP (Boyles *et al.*, 2015; Chen *et al.*, 2011; Ge *et al.*, 2009). In addition to their ability to strongly interact with anionic cell membranes, Fleischer and Payne, (2012) suggested that the uptake of cationic NP may be enhanced by binding of anionic serum proteins that facilitate uptake by receptor-mediated endocytosis. Anionic NP may interact with cationic domains within the membrane to facilitate uptake, or they may be functionalised with cationic polymers. GSH-AuNC encapsulated with the cationic polymers glycol chitosan and poly(allyl amine hydrochloride), for example, have shown increased uptake compared to the anionic uncoated GSH-AuNC (Yahia-Ammar *et al.*, 2016; Zhu *et al.*, 2019). However, the increased cellular uptake observed for cationic NP *in vitro* may not be observed *in vivo* due to the increased interaction of cationic NP with opsonins - Wang *et al.*, (2016)

observed increased tumour uptake of anionic AuNC compared to cationic AuNC *in vivo*, which was attributed opsonisation of the cationic AuNC.

2.7.3. Endosomal escape

Following uptake by endocytosis, endosomes fuse with the early endosome and undergo a complex sorting process in which they may either be recycled back to the membrane or degraded in the endosomal-lysosomal pathway. In this pathway, contents are transported in endosomal carrier vesicles to the late endosome, which fuses with lysosomes containing hydrolytic enzymes, leading to degradation of the internalised contents (Naslavsky & Caplan, 2018; Scott *et al*., 2014; Song *et al*., 2020). Efficient therapy thus requires the vector be capable of escaping from the endosome or lysosome following uptake, avoiding degradation and releasing the therapeutic cargo into the cytoplasm. Most delivery systems attempt to take advantage of the acidic conditions in the endosome and lysosome, created by membrane-bound ATP-dependent proton pumps that lower the pH from neutral to slightly acidic in the early endosome and approximately 4.5 in the lysosome (Huotari & Helenius, 2011). These vectors may be designed to undergo pH-induced swelling, leading to physical disruption of the membrane, or exploit the proton sponge effect, which is theorised to lead to osmotic rupture of the endosome.

The proton sponge effect proposes that cationic polymers with high buffering capacities are able to sequester the protons pumped into endosome by the ATPases, preventing acidification (Figure 2.21). The ATPases thus continue to pump protons into the endosome, leading to an influx of chloride ions (Cl^-) via ion channels to neutralise the charge. The increased Cl^- ion concentration in the endosome creates an osmotic imbalance. Water molecules thus diffuse into the endosome, causing it to swell and eventually burst (Bus *et al*., 2018; Vermeulen *et al*., 2018). The theory was first proposed to explain the high transfection efficiency of PEI, which has a high buffering capacity in the endosomal pH range due to the high density of protonable primary, secondary, and tertiary amines in its backbone (Bus *et al*., 2018). The polymer is thought to be only partially protonated at physiological pH, allowing it to bind protons in the acidic endo/lysosome and induce the proton sponge effect (Ziebarth & Wang, 2010). CS, in contrast, contains only primary amines and has often been shown to display a poor buffering capacity, suggesting that it is a poor proton sponge (Mao *et al*., 2001; Santos-Carballal *et al*., 2018): however, Richard *et al*., (2013) suggested that the buffering capacity of CS is higher than PEI when the polymers are compared at equal molar concentration of amines rather than

mass concentrations. Thibault *et al*., (2010) reported that CS polyplexes accumulate in lysosomes and escape slowly over a period of 48 hours, suggesting that endosomal escape is a rate-limiting step for CS. However, addition of excess CS improved transfection efficiencies, possibly due the requirement for a minimum amount of polymer for the proton sponge effect (Thibault *et al.*, 2011). Lysosomal escape has also been reported for CS-AuNC (Zhu *et al*., 2019).

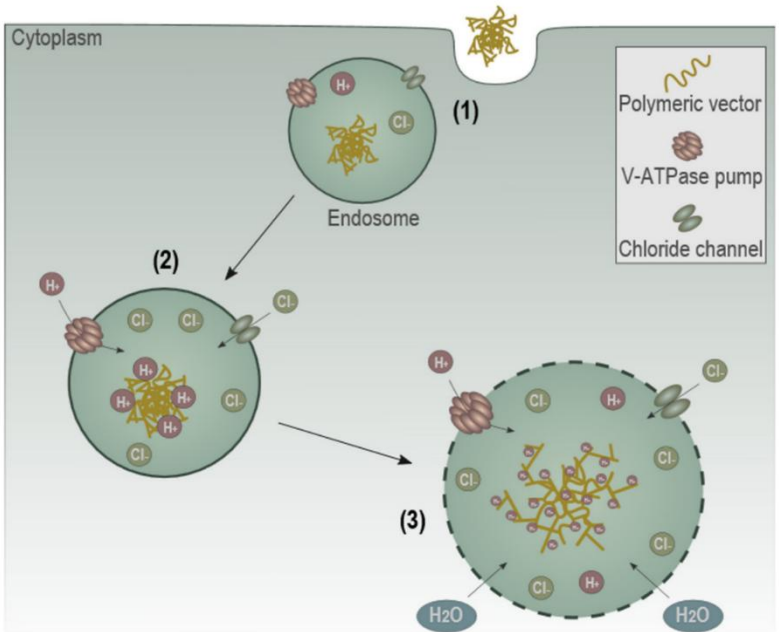

Figure 2.21: The suggested mechanism of the proton sponge effect whereby polymers with high buffering capacities are able to rupture the endosome. (1) The polymer enters the cell by endocytosis, (2) The polymer binds the protons pumped into the endosome, leading to the influx of Cl^-, (3) This leads to the inflow of water, swelling the endosome and causing it to burst (Vermeulen *et al*., 2018).

Notably, several studies have questioned the validity of the proton sponge effect. Evidence for the hypothesis has been provided by observations of increased endosomal Cl^- concentration and volume, buffering of the endo/lysosomal drop in pH, and reduced transfection efficiencies in the presence ATPase inhibitors (Akinc *et al*., 2005; Sonawane *et al*., 2003). In contrast, several studies have reported no increases in endo/lysosomal pH following PEI treatment, suggesting that ATPases are able to reduce the pH despite buffering by PEI (Benjaminsen *et al*., 2013; Forrest & Pack, 2002). Rehman *et al*., (2013) also reported lipoplex and polyplex escape to occur in HeLa cells without rupture of the endosome. It is possible that few endo/lysosomes contain enough polymer to induce the proton sponge effect, and escape instead results from a combination of polymer buffering swelling the endo/lysosome, particle swelling

due to electrostatic repulsion between the protonated groups, and membrane destabilisation (Vermeulen *et al*., 2018).

CHAPTER 3
MATERIALS AND METHODS

3.1. Materials

3.1.1. Synthesis and functionalisation

Gold (III) chloride trihydrate ($HAuCl_4.3H_2O$), L-glutathione reduced (L-GSH), chitosan (CS, medium MW, 75 – 85% deacetylated), and 14 kDa dialysis tubing were obtained from Sigma Aldrich (St Louis, USA). Polyethylene glycol 2000 (PEG_{2000}) was purchased from Merck (Darmstadt, Germany). Anhydrous glycerol was obtained from Sisco Research Laboratories Pvt. Ltd. (Maharashtra, India). Ultrapure 18 Mohm water was used in all experiments.

3.1.2. siRNA duplexes

The BLOCK-iT™ Fluorescent Oligo was purchased from Invitrogen, Thermo Fisher Scientific (Waltham, USA). The following siRNA duplexes were purchased from Dharmcon (Lafayette, USA): the siGENOME Non-Targeting siRNA #1; the ON-TARGET plus Human TNF (7124) SMARTpool siRNA; and the ON-TARGET plus Human MYC (4609) SMARTpool siRNA. The sequences of the individual siRNA duplexes are shown in Table 3.1. The 5x siRNA buffer and nuclease-free water were also obtained from Dharmacon (Lafayette, USA).

Table 3.1: Sequences of non-targeted siRNA and individual siRNA duplexes in the SMARTpool mixture.

siRNA reagent	Sequence (5′ – 3′)
siGENOME Non-Targeted siRNA	UAGCGACUAAACACAUCAA
ON-TARGET plus Human TNF SMARTpool siRNA	GCCCGACUAUCUCGACUUU
	GCGUGGAGCUGAGAGAUAA
	UGACAAGCCUGUGCCCAU
	CCAGGGACCUGUGUGUAAU
ON-TARGET plus Human MYC SMARTpool siRNA	ACGGAACUCUUGUGCGUAA
	GAACACACAACGUCUUGGA
	AACGUUAGCUUCACCAACA
	CGAUGUUGUUUCUGUGGAA

3.1.3. Binding studies

Tris (hydroxymethyl)-aminomethane (Tris-base), sodium dihydrogen phosphate (NaH_2PO_4), 4-(2-hydroxyethyl)-1-piperazine ethanesulfonic acid (HEPES), ethylenediaminetetraacetic acid (EDTA disodium salt), sodium dodecyl sulphate (SDS), bromophenol blue and ethidium

bromide (EtBr) were purchased from Merck (Darmstadt, Germany). Ultrapure grade agarose was obtained from Bio-Rad Laboratories, Inc., (Hercules, USA). Sucrose was purchased from NT Laboratory Supplies (Johannesburg, South Africa). RNase A was obtained from Calbiochem (San Diego, USA). All other reagents were of analytical grade.

3.1.4. *In vitro* cell culture studies

Minimum Essential Medium (MEM) was obtained from Gibco, Thermo Fisher Scientific (Waltham, USA). Dulbecco's Phosphate Buffered Saline (PBS) was purchased from Capricorn Scientific GmbH (Ebsdorfergrund, Germany). Foetal Bovine Serum (FBS) was purchased from Cytiva (Marlborough, United States.). Trypsin-versene and penicllin-streptomycin were obtained from Lonza BioWhittaker, (Walkersville, USA). Dimethylsulfoxide (DMSO) was purchased from Lichro Chemicals and Laboratory Supplies (Durban, South Africa). The 3-[4,5-dimethylthiazol-2-yl]-2,5-diphenyltetrazolium bromide (MTT) reagent was purchased from Merck (Darmstadt, Germany). Lipofectamine™ 3000 (LF3K) was supplied by Invitrogen, Thermo Fisher Scientific (Waltham, USA). The Muse® Caspase 3/7, Oxidative Stress, and Cell Cycle kits were sourced from Luminex Corporation (Austin, USA). All sterile plasticware was purchased from Nest Biotechnologies (Wuxi, China) and Corning Incorporated (New York, USA). The HEK293, MCF-7, and MDA-MB-231 cell lines were originally obtained from the American Type Culture Collection (ATCC, Manassas, USA).

3.1.5. Gene knockdown

TRIzol™ was obtained from Thermo Fisher Scientific (Waltham, USA). The following chemicals and plasticware were purchased from Bio-Rad (Hercules, USA): iScript™ cDNA Synthesis kit, 2x SsoAdvanced™ Universal Supermix, PrimePCR™ SYBR® Green Assays, PrimePCR™ Templates, Hard Shell® PCR 96 well plates, Microseal® 'B' adhesive seals, 10% Tween 20 and Blotting grade blocker. Bicinchoninic acid (BCA) and radioimmunoprecipitation assay (RIPA) buffer were obtained from Sigma-Aldrich (St. Louis, USA). The anti-β-actin primary antibody was obtained from Novus Biologicals (Littleton, USA); while the mouse monoclonal antibody anti-human c-myc and goat anti-mouse IgG2A secondary antibody, horseradish peroxidase (HRP) were purchased from Invitrogen, Thermo Fisher Scientific (Waltham, USA). The 3,3′,5,5′-tetramethylbenzidine (TMB) substrate was obtained from Life Technologies (Frederick, USA).

3.2. Methods

3.2.1. Synthesis and functionalisation of nanoclusters

3.2.1.1. Synthesis of AuNC

AuNC were synthesised according to Luo *et al*., (2012). Briefly, 20 x 10^{-3} M $HAuCl_4$ (1 mL) was mixed with 300 µL of a 100 x 10^{-3} M GSH solution and 8.7 mL deionised water under gentle stirring at room temperature. The solution turned orange upon addition of GSH, before becoming colourless with stirring. It was then maintained at 70 °C with stirring in a glycerol bath for 24 hrs. The resulting AuNC were purified by centrifugation at 16 000 xg for 1 min, to remove large NP, and then dialysed for 48 hrs against deionised water using a 14 kDa dialysis tube, to remove unreacted gold ions and GSH molecules.

3.2.1.2. Functionalisation of AuNC

AuNC were functionalised with CS, and PEG in two weight ratios of 1% and 2% (w/w). Functionalisation with CS was carried out according to Goswami *et al*., (2016). Briefly, 2 mL of the AuNC was added to a round bottom flask. Thereafter, a stock CS solution (2 mg/mL in 1% acetic acid) was added dropwise to the AuNC with stirring, to a final concentration of 1 mg/mL. The solution was made up to 5 mL with deionised water, adjusted to pH 6.5 through addition of 1 M NaOH, and stirred at room temperature for 30 min. The resulting AuCS NPs were dialysed as described in section 3.2.1.1.

Functionalisation with PEG was carried out using PEG conjugated to 1,1-carbonyldiimidazole (PEG-CDI). The appropriate volume of a 1 mg/mL stock PEG-CDI solution was first added to 1 mL CS (2 mg/mL) and stirred overnight to allow for binding of the PEG-CDI to the CS. The resulting CS-1% PEG and CS-2% PEG solutions were then used to produce AuCS-1% PEG and AuCS-2% PEG using the same protocol as for AuCS synthesis.

3.2.1.3. Preparation of nanocomplexes

Nanocomplexes were prepared by mixing varying amounts of functionalised AuNC (FAuNC) with a constant amount of siRNA (0.30 µg). Solutions were made up to 10 µL with HEPES buffered saline (HBS) (20 mM HEPES, 150 mM NaCl, pH 7.4), and incubated at room temperature for 1 hr to allow for binding. These nanocomplexes were used further in binding and *in vitro* studies. Complexation with Lipofectamine® 3000 (LF3K) was carried out according to the manufacturer's protocols. Briefly, LF3K and siRNA were mixed in serum-

free media according to the values shown in Table 3.2, vortexed briefly, and incubated at room temperature for 10 min.

Table 3.2: Quantities of LF3K and siRNA used for transfection in various plate formats.

Plate format	siRNA		LF3K (µL)	Total volume (µL)
	(pmol)	(µg)		
48-well	7.5	0.1	0.75	25
24-well	15	0.2	1.5	50
6-well	75	1.0	7.5	250

3.2.2. Characterisation of nanoclusters and nanocomplexes

The absorbance spectra of the AuNC and FAuNC were analysed by UV-visible (UV-vis) spectroscopy using a Jasco V-730 Bio Spectrophotometer (Jasco Inc, Japan). Briefly, 2 µL of samples was loaded onto the spectrophotometer, and the absorbance of light between 200 – 800 nm was measured to produce an absorbance spectrum. The presence or absence of peaks was noted for further analysis. Transmission electron microscopy (TEM) was used to determine the size and morphology of AuNC and FAuNC. Viewing was conducted on a Jeol T1010 TEM, using samples that were air-dried on a 400 mesh copper grid (Ted Pella Inc. Redding, USA). ImageJ software was used to measure the size of the NC and determine their average diameter. Fourier-transform infrared spectroscopy (FTIR) was conducted using a Perkin Elmer Spectrum 100 FT-IR spectrometer fitted with a universal ATR sampling accessory. The peaks in the spectra and the bonds corresponding to them were identified through comparison with literature. The hydrodynamic diameters and zeta potentials were determined using a Nanosight NS500 (Malvern Instruments, Worcestershire, UK), using samples diluted (1:1000) in deionised water to a final volume of 1 mL. Samples are exposed to a laser beam following loading into the machine. A camera captures and analyses the light scattered by individual particles to provide the hydrodynamic diameter. The polydispersity indices (PI) of the hydrodynamic diameters were calculated using the following formula:

$$PI = \left(\frac{SD}{Mean}\right)^2$$

The zeta potentials are determined through analysis of particle movement under an electric current. Nanocomplexes were prepared for NTA as described in section 3.2.1.3, according to

their optimum ratios determined in the band shift assay (section 3.2.3.1). The volume of FAuNC and siRNA was doubled, and nanocomplexes diluted as for the NPs.

3.2.3. Binding studies

3.2.3.1. Band shift assay

The band shift assay was used to assess FAuNC and siRNA interactions. Nanocomplexes were prepared as described in section 3.2.1.3 using a constant amount of non-targeted siRNA (0.30 µg) and increasing amounts of FAuNC. Following incubation, 2 µL of 6X gel loading dye (40% sucrose, 0.25% bromophenol blue) was added to the solutions. The nanocomplexes were then run in 1X TBE buffer on a 2% agarose gel containing 2 µL of ethidium bromide (EtBr) (10 mg/mL) at 50V for 30 min. Gels were then viewed under UV light (λ = 300 nm) in a Vacutec Syngene G: Box BioImaging system (Syngene, Cambridge, UK) and images were taken using GeneSnap software, version 7.05.02 (Syngene, Cambridge, UK). The optimum, sub-optimum, and supra-optimum siRNA:FAuNC ratios were recorded and studied further in the nuclease protection assay (section 3.2.3.3) and *in vitro* assays.

3.2.3.2. Ethidium Bromide (EtBr) intercalation assay

Dye displacement studies were conducted using the Glomax®-Multi Detection System (Promega Biosystems, Sunnyvale, USA). Briefly, 100 µL of HBS was added to a 96-well flat-bottom black FluorTrac plate. Approximately 2 µL of EtBr (100 µg/mL) was added to the HBS, and the fluorescence was measured at excitation and emission wavelengths of 525 and 600 nm, respectively, to establish a baseline. Thereafter, 0.30 µg siRNA was added to the wells and mixed to allow for binding. The fluorescence was measured to establish the maximum fluorescent intensity of the fully-bound siRNA. The FauNC were then added to the solution in 1 µL increments, and fluorescence recorded after each addition until a plateau was reached. The relative fluorescence was then calculated using the following formula:

$$F_R\ (\%) = \left(\frac{F_i - F_0}{F_{max} - F_0}\right) \times 100$$

Where F_0 = baseline fluorescence; F_i = fluorescent intensity following addition of FauNC; and F_{max} = maximum fluorescent intensity of intercalated siRNA. The approximate siRNA:FauNC weight ratio was determined after each addition, and the data was plotted as the relative fluorescence against the siRNA:FauNC ratio.

3.2.3.3. Nuclease protection assay

The nuclease protection assay assessed the ability of FAuNC to protect siRNA from degradation by RNase A. Nanocomplexes were prepared according to the optimum, sub-optimum, and supra-optimum ratios obtained in the band shift assay and incubated for one hour. Following incubation, approximately 1 µL of RNase A (1 mg/mL) was added to the nanocomplexes. Two siRNA-only controls were also set up: a positive control which was not subject to RNase A treatment, and a negative control treated with RNase A. The reactions were then incubated at 37 °C for 2 hrs and thereafter terminated by the addition of EDTA (110 mM) to a final concentration of 10 mM ($^{V}/_{V}$). SDS (6%) was then added to a final concentration of 0.5% ($^{V}/_{V}$), and the reactions were incubated at 55 °C for 20 min to permit release of the siRNA from the nanocomplexes. Samples were then run a 2% agarose gel and analysed as described in section 3.2.3.1.

3.2.4. *In vitro* cell culture maintenance

In vitro studies were conducted in three cell lines: two BC cell lines (HR+ MCF-7 and TNBC MDA-MB-231) and the non-cancer human embryonic kidney (HEK293) cells. MDA-MB-231 were maintained in DMEM:HAM's F12 (1:1) supplemented with 2% ($^{V}/_{V}$) FBS and 1% ($^{V}/_{V}$) penicillin/streptomycin antibiotic, while the other cell lines were grown in DMEM supplemented with 10% ($^{V}/_{V}$) FBS and 1% ($^{V}/_{V}$) penicillin/streptomycin. Cells were propagated in a Steri-cult CO_2 incubator (Thermo-Electron Corporation**,** Waltham, Massachusetts, USA) at 37 °C under 5% CO_2. All cell work was conducted under sterile conditions in a class II biohazard hood.

3.2.5. Cell viability studies

3.2.5.1. MTT cytotoxicity assay

The cells were plated in 48-well plates at a density of approximately 2 x 10^4 cells per well and incubated overnight to allow for attachment. Nanocomplexes containing the siRNA with FAuNC and LF3K were prepared as described in section 3.2.1.3, and the cells were thereafter treated with the nanocomplexes in triplicate. Untreated cells served as the control, which was assumed to have 100% cell survival. The cells were incubated at 37 °C for 48 hrs, after which the spent medium was removed and replaced with fresh medium containing 20 µL MTT reagent

(5 mg/mL in PBS). Cells were incubated at 37 °C for 4 hrs to allow for formation of the formazan crystals. The medium was then removed and replaced with DMSO. Plates were shaken to allow for development of a clear, purple solution. The absorbance was then read at 540 nm using a Mindray MR-96A microplate reader (Vacutec, Hamburg, Germany) against DMSO as a blank. Cell viability was then calculated using the following formula:

$$\text{Cell viability} = \frac{A_{540} \text{ of treated cells}}{A_{540} \text{ of control}} \times 100$$

3.2.5.2. Apoptosis assay

Apoptosis was evaluated using dual ethidium bromide/acridine orange (EtBr/AO) staining. The cells were plated at a density of approximately 2 x 10^4 cells per well and incubated overnight. The medium was then replaced with fresh medium, and cells were treated with nanocomplexes at the optimum ratios and incubated for a further 24 hrs. Subsequently, the medium was removed, and the cells were washed with PBS. The cells were stained with 15 µL of EtBr/AO dye (0.1 mg/mL: 0.1 mg/mL in PBS) for 5 min at room temperature, washed with PBS to remove unbound dye, and viewed using an inverted fluorescence microscope (CKX41, Olympus, Japan). Images were taken using Analysis Five Software (Olympus Soft Imaging Solutions, Olympus, Japan). The apoptotic index was calculated using the following formula, where the total number of apoptotic cells included cells in both early and late apoptosis:

$$\text{Apoptotic index} = \frac{\text{number of apoptotic cells}}{\text{total number cells counted}}$$

3.2.6. Cellular uptake studies

Cells were plated and incubated as in section 3.2.5. Thereafter, cells were treated with FAuNC complexed with BLOCK-iT™ Fluorescent Oligo and incubated for a further 24 hrs. Following incubation, the medium was removed, and cells were rinsed with PBS. Cells were viewed under a fluorescent microscope and images taken as in section 3.2.5.2.

3.2.7. Flow cytometry studies

All flow cytometry experiments were carried out using the Guava® Muse Cell Analyzer (Luminex Corporation, Austin, TX, USA). Cells were plated in 24-well plates at a density of approximately 4 x 10^4 cells per well and incubated overnight. Thereafter, cells were treated

with *TNF-α*-targeted siRNA complexed with LF3K and FAuNC at optimum ratios, and incubated for a further 48 hrs. The medium was then removed from the wells, and cells were washed with PBS. Cells were removed from the plate through trypsinisation, centrifuged at 300 xg for 5 min, and resuspended and treated according to the manufacturer's protocols, briefly described below.

3.2.7.1. Caspase 3/7 analysis

Cells were resuspended in 50 µL 1X Assay Buffer BA and treated with 5 µL of Muse® Caspase-3/7 Reagent working solution. The samples were briefly vortexed and incubated at 37 °C for 30 min. Samples were then treated with 150 µL of Muse® Caspase 7-AAD working solution, mixed, and incubated in the dark at room temperature for a further 5 min. Analysis was then carried out using the Muse® Cell Analyzer.

3.2.7.2. Cell cycle analysis

Trypsinised cells were washed with PBS and fixed in 70% ethanol at -20 °C overnight. Following cell fixation, the ethanol was removed by centrifugation at 300 xg for 5 min and cells were washed with PBS. Cells were resuspended in 200 µL of the Muse® Cell Cycle Reagent and incubated in the dark at room temperature for 30 min. Samples were finally analysed using the Muse® Cell Analyzer.

3.2.7.3. Oxidative stress analysis

Cells removed from the plate were resuspended in 1X Assay Buffer to a concentration between 1 x 10^6 and 1 x 10^7 cells/mL. Approximately 10 µL of the cell suspension was then treated with 190 µL of Muse® Oxidative Stress Reagent working solution, mixed, and incubated at 37 °C for 30 min. Samples were then analysed on the Muse® Cell Analyzer.

3.2.8. Analysis of gene knockdown

Gene knockdown studies were conducted in the HR+ MCF-7 cell line and targeted the *c-MYC* oncogene. Cells were plated in a 6-well plate at a density of approximately 2.5 x 10^5 cells per well. Following overnight incubation, the medium was replaced, and cells were treated with LF3K and FAuNC complexed to non-targeted and anti-*c-MYC* siRNA. Untreated cells and cells treated with uncomplexed siRNA were included as controls. Cells were incubated for a

further 48 hrs prior to RNA and protein extraction for reverse transcription quantitative PCR (RT-qPCR) and Enzyme Linked Immunosorbent Assay (ELISA), respectively.

3.2.8.1. Analysing knockdown at the mRNA level

3.2.8.1.1. RNA extraction

Total RNA was extracted using TRIzol™ Reagent according to the manufacturer's protocols, with minor modifications. Briefly, the medium was discarded and replaced with 1 mL of TRIzol™ Reagent. Cells were lysed by pipetting the solution several times and incubated at RT for 5 min. The cell solutions were then transferred to a sterile eppendorf tubes, followed by the addition of 200 µL of chloroform to the solution. The tubes were shaken vigorously for 15 sec and incubated at RT for 3 min, prior to centrifugation at 12 000 xg for 15 min at 4 °C. The upper aqueous phase containing the RNA was transferred to a new tube and treated with 500 µL of 100% isopropanol. The samples were mixed by inverting the tubes and incubated at RT for 20 min. Total RNA was then pelleted through centrifugation at 16 000 xg for 10 min at 4 °C. The supernatant was discarded, and the pellet was washed 3 times by centrifugation at 7500 xg for 10 min at 4 °C; twice with 75% ethanol and once with 95% ethanol. Following the final wash step, the supernatant was discarded, and the pellet was allowed to airdry at RT for 10 min to remove residual ethanol. The RNA was then resuspended in 30 µL of nuclease-free water by pipetting and incubating the solution at 55 °C for 15 min. The isolated RNA was then analysed through UV spectroscopy and agarose gel electrophoresis, to determine the concentration and quality, and integrity of the RNA, respectively.

3.2.8.1.2. cDNA synthesis

Prior to RT-qPCR, the isolated RNA was converted to cDNA using the iScript™ gDNA Clear cDNA Synthesis Kit according to the manufacturer's protocol. The reactions were carried out using a Bio-Rad C1000 Touch™ Thermal Cycler. Approximately 500 ng of the isolated RNA was diluted to 15 µL in nuclease-free water and mixed with 4 µL of the iScript Reaction Mix and 1 µL of the iScript Reverse Transcriptase (RT). A no-RT control, to which nuclease-free water was added instead of iScript RT, was included for each sample. The solutions were mixed and incubated according to the conditions shown in Table 3.3. The resulting cDNA solutions were quantified using a Nanodrop spectrophotometer and diluted for use in RT-qPCR.

Table 3.3: Reaction conditions for cDNA synthesis using isolated RNA.

Reaction step	Temperature (°C)	Time (min)
Priming	25	5
Reverse transcription	46	20
Reverse transcriptase inactivation	95	1

3.2.8.1.3. RT-qPCR

The PrimePCR™ Assay primers used for qPCR targeted the housekeeping gene *ACTB*, or β-actin, (Assay ID: qHsaCED0036269); and the target gene *c-MYC* (Assay ID: qHsaCID0012921). Reactions were set up in duplicate as shown in Table 3.4 for both the RT samples and no-RT controls in Hard Shell® PCR 96 well plates. Positive and negative controls were included for each gene; these replaced cDNA with PrimePCR™ Templates (1 µL) and nuclease-free water, respectively. Reactions were carried out using the C1000 Touch™ Thermal Cycler (CFX 96 Touch™ Real-Time PCR Detection System, Bio-Rad Laboratories (PTY) Ltd.), according to the protocol shown in Table 3.5. Results were presented as the fold change in *MYC* gene, determined using the $2^{-\Delta\Delta Ct}$ method shown below.

$$\Delta Ct \text{ sample} = Ct\ GOI_s - Ct\ norm_s$$

$$\Delta Ct \text{ calibrator} = Ct\ GOI_c - Ct\ norm_c$$

$$\Delta\Delta Ct = \Delta Ct \text{ sample} - \Delta Ct \text{ calibrator}$$

$$\text{Fold change} = 2^{-\Delta\Delta Ct}$$

Table 3.4: Components of PrimePCR™ assays and their final concentrations.

Reaction component	Volume added (µL)	Final concentration/amount
2x SsoAdvanced Universal SYBR Green Supermix	10	1x
20x PrimePCR™ Assay	1	1x
cDNA sample	5	100 ng
Nuclease-free water	4	-

Table 3.5: PrimePCR™ Assay cycling conditions.

Reaction step	Temperature (°C)	Time (sec)	No. of cycles
Activation	95	120	1
Denaturation	95	5	40
Annealing/extension	60	30	
Melt curve	65 – 95	5 sec/step	1

3.2.8.2. Analysing knockdown at the protein level

3.2.8.2.1. Protein extraction

Extraction of the cellular protein was carried out using RIPA buffer. Following the 48-hour incubation, the growth medium was removed, and cells were washed twice with 1 mL of ice-cold PBS. Cells were then treated with 250 µL of cold RIPA buffer and incubated at 4 °C for 5 min. Wells were thereafter scraped with a pipette tip to lyse the cells, and the samples were transferred to Eppendorf tubes and spun down at 8000 xg for 10 min at 4 °C. The supernatants were quantified using the BCA assay, aliquoted, and stored at -80°C until use.

3.2.8.2.2. BCA assay

Protein concentrations were determined using the BCA assay. Briefly, BCA working reagent ($CuSO_4$: bicinchoninic acid (BCA) (1:50 $^{V}/_{V}$), was mixed with the protein sample in a ratio 1: 20 (sample: working reagent). The solutions were then incubated at 37 °C for 30 min, cooled, and their absorbances were read at 450 nm using a Mindray MR-96A microplate reader (Vacutec, Hamburg, Germany).

3.2.8.2.3. Enzyme-linked Immunosorbent Assay (ELISA)

Protein isolates were diluted to 100 µg/mL in 50 mM carbonate-bicarbonate coating buffer, and 100 µL was dispensed into a 96-well plate. Samples were plated in duplicate for detection of the housekeeping protein β-actin and the protein of interest c-MYC. Plates were incubated overnight at 4°C to allow for protein attachment to the wells. Following incubation, the coating buffer was removed, and plates were washed twice with 200 µL of TBS-T (20 mM Tris-base, 150 mM NaCl, 0.1% Tween 20). Wells were then treated with 100 µL of 5% blocking buffer (non-fat dry milk in TBS-T) for 1 hr at room temperature with constant shaking. The blocking buffer was thereafter removed, and wells were washed twice with 200 µL TSB-T. Samples were then treated with the primary antibodies: MYC (diluted in1:2000 in 1% blocking buffer), and β-actin (diluted 1:10 000 in 1% blocking buffer). The plates were incubated at room temperature for 1 hr with shaking to allow for attachment. The antibodies were thereafter removed, and the plates were washed with 4 times with 200 µL TBS-T for 5 min with shaking each. Wells were then treated with the secondary antibody, goat anti mouse IgG2a-HRP (diluted 1:2000 in 1% blocking buffer) and incubated at room temperature for 1 hr with shaking. The solutions were then removed, and plates were washed 4 times as previously

described. Approximately 100 µL of TMB solution was then added to the samples and incubated protected from light for 30 min at room temperature to allow for colour change from colourless to blue. Stop solution (2M H_2SO_4) was thereafter added to the wells, changing the colour of the solutions from blue to yellow, and the absorbance was read at 450 nm using the Mindray MR-96A microplate reader (Vacutec, Hamburg, Germany).

3.2.9. Statistical analysis

All assays were performed in triplicate, except for the gene expression assays, which were performed in duplicate. Data are presented as means ± SD. Statistical analysis was conducted using GraphPad Prism version 6.01 (GraphPad Software Inc., USA). Groups were compared using two-way analysis of variance (ANOVA) followed by Tukey's multiple comparisons test. P-values < 0.05* and p-values < 0.01** were considered statistically significant.

CHAPTER 4
RESULTS AND DISCUSSION

4.1. Synthesis and functionalisation of AuNPs

The FAuNC used in this study consisted of AuNC functionalised with CS and PEG_{2000} in two weight ratios. AuNC were synthesised according to Luo *et al*., (2012), through AIE of non-luminescent Au(I)-thiolate complexes into luminescent AuNC (Figure 4.1). The solution initially turned colourless upon combination of the two reagents as the Au(I)-thiolate and Au(I)-non-thiolate complexes formed, before gradually turning light yellow over a 24 hr period as the Au(0)-on-Au(I)-thiolate complexes aggregated into the core-shell structured AuNC.

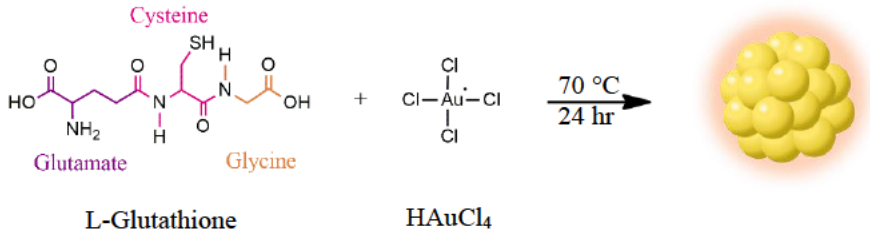

L-Glutathione $HAuCl_4$

Figure 4.1: Scheme showing synthesis of AuNC through GSH-induced reduction of $HAuCl_4$.

The GSH-AuNC were functionalised with the cationic CS to facilitate interactions with the anionic siRNA. CS functionalisation is dependent on electrostatic interactions between the CS polymer and GSH molecules capping the AuNC. The carboxyl groups of GSH bear low pKa values (2.06 for Glu-COOH and 3.50 for Gly-COOH), and are thus deprotonated at the weakly acidic pH of 6.5 used during AuCS synthesis (Neupane & Pecoraro, 2011). This gives the AuNC an overall negative charge. In contrast, the amine groups of the CS are protonated at pH 6.5, giving the polymer a positive charge. Mixing of the two reagents thus allows for the formation of cationic nanogels through electrostatic interactions (Figure 4.2). A high polymeric charge density is required to efficiently bind siRNA (Wang *et al*., 2021a). For CS, the charge density was influenced by the degree of deacetylation and molecular weight (MW) of the polymer. The deacetylation degree provides the fraction of N-acetyl groups that have deacetylated into the protonable glucosamine groups that give CS its positive charge (Layek & Singh, 2017). CS with a low deacetylation may thus be unable to form stable nanocomplexes with siRNA (Liu *et al*., 2007). Studies have also reported a minimum MW of 10 kDa to be

required for the formation of stable nanocomplexes that lead to efficient gene knockdown (Alameh *et al*., 2018; Liu *et al*., 2007). The CS used in this study was of a medium MW (190-310 kDa) and a deacetylation degree of 75 – 85%, and thus met these criteria.

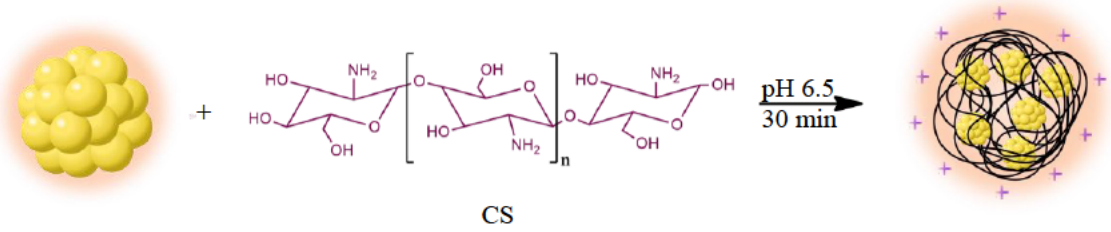

CS

Figure 4.2: Scheme showing synthesis of AuCS nanoconjugates.

Steric stabilisation was achieved through the addition of PEG. PEGylation was carried out using PEG-CI, which has been modified to carry a carbonyl-imidazole group. When reacted with CS, a covalent bond is formed between the carbonyl group of the PEG-CI and the amine group of the CS (Figure 4.3). To ensure successful protection and transfection, the MW and grafting density of the PEG chains must be optimised. PEG with an average chain MW of 2000 kDa (PEG_{2000}) was used in this study. Higher MW PEG generally provides more protection against opsonisation due to its increased flexibility; however, this increased flexibility may also inhibit cellular uptake by preventing interactions with the cell membrane (Rheiner & Bae, 2016; Suk *et al*., 2016). The grafting density must similarly be balanced, as high grafting densities may inhibit cellular uptake. Studies have reported improved knockdown with lower grafting densities of PEG_{2000} and PEG_{5000} compared to higher grafting densities. Guţoaia *et al*., (2016), for example, reported efficient knockdown with CS-PEG with grafting densities of 1.5 – 4%, while polyplexes with higher densities of 6 and 8% were unable to significantly knockdown GFP expression. Santel *et al*., (2006) similarly reported improved knockdown with lipoplexes functionalised with PEG molar ratios of 1, 2, and 3%, compared to 4 and 5 mol% PEG-lipoplexes. In this study, grafting densities of 1% ($^{w}/_{w}$) and 2% ($^{w}/_{w}$) were tested.

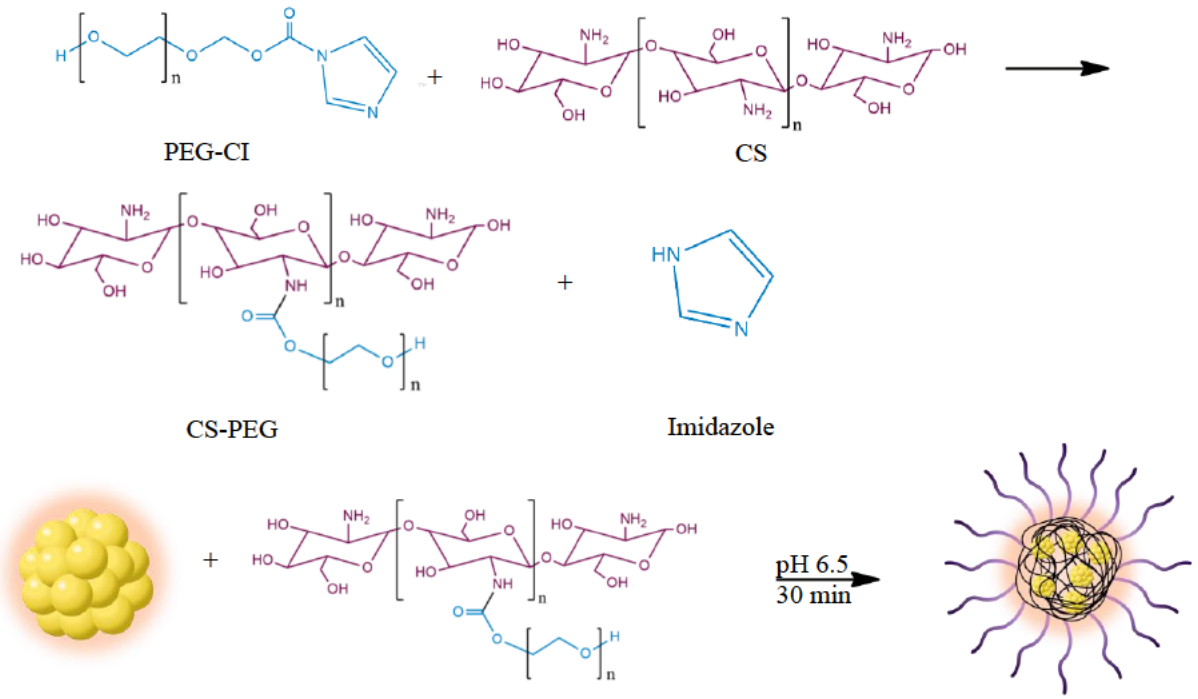

Figure 4.3: Scheme showing synthesis of PEGylated chitosan functionalised AuNC.

4.2. Physicochemical characterisation of AuNC

4.2.1. Optical characterisation

UV-vis spectrophotometry plays an important role in the characterisation of NPs, as it provides information regarding the optical properties, size, aggregation, and concentration of the NP solution (Mourdikoudis *et al*., 2018). The UV-vis spectra for the AuNC and FAuNC are shown in Figure 4.4.

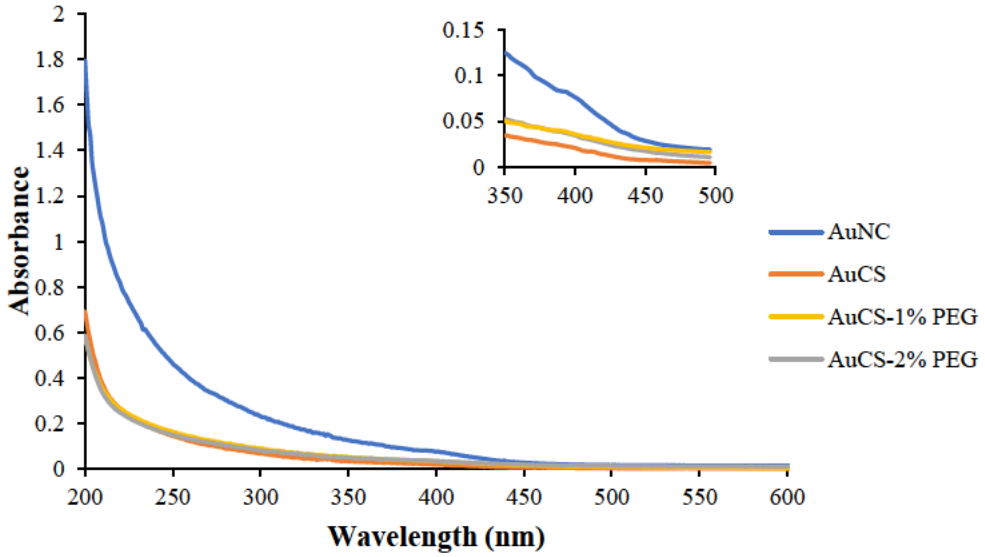

Figure 4.4: UV-vis spectra of AuNC and FAuNC. Inset shows the shoulder peak present at ~390 nm in the spectrum of the AuNC.

The spectrum for the unfunctionalised AuNC shows an increase in absorbance from approximately 450 nm, but displays no prominent peaks, except for a small shoulder peak at approximately 390 nm, shown in the inset. The absence of an LSPR peak at ~520 nm indicates that ultrasmall AuNC were successfully synthesised, and that no large AuNP were present in the AuNC solution following purification. The onset of absorbance from approximately 450 nm further indicates that AuNC which absorb strongly in the UV range of the light spectrum were synthesised (Chen *et al*., 2009). The shoulder peak is similar to that observed by Luo *et al*., (2012). Shoulder peaks at ~400 nm are commonly reported in the UV-vis spectra of thiolate-capped AuNC (Ju *et al*., 2019; Li *et al*., 2018b; Xia *et al*., 2019; Zhang *et al*., 2012b). Le Guével *et al*., (2012) reported a broad shoulder peak around 530 nm for BSA-AuNC, which was attributed to the LSPR of some AuNP slightly larger than 2 nm, or charge transfer between the gold core and cysteine groups of the ligand. The shoulder peak observed in this study is unlikely to result from LSPR due to its position, and may thus instead result from electron transfer between the ligand and metal or within the ligand, or due to electron excitation. Liang *et al*., (2015), for example, reported a shoulder peak in the UV spectrum of graphene oxide, which was attributed to transition of the lone electron pair of an oxygen to carbon. Shoulder peaks observed in the spectra of carboranealkynyl-protected AuNC have also been attributed to electron HOMO-LUMO transitions (Wang *et al*., 2021b).

UV-vis spectra may also indicate the success of functionalisation by showing changes in the optical characteristics of solutions following functionalisation. Both the CS- and PEG-functionalised AuNC lack a peak at 520 nm, indicating that functionalisation did not induce aggregation of the AuNC, and they maintained their ultrasmall structure. The shoulder peak at ~390 nm also appears to be absent from the spectra for the FAuNC, as shown in the inset. A similar observation can be made in the CS-coated AuNC UV spectra of Zhu *et al*., (2019). This may indicate the success of CS functionalisation onto the AuNC, and may result from differences in charge transfer in the CS-coated AuNC. Musnier *et al*., (2019) and Yuan *et al*., (2016) reported a shoulder peak at 440 nm in the spectrum of anionic mercaptohexanoic acid-coated AuNC, which disappeared for AuNC capped with both mercaptohexanoic acid and neutral or cationic ligands. This was attributed to a change in the anisotropy of the surface charge of the dual-capped AuNC. It is possible that a change in the surface charge of the AuNC following functionalisation with CS may have similarly influenced the UV spectra of the FAuNC.

The visual characteristics of the AuNC and FAuNC are shown in Figure 4.5. Under visible light, the solutions appeared yellow in colour, with the FAuNC appearing a lighter colour then the plain AuNC. Upon irradiation with UV light with a wavelength of 366 nm, the solutions emitted bright orange fluorescence. The AuCS (Figure 4.5C) can be observed to fluoresce brighter than the AuNC (Figure 4.5B), which may be attributed to the phenomenon of AIE. The fluorescence intensity of the PEGylated AuNC appears to be similar to that of the unfunctionalised AuNC, and weaker than the AuCS. This may suggest that functionalisation with the CS-PEG disrupted the circular structures of the AuCS that promoted AIE; however, fluorescence spectroscopy would be required to accurately quantify the fluorescent intensities.

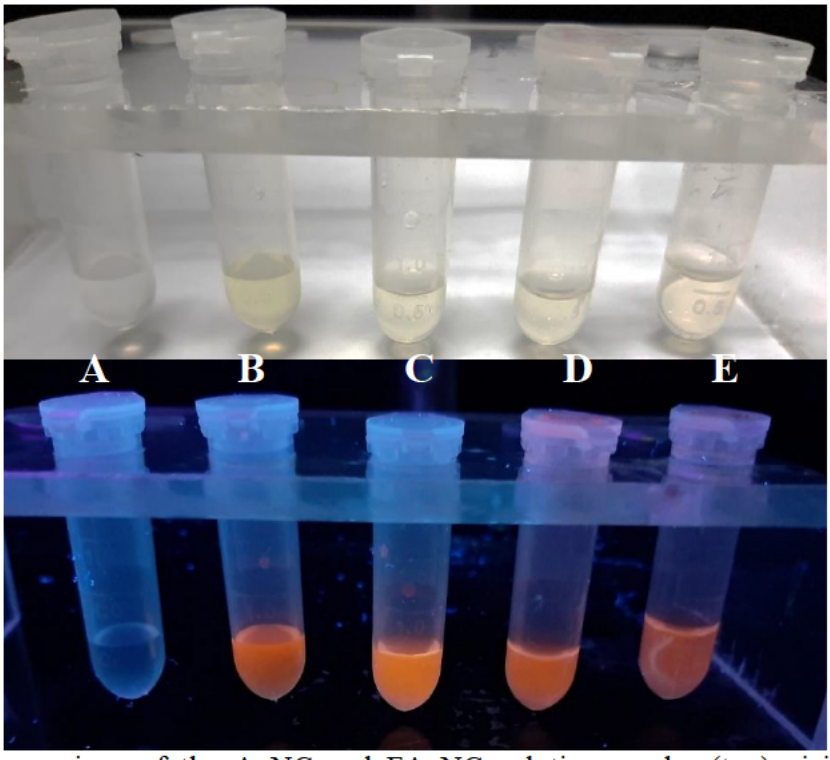

Figure 4.5: Comparison of the AuNC and FAuNC solutions under (top) visible light and (bottom) UV light (λ = 366 nm). (A) ddH_20 (B) AuNC (C) AuCS (D) AuCS-1% PEG (E) AuCS-2% PEG.

4.2.2. FTIR analysis

FTIR provides information on the types of bonds present in NP depending on their absorption of infrared radiation (Mourdikoudis *et al*., 2018). This allows for confirmation of ligand binding. The spectra for the plain AuNC and FAuNC is shown in Figure 4.6. Peaks were assigned according to literature.

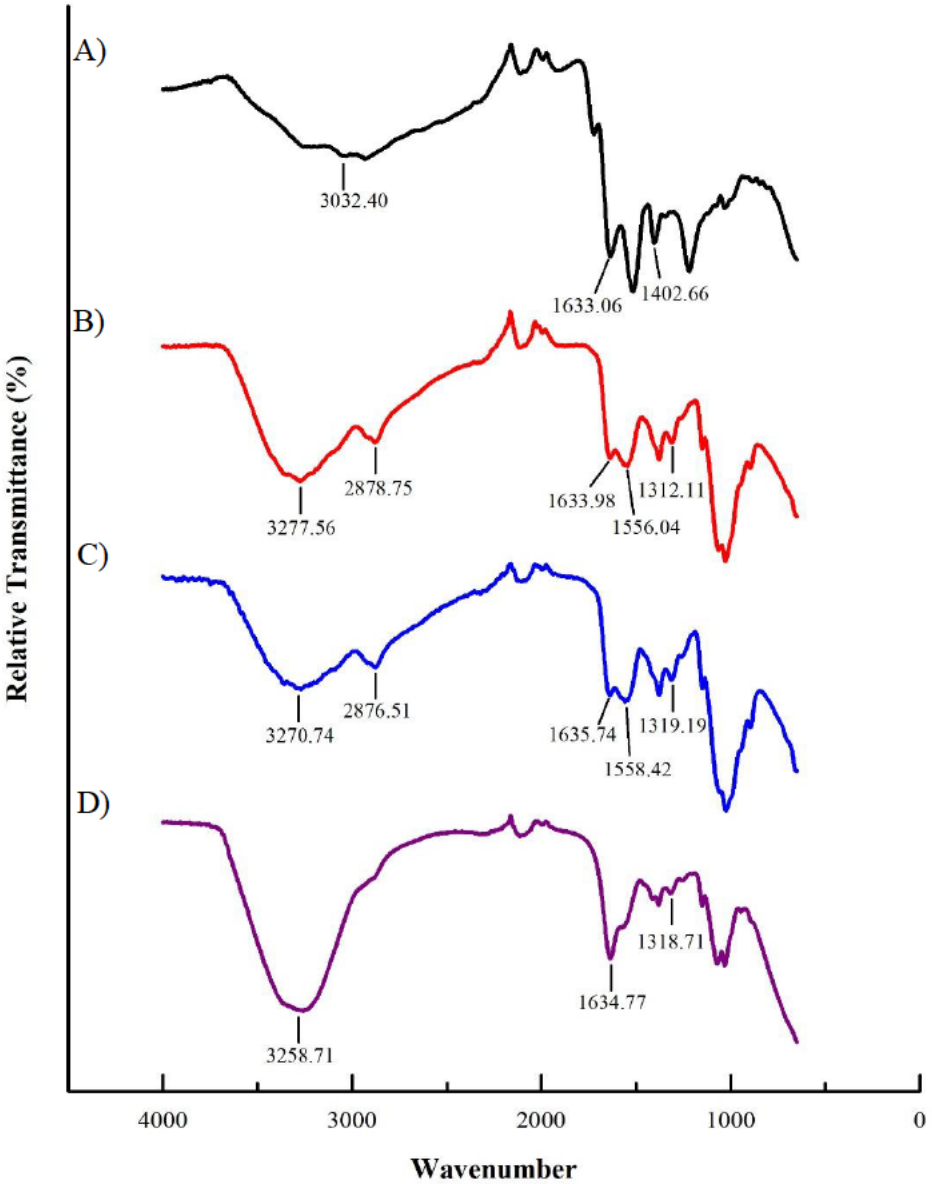

Figure 4.6: FTIR spectra of AuNC and FAuNC with major peaks labelled. A) AuNC, B) AuCS, C) AuCS-1% PEG, and D) AuCS-2% PEG.

The successful synthesis of the GSH-AuNC can be inferred from the spectrum in two ways. Firstly, the presence of amide bonds in the GSH-AuNC may be inferred by the peaks at 1633.06 and 1402.66 cm^{-1}, which correspond to C = O and C – N stretching, respectively (Zhao *et al*.,

2021). Secondly, the FTIR spectrum of GSH displays a peak in the 2600 – 2550 cm^{-1} region corresponding to S-H stretching in the thiol group (Farrag & Mohamed, 2016; Negishi *et al*., 2005; Zhao *et al*., 2021). This peak cannot be observed in the spectrum of the AuNC, indicating that the sulphur successfully bound the gold to form GSH-capped AuNC.

The success of CS functionalisation is suggested by the change in the shape of the peak at 3277.56 cm^{-1} and the appearance of a small peak at 2878.75 cm^{-1} in the spectrum of the AuCS. These peaks correspond to free amine and hydroxyl groups, and C-H stretching, respectively (Parveen & Sahoo, 2011; Queiroz *et al*., 2014). The peaks seen at 1633.98 cm^{-1}, 1556.04 cm^{-1}, and 1312.11 cm^{-1} are characteristic of CS, and indicate the C=O stretching of amide I, N-H bending in amide II, and C-N stretching in amide III, respectively (Liu *et al*., 2012; Queiroz *et al*., 2014). PEG has commonly been reported to display characteristic peaks at approximately 3430, 2870, and 1110 cm^{-1}. These correspond to intra-molecular hydrogen bonds, C-H stretching, and C-O-C stretching within the PEG backbone, respectively (Parveen & Sahoo, 2011; Yang *et al*., 2017b; Zhang *et al*., 2015a). However, these cannot be distinguished on the spectra for AuCS-1% PEG or AuCS-2% PEG, possibly due to masking by the CS. The spectrum of AuCS-2% PEG shows a change in the shape of the peak at 3258.71 cm^{-1}, and the absence of the peaks at 2878.75 and 1556.04 cm^{-1}. This is possibly due to masking of peaks by the PEG or masking by residual water.

4.2.3. Sizing and zeta potential

4.2.3.1. TEM

TEM analysis allows for a visual assessment of shape, size, and aggregation (Kaliva & Vamvakaki, 2020). The TEM images for the plain AuNC and FAuNC are shown in Figure 4.7, and the sizes obtained from the TEM images are given in Table 4.1. From Figure 4.7A, it can be seen that AuNC are relatively circular in shape and monodisperse, displaying an average size of 1.86 nm. This size is close to the critical size at which energy levels become discrete, and is thus characteristic of AuNC (Jin, 2010). Luo *et al*., (2012) reported similar sizes below 2 nm for the as-synthesised Au(0)@Au(I)-thiolate NCs. The size of the AuNC did not change significantly following functionalisation with CS (1.86 nm vs 1.82 nm); or PEG (1.86 vs 1.89 nm for AuCS-1% PEG and 1.99 nm for AuCS-2% PEG). This is in accordance with the UV-vis spectra, which showed the absence of an LSPR peak for the AuNC and all FAuNC (Figure 4.4).

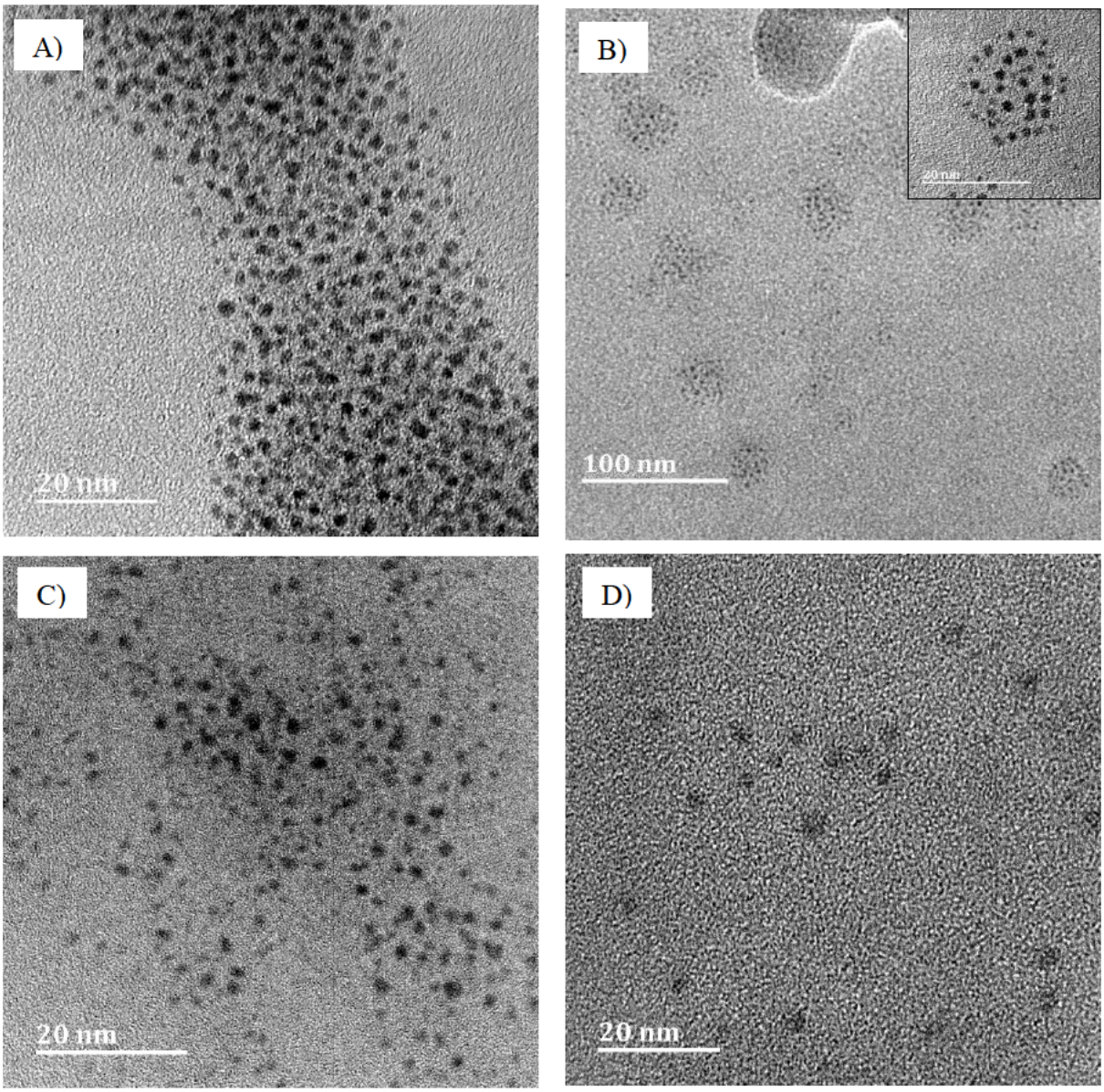

Figure 4.7: TEM images of AuNC and FAuNC. A) AuNC, B) AuCS, inset shows organisation of AuNC in circular AuCS nanogels, C) AuCS-1% PEG, and D) AuCS-2% PEG. Scale bars represent 20 nm on all figures except B), where the scale bar represents 100 nm.

Table 4.1: Average sizes of the plain and functionalised AuNC obtained using TEM.

NC	Size (nm ± SD)
AuNC	1.86 ± 0.45
AuCS (single)	1.82 ± 0.37
AuCS (nanogel)	21.23 ± 3.83
AuCS-1% PEG	1.89 ± 0.29
AuCS-2% PEG	1.99 ± 0.38

Biological compounds such as CS and PEG cannot be observed by TEM without staining, as they lack the density to deflect the electron beam to produce an image (Hall *et al*., 2007). However, the success of CS functionalisation can be inferred from the difference in NC organisation. Due to electrostatic interactions between the anionic carboxyl groups of GSH and the cationic CS amine groups, the AuCS self-assembled into larger, spherical nanogels of approximately 21 m in diameter, consisting of multiple AuNC encapsulated within the CS polymer (Figure 4.7B). Several studies have thus reported the self-assembly of GSH-capped nanoclusters into nanogels with cationic polymers, with TEM sizes ranging from approximately 20 nm in diameter for CS-encapsulated AgNC to 100 nm for poly(allylamine hydrochloride)-coated AuNC (Goswami *et al*., 2016; Liu *et al*., 2021; Yahia-Ammar *et al*., 2016; Zhu *et al*., 2019). PEGylation appeared to disrupt the formation of the circular nanogels, as shown in Figures 4.7C and D. These results may correlate with the apparent absence of AIE as observed for the PEGylated FAuNC in Figure 4.5.

While TEM may provide important structural information about the NC, it has two major shortcomings. Since staining of the FAuNC solutions was not conducted, the images only provide the sizes of the metallic AuNC excluding the ligands. Moreover, since solutions are air-dried before analysis, TEM provides the NP size in the dry state; however, the "wet" size of the NP in solution may differ from the "dry" size. This is especially important for polymeric nanogels, which may swell in solution. Thus, the AuNC and FAuNC size was also assessed using nanoparticle tracking analysis (NTA), which further provides the zeta potentials of the NC.

4.2.3.2. NTA sizing and zeta potential

A more biologically relevant estimate of AuNC and FAuNC properties in solution may be obtained using NTA, which provides an indication of the NP size and charge in solution. The hydrodynamic diameter given by NTA, which takes into account any ligands present on the NP surface as well as the electronic double layer (EDL) of ions that forms around NP in solution, is a more accurate estimation of the size of functionalised NP than given by TEM (Maguire *et al*., 2018). The polydispersity index (PI) is an indication of the uniformity of the solution, with values ranging from 0, indicating uniformity, to 1, indicating polydispersity. PI values below 0.2 are generally accepted as being indicative of monodisperse solutions (Danaei *et al*., 2018). NTA further provides the zeta potential, which is the potential at the slipping plane between the EDL and the surrounding solution. Measurement of the zeta potential in

deionised water can be used as an indication of the magnitude of the surface charge of the NP, or the Nernst potential (Radomska-Soukharev, 2007). The zeta potentials, PI, and hydrodynamic diameters of AuNC and FAuNC are shown in Table 4.2.

Table 4.2: Sizes and zeta potentials of AuNC and FAuNC as determined using NTA.

	NC			**Nanocomplex**		
	Size (nm ± SD)	PI	Zeta potential (mV ± SD)	Size (nm ± SD)	PI	Zeta potential (mV ± SD)
AuNC	73.6 ± 4.7	0.13	-19.5 ±7.5	-	-	-
AuCS	267.8 ± 34.4	0.10	31.9 ± 0.1	97.7 ± 8.0	0.28	-8.0 ±0.2
AuCS-1% PEG	194.5 ± 24.7	0.16	13.9 ± 0.3	108.5 ± 16.2	0.23	-0.8 ± 0.9
AuCS-2% PEG	97.5 ±9.2	0.20	17.1 ± 2.2	151.5 ±0.3	0.23	-1.6 ± 0.0

The hydrodynamic diameter of the uncoated AuNC was observed to be 73.6 nm, much larger than the size of 1.86 nm determined using TEM. This large discrepancy is likely due to the hydrodynamic diameter including the bulky GSH molecules capping the AuNC. Rogers *et al*., (2018) suggested that larger NTA and DLS than TEM sizes for AgNP may result from inclusion of the capping agent or from aggregation. Since NTA measures the light scattered by NP, it is also possible that the hydrodynamic size result was biased towards larger NC or aggregates that may have appeared brighter than individual AuNC, which may have scattered only small amounts of light due to their ultrasmall size. The zeta potential of uncoated AuNC was determined to be strongly negative (-19.5 mV) due to the presence of anionic GSH peptides capping the NC.

Functionalisation with CS led to an increase in the hydrodynamic diameter and zeta potential to 267.8 nm and +31.9 mV, respectively. The positive surface charge indicates that the anionic AuNC had successfully become encapsulated within the CS polymer to form cationic nanogels. The large size may indicate aggregation. However, the hydrodynamic diameter of nanogels is often reported to be significantly larger than the TEM size (Goswami *et al*., 2016; Guaresti *et al*., 2020; Kumar *et al*., 2016; Radnia *et al*., 2021). This difference can be attributed to the swelling behaviour displayed by nanogels in aqueous solutions, which is affected by the

different sample preparation procedures before NTA and TEM analysis. In aqueous solutions, CS hydro- and nanogels become hydrated and swell as water molecules move into the nanogel and interact with free hydrophilic amine groups (Ahmadi *et al*., 2015). NTA thus provides the size of this swollen nanogel. TEM, in contrast, reports the size of the dehydrated, collapsed nanogel, as samples are air-dried before viewing. The high swelling capacity of the AuCS highlights its high loading capacity and potential as a delivery vector.

FAuNC displayed smaller hydrodynamic diameters and lower zeta potentials than AuCS following PEGylation, confirming the addition of PEG chains to the amine groups of CS. The hydrodynamic diameters decreased in a grafting density-dependent manner, to 194.5 nm for AuCS-1% PEG and 97.5 nm for AuCS-2% PEG. The swelling behaviour of nanogels is dependent on their physicochemical properties, and is influenced by factors such as crosslinking and charge density (Neamtu *et al*., 2017). Abolmaali *et al*., (2016), for example, observed crosslinked PEGylated L-histidine-substituted PEI nanogels to display a smaller size than uncrosslinked nanogels. Increasing crosslinking ratios further reduced nanogel size. Reduced swelling capacity has also been observed for increasing grafting densities of PEG (Tamura *et al*., 2011).

Decreased surface charges of cationic NP are also expected following PEGylation, as the PEG molecules interact with, and thus reduce the number of, free protonable amine groups; and shield the positive surface charge. Buschmann *et al*., (2013) also noted that bulky ligands such as PEG may significantly reduce the zeta potential by moving the slip plane further away from the NP surface. PEGylation thus brings the zeta potential closer to neutral. It is, however, unexpected for lower PEG grafting density of 1% to have reduced the zeta potential to a greater degree than the 2%. Higher PEG grafting densities have generally been observed to lower zeta potentials (Gu *et al*., 2020; Kumar *et al*., 2014; Tamura *et al*., 2011). The AuCS-1% PEG may have assumed a different conformation that shielded the surface charge to a greater degree than the AuCS-2% PEG.

The zeta potentials of all nanocomplexes dropped to negative or close to neutral, indicating successful complexation with siRNA. As with the uncomplexed FAuNC, PEGylation shielded the surface charge, resulting in increased, near neutral zeta potentials compared to the AuCS/siRNA. Rudzinski *et al*., (2016) similarly noted a near neutral zeta potential on PEGylated CS nanocomplexes, which was attributed to the shielding effect of PEG and the low N:P ratio. The AuCS and AuCS-1% PEG formed highly condensed nanocomplexes, as

suggested by the decrease in hydrodynamic diameter following complexation: the AuCS decreased from 267.8 nm to 97.7 nm, and the AuCS-1% PEG decreased from 194.5 nm to 108.5 nm. Smaller sizes following complexation have been observed for CS nano- and hydrogels, and have been attributed to the strong interaction between the cationic nanogel and anionic nucleic acid, which promotes the formation of smaller, more condensed nanocomplexes (Abdul Ghafoor Raja *et al*., 2015; Radnia *et al*., 2021). In contrast, the AuCS-2% PEG increased in size following complexation. This may be due to its smaller size (97.5 nm) and limited swelling capacity in solution compared to the other FAuNC, which may have limited its condensation ability.

Zeta potential is often used as an indication of NP stability. According to the classical DLVO theory, colloidal stability is dependent on the net force of attractive van der Waals forces and repulsive electrostatic forces (Hill & Sarkar, 2017). NP with sufficiently high potentials will be able to repel each other, thus preventing aggregation, while those with low potentials will be unable to overcome the attractive forces and agglomerate. Generally, zeta potentials of >±30 mV, ±20-30 mV, ±10-20 mV, and ±0-10 mV are considered to be highly stable, moderately stable, relatively stable, and highly unstable, respectively (Bhattacharjee, 2016). According to these criteria, both the uncoated AuNC and AuCS can be classified as highly stable, while the PEGylated NC are only relatively stable. However, it is important to note that the DLVO theory does not take into account additional forces acting between colloids, such as the presence of steric stabilisers. Thus, while PEGylation reduces the magnitude of the zeta potential and the electrostatic repulsion between NP, it confers stability by physically preventing interactions between the NP.

4.3. Binding studies

The ideal vector for gene delivery should be able to strongly bind nucleic acids and protect them from degradation by circulating serum nucleases. To assess these qualities in the FAuNC, the band shift, EtBr intercalation, and nuclease protection assays were conducted.

4.3.1. Band shift assay

The ability of the FAuNC to bind siRNA was assessed using the band shift, or gel retardation, assay. This assay is dependent on the formation of an electroneutral complex when a set amount of anionic siRNA (0.30 μg) has been completely bound and neutralised by the cationic FAuNC.

The migration of these complexes is thus hindered during gel electrophoresis. The optimum ratio at which all siRNA is bound, as well as the ratios above (supra-optimum) and below (sub-optimum) the optimum, were used in further assays (Table 4.3). The agarose gel images of the endpoints are shown in Figure 4.8. Binding can be observed as a decrease in the fluorescence of the free siRNA, with endpoints being indicated by the absence of a free siRNA band.

Table 4.3: The sub-optimal, optimal, and supra-optimal siRNA:FAuNC ($^{w}/_{w}$) ratios determined using the band shift assay.

	Sub-optimal	Optimal	Supra-optimal
AuCS	1:2	1:2.5	1:3
AuCS-1% PEG	1:10	1:10.5	1:11
AuCS-2% PEG	1:8	1:8.5	1:9

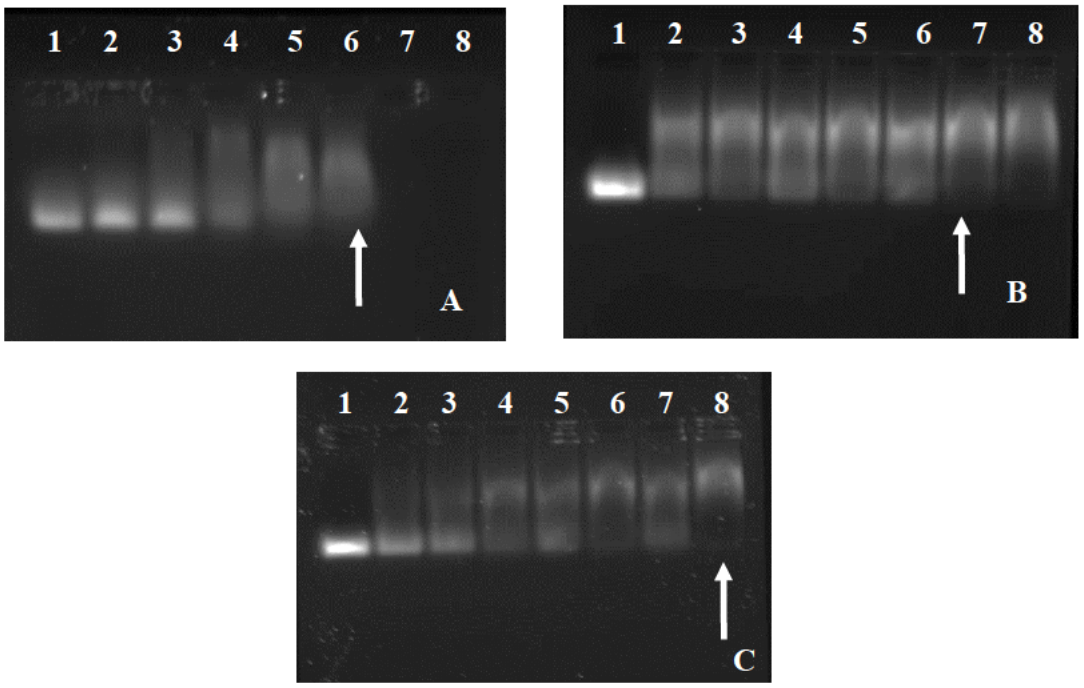

Figure 4.8: Band shift assay results for A) AuCS, B) AuCS-1% PEG, and C) AuCS-2% PEG run on a 2% agarose gel. Lane 1 contains uncomplexed siRNA, lanes 2-8 contain increasing siRNA:FAuNC weight ratios. Endpoints are indicated by arrows.

The gel images show that FAuNC were able to bind the siRNA. The AuCS were capable of completely binding the siRNA at a relatively low binding ratio of 1:2.5 (Figure 4.8A). This efficient binding is due to their high charge density and zeta potential, which promoted interactions with the siRNA. The high swelling capacity suggested by NTA measurements may have further allowed siRNA to move and bind within the nanogels.

The addition of PEG to the AuCS increased the binding ratios to 1:10.5 and 1:8.5 for AuCS-1% PEG and AuCS-2% PEG, respectively (Figure 4.8B and C). These results correspond with the significantly reduced zeta potentials observed for the PEGylated FAuNC compared to AuCS, which suggested that these FAuNC may exhibit weaker interactions with siRNA. Both PEGylated FAuNC were nevertheless able to completely complex the siRNA, despite their reduced zeta potentials. The mechanisms by which PEGylation reduces the zeta potential – by reducing the number of free positive groups and shielding the surface of the vector – also inhibit interactions with nucleic acids, and the addition of PEG to cationic polymers has thus often been reported to reduce their nucleic acid binding abilities. Le Bohec *et al*., (2019) suggested the weakened DNA binding displayed by PEGylated aminoethyl-based polyacrylates was due to the PEG preventing access to the positive groups. PEGylation has similarly been reported to increase the siRNA binding ratios of PLL (Guo *et al*., 2012) and interfere with siRNA encapsulation by CS NP (Rudzinski *et al*., 2016). It is also possible that PEGylation may have reduced siRNA binding by inhibiting the swelling capacity of the AuCS nanogel structure, which may have exposed both internal and external surfaces of the nanogel for siRNA binding.

Studies have also observed increasing PEG grafting densities to further increase binding ratios. Huo *et al*., (2015), for example, reported increasing siRNA binding ratios ($^{W}/_{W}$) of PEGylated polyasparthydrazide derivatives of 1:50, 1:75, 1:150 for grafting densities of 1%, 3% and 5%, respectively. Similar observations have also been made for 2% and 5% PEG-grafted AuNP (Daniels & Singh, 2019) and liposomes (Daniels *et al*., 2011); and 1% and 5% PEG-grafted 6-amino-6-deoxy-curdlan (Altangerel *et al*., 2016). It was thus unexpected that the AuCS-1% PEG bound the siRNA at a higher ratio than the AuCS-2% PEG. The lower grafting density and higher swelling capacity of the AuCS-1% PEG might have been expected to lead to a lower binding ratio. However, this result does correlate with the lower zeta potential displayed by the AuCS-1% PEG compared to the AuCS-2% PEG. It is possible that the lower surface charge displayed by the AuCS-1% PEG reduced interactions between the external surface of the AuCS-1% PEG and the siRNA, and more vector was thus required to completely bind the siRNA.

4.3.2. Ethidium bromide (EtBr) intercalation assay

Efficient nucleic acid condensation facilitates the formation of small nanocomplexes in which the payload is protected from degradation; however, efficient siRNA condensation is hampered by the short, rigid structure and low charge density of the oligonucleotide (Hong *et al.*, 2018). Moreover, siRNA that is condensed too tightly by the vector may be prevented from releasing into the cytoplasm following cellular uptake, thus reducing transfection efficiency (Zhang *et al.*, 2018b). The EtBr intercalation assay was thus conducted to assess the abilities of the FAuNC to condense siRNA. EtBr is a fluorescent dye that emits strong fluorescence when intercalated between the bp of double-stranded nucleic acids. The assay is dependent on the decrease in fluorescence intensity that occurs when siRNA-bound EtBr is displaced upon complexation by cationic polymer-coated vectors. The addition of increasing amounts of NP leads to a plateau or point of inflection, at which the siRNA is completely condensed by the vector. The graphs obtained from the assay are shown in Figure 4.9. Table 4.4 shows the maximum dye displacement and siRNA:FAuNC weight ratios at the points of inflection.

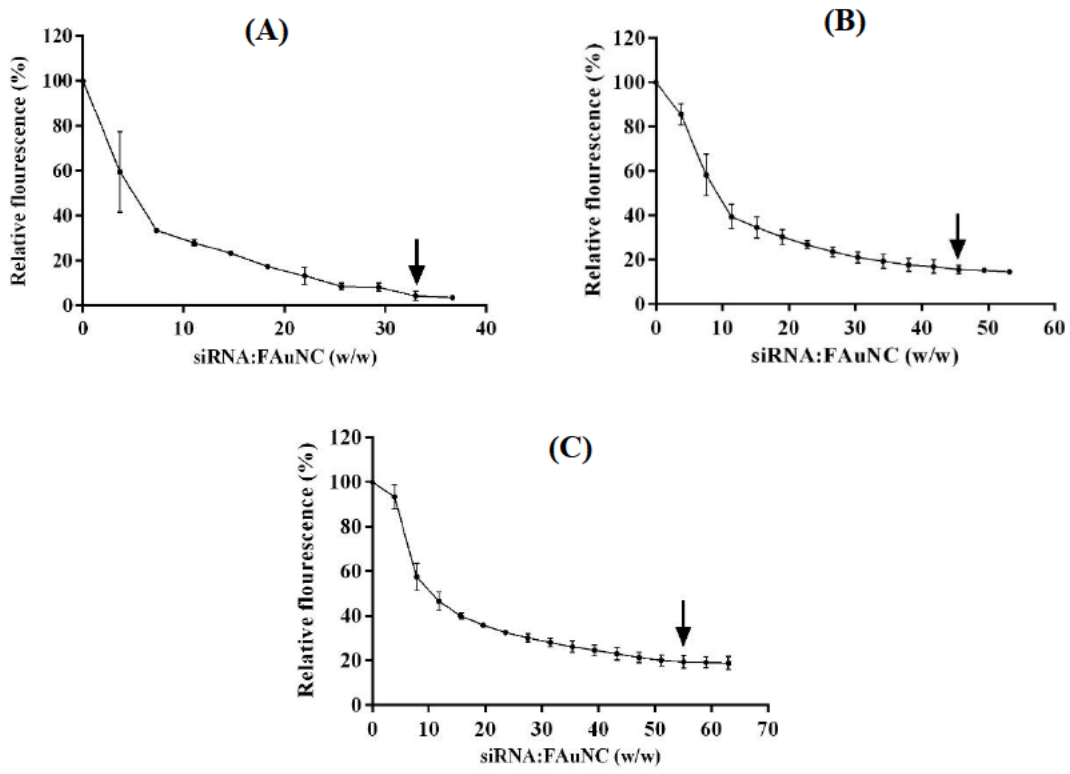

Figure 4.9: EtBr intercalation assays for A) AuCS, B) AuCS-1% PEG, and C) AuCS-2% PEG. Points of inflection are indicated by arrows.

Table 4.4: The siRNA:FAuNC ($^{w}/_{w}$) ratios and decays in fluorescence observed at the point of inflection for all nanocomplexes in the EtBr intercalation assay.

Nanocomplex	siRNA:FAuNC ($^{w}/_{w}$) at endpoint	Maximum dye displacement (%)
AuCS	1:33	95.6 ± 2.1
AuCS-1% PEG	1:45.6	84.4 ± 1.8
AuCS-2% PEG	1:55.1	80.6 ± 2.9

All FAuNC were able to condense the siRNA to a significant degree, with fluorescence decays of 80% and above. The AuCS displayed the strongest condensation ability of all FAuNC, condensing the siRNA at the lowest siRNA:FAuNC ratio (1:33) and to the greatest degree (95.6% dye displaced). This correlates with the strong binding ability displayed by the AuCS in the band shift assay and is in accordance with the NTA results for the AuCS, which displayed a highly positive charge promoting siRNA condensation and formed the most compact nanocomplexes out of all FAuNC tested.

Some studies have reported improved or similar nucleic acid condensation by PEGylated NP compared to their unPEGylated counterparts (Sutton *et al*., 2006; Urbiola *et al*., 2018). However, PEGylation may also interfere with condensation by reducing the number of positive groups available to interact with the siRNA, or by sterically interfering with siRNA condensation. Bhang *et al*., (2018) reported reduced fluorescence decay for PEGylated poly(disulfide spermine) polyplexes compared to unPEGylated polyplexes at equivalent N/P ratios, which was attributed to the reduced cationic density in PEGylated polymers. PEG-PEI has also been reported to fully condense pDNA and siRNA at higher N/P ratios than unmodified PEI (Merkel *et al*., 2009a, 2009b). In this study, PEGylation inhibited the ability of the FAuNC to condense siRNA in a grafting density-dependent manner, with PEGylated FAuNC plateauing later and at lower fluorescence decays than AuCS nanocomplexes (Table 4.4). This correlates with the reduced zeta potentials and larger nanocomplex sizes observed for the PEGylated FAuNC compared to AuCS. It is also possible that different structure of the PEGylated FAuNC compared to the AuCS, as suggested by TEM, may have contributed to their reduced condensation abilities. The circular structure of the AuCS may have allowed condensation into compact nanocomplexes; however, the addition of PEG disrupted the formation of the circular nanogels and may have thus disrupted condensation into small nanocomplexes.

The higher condensation ability of AuCS-1% PEG deviates slightly from the band shift assay results, where it showed inferior binding compared to the AuCS-2% PEG. It should be noted that, despite its lowered surface potential, the AuCS-1% PEG still contain more available amine groups than the AuCS-2% PEG due to the lower number of PEG molecules binding the CS. This higher charge density may have allowed it to condense the siRNA to a greater degree than the AuCS-2% PEG.

The siRNA:FAuNC ($^{w}/_{w}$) ratios at the points of inflection are notably higher than those obtained in the band shift assay. This discrepancy occurs due to the band shift assay measuring charge neutralisation rather than EtBr exclusion from the siRNA. However, this result suggests that the siRNA is relatively poorly condensed at the optimum weight ratios obtained in the band shift assay. This could be beneficial, as less tightly condensed siRNA will dissociate more rapidly from the vector following uptake. This principle has been demonstrated in early studies by Forrest *et al*., (2004) and Gabrielson and Pack, (2006), who reported acetylation of PEI to improve transfection efficiency by lowering the charge density, thus weakening the interactions between PEI and DNA and promoting unpackaging. Since RNAi occurs in the cytoplasm, rapid siRNA dissociation from the vector is vital for efficient gene silencing (Shim *et al*., 2010). On the other hand, siRNA that is loosely bound by the vector may be accessible to degradation by circulating nucleases. To verify the protective capabilities of the FAuNC at the optimum ratios, a nuclease protection assay was conducted.

4.3.3. Nuclease protection assay

The nuclease protection assay assessed the ability of the FAuNC to protect their siRNA payload from degradation by RNase A. Nanocomplexes were incubated with RNase A for 2 hours at physiological temperature and thereafter treated with SDS to release siRNA from the FAuNC. The integrity of the released siRNA was then analysed on an agarose gel. The results are shown in Figure 4.10.

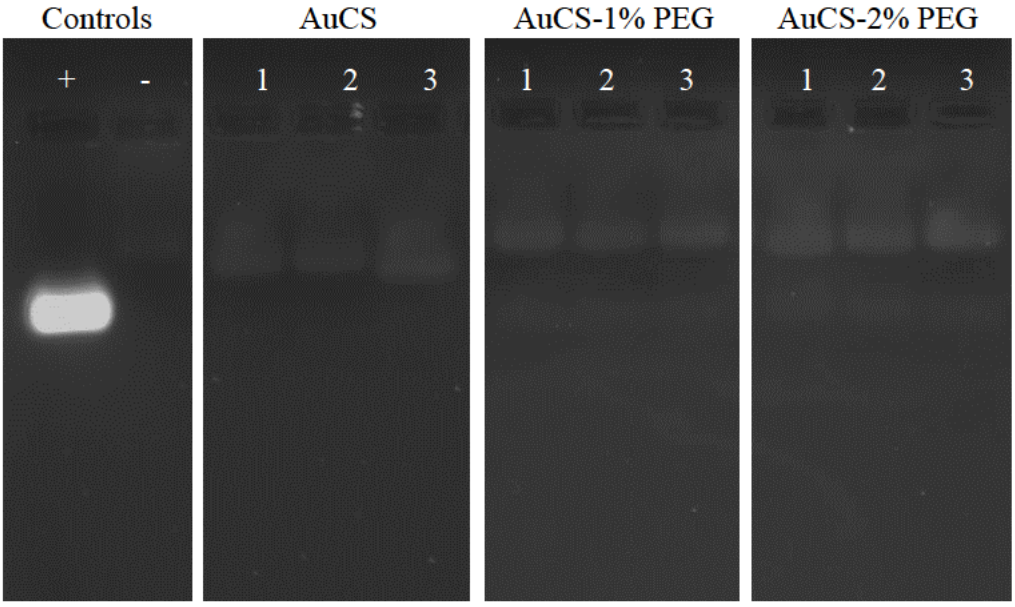

Figure 4.10: RNase protection assay for FAuNC nanocomplexes. +) Positive control of untreated siRNA; -) negative control of RNase-treated siRNA; lanes 1, 2, and 3 contain the sub-optimal, optimal, and supra-optimal ratios, respectively, of the indicated FAuNC.

From lane 2 Figure 4.10, it can be seen that naked siRNA was fully degraded following a 2 hr incubation with RNase A. In contrast, the FAuNC were capable of protecting the siRNA from complete degradation, as indicated by the presence of bands in lanes 1-3 for the FAuNC samples. This agrees with the strong condensation abilities of the FAuNC as observed in intercalation studies, which would have inhibited RNase access to the siRNA. The bands are significantly fainter and show reduced mobility compared to the free siRNA in the positive control. The faintness may result from partial degradation, or improper release of the siRNA from the FAuNC by the SDS treatment. SDS is an anionic surfactant used to destabilise the nanocomplex and release the nucleic acids and was added to a final concentration of 0.5%. However, this concentration may not have been sufficient to fully release the siRNA from the FAuNC. Ishii *et al*., (2001), for example, only observed complete release of plasmids from CS nanocomplexes at SDS concentrations of 1% and above. Incomplete siRNA release may also

account for the reduced mobility of the band, which may indicate to the presence of a complex between the cationic FAuNC and polyanionic SDS. A similar observation was made by Zhang *et al*., (2006) for siRNA released from liposomes through SDS treatment. They attributed the reduced siRNA mobility to the formation of complexes between the siRNA, SDS, cationic lipid molecules, and serum components, which would have had a higher MW and more cationic charge than free siRNA and thus migrated slower than free siRNA. It may be noted that no smears can be seen on the lower end of the gel, which may suggest that the siRNA was not degraded.

The AuCS were able to provide protection from complete degradation without the need for stabilisers. This may have been due to incorporation of the siRNA into the nanogel, where it may have been less exposed to RNases. The bound siRNA may also have assumed a conformation that prevented RNase binding: Liu *et al*., (2015) attributed protection by red fluorescent protein/CS NP to stiffening of the siRNA, which prevented it from binding the active site of RNase. Protection by the PEGylated FAuNC may thus be due a combination of compaction by CS and stabilisation by PEG, as suggested by Guzman-Villanueva *et al*., (2014). Some studies have reported improved protection by PEGylated polymers compared to unPEGylated polymers (Mao *et al*., 2006; Miteva *et al*., 2015). This does not appear to have been the case for the PEGylated FAuNC - as shown in Figure 4.10, the bands for the PEGylated FAuNC appear to be of the same intensity as the bands for the AuCS. This suggests that both unPEGylated and PEGylated FAuNC provided a similar degree of protection against RNase degradation. However, it is possible that the effects of PEGylation may be more apparent when tested in an *in vivo* setting, where the PEG chains may provide greater protection against degradation by preventing nanocomplex destabilisation in the plasma.

Overall, the FAuNC synthesised in this study were shown to be capable of binding, condensing, and protecting siRNA. While PEGylation reduced zeta potentials and significantly inhibited interactions with siRNA compared to the unPEGylated AuCS, it did not significantly affect siRNA condensation and protection. Thus, the FAuNC were investigated further in *in vitro* studies.

4.4. *In vitro* cell culture assays

4.4.1. MTT cytotoxicity assay

The MTT assay is dependent on the reduction of 3-(4,5-dimethylthiazol-2-yl)-2,5-diphenyltetrazolium bromide dye (MTT) by mitochondrial and cell plasma enzymes of viable cells to purple formazan crystals (Präbst *et al*., 2017). Solubilisation of the crystals by DMSO produces a purple solution, which may be measured spectrophotometrically at 550 nm. The intensity of the solution is an indication of the degree of MTT reduction, and, by extension, the number of viable cells present. MTT assays were conducted using FAuNC complexed with non-targeted siRNA (NT siRNA), allowing for assessment of the toxicity of the FAuNC vector. The results are shown in Figure 4.11.

Nanocarriers for siRNA delivery should ideally be non-toxic. Thus, any adverse effects observed after transfection can be attributed to the siRNA mediated silencing. According to the International Standards Organisation, medical devices that reduce cell viability by 30% or more can be considered cytotoxic (ISO, 2009). From Figure 4.11, it can be seen that viabilities remained above this threshold, indicating that all nanocomplexes were non-toxic in the cell lines tested. The lowest viability was observed in MCF-7 cells following treatment with the sub-optimal ratio of AuCS-1% PEG, which inhibited growth by approximately 22.5% (Figure 4.11B). In MDA-MB-231 cells, treatment with AuCS-1% PEG was observed to lead to slightly reduced viabilities (83-86%) as compared to treatment with AuCS and AuCS-2% PEG, where viabilities remained above 90%. Minimal toxicity was observed in the non-cancer HEK293 cells, with viabilities close to or exceeding the control for all FAuNC (Figure 4.11A). The LF3K complexes were similarly well tolerated, with the lowest viability following LF3K treatment being 80.1% in MCF-7 cells ($p<0.01$).

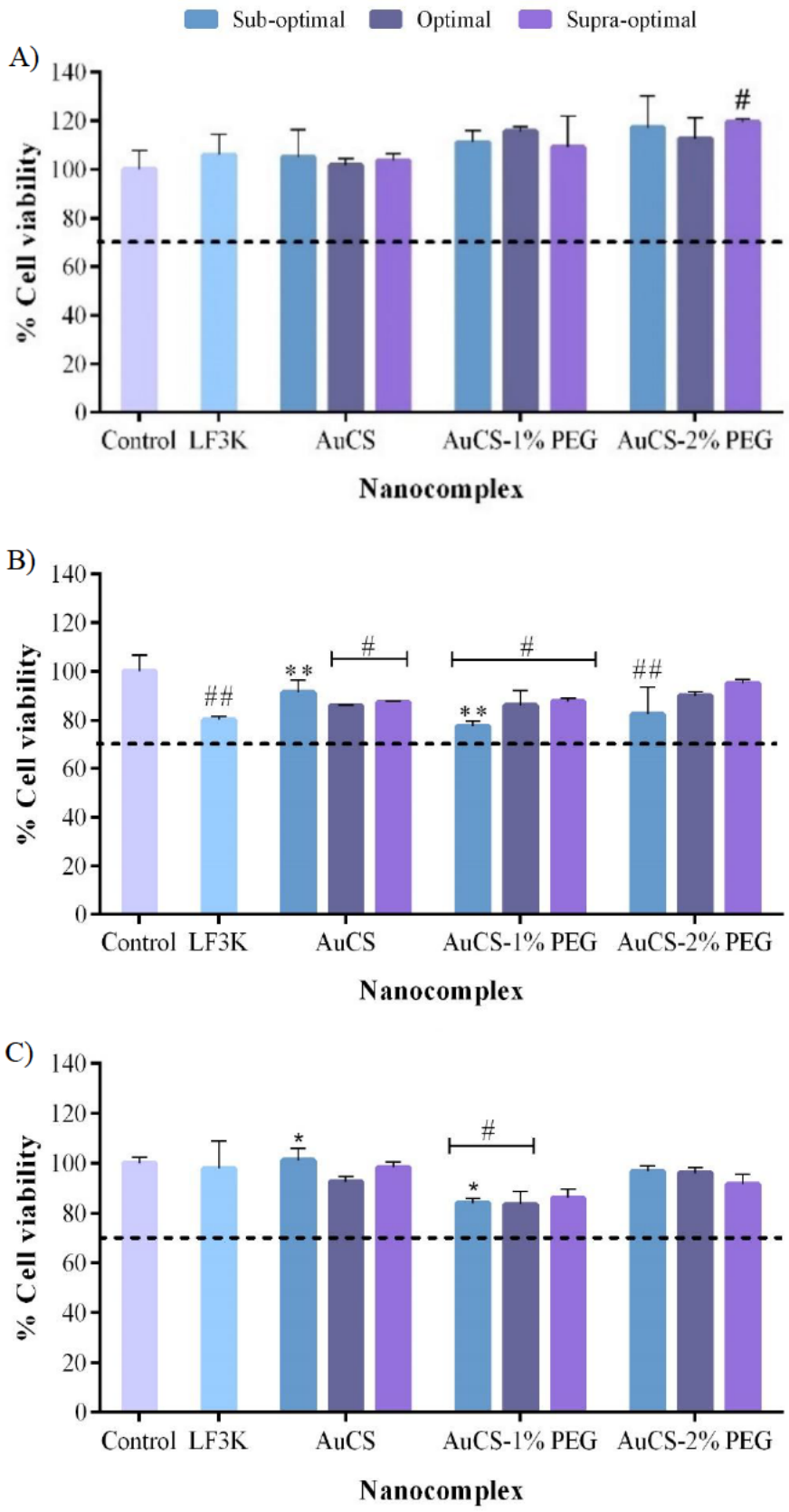

Figure 4.11: MTT assay results in the A) HEK293, B) MCF-7, and C) MDA-MB-231 cell lines. *p<0.05 was considered statistically significant between nanocomplex ratios; #p<0.05, ##p<0.01 were considered statistically significant vs. the control.

Several studies have reported LF3K to induce toxicity. This toxicity may be dependent on the cell line transfected and the presence/nature of the nucleic acid cargo. GFP-plasmid delivery by LF3K, for example, has been reported to show significant toxicity in the human oesophageal squamous cell carcinoma cell line KYSE-30 and the mouse myoblast cell line C2C12 (Cocchiararo *et al*., 2022; Mahmoudian *et al*., 2020); while miRNA-expressing plasmids were non-toxic in the monkey kidney cell line Vero (Zhu *et al*., 2023). Wang *et al*., (2018) demonstrated toxicity of LF3K-single strand oligonucleotide (SSO) complexes to vary among 10 mammalian cell lines. Toxicity was found to be exacerbated by the P3000 reagent required for plasmid transfection, and complexation with SSO. Differing results have also been reported for LF3K-siRNA delivery. Cytotoxicity has been reported in bladder cancer T24 cells and mesenchymal stromal cells following 72 hr and 7 day incubations, respectively (Galitsyna *et al*., 2021; Liu *et al*., 2019); while non-toxicity has been reported following a 72 hr treatment in zebrafish ZF4 cells (Hu *et al*., 2021). In this study, LF3K toxicity was found to be minimal in HEK293 and MDA-MB-231 cells after 48 hrs, with viabilities similar to the control (106% for HEK293 and 97.8% for MDA-MB-231); while MCF-7 cells showed a decrease in viability but remained above 70%. This is similar to the results of Habib *et al*., (2021), who reported LF3K-siRNA complexes to be non-toxic in MCF-7 and HT-29 cells after a 48 hr incubation.

The toxicity of AuNC is dependent on their surface coating. Some studies have reported CS-induced toxicity due to its high charge densities, which may disrupt cell membranes or interfere with intracellular enzymes. Casettari *et al*., (2010), for example, reported 50-150 kDa CS to induce dose-dependent toxicity in lung cancer Calu-3 cells. In contrast, Duan *et al*., (2018) reported viabilities of over 90% following treatment with CS-coated AuNC in MCF-7, cervical cancer HeLa, and mouse embryonic fibroblast 3T3 cells. AuNCs@CS-TPP have also been reported to be non-toxic to HeLa and liver cancer HepG2 cells (Zhuang *et al*., 2014). These results are similar to the results obtained in this study, where viabilities of 102% in HEK293, 86% in MCF-7, and 93% in MDA-MB-231 cells were observed following treatment with the optimum ratios of AuCS complexes. The AuCS's non-toxicity may be attributed to the low final concentrations of the polymer used to treat cells. The charge density and morphology of the CS would moreover have been modified by AuNC binding and complexation with nucleic acids. The AuCS nanocomplexes produced showed anionic zeta potentials and would thus not be expected to exert toxic effects as highly cationic particles might. Toxicity following FAuNC dissociation would also have been avoided due to the biodegradability of CS and non-toxicity of GSH-capped AuNC.

Several studies have reported PEGylation to improve the cytotoxicity profiles of lipophilic and polymeric vectors *in vitro*; a characteristic often attributed to PEG reducing the cationic charge of the polymer (Casettari *et al*., 2010; Lechanteur *et al*., 2016; Tamura *et al*., 2011). This was not observed in this study due to the non-toxicity of the AuCS, although PEGylated FAuNC showed slightly higher viabilities than AuCS in HEK293 cells. The non-toxic nature of the PEGylated nanocomplexes is especially important given that a much higher amount was required to fully bind the siRNA. No significant differences were seen when comparing between the two different ratios of PEG; however, some cell line specific interactions can be observed. In the HEK293 cells, PEGylation appeared to induce a density-dependent increase in cell growth. In contrast, in MDA-MB-231 cells, the AuCS-1% PEG showed lower viabilities than both the AuCS and AuCS-2% PEG. This reduced viability was significant at the sub- and optimal ratios against the control, and at the sub-optimal ratio against the AuCS ($p<0.05$). This may have been due to the higher amount of AuCS-1% PEG required to fully bind the siRNA, which may have slightly exacerbated any toxic effect displayed by the CS or PEG polymers. The 2% PEG coating seemed to attenuate any toxicity induced by the AuCS-1% PEG, possibly by greater shielding of FAuNC surface and inhibiting cellular interactions to a greater extent.

In addition to potential cytotoxicity of the carriers, siRNA delivery must also avoid adverse side effects induced by the siRNA itself. High concentrations of siRNA may induce RISC oversaturation or adverse off-target silencing, although RISC oversaturation is less likely with siRNA due the difficulties in achieving high intracellular concentrations (Varley & Desaulniers, 2021). The high cell viabilities obtained suggest that, while the FAuNC facilitated uptake of siRNA (see section 4.4.3), they were able to avoid deleterious effects that may be induced by the vector and siRNA. Overall, the low toxicity of the FAuNC indicates their suitability as delivery vectors and live cell imaging agents.

4.4.2. Ethidium bromide/acridine orange apoptosis assay

Dual ethidium bromide/acridine orange staining was performed to determine whether any reductions in cell viability observed in the MTT cytotoxicity assay were due to the induction of apoptosis in response to FAuNC treatment, or necrosis. Apoptosis is a form of programmed cell death that eliminates damaged or abnormal cells (Liu *et al*., 2015a); while necrosis is a non-specific form of cell death, and is generally undesirable as it may promote inflammation (Lekshmi *et al*., 2017). The assay is based on differential uptake of the EtBr and acridine orange dyes depending on the cell state. Acridine orange is a membrane-permeable nucleic acid dye,

which enters live cells and fluoresces green when bound to dsDNA. EtBr, in contrast, cannot permeate cell membranes and thus can only enter apoptotic or dead cells with damaged membranes, where it fluoresces orange upon DNA intercalation (Ude *et al.*, 2022). The assay was conducted using the optimum ratios in the MDA-MB-231 cell line, as it is the TNF-α-producing TNBC cell line. This allowed for confirmation of the non-toxicity of the FAuNC before investigation of the effects of anti-*TNF-α* siRNA delivery. Cells were stained and photographed 24 hrs after treatment with FAuNC complexed with NT siRNA and the apoptotic indices calculated. The results are shown in Figure 4.12, and the apoptotic indices are presented in Table 4.5.

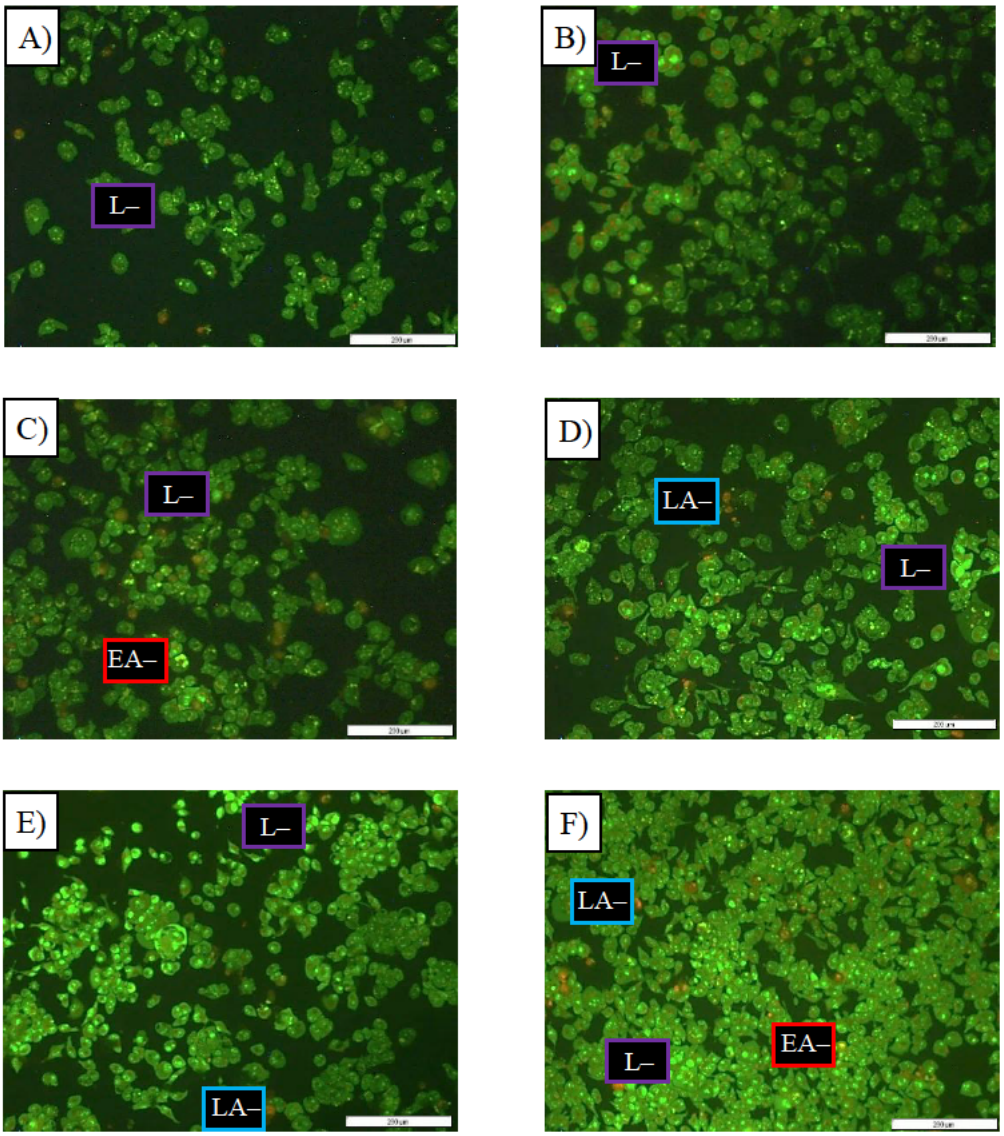

Figure 4.12: Dual EtBr/AO assay in MDA-MB-231 treated with B) free siRNA, C) LF3K, D) AuCS, E) AuCS-1% PEG, and F) AuCS-2% PEG complexes. A) represents the untreated control. The scale bar represents 200 µm for all images. L = live cells, EA = early apoptosis, LA = late apoptosis.

Table 4.5: Apoptotic indices in the MDA-MB-231 cell line following treatment with FAuNC complexes.

Treatment	Apoptotic index
Control	0.03
Free siRNA	0.02
LF3K	0.04
AuCS	0.03
AuCS-1% PEG	0.02
AuCS-2% PEG	0.04

Cells in early apoptosis show damaged or yellow-green nuclei, while cells in late apoptosis display orange/red nuclear staining. Necrotic cells appear orange/red or enlarged (Liu *et al*., 2015a). The results show that the FAuNC were non-toxic at the ratio tested. Treatment with LF3K and FAuNC complexes led to small increases in apoptosis levels; however, levels remained below 5% and were similar to the untreated control cells. Cells treated with AuCS-2% PEG showed the highest level of apoptosis of the FAuNC but were still non-toxic and comparable to the LF3K. This correlates with the results observed in the MTT cytotoxicity assay.

4.4.3. Cellular uptake

Cellular uptake was assessed qualitatively by observing uptake of FAuNC complexed with siRNA labelled with a fluorescent tag. Cells were transfected with nanocomplexes prepared at the optimum ratios, and images were taken 24 hr later using a fluorescent microscope. The images are for HEK293, MCF-7, and MDA-MB-231 cells are shown in Figure 4.13, Figure 4.14, and Figure 4.15, respectively. The presence of fluorescence indicates all FAuNC were able to effectively interact with cells. In contrast, untreated cells and cells treated with naked siRNA show no fluorescence.

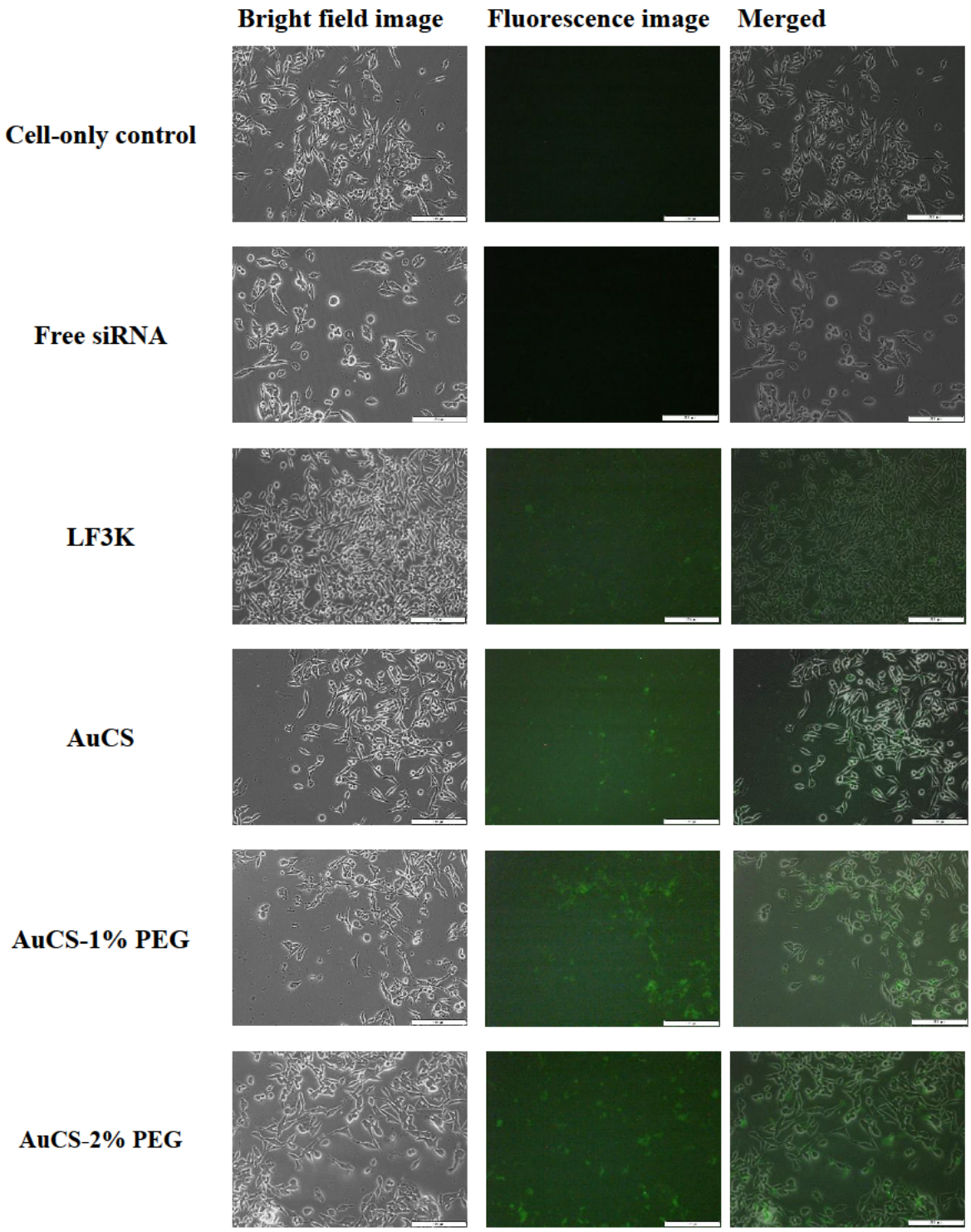

Figure 4.13: Cellular uptake of FAuNC and LF3K complexed with BLOCK-iT™ fluorescent siRNA in HEK293 cells. Images were taken on a fluorescence microscope. The scale bar represents 200 µm for all images.

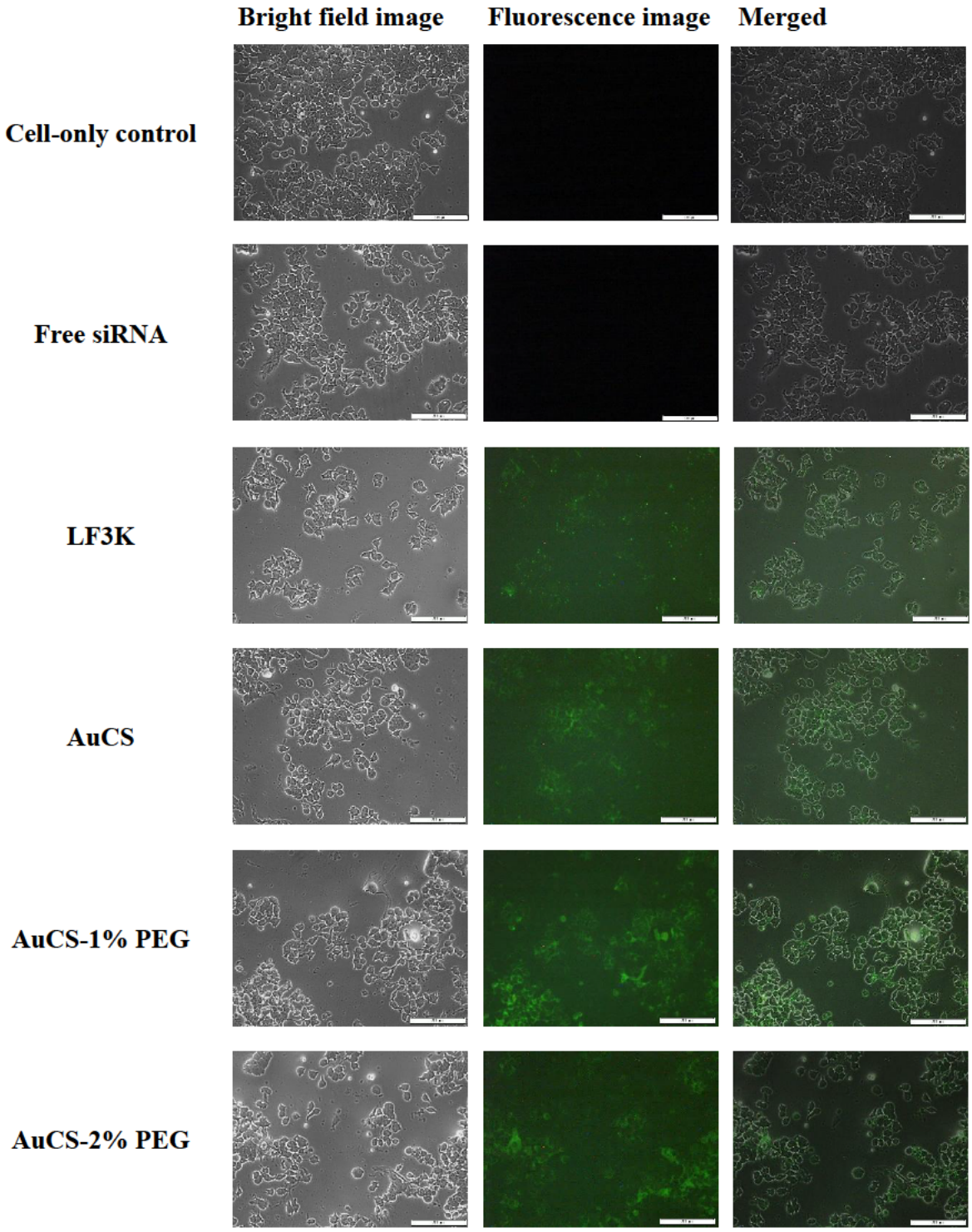

Figure 4.14: Cellular uptake of FAuNC and LF3K complexed with BLOCK-iT™ fluorescent siRNA in MCF-7 cells. Images were taken on a fluorescence microscope. The scale bar represents 200 µm for all images.

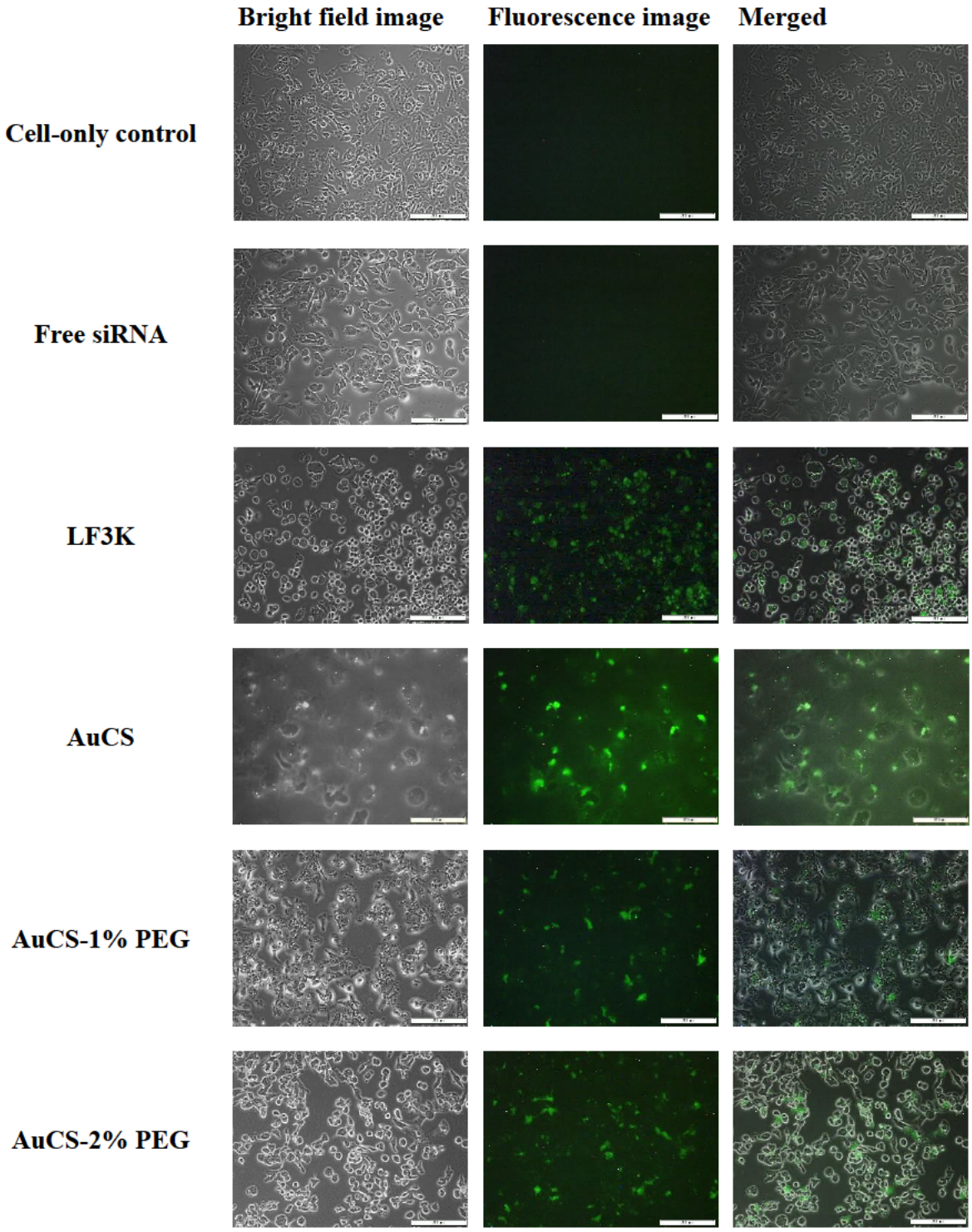

Figure 4.15: Cellular uptake of FAuNC and LF3K complexed with BLOCK-iT™ fluorescent siRNA in MDA-MB-231 cells. Images were taken on a fluorescence microscope. The scale bar represents 200 μm for all images except AuCS; scale bar represents 100 μm for AuCS.

The uptake of the nanocomplexes is notable given their weakly negative and neutral zeta potentials, which may have impaired interactions with the cell membrane. However, it is possible that the zeta potentials reported in section 4.2.3.2, which were obtained in ddH_20 at pH 7, are not an accurate reflection of the zeta potentials of the nanocomplexes in DMEM or in *in vivo* environments. Studies have reported differences in zeta potentials for gold and metal oxide NP dispersed in water and in both serum-free and supplemented medium (Limbach *et al*., 2005; Lojk *et al*., 2017; Sabuncu *et al*., 2012; Shannahan *et al*., 2013). This may be attributed to the formation of an EDL as ions interact with the NP surface, and the adsorption of serum proteins onto the NP surface, thus modifying the surface charge (Lojk *et al*., 2017). This potential difference in zeta potential may be more relevant for the non-stabilised AuCS nanocomplexes, which lack the PEG chains to shield the FAuNC surface and inhibit protein interactions. *In vivo*, the CS may also take on a more positive charge due to protonation of its amine groups in the acidic TME, thus promoting cellular interactions (Amoozgar *et al*., 2012).

Studies have reported both decreased transfection in the presence of serum, due to the formation of a protein corona (Krishnamoorthy *et al*., 2017); and increased transfection, due to binding of proteins that promote uptake (Chithrani *et al*., 2006). Proteins may interact with vectors via electrostatic, hydrophobic, van der Waals, or hydrogen bonding interactions. The charges of the FAuNC may be expected to reduce electrostatic interactions with serum proteins, as most are anionic at physiological pH and thus interact more strongly with cationic nanocomplexes (Tekie *et al*., 2020). However, as mentioned, the zeta potentials may differ in cell culture media. While CS with a high DD is regarded as hydrophilic, it may mediate hydrophobic interactions with serum proteins through hydrophobic functional groups (Bekale *et al*., 2015; Santander-Ortega *et al*., 2011). These groups may also mediate hydrogen or van der Waals bonding to serum proteins (Li *et al*., 2012b; Lü *et al*., 2018). PEGylation is expected to reduce these interactions due to its electroneutral and hydrophilic nature inhibiting electrostatic and hydrophobic interactions (Alberg *et al*., 2020). The uptake studies were conducted using DMEM supplemented with FCS. Despite potential interactions with serum proteins, the FAuNC were able to transfect the cells, indicating that they can maintain their stability in the presence of serum. This may signify their potential suitability for use in *in vivo* applications, although *in vivo* uptake studies would be required to accurately determine the effects of protein adsorption on uptake as the *in vivo* protein corona has been reported to differ from the corona formed in *ex vivo* experiments (Hadjidemetriou *et al*., 2019).

The nanocomplexes may utilise multiple endocytic pathways to enter cells. The choice of pathway is influenced by the nanocomplexes' characteristics, such as their size, composition, and rigidity. However, conflicting results have been reported regarding the influence of these factors on uptake, possibly due to differences in NP composition or between cell lines, or due to non-specific action of endocytosis inhibitors. For example, Wright *et al*., (2021) reported clathrin- and caveolae-independent uptake mechanisms for CS, mesoporous silica, and poly(lactic-co-glycolic) acid NP following siRNA knockdown of proteins involved in these pathways. This was suggested to be due to the NP sizes reaching or exceeding the maximum vesicle sizes (~100 nm and ~150 nm for caveolae- and clathrin-coated vesicles, respectively). In contrast, studies using endocytosis inhibitors have reported clathrin-dependent uptake of NP >200 nm, with larger NP (200 nm - 1 μm) being primarily internalised by caveolae-mediated endocytosis and micropinocytosis (Li *et al*., 2015b; Rejman *et al*., 2004). Clathrin-mediated endocytosis was suggested to be rapid process with an upper limit of 200 nm, while caveolae-mediated pathways were suggested to recruit additional internalisation machinery to facilitate uptake of large particles (Rejman *et al*., 2004).

Differing results have also been obtained regarding the uptake of CS and CS-coated NP. Several studies using inhibitors have reported their uptake via endocytic pathways (Apirakaramwong *et al*., 2012; Liu *et al*., 2018; Tahara *et al*., 2009; Zhao *et al*., 2015). However, siRNA knockdown of proteins involved in uptake led Pereira *et al*., (2015) to suggest that folate-targeted glycol CS nanogels primarily exploited clathrin- and caveolae-independent pathways. Macropinocytosis, an actin-dependent endocytic pathway, may also be exploited to enter cells (Pereira *et al*., 2015).

The results from these studies suggest that the FAuNC nanocomplexes may exploit several uptake pathways. All nanocomplexes displayed hydrodynamic diameters below 200 nm, with sizes of 97.7 nm, 108.5 nm, and 151.5 for AuCS, AuCS-1% PEG, and AuCS-2% PEG, respectively. This suggests that they may exploit clathrin-mediated endocytosis to enter cells; however, according to the results of Wright *et al*., (2021), the AuCS-2% PEG may have to enter via clathrin- and caveolae-independent uptake pathways. The nanocomplexes may also exploit all mentioned uptake pathways to varying degrees to enter cells.

It is also important to note that different cell types may utilise different uptake pathways. Peñaloza *et al*., (2017), for example, reported the uptake mechanisms for poly (3-hydroxybutyric acid-co-hydroxyvaleric acid) NPs to differ between HeLa cells, which utilised

endocytic and macropinocytic pathways, and ovarian cancer SKOV-3 cells, which primarily utilised endocytic-independent uptake pathways. Different cell lines may also express different amounts of endocytic proteins (Kumari *et al*., 2010).

4.4.4. Flow cytometry studies

The *in vitro* effects of *TNF-α* knockdown were investigated using flow cytometry assays. Flow cytometry is a technique that allows for analysis of the characteristics of single cells in a population based on their fluorescence profiles (McKinnon, 2018). FAuNC were complexed with anti-*TNF-α* siRNA according to the optimum ratios obtained in the band shift assay, and used to treat HEK293, MCF-7, and MDA-MB-231 cells. Following incubation, the effects of knockdown on Caspase 3/7 activation, ROS levels, and cell cycle distribution were investigated using the Guava® Muse® Cell Analyser.

4.4.4.1. Caspase 3/7 Activity

Caspases proteins are cysteine proteases which function in regulating multiple cellular processes, most notably cell death such as apoptosis (Julien & Wells, 2017). The effector caspases 3 and 7 are particularly well-known due to their involvement in the caspase cascade that initiates apoptosis. Their activation in response to *TNF-α* knockdown was evaluated using the Muse® Caspase-3/7 Kit. The kit distinguishes between live, apoptotic, and necrotic cells using a Caspase 3/7 reagent and the cell death marker 7-aminoactinomycin D (7-AAD) (Table 4.6). The Caspase 3/7 reagent is composed of a DNA-binding dye linked to a peptide containing a Caspase 3 recognition sequence. In apoptotic cells, the peptide is cleaved by active Caspase 3/7, freeing the dye and allowing it to migrate to the nucleus and bind the DNA (Cen *et al*., 2008). 7-AAD is an intercalating dye that is impermeable to the cell membrane. It thus only stains late apoptotic or necrotic cells, which exhibit weakened membrane integrity (Zimmermann & Meyer, 2011). The results for the cell lines are shown in Figure 4.16.

Table 4.6: The fluorescent profiles of live, apoptotic, and necrotic cells determined by the Muse® Caspase-3/7 kit.

	Caspase 3/7	7-AAD
Live cells	-	-
Early apoptotic cells	+	-
Late apoptotic/necrotic cells	+	+
Necrotic cells	-	+

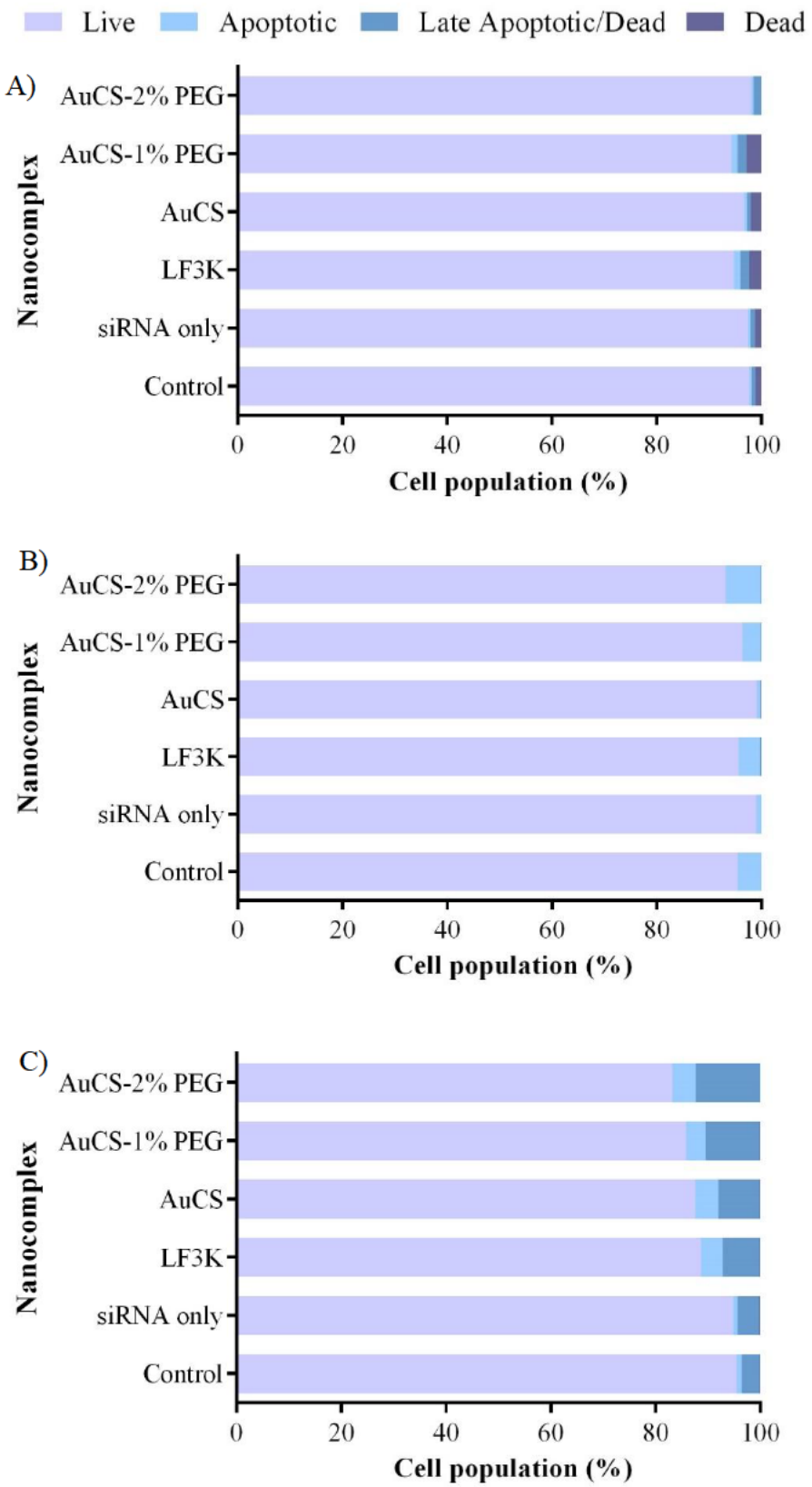

Figure 4.16: Graphical representation of the apoptotic profiles following *TNF-α* knockdown in A) HEK293, B) MCF-7, and C) MDA-MB-231 cells. Control = cell-only control; siRNA only = anti-*TNF-α* siRNA only; LF3K = Lipofectamine 3000.

The viabilities of the cell-only controls for all cells were approximately 95%, indicating that the cells were healthy. Delivery of the naked siRNA had little effect on apoptosis levels. FAuNC-mediated delivery of the anti-*TNF-α* siRNA was found to be non-toxic to the HEK293 cells. As shown in Figure 4.16A, over 94% of the cell population remained viable after treatment. Caspase 3/7 activation was similarly low in MCF-7 cells, with the proportion of live cells in all samples similar to or exceeding that of the control. In contrast, anti-*TNF-α* siRNA delivery in the MDA-MB-231 cells was observed to lead to slightly increased levels of caspase 3/7 activation compared to the control. AuCS and LF3K-mediated delivery produced similar increases in caspase 3/7 activation, leading to increases in percentage of apoptotic cells from 4.4% in the control to 12.4% and 11.3%, respectively. The PEGylated FAuNC produced slightly higher apoptosis levels of 14.1% and 16.7% for AuCS-1% PEG and AuCS-2% PEG, respectively. This result would suggest that the FAuNC were successful in delivering the anti-*TNF-α* siRNA to the MDA-MB-231 cells, where it may have induced apoptosis of the TNF-α-producing TNBC cells.

TNF-α inhibition has been reported to lead to increased apoptosis in cancer cells. Shirmohammadi *et al*., (2020) showed that treatment with the TNF-α inhibitor etanercept led to increased apoptosis in MDA-MB-231 cells, similar to the results presented in Figure 4.16C. Antibody targeting of tmTNF-α in mice with MDA-MB-231 tumours was reported by Yu *et al*., (2013) to induce caspase 8 cleavage, and thus apoptosis, in tumour cells. Delivery of anti-*TNF-α* siRNA using the lipid-based siPORT™ NeoFX™ Transfection Agent has also been reported to induce apoptosis in TNBC Hs578T cells, leading to a decrease in cell viability from 98.5% to 68.8% (Pileczki *et al*., 2012). Analyses of gene expression following knockdown showed downregulation of TRADD, indicating inhibition of TNF-α signalling; and upregulation of p53 and several genes involved in apoptosis, including TNF superfamily member 10, or TNF-related apoptosis-inducing ligand (*TRAIL*). TRAIL selectively induces apoptosis in cancer cells through the receptors TRAIL-R1 and TRAIL-R2 (Dai *et al*., 2015). *TNF-α* knockdown thus led to reduced activation of the cell growth and inflammatory pathways transcribed by NF-κB, which, together with the increased expression of TRAIL, led to activation of apoptotic pathways.

Very little necrosis was observed in the cell populations. The highest levels of necrosis were 2.2 - 2.9%, observed following treatment with LF3K and AuCS-1% PEG in the HEK293 cells (Figure 4.16A). It is thus ideal that no necrosis was observed in the MDA-MB-231 cells, which showed increased cell death in response to the treatments.

4.4.4.2. Oxidative stress

Reactive oxygen species (ROS) include hydrogen peroxide (H_2O_2), superoxide anions (O^{2-}), and hydroxyl ions (OH^-). They are produced through aerobic respiration, and play important roles in mediating signalling processes, including TNF-α signalling, and phagocytosis. However, they may also cause damage to cellular macromolecules, such as proteins, lipids and DNA, and induce transformation (Schieber & Chandel, 2014). The ROS levels following transfection were analysed using the Muse® Oxidative Stress kit, which utilises the dihydroethidium (DHE) dye that detects intracellular O^{2-} anions. Upon entry into the cell, DHE is oxidised by O^{2-} ions to 2-hydroxyethidium, which intercalates within DNA and fluoresces red (Chen *et al*., 2013). Figure 4.17 depicts the results as the percentage of the cell populations that are ROS(-) and ROS(+).

Figure 4.17A shows that the majority of the HEK293 cells had reduced oxidative stress. The percentage of the cell population with elevated ROS remained below 10% for all samples except for the PEGylated FAuNC-treated samples, which showed slightly increased ROS(+) populations of 12.1 – 13.1% compared to the control of 7.6%. Very little change in the distribution of the ROS(+) and ROS(-) populations was observed in the luminal MCF-7 cells (Figure 4.17B). Treatment in the MDA-MB-231 cells, however, was observed to produce a shift. Anti-*TNF-α* siRNA delivery by the FAuNC led to an increase in the proportion of the cell population with elevated ROS levels, from 60.8% in the control to 60.7%, 67.5% and 73.4% for AuCS, AuCS-1% PEG, and AuCS-2% PEG samples, respectively. The shifts produced by treatment with the PEGylated FAuNC were similar to that produced by LF3K, where 70.2% of cells were ROS(+). Both cancer cell lines showed a larger base ROS(+) population compared to the HEK293.

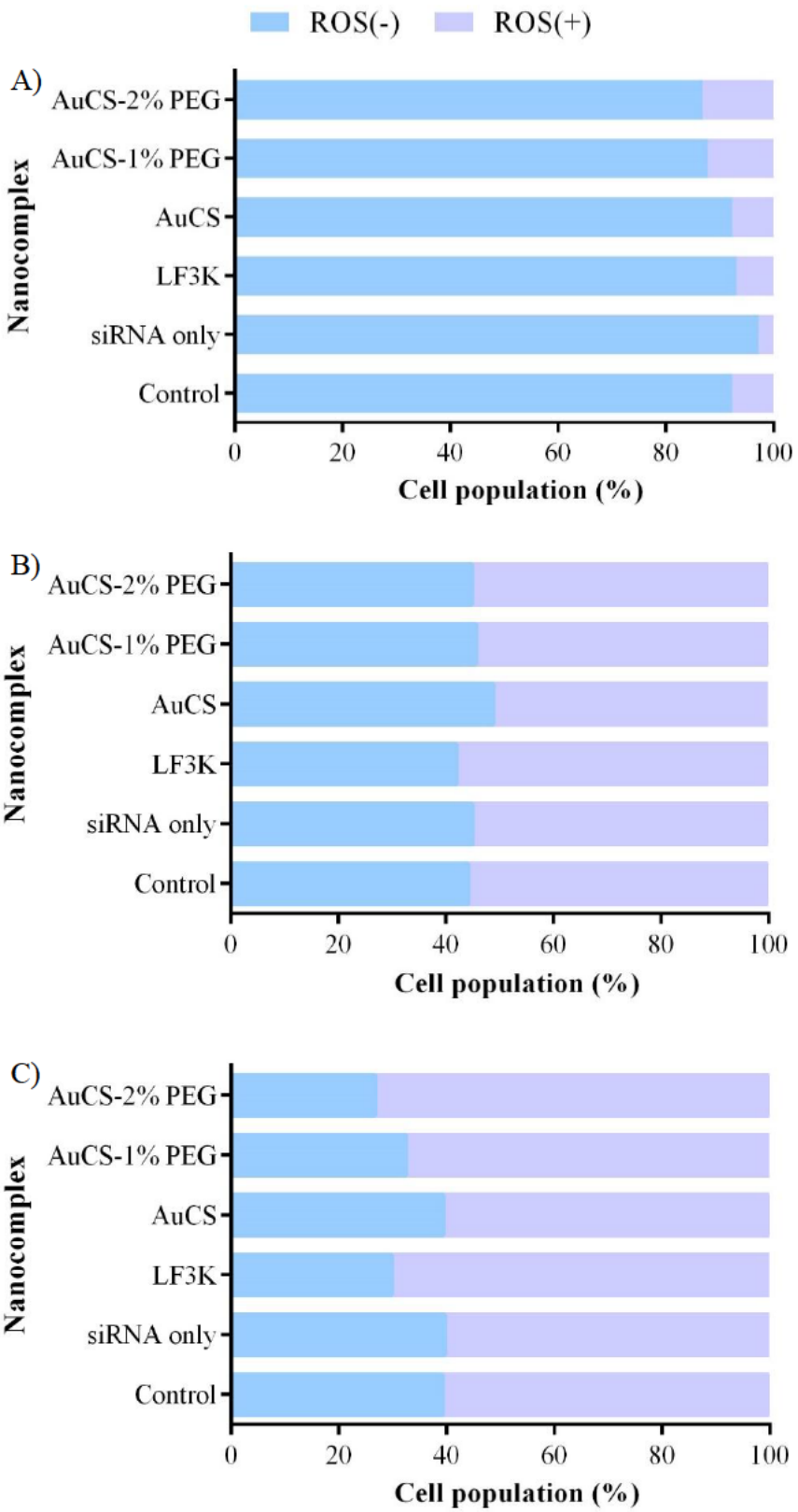

Figure 4.17: Graphical representation of the ROS levels following TNF-α knockdown in A) HEK293, B) MCF-7, and C) MDA-MB-231 cells. Control = cell-only control; siRNA only = anti-*TNF-α* siRNA only; LF3K = Lipofectamine 3000.

It is generally accepted that cancer cells produce more ROS than non-cancerous cells. Normal cells utilise ROS-scavenging systems composed of several antioxidant proteins to prevent their toxic build-up (Perillo *et al*., 2020). Several factors contribute to the increase ROS production in malignant cells. These include, increased mitochondrial activity, loss of TSGs that may have antioxidant functions, and the hypoxic and inflammatory tumour microenvironment, which contains ROS-producing macrophages (Brown & Bicknell, 2001; Reczek & Chandel, 2017). This increased oxidative stress is reflected in Figure 4.17. Less than 10% of the control HEK293 cells showed increased ROS, in contrast to the cancer cell lines where over 55% of the control population displayed elevated ROS levels.

TNF-α induces both intracellular ROS generation and antioxidant expression through NF-κB (Morgan & Liu, 2010). TNF-α-induced ROS generation is implicated in the pathology of inflammatory and cardiovascular disorders, and studies in *in vitro* and *in vivo* models have shown TNF-α inhibition to reduce oxidative stress (Carvalho-Galvão *et al*., 2019; Mattos *et al*., 2020; Zhang *et al*., 2018a). Kastl *et al*., (2014) reported TNF-α stimulation to increase mitochondrial ROS generation in liver cancer cells. ROS play a significant role in mediating NF-κB activation, and this increased oxidative stress was thus observed to lead to increased cell migration. It was thus unexpected to observe an apparent increase in the ROS(+) population in MDA-MB-231 cells in response to anti-*TNF-α* siRNA delivery. This would appear to indicate that delivery of the anti-*TNF-α* siRNA might lead to increased TNBC cell proliferation, and potentially increased TNF-α release. However, it is possible that the increased ROS in MDA-MB-231 cells correlates with the results of the other flow cytometry assays, which indicated a decrease in cell proliferation.

Cancer cells must still maintain ROS homeostasis to prevent the excessive levels inducing cell death; this is achieved by upregulating antioxidant pathways to scavenge excess ROS (Reczek & Chandel, 2018). Tumours are thus still be sensitive to exogenous treatments that induce ROS; their already elevated ROS levels are thought to make them more sensitive to these treatments than normal cells (Trachootham *et al*., 2009). Studies have linked treatment-induced ROS generation in MDA-MB-231 cells to apoptosis. Zhang *et al*., (2015) reported polyphenol extracts from the *Annurca* apple fruit to selectively induce oxidative stress in MDA-MB-231, but not non-cancer MCF10A, cells. The increased ROS levels led to sustained JNK activation, and thus apoptosis. The apparently selective pro-oxidant activity of these polyphenols may result from the higher concentration of metal ions in cancerous cells, which react with plant-derived polyphenols to produce ROS (Farhan & Rizvi, 2022). Similar results were reported by

Martino *et al*., (2019) using the isoliensinine alkaloid isolated from lotus seed embryos. Elevated ROS levels may also trigger apoptosis by damaging cellular macromolecules, or disrupting the mitochondrial membrane (Alsaedi *et al*., 2019). Thus, the elevated ROS may correlate with the increased levels of apoptosis observed in the Caspase 3/7 assay, and the decreased proliferation observed in the cell cycle assay.

It is important to note the double-edged nature of ROS therapy. Treatments that induce only moderate increases in ROS levels may promote malignancy rather than apoptosis. It is thus notable that the HEK293 cells showed no increase or very small increases in ROS levels following treatment. This would suggest that the FAuNC are non-toxic and may not significantly impact expression pathways in non-cancer cells. The effects of the increased ROS on gene expression could be more accurately determined using gene expression assays, to verify that the expression of proliferation genes was unaffected by the slight increase in ROS levels.

4.4.4.3. Cell cycle

The cell cycle is composed of four stages: a quiescent G0/G1 phase, the S phase in which DNA replication occurs, the G2 phase in which the cell prepares for mitosis, and the M phase in which the cell splits. The Muse® Cell Cycle Assay utilises the intercalating agent propidium iodide to distinguish between the different phases according to the DNA content in the cells. Cells in the G0/G1 phase will exhibit the lowest intercalation, and thus fluorescence. Fluorescence intensity will increase during the S phase as DNA replicates, until it is double that of cells in the G0/G1. This doubled intensity is indicative of cells in the G2/M phase where DNA has replicated. RNase A is included in the assay to improve the specificity of DNA binding by the propidium iodide. The results are shown in Figure 4.18, and give the proportion of the cell populations in the G0/G1, S, and G2/M phases.

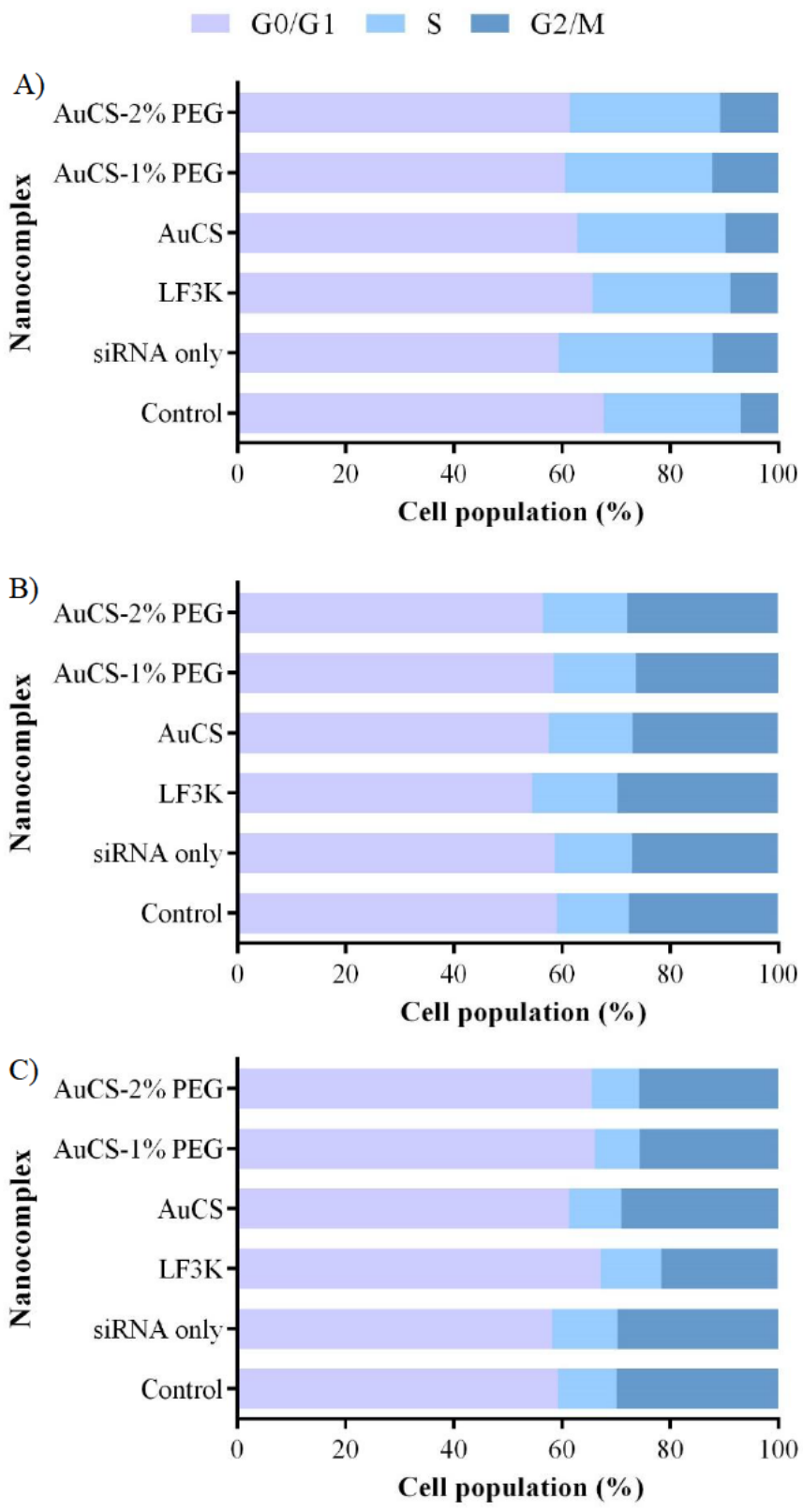

Figure 4.18: Graphical representation of the cell cycle distribution following *TNF-α* knockdown in A) HEK293, B) MCF-7, and C) MDA-MB-231 cells. Control = cell-only control; siRNA only = anti-*TNF-α* siRNA only; LF3K = Lipofectamine 3000.

In this study, the HEK293 and MCF-7 cells were minimally affected by treatment with the *TNF-α*-targeting FAuNC nanocomplexes. HEK293 cells displayed a slight increase in the proportion of cells in the S- and G2 phases as compared to the control, suggesting that the cells are actively proliferating and were not adversely affected by FAuNC delivery. In contrast, delivery of anti-*TNF-α* siRNA in MDA-MB-231 cells was observed to lead to slight increases in the proportion of cells in the G0/G1 phase, together with a slight decrease in cells in the S and G2/M phases (Figure 4.18C). This shift was minimal for the AuCS-treated cells, which showed an increase from 59.2% cells in the G0/G1 phase for the control to 61.3%. The shift was, however, slightly more prominent for cells treated with the PEGylated FAuNC, which produced shifts equivalent to that observed for LF3K-mediated knockdown. The observed proportion of cells in the G0/G1 phase following treatment was 67.1% for LF3K, 66.1% for AuCS-1% PEG, 65.5% for AuCS-2% PEG.

A shift in the distribution of the cell population in the different cell cycle phases may occur in response to DNA damage, which may prevent DNA replication from occurring or prevent entry into mitosis. Damaged cells thus undergo cycle arrest to allow for DNA repair to take place. If the damage cannot be repaired, cells may undergo permanent arrest or apoptosis (Chao *et al*., 2017). Shifts may also occur if the treatment alters the expression of genes involved in cell cycle progression. NF-κB has been implicated in the regulation of several proteins involved in cell cycle progression, including the cyclin D proteins and *c-MYC* oncogene (Ledoux & Perkins, 2014; Mussbacher *et al*., 2019). TNF-α may thus promote cell cycle progression through NF-κB activation. TNF-α treatment in MDA-MB-231 and MCF-7 cells has, for example, been reported to shift cells from the G0 to the S phase, sensitising them to chemotherapy (Wu *et al*., 2017). Several studies have also reported cell cycle arrest following *TNF-α* knockdown. Shen *et al*., (2019) observed *TNF-α*-knockout leukaemia cells to display a shift to the G0 phase as compared to wild type cells. This was accompanied by a decrease in the expression of CDC6 and CDC23 proteins, which mediate cell cycle progression. Knockout was thus suggested to lead to cell cycle arrest. A similar shift was reported in MDA-MB-231 cells, where shRNA-mediated knockdown of tmTNF-α led to an increase of cells in the quiescent G0 phase and a decrease of cells in the S phase (Zhang *et al*., 2018c). These results are similar to those shown in Figure 4.15C and suggest that PEGylated FAuNC-mediated delivery of the anti-*TNF-α* siRNA selectively induced cell cycle arrest in the TNBC MDA-MB-231 cells.

Overall, FAuNC were consistently well-tolerated in the non-cancer HEK293 cells, indicating their safety. The effects of anti-*TNF-α* delivery appeared to be selective in the TNBC MDA-MB-231 cells. Studies have reported low or absent TNF-α production in the HEK293 and MCF-7 cells (Hamaguchi *et al*., 2011). Subramoniam *et al*., (2012) has also reported no TNF-α expression in unstimulated, control HEK293 cells. This may suggest the success of the vector in delivering anti-*TNF-α* siRNA and initiating gene silencing. However, the results were minimal, and thus the extent of gene knockdown must be analysed through RT-qPCR and ELISA.

Based on the results obtained thus far, the AuCS-2% PEG were chosen for further investigation. These FAuNC displayed a nanocomplex size within the ideal range for uptake (<200 nm in diameter) and a slightly less neutral zeta potential than the AuCS-1% PEG. They showed favourable interactions with siRNA, and optimal toxicity profiles in all cell lines. The results obtained in the Muse® assays further suggest that AuCS-2% PEG-mediated anti-*TNF-α* siRNA delivery more effectively than other FAuNC while showing non-toxicity in the HEK293 cells.

4.4.5. Gene knockdown studies

Effective gene silencing requires the vector to deliver the siRNA to the cytoplasm of the target cells, where it can mediate formation of the RISC and degradation of complementary mRNA. The transfection efficiency of the AuCS-2% PEG vectors was evaluated by evaluating knockdown of the *c-MYC* oncogene, as the assays assessing *TNF-α* expression were unsuccessful and could not be optimised to provide reliable results. Knockdown was investigated in MCF-7 cells following procedures previously described (Daniels & Singh, 2019; Habib *et al*., 2021). The *c-MYC* gene is induced by oestrogen stimulation, leading to its overexpression in HR+ MCF-7 cells (Dubik & Shiu, 1988; Wang *et al*., 2011b).

The techniques of RT-qPCR and ELISA allow for sensitive and accurate determination of the expression levels of specific genes and proteins, respectively. RT-qPCR combines the techniques of RT-PCR, which utilises DNA produced through reverse transcription of mRNA as a PCR template, and qPCR, which allows for quantification of the PCR product in real time (Adams, 2020). A commonly used method for analysing the data is through relative quantification of the gene expression levels. This method, also called the $2^{-\Delta\Delta Ct}$ method, compares the expression of the target gene in the treated samples to its expression in the

untreated control sample. Thus, any changes in gene expression in response to treatment can be quantified (Adams, 2020; Livak & Schmittgen, 2001). The indirect ELISA technique was used in this study to evaluate changes in protein expression. This two-step process utilises both a primary antibody that binds the target protein, and a tagged secondary antibody that binds the primary antibody. The horseradish peroxidase (HRP) enzyme used as a tag produces a colourimetric reaction that can be measured using a spectrophotometer (Wang & Kobayashi, 2013). Relative quantification of protein expression can be determined by comparing the absorbance of treated samples to the untreated control. For both techniques, the level of *c-MYC* expression was normalised to the expression of *β-actin*, a housekeeping gene whose expression is uninfluenced by treatments. The results for the RT-qPCR and ELISA are shown in Figure 4.19A and B, respectively.

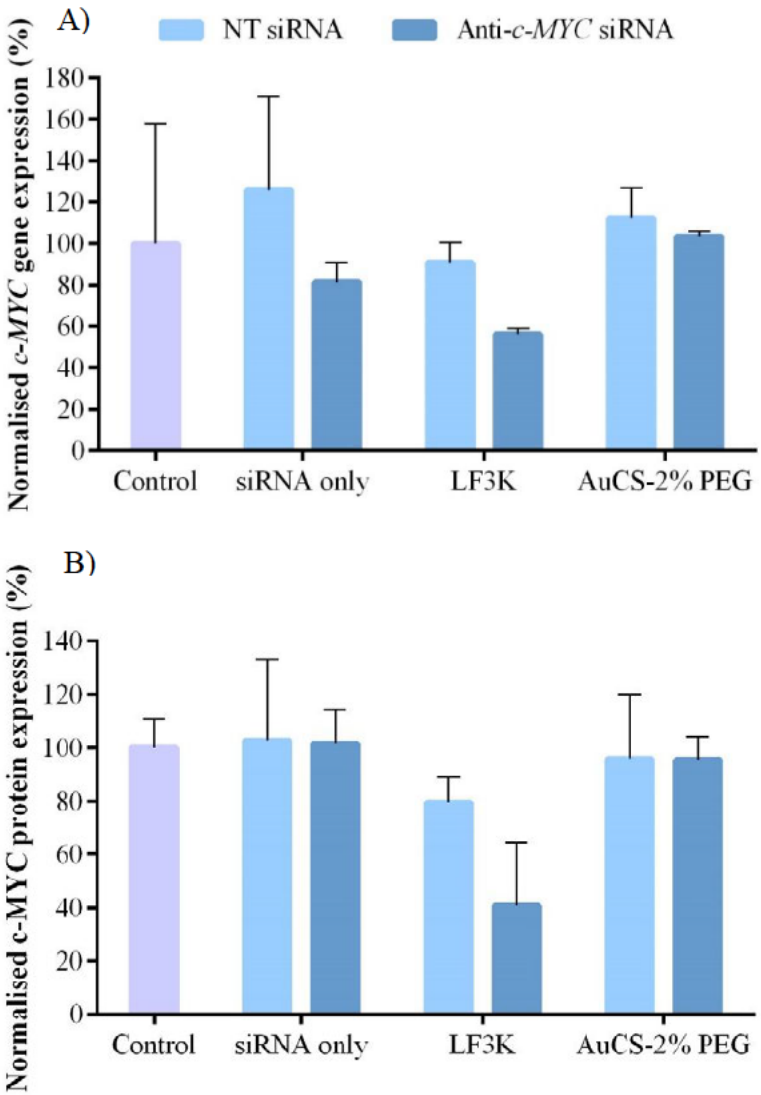

Figure 4.19: Gene knockdown studies in MCF-7 cells, showing the relative (A) gene and (B) protein expression of *c-MYC* following treatment with naked siRNA and LF3K and AuCS-2% PEG complexes. Data are presented as means ± SD (n=2).

The results show that naked siRNA had no significant effect on the level of c-MYC gene and protein expression. Cells treated with free non-targeting (NT) siRNA showed gene and protein expression levels close to or exceeding the untreated control cells, while those treated with anti-*c-MYC* siRNA showed gene and protein expression levels of 81.6% and 101.7%, respectively. This inability to induce knockdown was expected as free siRNA is highly susceptible to degradation and impervious to cellular uptake mechanisms. Both LF3K- and AuCS-2% PEG-mediated transfection with the NT siRNA did not significantly affect *c-MYC* levels. In contrast, LF3K delivery of anti-*c-MYC* siRNA led to a large decrease in gene and protein expression. However, anti-*c-MYC* delivery with the AuCS-2% PEG did not lead to the expected decrease in *c-MYC* expression levels. The gene and protein expression levels were found to be 103.6% and 95.3%, respectively. This result suggests that transfection with the AuCS-2% PEG did not efficiently induce *c-MYC* knockdown as the LF3K did.

LF3K is a commercially available transfection agent that is often considered to be a gold standard in transfection (Mikheev *et al*., 2020). It was thus used as a positive control for comparison with the FAuNC. Lipofectamine is a liposomal vector, composed of the lipids 2,3-dioleoyloxy-N- [2(sperminecarboxamido) ethyl]- N,N-dimethyl-1-propaniminium trifluoroacetate (DOSPA) and 1,2-dioleoyl-sn-glycerophosphoethanolamine (DOPE) in a 3:1 (w/w) ratio, although the exact composition of LF3K is proprietary (Ma *et al*., 2016; Yang & Huang, 1998; Zhang *et al*., 2021c). DOSPA is a cationic lipid that promotes interactions with negative nucleic acids and cell membrane components, while the neutral lipid DOPE improves transfection efficiency (Beg *et al*., 2021). Lipofectamine-based reagents are able to enter cells through diffusion, which may avoid lysosomal degradation (Cardarelli *et al*., 2016). With optimisation, LF3K can efficiently transfect multiple types of cell lines, and facilitate uptake of a variety of gene therapy agents, from SSOs to genome editing systems (de Carvalho *et al*., 2018; Liu *et al*., 2020b; Wang *et al*., 2018). The results of this study support the widespread use of LF3K as a transfection agent, as it showed minimal toxicity in the cell lines tested and sufficient uptake to induce gene silencing.

There are several possible reasons why the AuCS-2% PEG failed to induce knockdown. Further experiments would be required to determine the exact step(s) at which transfection and knockdown failed.

It is firstly possible that the siRNA payload was subject to degradation by nucleases. siRNA must avoid both extra- and intracellular nucleases before integration into the RISC (Nair *et al*.,

2017). As mentioned in the results of the RNase protection assay (section 4.3.3), the siRNA may potentially have been subject to partial degradation by the nuclease. If a significant portion of the siRNA cargo was degraded, this may result in the intracellular concentration being too low to induce effective knockdown. To confirm the cause of the lowered intensity, different release agents may be investigated to ensure the complete release of bound siRNA. Ma *et al*., (2017), for example, showed heparin sulphate to effectively dissociate CS-DNA complexes, and it may thus dissociate the FAuNC complexes more effectively than SDS. Different concentrations of SDS may also be investigated. Mannose-modified trimethyl chitosan-cysteine (MTC) NP, for example, have been observed to require different concentrations of heparin to completely dissociate siRNA depending on their level of crosslinking with different polymers (He *et al*., 2020).

It is also possible that PEGylation interfered with transfection, due to the "PEG dilemma". PEG shields cationic sites on the CS. This may reduce uptake by inhibiting interactions between CS and the cell membrane, and by lowering the zeta potential of nanocomplexes. Both PEGylated FAuNC complexes showed close to neutral zeta potentials, although whether the zeta potential in medium containing serum is neutral needs to be verified. Some studies have reported neutral PEGylated nanocomplexes to show reduced transfection compared to cationic nanocomplexes. Niu *et al*., (2018) reported neutral r8-insulin nanocomplexes encapsulated with PGA-PEG to efficiently transfect colon cancer Caco-2 cells, although transfection was markedly lower than cationic unencapsulated nanocomplexes. It was, however, noted that this would not be the case *in vivo* due to the inherent instability of the unencapsulated nanocomplexes. Rudzinski *et al*., (2016) reported neutral PEGylated CS-PEG complexes to induce slightly reduced *β-catenin* knockdown (expression reduced by 27.8%) compared to CS (30.4%) and Lipofectamine 2000 (33.4%) after 48 hrs. It is possible that the neutral zeta potential of the AuCS-2% PEG together with the steric hindrance may have reduced interactions with cell membrane components, thus reducing uptake.

If sufficient uptake did occur, it is possible that the AuCS-2% PEG were not able to efficiently escape the endosome or lysosome. Zhu *et al*., (2019) reported CS-encapsulated AuNC to be capable of escaping from the lysosome. This efficient escape was attributed to the acidic pH of the lysosome increasing the surface charge of the AuCS, thus inducing lysosomal membrane disruption through the proton sponge effect. This would notably rely on sufficient free protonable sites on the CS. However, this may not have been the case for the near-neutral AuCS-2% PEG nanocomplexes, in which the number of positive amine groups of the CS was

reduced through binding with PEG and siRNA. It has also been suggested that polyplexes may require interactions with the endosomal membrane to induce escape, as lipoplexes do (Degors *et al*., 2019). PEG may again inhibit this interaction through steric hindrance.

If PEGylation did interfere with transfection, this would be in contrast to the results of Daniels and Singh, (2019), who reported CS-encapsulated AuNP functionalised with PEG in weight ratios of 2% and 5% to effectively induce *c-MYC* silencing. In a study on the effect of PEGylation on transfection efficiency of PEI-siRNA complexes, Rheiner *et al*., (2016) observed increased PEGylation with PEG_{2000} and PEG_{5000} to inhibit knockdown. It was noted that, since both PEG and PEI are hydrophilic, this may have led to entanglement of the two polymers and efficient blocking of cationic sites on the PEI. This may have occurred with the AuCS-2% PEG, as CS is also a hydrophilic polymer. It is possible that such entanglement would occur less on CS-AuNP where the CS was stabilised on a solid AuNP core, in contrast to the nanogel structure of the AuCS. This conflicting result may thus possibly result from the difference in structure of the functionalised AuNP and FAuNC.

Other characteristics of the nanocomplexes may also affect their ability to transfect cells. In a study evaluating the uptake of novel polymeric poly(propargyl glycolide) NP modified to contain disulfide linkages or cholesterol groups, Portis *et al*., (2010) reported successful uptake of complexes with anti-*GFP* siRNA in GFP expressing H1299 cells using confocal laser scanning microscopy. However, this did not produce significant knockdown of GFP expression, in contrast to treatment with Lipofectamine 2000 and LPEI complexes. This was attributed to a low intracellular concentration of siRNA being achieved by the novel polymeric NP. The authors further suggested that the transfection efficacy of nanocomplexes is dependent not only on the physical structure of the nanocomplexes formed through binding with siRNA, but also the formation of higher-order structures through interactions between complexes. These structures may be predicted and assessed using modelling software to determine whether they would promote or interfere with uptake.

Further studies may be done to accurately assess the cellular uptake and endosomal escape of all FAuNC. Although the fluorescence images (section 4.4.3) do not appear to show reduced transfection by PEGylated FAuNC compared to AuCS and LF3K, more comprehensive analyses would be required to accurately measure cellular uptake. These may include inductively-coupled plasma (ICP) techniques that measure that amount of gold present in cell lysates, or flow cytometry to measure the level fluorescence in a cell population (Shin *et al*.,

2020). Fluorescence studies may be performed to determine uptake and release of FAuNC from endosomes or lysosomes. This may be achieved using dyes or markers that bind or accumulate within endosomes or lysosomes, such as LysoTracker dyes that accumulate in acidic late endosomes and lysosomes (Zhitomirsky *et al*., 2018). A fluorescent microscope may then be used to visualise any overlap between the FAuNC and labelled vesicles. Endosomal escape may also be monitored using confocal microscopy, which allows for detection of changes in the fluorescence of FAuNC in response to changes in the pH in the lysosome and cytoplasm (Zhu *et al*., 2019).

Following entry into the cell, the vector would also be required to "unpack" and release the free siRNA, which is then incorporated into the RISC. Vector unpacking may occur during endosomal escape. Alternatively, the bound nanocomplex must dissociate in the cytoplasm after escaping the endo-/lysosome (Gary *et al*., 2007). It has been suggested that vector unpacking is a smaller obstacle to siRNA delivery than DNA delivery, as the small size of siRNA results in weaker interactions with vectors, thus promoting dissociation (Gary *et al*., 2007). Nevertheless, ineffective or slow release of the siRNA may lead to inefficient gene silencing. In their study on MTC NP with different kinds and amounts of crosslinkers, He *et al*., (2020) reported formulations that showed slow siRNA release to be ineffective at silencing *TNF-α* expression in the macrophage cell line Raw 264.7. However, it may be noted that the binding studies showed PEGylation to weaken the binding and compaction abilities of the FAuNC. This would suggest that vector dissociation may have been more likely to occur for the AuCS-2% PEG. There are several techniques that may verify the release kinetics of the FAuNC. A procedure similar to drug release assays may be used, in which siRNA released from nanocomplexes into a PBS solution is quantified at different time intervals using UV spectroscopy, or fluorescence intensity in the case of tagged siRNA (Abdul Ghafoor Raja *et al*., 2015; Shi *et al*., 2014). *In vitro* release may be investigated using confocal microscopy, which would allow for detection of signals from the fluorescent FAuNC and tagged siRNA. Divergence of the signals would suggest that the siRNA has dissociated from the FAuNC (Lee *et al*., 2010).

Overall, both gene expression assays showed that the AuCS-2% PEG did not affect knockdown of the *c-MYC* oncogene in MCF-7 cells. This may have resulted from a combination of the above-mentioned factors that led to insufficient uptake and a low intracellular concentration of siRNA.

CHAPTER 5
CONCLUSION AND FUTURE STUDIES

5.1. Conclusion

siRNA have emerged as potentially powerful tools in the treatment of aggressive cancers. By exploiting the natural gene regulation mechanism of RNAi, they allow for sequence-specific silencing of aberrant genes. siRNA therapies show particular promise in treating diseases previously considered undruggable and cancers with high mutagenic diversity, such as TNBC. However, their *in vivo* efficacy is limited due to the unfavourable physicochemical properties of siRNA molecules, and much research has thus focussed on the development of delivery systems. Concerns over vector toxicity and immunogenicity has resulted in a shift in focus from viral to non-viral vectors. AuNC form part of a novel class of ultra-small NP, which show unique optical and physicochemical characteristics. They display a large surface area, strong photoluminescence, and high biocompatibility, making them viable candidates as gene delivery vectors. Functionalisation with the polymer CS produces nanogels that can easily interact with therapeutic nucleic acids. Addition of the stealth polymer PEG may lead to reduced opsonisation and thus increased circulation times *in vivo*.

This study focussed on the development of AuNC vectors coated with CS, and PEG_{2000} in two weight ratios, and the evaluation of their *in vitro* toxicity and ability to deliver siRNA. Ultra-small AuNC (<2 nm) were successfully synthesised and functionalised. FAuNC showed minimal aggregation and strong fluorescence upon excitation with UV light. NTA showed the FAuNC to display good colloidal stability and physiologically relevant sizes. These characteristics may facilitate their potential use as imaging or detection agents. The band shift and EtBr intercalation assays further showed FAuNC to successfully bind and condense siRNA into compact nanocomplexes with ideal sizes for cellular uptake. The nuclease protection assay further showed that the FAuNC were capable of providing protection against complete degradation by RNase A.

In vitro studies, conducted in BC and non-cancerous cell lines, involved evaluation of the toxicity and uptake of the FAuNC. All complexes were found to be well-tolerated, further signifying their potential for *in vivo* applications. Fluorescent assays to assess the induction of apoptosis in MDA-MB-231 cells further confirmed the safety of the FAuNC. Cellular uptake studies showed all FAuNC to be capable of interacting with all cells tested, with all samples

showing fluorescence compared to the untreated and siRNA-only controls that displayed minimal fluorescence.

Based on the results of the flow cytometry assays *in vitro*, the AuCS-2% PEG were chosen as subjects for the gene expression assays. However, RT-qPCR and ELISA showed that the AuCS-2% PEG failed to elicit sufficient knockdown of mRNA and protein levels of the *c-MYC* oncogene. This was in contrast to the commercially available vector LF3K, which led to a reduction in expression relative to the untreated control.

Steric stabilisation was achieved through the conjugation of PEG_{2000} to the CS polymer. This was observed to result in weakened interactions between the FAuNC and siRNA: more of the PEGylated FAuNC was required to fully bind the siRNA, and both PEGylated FAuNC condensed siRNA to a lesser degree than AuCS. PEGylation also appeared to slightly reduce the fluorescence of the AuNC, which may be an obstacle for imaging purposes. Furthermore, it is possible that PEGylation interfered with knockdown. The AuCS showed strong interactions with siRNA, provided protection against RNase A degradation without the need for stabilisers, and showed high biocompatibility.

Overall, all FAuNC formulated and tested in this study were capable of interacting with siRNA and showed favourable characteristics *in vitro* in BC and non-cancer cells. However, the AuCS-2% PEG that was selected was unable to successfully induce knockdown of the *c-MYC* oncogene, and further optimisation would be needed to take this nano-delivery system further.

5.2. Future Studies

Based on the results obtained further studies may be needed, such as optimisation of the enzyme protection assay to fully assess the level of protection of the siRNA. This may involve investigation of releasing agents other than SDS that can completely destabilise the nanocomplex. Comprehensive uptake studies that can provide more detailed information on the level of uptake in into the cells, may be undertaken. This may include measurement of the fluorescence from cell lysates or the use of Tox, anti-*Luc*, or anti-*GFP* siRNA. Tox siRNA induces apoptosis following transfection, and the transfection efficiency of NP can thus be assessed using a cytotoxicity assay. Anti-*Luc* and anti-*GFP* siRNA, which silence the Luciferase and GFP genes respectively, allow for the use of luciferase assays or fluorescence microscopy to assess transfection efficiency. Such assays may provide more accurate, quantitative information on the impact of PEGylation on uptake, and reveal any cell-specific

interactions, such as whether the FAuNC are preferentially taken up by particular cell types. This may ultimately influence the choice of disease that the FAuNC vectors may be designed to target. Further investigation into the cellular uptake and intracellular trafficking pathways is vital to understanding why knockdown was inadequate. Further optimisation of the assays evaluating TNF-α expression will be needed.

The necessity of PEGylation should also be investigated further. The ability of PEGylation to prevent serum protein binding may be assessed through incubation of the FAuNC with FBS, and quantification of the amount of protein bound to the FAuNC. However, *in vivo* studies may be required to accurately assess the influence of the different PEG grafting densities on the circulation time of the FAuNC. Future studies may also investigate the use of smaller PEG chains, such as PEG_{400}, or cleavable PEG chains that dissociate from the CS in acidic environments. Different methods of binding PEG to the CS may also be investigated.

In addition to the studies mentioned above, future work may include further investigation into the optical properties of the FAuNC, and evaluation of their abilities as imaging agents. This would broaden their application to include biomedical imaging for research or disease diagnosis. Possible *in vivo* studies may also include evaluation of the fate of the FAuNC to determine how they are excreted. This is of particular importance as gold is not biodegradable. The formulations may also benefit from the addition of targeting molecules. Ligands such as transferrin, folic acid, or asialoglycoprotein may be used to promote delivery to and uptake by specific cells, while cell-penetrating peptides can promote better cellular uptake.

BIBLIOGRAPHY

Abdul Ghafoor Raja, M., Katas, H., Jing Wen, T., Malaysia, K., Raja Muda Abdul Aziz, J., & Lumpur, K. (2015). Stability, Intracellular Delivery, and Release of siRNA from Chitosan Nanoparticles Using Different Cross-Linkers. *PLOS ONE*, *10*(6), e0128963.

Abolmaali, S. S., Tamaddon, A. M., Mohammadi, S., Amoozgar, Z., & Dinarvand, R. (2016). Chemically crosslinked nanogels of PEGylated poly ethyleneimine (l-histidine substituted) synthesized via metal ion coordinated self-assembly for delivery of methotrexate: Cytocompatibility, cellular delivery and antitumor activity in resistant cells. *Materials Science and Engineering C*, *62*, 897–907.

Adams, G. (2020). A beginner's guide to RT-PCR, qPCR and RT-qPCR. *The Biochemist*, *42*(3), 48–53.

Aderka, D., Engelmann, H., Maor, Y., Brakebusch, C., & Wallach, D. (1992). Stabilization of the bioactivity of tumor necrosis factor by its soluble receptors. *Journal of Experimental Medicine*, *175*(2), 323–329.

Ades, F., Tryfonidis, K., & Zardavas, D. (2017). The past and future of breast cancer treatment-from the papyrus to individualised treatment approaches. *Ecancermedicalscience*, *11*, 746.

Aggarwal, B. B., Gupta, S. C., & Kim, J. H. (2012). Historical perspectives on tumor necrosis factor and its superfamily: 25 years later, a golden journey. *Blood*, *119*(3), 651–665.

Ahmadi, F., Oveisi, Z., Samani, S. M., & Amoozgar, Z. (2015). Chitosan based hydrogels: characteristics and pharmaceutical applications. *Research in Pharmaceutical Sciences*, *10*(1), 1–16.

Ahmadi, S. E., Rahimi, S., Zarandi, B., Chegeni, R., & Safa, M. (2021). MYC: a multipurpose oncogene with prognostic and therapeutic implications in blood malignancies. *Journal of Hematology & Oncology*, *14*(1), 1–49.

Akinc, A., Thomas, M., Klibanov, A. M., & Langer, R. (2005). Exploring polyethylenimine-mediated DNA transfection and the proton sponge hypothesis. *The Journal of Gene Medicine*, *7*(5), 657–663.

Alameh, M., Lavertu, M., Tran-Khanh, N., Chang, C. Y., Lesage, F., Bail, M., Darras, V., Chevrier, A., & Buschmann, M. D. (2018). SiRNA Delivery with Chitosan: Influence of Chitosan Molecular Weight, Degree of Deacetylation, and Amine to Phosphate Ratio on in Vitro Silencing Efficiency, Hemocompatibility, Biodistribution, and in Vivo Efficacy. *Biomacromolecules*, *19*(1), 112–131.

Alamolhodaei, N. S., Rashidpoor, H., Gharaee, M. E., Behravan, J., & Mosaffa, F. (2020). Overexpression of ABCC2 and NF-/p65 with reduction in cisplatin and 4OH-Tamoxifen sensitivity in MCF-7 breast cancer cells: The influence of TNF-α. *Pharmaceutical Sciences*, *26*(2), 150–158.

Alberg, I., Kramer, S., Schinnerer, M., Hu, Q., Seidl, C., Leps, C., Drude, N., Möckel, D., Rijcken, C., Lammers, T., Diken, M., Maskos, M., Morsbach, S., Landfester, K., Tenzer, S., Barz, M., & Zentel, R. (2020). Polymeric Nanoparticles with Neglectable Protein Corona. *Small*, *16*(18), 1907574.

Alitalo, K., Schwab, M., Lin, C. C., Varmus, H. E., & Bishop, J. M. (1983). Homogeneously staining chromosomal regions contain amplified copies of an abundantly expressed cellular

oncogene (c-myc) in malignant neuroendocrine cells from a human colon carcinoma. *Proceedings of the National Academy of Sciences of the United States of America*, *80*(6), 1707–1711.

Alles, M. C., Gardiner-Garden, M., Nott, D. J., Wang, Y., Foekens, J. A., Sutherland, R. L., Musgrove, E. A., & Ormandy, C. J. (2009). Meta-analysis and gene set enrichment relative to ER status reveal elevated activity of MYC and E2F in the "Basal" breast cancer subgroup. *PLoS ONE*, *4*(3), e4710.

Allevato, M., Bolotin, E., Grossman, M., Mane-Padros, D., Sladek, F. M., & Martinez, E. (2017). Sequence-specific DNA binding by MYC/MAX to low-affinity non-E-box motifs. *PLOS ONE*, *12*(7), e0180147.

Alsaedi, I. I. J., Taqi, Z. J., Hussien, A. M. A., Sulaiman, G. M., & Jabir, M. S. (2019). Graphene nanoparticles induces apoptosis in MCF-7 cells through mitochondrial damage and NF-KB pathway. *Materials Research Express*, *6*(9), 095413.

Alshaer, W., Zureigat, H., Al Karaki, A., Al-Kadash, A., Gharaibeh, L., Hatmal, M. M., Aljabali, A. A. A., & Awidi, A. (2021). siRNA: Mechanism of action, challenges, and therapeutic approaches. *European Journal of Pharmacology*, *905*, 174178.

Altangerel, A., Cai, J., Liu, L., Wu, Y., Baigude, H., & Han, J. (2016). PEGylation of 6-amino-6-deoxy-curdlan for efficient in vivo siRNA delivery. *Carbohydrate Polymers*, *141*, 92–98.

Amoozgar, Z., Park, J., Lin, Q., & Yeo, Y. (2012). Low molecular-weight chitosan as a pH-sensitive stealth coating for tumor-specific drug delivery. *Molecular Pharmaceutics*, *9*(5), 1262–1270.

Angart, P., Vocelle, D., Chan, C., & Walton, S. (2013). Design of siRNA Therapeutics from the Molecular Scale. *Pharmaceuticals*, *6*(4), 440–468.

Annunziato, S., de Ruiter, J. R., Henneman, L., Brambillasca, C. S., Lutz, C., Vaillant, F., Ferrante, F., Drenth, A. P., van der Burg, E., Siteur, B., van Gerwen, B., de Bruijn, R., van Miltenburg, M. H., Huijbers, I. J., van de Ven, M., Visvader, J. E., Lindeman, G. J., Wessels, L. F. A., & Jonkers, J. (2019). Comparative oncogenomics identifies combinations of driver genes and drug targets in BRCA1-mutated breast cancer. *Nature Communications*, *10*(1), 397.

Anselmo, A. C., and Mitragotri, S. (2015). A Review of Clinical Translation of Inorganic Nanoparticles. *AAPS Journal*, *17*(5), 1041–1054.

Antunes, R. F., Kaski, J. C., & Dumitriu, I. E. (2012). The Role of Costimulatory Receptors of the Tumour Necrosis Factor Receptor Family in Atherosclerosis. *Journal of Biomedicine and Biotechnology*, *2012*, 464532.

Apirakaramwong, A., Pamonsinlapatham, P., Techaarpornkul, S., Opanasopit, P., Panomsuk, S., & Soksawatmaekhin, W. (2012). Mechanisms of Cellular Uptake with Chitosan/DNA Complex in Hepatoma Cell Line. *Advanced Materials Research*, *506*, 485–488.

Araújo, T., Aresta, G., Castro, E., Rouco, J., Aguiar, P., Eloy, C., Polónia, A., & Campilho, A. (2017). Classification of breast cancer histology images using Convolutional Neural Networks. *PLOS ONE*, *12*(6), e0177544.

Arthur, N. B., Christensen, K. A., Mannino, K., Ruzinova, M. B., Kumar, A., Gruszczynska, A., Day, R. B., Erdmann-Gilmore, P., Mi, Y., Sprung, R., York, C. R., Townsend, R. R., Spencer, D. H., Sykes, S. M., & Ferraro, F. (2023). Missense mutations in Myc Box I influence MYC cellular localization, mRNA partitioning and turnover to promote leukemogenesis.

BioRxiv, 2023.10.22.563493.

Asano, Y., Kashiwagi, S., Goto, W., Tanaka, S., Morisaki, T., Takashima, T., Noda, S., Onoda, N., Ohsawa, M., Hirakawa, K., & Ohira, M. (2017). Expression and clinical significance of androgen receptor in triple-negative breast cancer. *Cancers*, *9*(1), 4.

Asher, A., Mulé, J. J., Reichert, C. M., Shiloni, E., & Rosenberg, S. A. (1987). Studies on the anti-tumor efficacy of systemically administered recombinant tumor necrosis factor against several murine tumors in vivo. *Journal of Immunology*, *138*(3), 963–974.

Atretkhany, K. N., Gogoleva, V. S., Drutskaya, M. S., & Nedospasov, S. A. (2020). Distinct modes of TNF signaling through its two receptors in health and disease. *Journal of Leukocyte Biology*, *107*(6), 893–905.

Azenshtein, E., Luboshits, G., Shina, S., Neumark, E., Shahbazian, D., Weil, M., Wigler, N., Keydar, I., & Ben-Baruch, A. (2002). The CC Chemokine RANTES in Breast Carcinoma Progression. *Cancer Research*, *62*(4), 1093–1102.

Babu, A., Muralidharan, R., Amreddy, N., Mehta, M., Munshi, A., & Ramesh, R. (2016). Nanoparticles for siRNA-Based Gene Silencing in Tumor Therapy. *IEEE Transactions on Nanobioscience*, *15*(8), 849–863.

Badowska-Kozakiewicz, A. M., Liszcz, A., Sobol, M., & Patera, J. (2017). Retrospective evaluation of histopathological examinations in invasive ductal breast cancer of no special type: An analysis of 691 patients. *Archives of Medical Science*, *13*(6), 1408–1415.

Bahia, M. S., & Silakari, O. (2010). Tumor Necrosis Factor Alpha Converting Enzyme: An Encouraging Target for Various Inflammatory Disorders. *Chemical Biology & Drug Design*, *75*(5), 415–443.

Balkwill, F., & Mantovani, A. (2001). Inflammation and cancer: Back to Virchow? In *Lancet* (Vol. 357, Issue 9255, pp. 539–545). Elsevier Limited.

Balkwill, F. R., Lee, A., Aldam, G., Moodie, E., Thomas, J. A., Tavernier, J., & Fiers, W. (1986). Human tumor xenografts treated with recombinant human tumor necrosis factor alone or in combination with interferons. *Cancer Research*, *46*(8), 3990–3993.

Bano, F., Sluysmans, D., Wislez, A., & Duwez, A. S. (2015). Unraveling the complexity of the interactions of DNA nucleotides with gold by single molecule force spectroscopy. *Nanoscale*, *7*(46), 19528–19533.

Barba, A. A., Bochicchio, S., Dalmoro, A., & Lamberti, G. (2019). Lipid delivery systems for nucleic-acid-based-drugs: From production to clinical applications. *Pharmaceutics*, *11*(8), 360.

Bardia, A., Mayer, I. A., Vahdat, L. T., Tolaney, S. M., Isakoff, S. J., Diamond, J. R., O'Shaughnessy, J., Moroose, R. L., Santin, A. D., Abramson, V. G., Shah, N. C., Rugo, H. S., Goldenberg, D. M., Sweidan, A. M., Iannone, R., Washkowitz, S., Sharkey, R. M., Wegener, W. A., & Kalinsky, K. (2019). Sacituzumab Govitecan-hziy in Refractory Metastatic Triple-Negative Breast Cancer. *New England Journal of Medicine*, *380*(8), 741–751.

Barton, V. N., D'Amato, N. C., Gordon, M. A., Christenson, J. L., Elias, A., & Richer, J. K. (2015). Androgen Receptor Biology in Triple Negative Breast Cancer: a Case for Classification as AR+ or Quadruple Negative Disease. In *Hormones and Cancer* (Vol. 6, Issues 5–6, pp. 206–213). Springer US.

Battey, J., Moulding, C., Taub, R., Murphy, W., Stewart, T., Potter, H., Lenoir, G., & Leder,

P. (1983). The human c-myc oncogene: structural consequences of translocation into the IgH locus in Burkitt lymphoma. *Cell*, *34*(3), 779–787.

Bauer, K. R., Brown, M., Cress, R. D., Parise, C. A., & Caggiano, V. (2007). Descriptive analysis of estrogen receptor (ER)-negative, progesterone receptor (PR)-negative, and HER2-negative invasive breast cancer, the so-called triple-negative phenotype: A population-based study from the California Cancer Registry. *Cancer*, *109*(9), 1721–1728.

Beaulieu, M. E., Castillo, F., & Soucek, L. (2020). Structural and Biophysical Insights into the Function of the Intrinsically Disordered Myc Oncoprotein. *Cells*, *9*(4), 1038.

Beg, S., Almalki, W. H., Khatoon, F., Alharbi, K. S., Alghamdi, S., Akhter, M. H., Khalilullah, H., Baothman, A. A., Hafeez, A., Rahman, M., Akhter, S., & Choudhry, H. (2021). Lipid/polymer-based nanocomplexes in nucleic acid delivery as cancer vaccines. *Drug Discovery Today*, *26*(8), 1891–1903.

Bekale, L., Agudelo, D., & Tajmir-Riahi, H. A. (2015). Effect of polymer molecular weight on chitosan–protein interaction. *Colloids and Surfaces B: Biointerfaces*, *125*, 309–317.

Benjaminsen, R. V, Mattebjerg, M. A., Henriksen, J. R., Moghimi, S. M., & Andresen, T. L. (2013). The Possible "Proton Sponge" Effect of Polyethylenimine (PEI) Does Not Include Change in Lysosomal pH. *Molecular Therapy*, *21*(1), 149–157.

Beutler, B., Greenwald, D., Hulmes, J. D., Chang, M., Pan, Y. C. E., Mathison, J., Ulevitch, R., & Cerami, A. (1985). Identity of tumour necrosis factor and the macrophage-secreted factor cachectin. *Nature*, *316*(6028), 552–554.

Beutler, B., Milsark, I. W., & Cerami, A. C. (1985). Passive immunization against cachectin/tumor necrosis factor protects mice from lethal effect of endotoxin. *Science*, *229*(4716), 869–871.

Bhang, S. H., Kim, K., Rhee, W. J., & Shim, M. S. (2018). Bioreducible Polyspermine-Based Gene Carriers for Efficient siRNA Delivery: Effects of PEG Conjugation on Gene Silencing Efficiency. *Macromolecular Research*, *26*(12), 1135–1142.

Bhattacharjee, S. (2016). DLS and zeta potential – What they are and what they are not? *Journal of Controlled Release*, *235*, 337–351.

Biswas, T., Efird, J. T., Prasad, S., Jindal, C., & Walker, P. R. (2017). The survival benefit of neoadjuvant chemotherapy and pCR among patients with advanced stage triple negative breast cancer. *Oncotarget*, *8*(68), 112712–112719.

Bjorge, J. D., Pang, A., & Fujita, D. J. (2017). Delivery of gene targeting siRNAs to breast cancer cells using a multifunctional peptide complex that promotes both targeted delivery and endosomal release. *PLOS ONE*, *12*(6), e0180578.

Blackwood, E. M., & Eisenman, R. N. (1991). Max: A Helix-Loop-Helix Zipper Protein That Forms a Sequence-Specific DNA-Binding Complex with Myc. *Science*, *251*(4998), 1211–1217.

Blackwood, E. M., Lugo, T. G., Kretzner, L., King, M. W., Street, A. J., Witte, O. N., & Eisenman, R. N. (1994). Functional analysis of the AUG- and CUG-initiated forms of the c-Myc protein. *Molecular Biology of the Cell*, *5*(5), 597–609.

Blanco, E., Shen, H., & Ferrari, M. (2015). Principles of nanoparticle design for overcoming biological barriers to drug delivery. *Nature Biotechnology*, *33*(9), 941–951.

Blaser, H., Dostert, C., Mak, T. W., & Brenner, D. (2016). TNF and ROS Crosstalk in Inflammation. *Trends in Cell Biology*, *26*(4), 249–261.

Booth, S. G., Uehara, A., Chang, S. Y., La Fontaine, C., Fujii, T., Okamoto, Y., Imai, T., Schroeder, S. L. M., & Dryfe, R. A. W. (2017). The significance of bromide in the Brust-Schiffrin synthesis of thiol protected gold nanoparticles. *Chemical Science*, *8*(12), 7954–7962.

Borghi, A., Haegman, M., Fischer, R., Carpentier, I., Bertrand, M. J. M., Libert, C., Afonina, I. S., & Beyaert, R. (2018). The E3 ubiquitin ligases HOIP and cIAP1 are recruited to the TNFR2 signaling complex and mediate TNFR2-induced canonical NF-κB signaling. *Biochemical Pharmacology*, *153*, 292–298.

Bowen, R. L., Duffy, S. W., Ryan, D. A., Hart, I. R., & Jones, J. L. (2008). Early onset of breast cancer in a group of British black women. *British Journal of Cancer*, *98*(2), 277–281.

Boyles, M. S. P., Kristl, T., Andosch, A., Zimmermann, M., Tran, N., Casals, E., Himly, M., Puntes, V., Huber, C. G., Lütz-Meindl, U., & Duschl, A. (2015). Chitosan functionalisation of gold nanoparticles encourages particle uptake and induces cytotoxicity and pro-inflammatory conditions in phagocytic cells, as well as enhancing particle interactions with serum components. *Journal of Nanobiotechnology*, *13*(1), 84–103.

Bray, F., Ferlay, J., Soerjomataram, I., Siegel, R. L., Torre, L. A., & Jemal, A. (2018). Global cancer statistics 2018: GLOBOCAN estimates of incidence and mortality worldwide for 36 cancers in 185 countries. *CA: A Cancer Journal for Clinicians*, *68*(6), 394–424.

Briot, D., Macé-Aimé, G., Subra, F., & Rosselli, F. (2008). Aberrant activation of stress-response pathways leads to TNF-α oversecretion in Fanconi anemia. *Blood*, *111*(4), 1913–1923.

Broekman, W., Amatngalim, G. D., de Mooij-Eijk, Y., Oostendorp, J., Roelofs, H., Taube, C., Stolk, J., & Hiemstra, P. S. (2016). TNF-aα and IL-1β-activated human mesenchymal stromal cells increase airway epithelial wound healing in vitro via activation of the epidermal growth factor receptor. *Respiratory Research*, *17*(1), 1–12.

Brouckaert, P. G. G., Leroux-Roels, G. G., Guisez, Y., Tavernier, J., & Fiers, W. (1986). In vivo anti-tumour activity of recombinant human and murine TNF, alone and in combination with murine IFN-γ, on a syngeneic murine melanoma. *International Journal of Cancer*, *38*(5), 763–769.

Brown, N. S., & Bicknell, R. (2001). Oxidative stress: Its effects on the growth, metastatic potential and response to therapy of breast cancer. *Breast Cancer Research*, *3*(5), 323–327.

Burman, A., Haworth, O., Bradfield, P., Parsonage, G., Filer, A., Thomas, A. M. C., Amft, N., Salmon, M., & Buckley, C. D. (2005). The role of leukocyte-stromal interactions in chronic inflammatory joint disease. *Joint Bone Spine*, *72*(1), 10–16.

Burow, M. E., Weldon, C. B., Tang, Y., Navar, G. L., Krajewski, S., Reed, J. C., Hammond, T. G., Clejan, S., & Beckman, B. S. (1998). Differences in susceptibility to tumor necrosis factor alpha-induced apoptosis among MCF-7 breast cancer cell variants. *Cancer Research*, *58*(21), 4940–4946.

Burstein, M. D., Tsimelzon, A., Poage, G. M., Covington, K. R., Contreras, A., Fuqua, S. A. W., Savage, M. I., Osborne, C. K., Hilsenbeck, S. G., Chang, J. C., Mills, G. B., Lau, C. C., & Brown, P. H. (2015). Comprehensive genomic analysis identifies novel subtypes and targets of triple-negative breast cancer. *Clinical Cancer Research*, *21*(7), 1688–1698.

Bus, T., Traeger, A., & Schubert, U. S. (2018). The great escape: how cationic polyplexes overcome the endosomal barrier. *Journal of Materials Chemistry B*, *6*(43), 6904–6918.

Buschmann, M. D., Merzouki, A., Lavertu, M., Thibault, M., Jean, M., & Darras, V. (2013). Chitosans for delivery of nucleic acids. *Advanced Drug Delivery Reviews*, *65*(9), 1234–1270.

Cabal-Hierro, L., Artime, N., Iglesias, J., Prado, M. A., Ugarte-Gil, L., Casado, P., Fernández-García, B., Darnay, B. G., & Lazo, P. S. (2014). A TRAF2 binding independent region of TNFR2 is responsible for TRAF2 depletion and enhancement of cytotoxicity driven by TNFR1. *Oncotarget*, *5*(1), 224–236.

Caforio, M., Sorino, C., Iacovelli, S., Fanciulli, M., Locatelli, F., & Folgiero, V. (2018). Recent advances in searching c-Myc transcriptional cofactors during tumorigenesis. *Journal of Experimental and Clinical Cancer Research*, *37*(1), 1–9.

Cai, X., Cao, C., Li, J., Chen, F., Zhang, S., Liu, B., Zhang, W., Zhang, X., & Ye, L. (2017). Inflammatory factor TNF-α promotes the growth of breast cancer via the positive feedback loop of TNFR1/NF-κB (and/or p38)/p-STAT3/HBXIP/TNFR1. *Oncotarget*, *8*(35), 58338–58352.

Carabet, L. A., Rennie, P. S., & Cherkasov, A. (2018). Therapeutic Inhibition of Myc in Cancer. Structural Bases and Computer-Aided Drug Discovery Approaches. *International Journal of Molecular Sciences 2019, Vol. 20, Page 120*, *20*(1), 120.

Cardarelli, F., Digiacomo, L., Marchini, C., Amici, A., Salomone, F., Fiume, G., Rossetta, A., Gratton, E., Pozzi, D., & Caracciolo, G. (2016). The intracellular trafficking mechanism of Lipofectamine-based transfection reagents and its implication for gene delivery. *Scientific Reports 2016 6:1*, *6*(1), 1–8.

Carey, L. A., Dees, E. C., Sawyer, L., Gatti, L., Moore, D. T., Collichio, F., Ollila, D. W., Sartor, C. I., Graham, M. L., & Perou, C. M. (2007). The triple negative paradox: Primary tumor chemosensitivity of breast cancer subtypes. *Clinical Cancer Research*, *13*(8), 2329–2334.

Carswell, E. A., Old, L. J., Kassel, R. L., Green, S., Fiore, N., & Williamson, B. (1975). An endotoxin induced serum factor that cuases necrosis of tumors. *Proceedings of the National Academy of Sciences of the United States of America*, *72*(9), 3666–3670.

Carvalho-Galvão, A., Guimarães, D. D., De Brito Alves, J. L., & Braga, V. A. (2019). Central inhibition of tumor necrosis factor alpha reduces hypertension by attenuating oxidative stress in the rostral ventrolateral medulla in renovascular hypertensive rats. *Frontiers in Physiology*, *10*(APR), 491.

Casettari, L., Vllasaliu, D., Mantovani, G., Howdle, S. M., Stolnik, S., & Illum, L. (2010). Effect of PEGylation on the toxicity and permeability enhancement of chitosan. *Biomacromolecules*, *11*(11), 2854–2865.

Cen, H., Mao, F., Aronchik, I., Fuentes, R. J., & Firestone, G. L. (2008). DEVD-NucView488: a novel class of enzyme substrates for real-time detection of caspase-3 activity in live cells. *The FASEB Journal*, *22*(7), 2243–2252.

Chakraborty, A. A., Scuoppo, C., Dey, S., Thomas, L. R., Lorey, S. L., Lowe, S. W., & Tansey, W. P. (2015). A common functional consequence of tumor-derived mutations within c-MYC. *Oncogene*, *34*(18), 2406–2409.

Chakravarthy, S., Sternberg, S. H., Kellenberger, C. A., & Doudna, J. A. (2010). Substrate-

specific kinetics of dicer-catalyzed RNA processing. *Journal of Molecular Biology*, *404*(3), 392–402.

Chandra, P., Noh, H. B., & Shim, Y. B. (2013). Cancer cell detection based on the interaction between an anticancer drug and cell membrane components. *Chemical Communications*, *49*(19), 1900–1902.

Chandrasekharan, U. M., Siemionow, M., Unsal, M., Yang, L., Poptic, E., Bohn, J., Ozer, K., Zhou, Z., Howe, P. H., Penn, M., & DiCorleto, P. E. (2007). Tumor necrosis factor α (TNF-α) receptor-II is required for TNF-α-induced leukocyte-endothelial interaction in vivo. *Blood*, *109*(5), 1938–1944.

Chang, C.-H., Huang, C.-W., Huang, C.-M., Ou, T.-C., Chen, C.-C., & Lu, Y.-M. (2019). The duration of endocrine therapy and breast cancer patients' survival: A nationwide population-based cohort study. *Medicine*, *98*(43), e17746.

Chang, L. Y., Lin, Y. C., Chiang, J. M., Mahalingam, J., Su, S. H., Huang, C. T., Chen, W. T., Huang, C. H., Jeng, W. J., Chen, Y. C., Lin, S. M., Sheen, I. S., & Lin, C. Y. (2015). Blockade of TNF-α signaling benefits cancer therapy by suppressing effector regulatory T cell expansion. *OncoImmunology*, *4*(10), e1040215.

Chao, H. X., Poovey, C. E., Privette, A. A., Grant, G. D., Chao, H. Y., Cook, J. G., & Purvis, J. E. (2017). Orchestration of DNA Damage Checkpoint Dynamics across the Human Cell Cycle. *Cell Systems*, *5*(5), 445-459.e5.

Chappell, D., Hofmann-Kiefer, K., Jacob, M., Rehm, M., Briegel, J., Welsch, U., Conzen, P., & Becker, B. F. (2009). TNF-α induced shedding of the endothelial glycocalyx is prevented by hydrocortisone and antithrombin. *Basic Research in Cardiology*, *104*(1), 78–89.

Chen, B. J., Wu, Y. L., Tanaka, Y., & Zhang, W. (2014). Small Molecules Targeting c-Myc Oncogene: Promising Anti-Cancer Therapeutics. *International Journal of Biological Sciences*, *10*(10), 1084–1096.

Chen, H., Liu, H., & Qing, G. (2018). Targeting oncogenic Myc as a strategy for cancer treatment. *Signal Transduction and Targeted Therapy*, *3*(1), 1–7.

Chen, J., Rogers, S. C., & Kavdia, M. (2013). Analysis of kinetics of dihydroethidium fluorescence with superoxide using xanthine oxidase and hypoxanthine assay. *Annals of Biomedical Engineering*, *41*(2), 327–337.

Chen, L., Mccrate, J. M., Lee, J. C. M., & Li, H. (2011). The role of surface charge on the uptake and biocompatibility of hydroxyapatite nanoparticles with osteoblast cells. *Nanotechnology*, *22*(10), 105708.

Chen, T., Yao, Q., Cao, Y., & Xie, J. (2020). Studying the Growth of Gold Nanoclusters by Sub-stoichiometric Reduction. *Cell Reports Physical Science*, *1*(9), 100206.

Chen, W., Tu, X., & Guo, X. (2009). Fluorescent gold nanoparticles-based fluorescence sensor for Cu 2+ ions. *Chemical Communications*, *13*, 1736–1738.

Chendrimada, T. P., Gregory, R. I., Kumaraswamy, E., Norman, J., Cooch, N., Nishikura, K., & Shiekhattar, R. (2005). TRBP recruits the Dicer complex to Ago2 for microRNA processing and gene silencing. *Nature*, *436*(7051), 740–744.

Cheng, D., Liu, R., & Hu, K. (2022). Gold nanoclusters: Photophysical properties and photocatalytic applications. *Frontiers in Chemistry*, *10*, 958626.

Cheng, X., & Lee, R. J. (2016). The role of helper lipids in lipid nanoparticles (LNPs) designed for oligonucleotide delivery. *Advanced Drug Delivery Reviews*, *99*(Pt A), 129–137.

Chernikova, S. B., Game, J. C., & Brown, J. M. (2019). Dynamin 2, cell trafficking, and the triple-negative paradox. *Oncotarget*, *10*(24), 2336–2337.

Chithrani, B. D., Ghazani, A. A., & Chan, W. C. W. (2006). Determining the Size and Shape Dependence of Gold Nanoparticle Uptake into Mammalian Cells. *Nano Letters*, *6*(4), 662–668.

Chocholata, P., Kulda, V., & Babuska, V. (2019). Fabrication of scaffolds for bone-tissue regeneration. *Materials*, *12*(4), 568.

Choi, E., Mun, G. im, Lee, J., Lee, H., Cho, J., & Lee, Y. S. (2023). BRCA1 deficiency in triple-negative breast cancer: Protein stability as a basis for therapy. *Biomedicine and Pharmacotherapy*, *158*, 114090.

Choi, S. H., Wright, J. B., Gerber, S. A., & Cole, M. D. (2010). Myc protein is stabilized by suppression of a novel E3 ligase complex in cancer cells. *Genes & Development*, *24*(12), 1236–1241.

Chou, L. Y. T., Ming, K., & Chan, W. C. W. (2011). Strategies for the intracellular delivery of nanoparticles. *Chemical Society Reviews*, *40*(1), 233–245.

Chua, H. L., Bhat-Nakshatri, P., Clare, S. E., Morimiya, A., Badve, S., & Nakshatri, H. (2007). NF-κB represses E-cadherin expression and enhances epithelial to mesenchymal transition of mammary epithelial cells: Potential involvement of ZEB-1 and ZEB-2. *Oncogene*, *26*(5), 711–724.

Clarke, C. A., Keegan, T. H. M., Yang, J., Press, D. J., Kurian, A. W., Patel, A. H., & Lacey Jr, J. V. (2012). Age-specific incidence of breast cancer subtypes: understanding the black-white crossover. *Journal of the National Cancer Institute*, *104*(14), 1094–1101.

Cocchiararo, I., Cornut, M., Soldati, H., Bonavoglia, A., & Castets, P. (2022). Back to basics: Optimization of DNA and RNA transfer in muscle cells using recent transfection reagents. *Experimental Cell Research*, *421*(2), 113392.

Coley, W. B. (1898). The treatment of inoperable sarcoma with the 'mixed toxins of erysipelas and bacillus prodigiosus.: Immediate and final results in one hundred and forty cases. *Journal of the American Medical Association*, *XXXI*(9), 456–465.

Collins, S., & Groudine, M. (1982). Amplification of endogenous myc-related DNA sequences in a human myeloid leukaemia cell line. *Nature*, *298*(5875), 679–681.

Conacci-Sorrell, M., McFerrin, L., & Eisenman, R. N. (2014). An overview of MYC and its interactome. *Cold Spring Harbor Perspectives in Medicine*, *4*(1), a014357.

Cooper, A. M. W., Silver, K., Zhang, J., Park, Y., & Zhu, K. Y. (2019). Molecular mechanisms influencing efficiency of RNA interference in insects. *Pest Management Science*, *75*(1), 18–28.

Cooper, G. M. (2000). Structure of the Plasma Membrane. In *The Cell: A Molecular Approach* (2nd ed.). Sinauer Associates.

Corbo, C., Molinaro, R., Parodi, A., Toledano Furman, N. E., Salvatore, F., & Tasciotti, E. (2016). The impact of nanoparticle protein corona on cytotoxicity, immunotoxicity and target drug delivery. *Nanomedicine*, *11*(1), 81–100.

Cowling, V. H., Chandriani, S., Whitfield, M. L., & Cole, M. D. (2006). A Conserved Myc Protein Domain, MBIV, Regulates DNA Binding, Apoptosis, Transformation, and G2 Arrest. *Molecular and Cellular Biology*, *26*(11), 4226–4239.

Croft, M., & Siegel, R. M. (2017). Beyond TNF: TNF superfamily cytokines as targets for the treatment of rheumatic diseases. *Nature Reviews Rheumatology*, *13*(4), 217–233.

Cruceriu, D., Baldasici, O., Balacescu, O., & Berindan-Neagoe, I. (2020). The dual role of tumor necrosis factor-alpha (TNF-α) in breast cancer: molecular insights and therapeutic approaches. *Cellular Oncology*, *43*(1), 1–18.

Cruz-Chu, E. R., Malafeev, A., Pajarskas, T., Pivkin, I. V., & Koumoutsakos, P. (2014). Structure and response to flow of the glycocalyx layer. *Biophysical Journal*, *106*(1), 232–243.

Cubasch, H., Dickens, C., Joffe, M., Duarte, R., Murugan, N., Tsai Chih, M., Moodley, K., Sharma, V., Ayeni, O., Jacobson, J. S., Neugut, A. I., McCormack, V., & Ruff, P. (2018). Breast cancer survival in Soweto, Johannesburg, South Africa: A receptor-defined cohort of women diagnosed from 2009 to 11. *Cancer Epidemiology*, *52*, 120–127.

Cubasch, H., Joffe, M., Hanisch, R., Schuz, J., Neugut, A. I., Karstaedt, A., Broeze, N., Van Den Berg, E., McCormack, V., & Jacobson, J. S. (2013). Breast cancer characteristics and HIV among 1,092 women in Soweto, South Africa. *Breast Cancer Research and Treatment*, *140*(1), 177–186.

Cui, J., De Rose, R., Alt, K., Alcantara, S., Paterson, B. M., Liang, K., Hu, M., Richardson, J. J., Yan, Y., Jeffery, C. M., Price, R. I., Peter, K., Hagemeyer, C. E., Donnelly, P. S., Kent, S. J., & Caruso, F. (2015). Engineering poly(ethylene glycol) particles for improved biodistribution. *ACS Nano*, *9*(2), 1571–1580.

Cui, L. F., Guo, X. J., Wei, J., Liu, F. F., Fan, Y., Lang, R. G., Gu, F., Zhang, X. M., & Fu, L. (2008). Overexpression of TNF-α and TNFRII in invasive micropapillary carcinoma of the breast: clinicopathological correlations. *Histopathology*, *53*(4), 381–388.

Dadou, S. M., El-Barghouthi, M. I., Alabdallah, S. K., Badwan, A. A., Antonijevic, M. D., & Chowdhry, B. Z. (2017). Effect of protonation state and N-acetylation of chitosan on its interaction with xanthan gum: A molecular dynamics simulation study. *Marine Drugs*, *15*(10), 298.

Dai, X., Zhang, J., Arfuso, F., Chinnathambi, A., Zayed, M., Alharbi, S. A., Kumar, A. P., Ahn, K. S., & Sethi, G. (2015). Targeting TNF-related apoptosis-inducing ligand (TRAIL) receptor by natural products as a potential therapeutic approach for cancer therapy. *Experimental Biology and Medicine*, *240*(6), 760.

Dalla-Favera, R., Bregni, M., Erikson, J., Patterson, D., Gallo, R. C., & Croce, C. M. (1982). Human c-myc onc gene is located on the region of chromosome 8 that is translocated in Burkitt lymphoma cells. *Proceedings of the National Academy of Sciences of the United States of America*, *79*(24), 7824–7827.

Dana, H., Chalbatani, G. M., Mahmoodzadeh, H., Karimloo, R., Rezaiean, O., Moradzadeh, A., Mehmandoost, N., Moazzen, F., Mazraeh, A., Marmari, V., Ebrahimi, M., Rashno, M. M., Abadi, S. J., & Gharagouzlo, E. (2017). Molecular Mechanisms and Biological Functions of siRNA. *International Journal of Biomedical Science*, *13*(2), 48–57.

Danaei, M., Dehghankhold, M., Ataei, S., Hasanzadeh Davarani, F., Javanmard, R., Dokhani, A., Khorasani, S., & Mozafari, M. (2018). Impact of Particle Size and Polydispersity Index on

the Clinical Applications of Lipidic Nanocarrier Systems. *Pharmaceutics*, *10*(2), 57.

Dang, C. V., O'Donnell, K. A., Zeller, K. I., Nguyen, T., Osthus, R. C., & Li, F. (2006). The c-Myc target gene network. *Seminars in Cancer Biology*, *16*(4), 253–264.

Dang, C. V, & Lee, W. M. F. (1988). Identification of the human c-myc protein nuclear translocation signal. *Molecular and Cellular Biology*, *8*(10), 4048–4054.

Daniels, A. N., & Singh, M. (2019). Sterically stabilized siRNA:gold nanocomplexes enhance *c-MYC* silencing in a breast cancer cell model. *Nanomedicine*, *14*(11), 1387–1401.

Daniels, A., Noor-Mahomed, N., Singh, M., & Ariatti, M. (2011). Cytofectin amine head group modification and degree of liposome pegylation: factors influencing gene transfer. *Indian Journal of Pharmaceutical Sciences*, *73*(4), 381–386.

Das, S. K., Lewis, B. A., & Levens, D. (2023). MYC: a complex problem. *Trends in Cell Biology*, *33*(3), 235–246.

de Carvalho, T. G., Pellenz, F. M., Laureano, A., da Rocha Silla, L. M., Giugliani, R., Baldo, G., & Matte, U. (2018). A simple protocol for transfecting human mesenchymal stem cells. *Biotechnology Letters*, *40*(3), 617–622.

Dealtry, G. B., Naylor, M. S., Fiers, W., & Balkwill, F. R. (1987). The effect of recombinant human tumour necrosis factor on growth and macromolecular synthesis of human epithelial cells. *Experimental Cell Research*, *170*(2), 428–438.

Degors, I. M. S., Wang, C., Rehman, Z. U., & Zuhorn, I. S. (2019). Carriers Break Barriers in Drug Delivery: Endocytosis and Endosomal Escape of Gene Delivery Vectors. *Accounts of Chemical Research*, *52*(7), 1750–1760.

Demidenko, Z. N., & Blagosklonny, M. V. (2004). Flavopiridol induces p53 via initial inhibition of Mdm2 and p21 and, independently of p53, sensitizes apoptosis-reluctant cells to tumor necrosis factor. *Cancer Research*, *64*(10), 3653–3660.

Dent, R., Trudeau, M., Pritchard, K. I., Hanna, W. M., Kahn, H. K., Sawka, C. A., Lickley, L. A., Rawlinson, E., Sun, P., & Narod, S. A. (2007). Triple-negative breast cancer: Clinical features and patterns of recurrence. *Clinical Cancer Research*, *13*(15), 4429–4434.

Depuydt, B., Van Loo, G., Vandenabeele, P., & Declercq, W. (2005). Induction of apoptosis by TNF receptor 2 in a T-cell hybridoma is FADD dependent and blocked by caspase-8 inhibitors. *Journal of Cell Science*, *118*(3), 497–504.

Dhanasekaran, R., Deutzmann, A., Mahauad-Fernandez, W. D., Hansen, A. S., Gouw, A. M., & Felsher, D. W. (2021). The MYC oncogene — the grand orchestrator of cancer growth and immune evasion. *Nature Reviews Clinical Oncology*, *19*(1), 23–36.

Dieci, M. V., Orvieto, E., Dominici, M., Conte, P., & Guarneri, V. (2014). Rare breast cancer subtypes: histological, molecular, and clinical peculiarities. *The Oncologist*, *19*(8), 805–813.

Díez, I., & Ras, R. H. A. (2010). Few-Atom Silver Clusters as Fluorescent Reporters. In A. P. Demchenko (Ed.), *Advanced Fluorescence Reporters in Chemistry and Biology* (II, pp. 307–332). Springer Berlin Heidelberg.

Dinarello, C. A., Cannon, J. G., Wolff, S. M., Bernheim, H. A., Beutler, B., Cerami, A., Figari, I. S., Palladino, M. A., & O'Connor, J. V. (1986). Tumor necrosis factor (cachectin) is an endogenous pyrogen and induces production of interleukin 1. *Journal of Experimental*

Medicine, *163*(6), 1433–1450.

Ding, W., Liu, Y., Li, Y., Shi, Q., Li, H., Xia, H., Wang, D., & Tao, X. (2014). Water-soluble gold nanoclusters with pH-dependent fluorescence and high colloidal stability over a wide pH range via co-reduction of glutathione and citrate. *RSC Advances*, *4*(43), 22651–22659.

Domonkos, A., Udvardy, A., László, L., Nagy, T., & Duda, E. (2001). Receptor-like Properties of the 26 kDa Transmembrane Form of TNF. *European Cytokine Network*, *12*(3), 411–419.

Donato, N. J., & Klostergaard, J. (2004). Distinct stress and cell destruction pathways are engaged by TNF and ceramide during apoptosis of MCF-7 cells. *Experimental Cell Research*, *294*(2), 523–533.

Dong, L., Li, M., Zhang, S., Li, J., Shen, G., Tu, Y., Zhu, J., & Tao, J. (2015). Cytotoxicity of BSA-Stabilized Gold Nanoclusters: In Vitro and In Vivo Study. *Small*, *11*(21), 2571–2581.

Dong, R., Wang, Q., He, X. L., Chu, Y. K., Lu, J. G., & Ma, Q. J. (2007). Role of nuclear factor kappa B and reactive oxygen species in the tumor necrosis factor-α-induced epithelial-mesenchymal transition of MCF-7 cells. *Brazilian Journal of Medical and Biological Research*, *40*(8), 1071–1078.

Dostert, C., Grusdat, M., Letellier, E., & Brenner, D. (2019). The TNF family of ligands and receptors: Communication modules in the immune system and beyond. *Physiological Reviews*, *99*(1), 115–160.

Duan, H., & Nie, S. (2007). Etching colloidal gold nanocrystals with hyperbranched and multivalent polymers: A new route to fluorescent and water-soluble atomic clusters. *Journal of the American Chemical Society*, *129*(9), 2412–2413.

Duan, Y., Duan, R., Liu, R., Guan, M., Chen, W., Ma, J., Chen, M., Du, B., & Zhang, Q. (2018). Chitosan-Stabilized Self-Assembled Fluorescent Gold Nanoclusters for Cell Imaging and Biodistribution in Vivo. *ACS Biomaterials Science and Engineering*, *4*(3), 1055–1063.

Dubik, D., & Shiu, R. P. C. (1988). Transcriptional regulation of c-myc oncogene expression by estrogen in hormone-responsive human breast cancer cells. *Journal of Biological Chemistry*, *263*(25), 12705–12708.

Duffy, M. J., O'Grady, S., Tang, M., & Crown, J. (2021). MYC as a target for cancer treatment. *Cancer Treatment Reviews*, *94*, 102154.

Eberhardy, S. R., & Farnham, P. J. (2002). Myc Recruits P-TEFb to Mediate the Final Step in the Transcriptional Activation of the cad Promoter. *Journal of Biological Chemistry*, *277*(42), 40156–40162.

Egberts, J. H., Cloosters, V., Noack, A., Schniewind, B., Thon, L., Klose, S., Kettler, B., Von Forstner, C., Kneitz, C., Tepel, J., Adam, D., Wajant, H., Kalthoff, H., & Trauzold, A. (2008). Anti-tumor necrosis factor therapy inhibits pancreatic tumor growth and metastasis. *Cancer Research*, *68*(5), 1443–1450.

El-Tahan, R. R., Ghoneim, A. M., & El-Mashad, N. (2016). TNF-α gene polymorphisms and expression. *SpringerPlus*, *5*(1), 1508.

Elahi, N., Kamali, M., & Baghersad, M. H. (2018). Recent biomedical applications of gold nanoparticles: A review. *Talanta*, *184*, 537–556.

Elbadawy, M., Usui, T., Yamawaki, H., & Sasaki, K. (2019). Emerging Roles of C-Myc in

Cancer Stem Cell-Related Signaling and Resistance to Cancer Chemotherapy: A Potential Therapeutic Target Against Colorectal Cancer. *International Journal of Molecular Sciences 2019, Vol. 20, Page 2340*, *20*(9), 2340.

Eliyahu, H., Barenholz, Y., & Domb, A. J. (2005). Polymers for DNA delivery. *Molecules*, *10*(1), 34–64.

Ellermann, V., & Bang, O. (1909). Experimentelle Leukämie bei Hühnern. II. *Zeitschrift Für Hygiene Und Infektionskrankheiten*, *63*(1), 231–272.

Escudero-Francos, M. A., Cepas, V., González-Menédez, P., Badía-Laíño, R., Díaz-García, M. E., Sainz, R. M., Mayo, J. C., & Hevia, D. (2017). Cellular Uptake and Tissue Biodistribution of Functionalized Gold Nanoparticles and Nanoclusters. *Journal of Biomedical Nanotechnology*, *13*(2), 167–179.

Faiola, F., Liu, X., Lo, S., Pan, S., Zhang, K., Lymar, E., Farina, A., & Martinez, E. (2005). Dual Regulation of c-Myc by p300 via Acetylation-Dependent Control of Myc Protein Turnover and Coactivation of Myc-Induced Transcription. *Molecular and Cellular Biology*, *25*(23), 10220–10234.

Fajardo, L. F., Kwan, H. H., Kowalski, J., Prionas, S. D., & Allison, A. C. (1992). Dual role of tumor necrosis factor-α in angiogenesis. *American Journal of Pathology*, *140*(3), 539–544.

Fakhraldeen, S. A., Clark, R. J., Roopra, A., Chin, E. N., Huang, W., Castorino, J., Wisinski, K. B., Kim, T. W., Spiegelman, V. S., & Alexander, C. M. (2015). Two Isoforms of the RNA Binding Protein, Coding Region Determinant-binding Protein (CRD-BP/IGF2BP1), Are Expressed in Breast Epithelium and Support Clonogenic Growth of Breast Tumor Cells. *The Journal of Biological Chemistry*, *290*(21), 13386–13400.

Fallah, Y., Brundage, J., Allegakoen, P., & Shajahan-Haq, A. N. (2017). MYC-Driven pathways in breast cancer subtypes. *Biomolecules*, *7*(3), 53.

Fam, S. Y., Chee, C. F., Yong, C. Y., Ho, K. L., Mariatulqabtiah, A. R., & Tan, W. S. (2020). Stealth Coating of Nanoparticles in Drug-Delivery Systems. *Nanomaterials*, *10*(4), 787.

Fang, C., Shi, B., Pei, Y. Y., Hong, M. H., Wu, J., & Chen, H. Z. (2006). In vivo tumor targeting of tumor necrosis factor-α-loaded stealth nanoparticles: Effect of MePEG molecular weight and particle size. *European Journal of Pharmaceutical Sciences*, *27*(1), 27–36.

Fang, Y., Xue, J., Gao, S., Lu, A., Yang, D., Jiang, H., He, Y., & Shi, K. (2017). Cleavable PEGylation: a strategy for overcoming the "PEG dilemma" in efficient drug delivery. *Drug Delivery*, *24*(2), 22–32.

Farhan, M., and Rizvi, A. (2022). Understanding the Prooxidant Action of Plant Polyphenols in the Cellular Microenvironment of Malignant Cells: Role of Copper and Therapeutic Implications. *Frontiers in Pharmacology*, *13*, 929853.

Farrag, M., & Mohamed, R. A. (2016). Ecotoxicity of ∼1 nm silver and palladium nanoclusters protected by l-glutathione on the microbial growth under light and dark conditions. *Journal of Photochemistry and Photobiology A: Chemistry*, *330*, 117–125.

Fechtner, S., Fox, D. A., & Ahmed, S. (2017). Transforming growth factor β activated kinase 1: a potential therapeutic target for rheumatic diseases. *Rheumatology*, *56*(7), 1060–1068.

Felgner, S., Kocijancic, D., Frahm, M., & Weiss, S. (2016). Bacteria in Cancer Therapy: Renaissance of an Old Concept. *International Journal of Microbiology*, *2016*.

Feng, Y., Spezia, M., Huang, S., Yuan, C., Zeng, Z., Zhang, L., Ji, X., Liu, W., Huang, B., Luo, W., Liu, B., Lei, Y., Du, S., Vuppalapati, A., Luu, H. H., Haydon, R. C., He, T. C., & Ren, G. (2018). Breast cancer development and progression: Risk factors, cancer stem cells, signaling pathways, genomics, and molecular pathogenesis. *Genes and Diseases*, *5*(2), 77–106.

Figueroa, J. D., Pfeiffer, R. M., Patel, D. A., Linville, L., Brinton, L. A., Gierach, G. L., Yang, X. R., Papathomas, D., Visscher, D., Mies, C., Degnim, A. C., Anderson, W. F., Hewitt, S., Khodr, Z. G., Clare, S. E., Storniolo, A. M., & Sherman, M. E. (2014). Terminal Duct Lobular Unit Involution of the Normal Breast: Implications for Breast Cancer Etiology. *Journal of the National Cancer Institute*, *106*(10), dju186.

Fire, A., Xu, S., Montgomery, M. K., Kostas, S. A., Driver, S. E., & Mello, C. C. (1998). Potent and specific genetic interference by double-stranded RNA in caenorhabditis elegans. *Nature*, *391*(6669), 806–811.

Fischer, R., Kontermann, R. E., & Pfizenmaier, K. (2020). Selective Targeting of TNF Receptors as a Novel Therapeutic Approach. *Frontiers in Cell and Developmental Biology*, *8*, 401.

Fischer, R., Maier, O., Siegemund, M., Wajant, H., Scheurich, P., & Pfizenmaier, K. (2011). A TNF Receptor 2 Selective Agonist Rescues Human Neurons from Oxidative Stress-Induced Cell Death. *PLoS ONE*, *6*(11), e27621.

Fleischer, C. C., & Payne, C. K. (2012). Nanoparticle surface charge mediates the cellular receptors used by protein-nanoparticle complexes. *Journal of Physical Chemistry B*, *116*(30), 8901–8907.

Forrest, M. L., Meister, G. E., Koerber, J. T., & Pack, D. W. (2004). Partial Acetylation of Polyethylenimine Enhances In Vitro Gene Delivery. *Pharmaceutical Research 2004 21:2*, *21*(2), 365–371.

Forrest, M. L., & Pack, D. W. (2002). On the Kinetics of Polyplex Endocytic Trafficking: Implications for Gene Delivery Vector Design. *Molecular Therapy*, *6*(1), 57–66.

Fotin-Mleczek, M., Henkler, F., Samel, D., Reichwein, M., Hausser, A., Parmryd, I., Scheurich, P., Schmid, J. A., & Wajant, H. (2002). Apoptotic crosstalk of TNF receptors: TNF-R2-induces depletion of TRAF2 and IAP proteins and accelerates TNF-R1-dependent activation of caspase-8. *Journal of Cell Science*, *115*(13), 2757–2770.

Fragomeni, S. M., Sciallis, A., & Jeruss, J. S. (2018). Molecular Subtypes and Local-Regional Control of Breast Cancer. *Surgical Oncology Clinics of North America*, *27*(1), 95–120.

Francisco, L. M., Salinas, V. H., Brown, K. E., Vanguri, V. K., Freeman, G. J., Kuchroo, V. K., & Sharpe, A. H. (2009). PD-L1 regulates the development, maintenance, and function of induced regulatory T cells. *Journal of Experimental Medicine*, *206*(13), 3015–3029.

Frasor, J., Weaver, A., Pradhan, M., Dai, Y., Miller, L. D., Lin, C. Y., & Stanculescu, A. (2009). Positive cross-talk between estrogen receptor and NF-κB in breast cancer. *Cancer Research*, *69*(23), 8918–8925.

Freire, M. O., & Van Dyke, T. E. (2013). Natural resolution of inflammation. *Periodontology 2000*, *63*(1), 149–164.

Frens, G. (1973). Controlled Nucleation for the Regulation of the Particle Size in Monodisperse Gold Suspensions. *Nature Physical Science*, *241*(105), 20–22.

Friedmann, E., Hauben, E., Maylandt, K., Schleeger, S., Vreugde, S., Lichtenthaler, S. F., Kuhn, P. H., Stauffer, D., Rovelli, G., & Martoglio, B. (2006). SPPL2a and SPPL2b promote intramembrane proteolysis of TNFα in activated dendritic cells to trigger IL-12 production. *Nature Cell Biology*, *8*(8), 843–848.

Fritsch, J., Stephan, M., Tchikov, V., Winoto-Morbach, S., Gubkina, S., Kabelitz, D., & Schutze, S. (2014). Cell Fate Decisions Regulated by K63 Ubiquitination of Tumor Necrosis Factor Receptor 1. *Molecular and Cellular Biology*, *34*(17), 3214–3228.

Fujinami, A., & Inamoto, K. (1914). Ueber Geschwülste bei japanischen Haushühnern, insbesondere über einen transplantablen Tumor. *Zeitschrift Für Krebsforschung*, *14*(1), 94–119.

Furtado, D., Björnmalm, M., Ayton, S., Bush, A. I., Kempe, K., & Caruso, F. (2018). Overcoming the Blood-Brain Barrier: The Role of Nanomaterials in Treating Neurological Diseases. *Advanced Materials*, *30*(46), 1801362.

Gabay, M., Li, Y., & Felsher, D. W. (2014). MYC activation is a hallmark of cancer initiation and maintenance. *Cold Spring Harbor Perspectives in Medicine*, *4*(6), a014241.

Gabrielson, N. P., & Pack, D. W. (2006). Acetylation of Polyethylenimine Enhances Gene Delivery via Weakened Polymer/DNA Interactions. *Biomacromolecules*, *7*(8), 2427–2435.

Galitsyna, E. V., Bukharova, T. B., Buianova, A. A., Davygora, K. S., & Goldshtein, D. V. (2021). Choice of an Effective System of Nonviral siRNA Delivery to Multipotent Mesenchymal Stromal Cells. *Applied Biochemistry and Microbiology*, *57*(7), 823–827.

Gao, X., Loggie, B. W., & Nawaz, Z. (2002). The roles of sex steroid receptor coregulators in cancer. *Molecular Cancer*, *1*, 7.

Gao, Z., Hao, Y., Zheng, M., & Chen, Y. (2017). A fluorescent dye with large Stokes shift and high stability: synthesis and application to live cell imaging. *RSC Advances*, *7*(13), 7604–7609.

García-Pinel, B., Porras-Alcalá, C., Ortega-Rodríguez, A., Sarabia, F., Prados, J., Melguizo, C., & López-Romero, J. M. (2019). Lipid-based nanoparticles: Application and recent advances in cancer treatment. *Nanomaterials*, *9*(4), 638.

García-Tuñón, I., Ricote, M., Ruiz, A., Fraile, B., Paniagua, R., & Royuela, M. (2006). Role of tumor necrosis factor-α and its receptors in human benign breast lesions and tumors (*in situ* and infiltrative). *Cancer Science*, *97*(10), 1044–1049.

Gary, D. J., Puri, N., & Won, Y. Y. (2007). Polymer-based siRNA delivery: Perspectives on the fundamental and phenomenological distinctions from polymer-based DNA delivery. *Journal of Controlled Release*, *121*(1–2), 64–73.

Ge, Y., Zhang, Y., Xia, J., Ma, M., He, S., Nie, F., & Gu, N. (2009). Effect of surface charge and agglomerate degree of magnetic iron oxide nanoparticles on KB cellular uptake in vitro. *Colloids and Surfaces B: Biointerfaces*, *73*(2), 294–301.

Geng, Y., Chandrasekaran, S., Hsu, J. W., Gidwani, M., Hughes, A. D., & King, M. R. (2013). Phenotypic Switch in Blood: Effects of Pro-Inflammatory Cytokines on Breast Cancer Cell Aggregation and Adhesion. *PLoS ONE*, *8*(1), e54959.

Gerratana, L., Fanotto, V., Bonotto, M., Bolzonello, S., Minisini, A. M., Fasola, G., & Puglisi, F. (2015). Pattern of metastasis and outcome in patients with breast cancer. *Clinical and Experimental Metastasis*, *32*(2), 125–133.

Ghasemiyeh, P., & Mohammadi-Samani, S. (2018). Solid lipid nanoparticles and nanostructured lipid carriers as novel drug delivery systems: Applications, advantages and disadvantages. *Research in Pharmaceutical Sciences*, *13*(4), 288–303.

Girija, A. R., Balasubramanian, S., Bright, R., Cowin, A. J., Goswami, N., & Vasilev, K. (2019). Ultrasmall Gold Nanocluster Based Antibacterial Nanoaggregates for Infectious Wound Healing. *ChemNanoMat*, *5*(9), 1176–1181.

Gong, X., Hou, Z., Endsley, M. P., Gronseth, E. I., Rarick, K. R., Jorns, J. M., Yang, Q., Du, Z., Yan, K., Bordas, M. L., Gershan, J., Deepak, P., Geethadevi, A., Chaluvally-Raghavan, P., Fan, Y., Harder, D. R., Ramchandran, R., & Wang, L. (2019). Interaction of tumor cells and astrocytes promotes breast cancer brain metastases through TGF-β2/ANGPTL4 axes. *Npj Precision Oncology*, *3*, 24.

Gonzalez, H., Hagerling, C., & Werb, Z. (2018). Roles of the immune system in cancer: From tumor initiation to metastatic progression. *Genes and Development*, *32*(19–20), 1267–1284.

Goswami, N., Lin, F., Liu, Y., Leong, D. T., & Xie, J. (2016). Highly Luminescent Thiolated Gold Nanoclusters Impregnated in Nanogel. *Chemistry of Materials*, *28*(11), 4009–4016.

Green, A. R., Aleskandarany, M. A., Agarwal, D., Elsheikh, S., Nolan, C. C., Diez-Rodriguez, M., Macmillan, R. D., Ball, G. R., Caldas, C., Madhusudan, S., Ellis, I. O., & Rakha, E. A. (2016). MYC functions are specific in biological subtypes of breast cancer and confers resistance to endocrine therapy in luminal tumours. *British Journal of Cancer*, *114*(8), 917–928.

Gref, R., Lück, M., Quellec, P., Marchand, M., Dellacherie, E., Harnisch, S., Blunk, T., & Müller, R. . (2000). 'Stealth' corona-core nanoparticles surface modified by polyethylene glycol (PEG): influences of the corona (PEG chain length and surface density) and of the core composition on phagocytic uptake and plasma protein adsorption. *Colloids and Surfaces B: Biointerfaces*, *18*(3–4), 301–313.

Gregory, M. A., & Hann, S. R. (2000). c-Myc Proteolysis by the Ubiquitin-Proteasome Pathway: Stabilization of c-Myc in Burkitt's Lymphoma Cells. *Molecular and Cellular Biology*, *20*(7), 2423–2435.

Grell, M., Douni, E., Wajant, H., Löhden, M., Clauss, M., Maxeiner, B., Georgopoulos, S., Lesslauer, W., Kollias, G., Pfizenmaier, K., & Scheurich, P. (1995). The transmembrane form of tumor necrosis factor is the prime activating ligand of the 80 kDa tumor necrosis factor receptor. *Cell*, *83*(5), 793–802.

Grimm, D. (2011). The dose can make the poison: lessons learned from adverse in vivo toxicities caused by RNAi overexpression. *Silence*, *2*, 8.

Grivennikov, S. I., Greten, F. R., & Karin, M. (2010). Immunity, Inflammation, and Cancer. *Cell*, *140*(6), 883–899.

Grushko, T. A., Dignam, J. J., Das, S., Blackwood, A. M., Perou, C. M., Ridderstråle, K. K., Anderson, K. N., Wei, M. J., Adams, A. J., Hagos, F. G., Sveen, L., Lynch, H. T., Weber, B. L., & Olopade, O. I. (2004). MYC Is Amplified in BRCA1-Associated Breast Cancers. *Clinical Cancer Research*, *10*(2), 499–507.

Gu, J., Clegg, J. R., Heersema, L. A., Peppas, N. A., & Smyth, H. D. C. (2020). Optimization of Cationic Nanogel PEGylation to Achieve Mammalian Cytocompatibility with Limited Loss of Gram-Negative Bactericidal Activity. *Biomacromolecules*, *21*(4), 1528–1538.

Gu, Y., Zhang, J., Ma, X., Kim, B. wook, Wang, H., Li, J., Pan, Y., Xu, Y., Ding, L., Yang, L., Guo, C., Wu, X., Wu, J., Wu, K., Gan, X., Li, G., Li, L., Forman, S. J., Chan, W. C., … Huang, W. (2017). Stabilization of the c-Myc protein by CAMKIIγ promotes T cell lymphoma. *Cancer Cell*, *32*(1), 115-128.e7.

Guaresti, O., Maiz–Fernández, S., Palomares, T., Alonso–Varona, A., Eceiza, A., Pérez–Álvarez, L., & Gabilondo, N. (2020). Dual charged folate labelled chitosan nanogels with enhanced mucoadhesion capacity for targeted drug delivery. *European Polymer Journal*, *134*, 109847.

Gun, S. Y., Lee, S. W. L., Sieow, J. L., & Wong, S. C. (2019). Targeting immune cells for cancer therapy. *Redox Biology*, *25*, 101174.

Gunnarsdóttir, F. B., Hagerling, C., Bergenfelz, C., Mehmeti, M., Källberg, E., Allaoui, R., Mohlin, S., Påhlman, S., Larsson, C., Jirström, K., Bexell, D., & Leandersson, K. (2020). Inflammatory macrophage derived TNFα downregulates estrogen receptor α via FOXO3a inactivation in human breast cancer cells. *Experimental Cell Research*, *390*(1), 111932.

Guo, J., Cheng, W. P., Gu, J., Ding, C., Qu, X., Yang, Z., & O'Driscoll, C. (2012). Systemic delivery of therapeutic small interfering RNA using a pH-triggered amphiphilic poly-l-lysine nanocarrier to suppress prostate cancer growth in mice. *European Journal of Pharmaceutical Sciences*, *45*(5), 521–532.

Guo, S., & Kemphues, K. J. (1995). par-1, a gene required for establishing polarity in C. elegans embryos, encodes a putative Ser/Thr kinase that is asymmetrically distributed. *Cell*, *81*(4), 611–620.

Gupta, G. K., Collier, A. L., Lee, D., Hoefer, R. A., Zheleva, V., Siewertsz van Reesema, L. L., Tang-Tan, A. M., Guye, M. L., Chang, D. Z., Winston, J. S., Samli, B., Jansen, R. J., Petricoin, E. F., Goetz, M. P., Bear, H. D., & Tang, A. H. (2020). Perspectives on Triple-Negative Breast Cancer: Current Treatment Strategies, Unmet Needs, and Potential Targets for Future Therapies. *Cancers*, *12*(9), 2392.

Gupta, N., Jung, K., Wu, C., Alshareef, A., Alqahtani, H., Damaraju, S., Mackey, J. R., Ghosh, S., Sabri, S., Abdulkarim, B. S., Bigras, G., & Lai, R. (2017). High Myc expression and transcription activity underlies intratumoral heterogeneity in triple-negative breast cancer. *Oncotarget*, *8*(17), 28101–28115.

Gustin, J. A., Ozes, O. N., Akca, H., Pincheira, R., Mayo, L. D., Li, Q., Guzman, J. R., Korgaonkar, C. K., & Donner, D. B. (2004). Cell Type-specific Expression of the IκB Kinases Determines the Significance of Phosphatidylinositol 3-Kinase/Akt Signaling to NF-κB Activation. *Journal of Biological Chemistry*, *279*(3), 1615–1620.

Guţoaia, A., Schuster, L., Margutti, S., Laufer, S., Schlosshauer, B., Krastev, R., Stoll, D., & Hartmann, H. (2016). Fine-tuned PEGylation of chitosan to maintain optimal siRNA-nanoplex bioactivity. *Carbohydrate Polymers*, *143*, 25–34.

Guzman-Villanueva, D., El-Sherbiny, I. M., Vlassov, A. V., Herrera-Ruiz, D., & Smyth, H. D. C. (2014). Enhanced cellular uptake and gene silencing activity of siRNA molecules mediated by chitosan-derivative nanocomplexes. *International Journal of Pharmaceutics*, *473*(1–2), 579–590.

Habib, S., Daniels, A., Ariatti, M., Singh, M., Arbuthnot, P., Ajiboye, B. O., & Babalola, A. (2021). Anti-*c-myc* cholesterol based lipoplexes as onco-nanotherapeutic agents *in vitro*. *F1000Research 2021* , *9*, 770.

Hadjidemetriou, M., Mcadam, S., Garner, G., Thackeray, C., Knight, D., Smith, D., Al-Ahmady, Z., Mazza, M., Rogan, J., Clamp, A., Kostarelos, K., Hadjidemetriou, M., Al-Ahmady, Z., Mazza, M., Kostarelos, K., Mcadam, S., Garner, G., Rogan, J., Thackeray, C., … Smith, D. (2019). The Human In Vivo Biomolecule Corona onto PEGylated Liposomes: A Proof-of-Concept Clinical Study. *Advanced Materials*, *31*(4), 1803335.

Hajifathaliha, F., Mahboubi, A., Nematollahi, L., Mohit, E., & Bolourchian, N. (2020). Comparison of different cationic polymers efficacy in fabrication of alginate multilayer microcapsules. *Asian Journal of Pharmaceutical Sciences*, *15*(1), 95–103.

Halawa, M. I., Lai, J., & Xu, G. (2018). Gold nanoclusters: synthetic strategies and recent advances in fluorescent sensing. *Materials Today Nano*, *3*, 9–27.

Halazonetis, T. D., & Kandil, A. N. (1991). Determination of the c-MYC DNA-binding site. *Proceedings of the National Academy of Sciences of the United States of America*, *88*(14), 6162–6166.

Hall, J. B., Dobrovolskaia, M. A., Patri, A. K., & McNeil, S. E. (2007). Characterization of nanoparticles for therapeutics. *Nanomedicine*, *2*(6), 789–803.

Hamaguchi, T., Wakabayashi, H., Matsumine, A., Sudo, A., & Uchida, A. (2011). TNF inhibitor suppresses bone metastasis in a breast cancer cell line. *Biochemical and Biophysical Research Communications*, *407*(3), 525–530.

Hanahan, D., & Coussens, L. M. (2012). Accessories to the Crime: Functions of Cells Recruited to the Tumor Microenvironment. *Cancer Cell*, *21*(3), 309–322.

Hann, S. R. (2014). MYC Cofactors: Molecular Switches Controlling Diverse Biological Outcomes. *Cold Spring Harbor Perspectives in Medicine*, *4*(9), a014399.

Haranaka, K., Satomi, N., & Sakurai, A. (1984). Antitumor activity of murine tumor necrosis factor (TNF) against transplanted murine tumors and heterotransplanted human tumors in nude mice. *International Journal of Cancer*, *34*(2), 263–267.

Harris, A. R., Perez, M. J., & Munson, J. M. (2018). Docetaxel facilitates lymphatic-tumor crosstalk to promote lymphangiogenesis and cancer progression. *BMC Cancer*, *18*(1), 718.

Hatakeyama, H., Akita, H., & Harashima, H. (2013). The polyethyleneglycol dilemma: advantage and disadvantage of PEGylation of liposomes for systemic genes and nucleic acids delivery to tumors. *Biological & Pharmaceutical Bulletin*, *36*(6), 892–899.

Hayden, M. S., & Ghosh, S. (2008). Shared Principles in NF-κB Signaling. *Cell*, *132*(3), 344–362.

He, C., Yue, H., Xu, L., Liu, Y., Song, Y., Tang, C., & Yin, C. (2020). siRNA release kinetics from polymeric nanoparticles correlate with RNAi efficiency and inflammation therapy via oral delivery. *Acta Biomaterialia*, *103*, 213–222.

Helleday, T. (2011). The underlying mechanism for the PARP and BRCA synthetic lethality: Clearing up the misunderstandings. *Molecular Oncology*, *5*(4), 387–393.

Hemann, M. T., Bric, A., Teruya-Feldstein, J., Herbst, A., Nilsson, J. A., Cordon-Cardo, C., Cleveland, J. L., Tansey, W. P., & Lowe, S. W. (2005). Evasion of the p53 tumour surveillance network by tumour-derived MYC mutants. *Nature*, *436*(7052), 807–811.

Heo, S. C., Jeon, E. S., Lee, I. H., Kim, H. S., Kim, M. B., & Kim, J. H. (2011). Tumor necrosis

factor-α-activated human adipose tissue-derived mesenchymal stem cells accelerate cutaneous wound healing through paracrine mechanisms. *Journal of Investigative Dermatology*, *131*(7), 1559–1567.

Herbst, A., Hemann, M. T., Tworkowski, K. A., Salghetti, S. E., Lowe, S. W., & Tansey, W. P. (2005). A conserved element in Myc that negatively regulates its proapoptotic activity. *EMBO Reports*, *6*(2), 177–183.

Herrera-Carrillo, E., Liu, Y. P., & Berkhout, B. (2017). Improving miRNA Delivery by Optimizing miRNA Expression Cassettes in Diverse Virus Vectors. *Human Gene Therapy Methods*, *28*(4), 177–190.

Hijdra, D., Vorselaars, A. D., Grutters, J. C., Claessen, A. M., & Rijkers, G. T. (2012). Differential expression of TNFR1 (CD120a) and TNFR2 (CD120b) on subpopulations of human monocytes. *Journal of Inflammation*, *9*(1), 38.

Hikita, A., Tanaka, N., Yamane, S., Ikeda, Y., Furukawa, H., Tohma, S., Suzuki, R., Tanaka, S., Mitomi, H., & Fukui, N. (2009). Involvement of a disintegrin and metalloproteinase 10 and 17 in shedding of tumor necrosis factor-α. *Biochemistry and Cell Biology*, *87*(4), 581–593.

Hill, M. J., & Sarkar, D. (2017). Polyurethane Microgel Based Microtissue: Interface-Guided Assembly and Spreading. *Langmuir*, *33*(24), 6167–6181.

Hillaireau, H., & Couvreur, P. (2009). Nanocarriers' entry into the cell: relevance to drug delivery. *Cellular and Molecular Life Sciences*, *66*(17), 2873–2896.

Hoeflich, K. P., O'Brien, C., Boyd, Z., Cavet, G., Guerrero, S., Jung, K., Januario, T., Savage, H., Punnoose, E., Truong, T., Zhou, W., Berry, L., Murray, L., Amler, L., Belvin, M., Friedman, L. S., & Lackner, M. R. (2009). In vivo antitumor activity of MEK and phosphatidylinositol 3-kinase inhibitors in basal-like breast cancer models. *Clinical Cancer Research*, *15*(14), 4649–4664.

Hofmann, S., Grasberger, H., Jung, P., Bidlingmaier, M., Vlotides, J., Janssen, O. E., & Landgraf, R. (2002). The tumour necrosis factor-alpha induced vascular permeability is associated with a reduction of VE-cadherin expression. *European Journal of Medical Research*, *7*(4), 171–176.

Hong, C. A., Son, H. Y., & Nam, Y. S. (2018). Layer-by-layer siRNA/poly(L-lysine) Multilayers on Polydopamine-coated Surface for Efficient Cell Adhesion and Gene Silencing. *Scientific Reports*, *8*(1), 1–7.

Hong, S., Wang, T. Y., Secombes, C. J., & Wang, T. (2019). Different origins of paralogues of salmonid TNR1 and TNFR2: Characterisation and expression analysis of four TNF receptor genes in rainbow trout Oncorhynchus mykiss. *Developmental and Comparative Immunology*, *99*, 103403.

Horiuchi, D., Kusdra, L., Huskey, N. E., Chandriani, S., Lenburg, M. E., Gonzalez-Angulo, A. M., Creasman, K. J., Bazarov, A. V., Smyth, J. W., Davis, S. E., Yaswen, P., Mills, G. B., Esserman, L. J., & Goga, A. (2012). MYC pathway activation in triple-negative breast cancer is synthetic lethal with CDK inhibition. *Journal of Experimental Medicine*, *209*(4), 679–696.

Horiuchi, T., Mitoma, H., Harashima, S., Tsukamoto, H., & Shimoda, T. (2010). Transmembrane TNF-alpha: structure, function and interaction with anti-TNF agents. *Rheumatology*, *49*(7), 1215–1228.

Howard, M. D., Jay, M., Dziubla, T. D., & Lu, X. (2008). PEGylation of nanocarrier drug

delivery systems: State of the art. *Journal of Biomedical Nanotechnology*, *4*(2), 133–148.

Hsu, H., Huang, J., Shu, H. B., Baichwal, V., & Goeddel, D. V. (1996). TNF-dependent recruitment of the protein kinase RIP to the TNF receptor-1 signaling complex. *Immunity*, *4*(4), 387–396.

Hu, X., Gao, S., Wang, P., Zhou, Y., Chen, K., Chen, Q., Wang, B., Hu, W., Cheng, P., Eid, R., Giraud-Panis, M. J., Wang, L., Gilson, E., Ye, J., & Lu, Y. (2021). The knockdown efficiency of telomere associated genes with specific methodology in a zebrafish cell line. *Biochimie*, *190*, 12–19.

Hu, X. Q., Chen, W. L., Ma, H. G., & Jiang, K. (2017). Androgen receptor expression identifies patient with favorable outcome in operable triple negative breast cancer. *Oncotarget*, *8*(34), 56364–56374.

Huang, H., Feng, W., Chen, Y., and Shi, J. (2020). Inorganic nanoparticles in clinical trials and translations. *Nano Today*, *35*, 100972.

Huang, Y., Cheng, Q., Ji, J. L., Zheng, S., Du, L., Meng, L., Wu, Y., Zhao, D., Wang, X., Lai, L., Cao, H., Xiao, K., Gao, S., & Liang, Z. (2016). Pharmacokinetic behaviors of intravenously administered siRNA in glandular tissues. *Theranostics*, *6*(10), 1528–1541.

Huang, Y., Fuksman, L., & Zheng, J. (2018). Luminescence mechanisms of ultrasmall gold nanoparticles. *Dalton Transactions*, *47*(18), 6267–6273.

Huo, H., Gao, Y., Wang, Y., Zhang, J., Wang, Z., Jiang, T., & Wang, S. (2015). Polyion complex micelles composed of pegylated polyasparthydrazide derivatives for siRNA delivery to the brain. *Journal of Colloid And Interface Science*, *447*, 8–15.

Huo, S., Chen, S., Gong, N., Liu, J., Li, X., Zhao, Y., & Liang, X. J. (2017). Ultrasmall gold nanoparticles behavior in vivo modulated by surface polyethylene glycol (PEG) grafting. *Bioconjugate Chemistry*, *28*(1), 239–243.

Huotari, J., & Helenius, A. (2011). Endosome maturation. *The EMBO Journal*, *30*(17), 3481–3500.

Ieda, T., Tazawa, H., Okabayashi, H., Yano, S., Shigeyasu, K., Kuroda, S., Ohara, T., Noma, K., Kishimoto, H., Nishizaki, M., Kagawa, S., Shirakawa, Y., Saitou, T., Imamura, T., & Fujiwara, T. (2019). Visualization of epithelial-mesenchymal transition in an inflammatory microenvironment–colorectal cancer network. *Scientific Reports*, *9*(1), 1–11.

Ilic, N., Utermark, T., Widlund, H. R., & Roberts, T. M. (2011). PI3K-targeted therapy can be evaded by gene amplification along the MYC-eukaryotic translation initiation factor 4E (eIF4E) axis. *Proceedings of the National Academy of Sciences of the United States of America*, *108*(37), E699–E708.

Imani, R., Prakash, S., Vali, H., & Faghihi, S. (2018). Polyethylene glycol and octa-arginine dual-functionalized nanographene oxide: an optimization for efficient nucleic acid delivery. *Biomaterials Science*, *6*(6), 1636–1650.

Inoue, M., Kamada, H., Abe, Y., Higashisaka, K., Nagano, K., Mukai, Y., Yoshioka, Y., Tsutsumi, Y., & Tsunoda, S. I. (2015). Aminopeptidase P3, a new member of the TNF-TNFR2 signaling complex, induces phosphorylation of JNK1 and JNK2. *Journal of Cell Science*, *128*(4), 656–669.

Ip, M. M., Shoemaker, S. F., & Darcy, K. M. (1992). Regulation of rat mammary epithelial

cell proliferation and differentiation by tumor necrosis factor-alpha. *Endocrinology*, *130*(5), 2833–2844.

Ishii, T., Okahata, Y., & Sato, T. (2001). Mechanism of cell transfection with plasmid/chitosan complexes. *Biochimica et Biophysica Acta (BBA) - Biomembranes*, *1514*(1), 51–64.

ISO. (2009). *Biological evaluation of medical devices — Part 5: Tests for in vitro cytotoxicity (ISO Standard No. 10993-5:2009)* (3rd ed.).

Iulia Irimie, A., Braicu, C., Zanoaga, O., Pileczki, V., Soritau, O., Berindan-Neagoe, I., & Septimiu Campian, R. (2015). Inhibition of tumor necrosis factor alpha using RNA interference in oral squamous cell carcinoma. *Journal of B.U.ON. : Official Journal of the Balkan Union of Oncology*, *20*(4), 1107–1114.

Jackson, A. L., Burchard, J., Schelter, J., Chau, B. N., Cleary, M., Lim, L., & Linsley, P. S. (2006). Widespread siRNA "off-target" transcript silencing mediated by seed region sequence complementarity. *RNA*, *12*(7), 1179–1187.

Jang, C., Blume, S. W., & Choi, H. S. (2023). Novel protein products encoded by upstream open reading frames of the MYCN gene in pediatric embryonal tumors. *Journal of Cellular Biochemistry*, *124*(10), 1615–1627.

Jassam, S. A., Maherally, Z., Smith, J. R., Ashkan, K., Roncaroli, F., Fillmore, H. L., & Pilkington, G. J. (2016). TNF-α enhancement of CD62E mediates adhesion of non-small cell lung cancer cells to brain endothelium via CD15 in lung-brain metastasis. *Neuro-Oncology*, *18*(5), 679–690.

Javier, R. T., & Butel, J. S. (2008). The History of Tumor Virology. *Cancer Research*, *68*(19), 7693–7703.

Jeon, S. I., Lee, J. H., Andrade, J. D., & De Gennes, P. G. (1991). Protein-surface interactions in the presence of polyethylene oxide. I. Simplified theory. *Journal of Colloid And Interface Science*, *142*(1), 149–158.

Jeoung, D. Il, Tang, B., & Sonenberg, M. (1995). Effects of tumor necrosis factor-α on antimitogenicity and cell cycle-related proteins in MCF-7 cells. *Journal of Biological Chemistry*, *270*(31), 18367–18373.

Jézéquel, P., Kerdraon, O., Hondermarck, H., Guérin-Charbonnel, C., Lasla, H., Gouraud, W., Canon, J. L., Gombos, A., Dalenc, F., Delaloge, S., Lemonnier, J., Loussouarn, D., Verrièle, V., & Campone, M. (2019). Identification of three subtypes of triple-negative breast cancer with potential therapeutic implications. *Breast Cancer Research*, *21*(1), 65.

Ji, M. H., Kim, S. K., Kim, C. Y., Phi, J. H., Jun, H. J., Blume, S. W., & Choi, H. S. (2016). Physiological Expression and Accumulation of the Products of Two Upstream Open Reading Frames mrtl and MycHex1 Along With p64 and p67 Myc From the Human c-myc Locus. *Journal of Cellular Biochemistry*, *117*(6), 1407–1418.

Ji, W., Li, Y., Wan, T., Wang, J., Zhang, H., Chen, H., & Min, W. (2012). Both internalization and AIP1 association are required for tumor necrosis factor receptor 2-mediated JNK signaling. *Arteriosclerosis, Thrombosis, and Vascular Biology*, *32*(9), 2271–2279.

Ji, X., Han, T., Kang, N., Huang, S., & Liu, Y. (2020). Preparation of RGD4C fused anti-TNFα nanobody and inhibitory activity on triple-negative breast cancer in vivo. *Life Sciences*, *260*, 118274.

Ji, X., Peng, Z., Li, X., Yan, Z., Yang, Y., Qiao, Z., & Liu, Y. (2017). Neutralization of TNFα in tumor with a novel nanobody potentiates paclitaxel-therapy and inhibits metastasis in breast cancer. *Cancer Letters*, *386*, 24–34.

Jiang, Y., Yu, M., Hu, X., Han, L., Yang, K., Ba, H., Zhang, Z., Yin, B., Yang, X. P., Li, Z., & Wang, J. (2017). STAT1 mediates transmembrane TNF-alpha-induced formation of death-inducing signaling complex and apoptotic signaling via TNFR1. *Cell Death and Differentiation*, *24*(4), 660–671.

Jin, R. (2010). Quantum sized, thiolate-protected gold nanoclusters. *Nanoscale*, *2*(3), 343–362.

Jokerst, J. V, Lobovkina, T., Zare, R. N., & Gambhir, S. S. (2011). Nanoparticle PEGylation for imaging and therapy. *Nanomedicine*, *6*(4), 715–728.

Josephs, S. F., Ichim, T. E., Prince, S. M., Kesari, S., Marincola, F. M., Escobedo, A. R., & Jafri, A. (2018). Unleashing endogenous TNF-alpha as a cancer immunotherapeutic. *Journal of Translational Medicine*, *16*(1), 242.

Ju, E., Li, T., Ramos Da Silva, S., & Gao, S. J. (2019). Gold Nanocluster-Mediated Efficient Delivery of Cas9 Protein through pH-Induced Assembly-Disassembly for Inactivation of Virus Oncogenes. *ACS Applied Materials and Interfaces*, *11*(38), 34717–34724.

Julien, O., & Wells, J. A. (2017). Caspases and their substrates. *Cell Death & Differentiation 2017 24:8*, *24*(8), 1380–1389.

Kaliva, M., & Vamvakaki, M. (2020). Nanomaterials characterization. *Polymer Science and Nanotechnology*, 401–433.

Kalkat, M., De Melo, J., Hickman, K. A., Lourenco, C., Redel, C., Resetca, D., Tamachi, A., Tu, W. B., & Penn, L. Z. (2017). MYC Deregulation in Primary Human Cancers. *Genes*, *8*(6), 2–30.

Kalkat, M., Resetca, D., Lourenco, C., Chan, P. K., Wei, Y., Shiah, Y. J., Vitkin, N., Tong, Y., Sunnerhagen, M., Done, S. J., Boutros, P. C., Raught, B., & Penn, L. Z. (2018). MYC Protein Interactome Profiling Reveals Functionally Distinct Regions that Cooperate to Drive Tumorigenesis. *Molecular Cell*, *72*(5), 836-848.e7.

Kalliolias, G. D., & Ivashkiv, L. B. (2016). TNF biology, pathogenic mechanisms and emerging therapeutic strategies. *Nature Reviews Rheumatology*, *12*(1), 49–62.

Kamali-Sarvestani, E., Gharesi-Fard, B., Sarvari, J., & Talei, A. A. R. (2005). Association of TNF-α and TNF-β gene polymorphism with steroid receptor expression in breast cancer patients. *Pathology and Oncology Research*, *11*(2), 99–102.

Kamola, P. J., Nakano, Y., Takahashi, T., Wilson, P. A., & Ui-Tei, K. (2015). The siRNA Non-seed Region and Its Target Sequences Are Auxiliary Determinants of Off-Target Effects. *PLoS Computational Biology*, *11*(12), e1004656.

Kang, H., Wu, Q., Sun, A., Liu, X., Fan, Y., & Deng, X. (2018). Cancer Cell Glycocalyx and Its Significance in Cancer Progression. *International Journal of Molecular Sciences*, *19*(9), 2484.

Kang, K., Lee, S. R., Piao, X., & Hur, G. M. (2019). Post-translational modification of the death receptor complex as a potential therapeutic target in cancer. *Archives of Pharmacal Research*, *42*(1), 76–87.

Kastl, L., Sauer, S. W., Ruppert, T., Beissbarth, T., Becker, M. S., Süss, D., Krammer, P. H., & Gülow, K. (2014). TNF-α mediates mitochondrial uncoupling and enhances ROS-dependent cell migration via NF-κB activation in liver cells. *FEBS Letters*, *588*(1), 175–183.

Katsuta, E., Yan, L., Takeshita, T., McDonald, K.-A., Dasgupta, S., Opyrchal, M., & Takabe, K. (2019). High MYC mRNA Expression Is More Clinically Relevant than MYC DNA Amplification in Triple-Negative Breast Cancer. *International Journal of Molecular Sciences*, *21*(1), 217.

Kaur, M., Tiwana, K., & Singla, N. (2019). Rare breast malignancy subtypes: A cytological, histological, and immunohistochemical correlation. *Nigerian Journal of Surgery*, *25*(1), 70.

Kaur, N., Aditya, R. N., Singh, A., & Kuo, T. R. (2018). Biomedical Applications for Gold Nanoclusters: Recent Developments and Future Perspectives. *Nanoscale Research Letters*, *13*(1), 302.

Kawasaki, H., Hamaguchi, K., Osaka, I., & Arakawa, R. (2011). ph-Dependent Synthesis of Pepsin-Mediated Gold Nanoclusters with Blue Green and Red Fluorescent Emission. *Advanced Functional Materials*, *21*(18), 3508–3515.

Kearney, C. J., Cullen, S. P., Tynan, G. A., Henry, C. M., Clancy, D., Lavelle, E. C., & Martin, S. J. (2015). Necroptosis suppresses inflammation via termination of TNF-or LPS-induced cytokine and chemokine production. *Cell Death and Differentiation*, *22*(8), 1313–1327.

Kennedy, T. A. C., MacLean, J. L., & Liu, J. (2012). Blue emitting gold nanoclusters templated by poly-cytosine DNA at low pH and poly-adenine DNA at neutral pH. *Chemical Communications*, *48*(54), 6845–6847.

Kerkhoff, E., Bister, K., & Klempnauer, K. H. (1991). Sequence-specific DNA binding by Myc proteins. *Proceedings of the National Academy of Sciences*, *88*(10), 4323–4327.

Kienle, G. S. (2012). Fever in Cancer Treatment: Coley's Therapy and Epidemiologic Observations. *Global Advances in Health and Medicine*, *1*(1), 92–100.

Kim, D. H., Behlke, M. A., Rose, S. D., Chang, M. S., Choi, S., & Rossi, J. J. (2005). Synthetic dsRNA Dicer substrates enhance RNAi potency and efficacy. *Nature Biotechnology*, *23*(2), 222–226.

Kim, D. H., & Rossi, J. J. (2008). RNAi mechanisms and applications. *BioTechniques*, *44*(5), 613–616.

Kim, Y. K., Na, K. S., Myint, A. M., & Leonard, B. E. (2016). The role of pro-inflammatory cytokines in neuroinflammation, neurogenesis and the neuroendocrine system in major depression. *Progress in Neuro-Psychopharmacology and Biological Psychiatry*, *64*, 277–284.

Kirchhofer, D., Tschopp, T. B., Hadvary, P., & Baumgartner, H. R. (1994). Endothelial cells stimulated with tumor necrosis factor-α express varying amounts of tissue factor resulting in inhomogenous fibrin deposition in a native blood flow system. Effects of thrombin inhibitors. *Journal of Clinical Investigation*, *93*(5), 2073–2083.

Kress, T. R., Sabò, A., & Amati, B. (2015). MYC: connecting selective transcriptional control to global RNA production. *Nature Reviews Cancer 2015 15:10*, *15*(10), 593–607.

Krippner-Heidenreich, A., Tübing, F., Bryde, S., Willi, S., Zimmermann, G., & Scheurich, P. (2002). Control of receptor-induced signaling complex formation by the kinetics of ligand/receptor interaction. *Journal of Biological Chemistry*, *277*(46), 44155–44163.

Krishnamoorthy, M., Li, D., Sharili, A. S., Gulin-Sarfraz, T., Rosenholm, J. M., & Gautrot, J. E. (2017). Solution Conformation of Polymer Brushes Determines Their Interactions with DNA and Transfection Efficiency. *Biomacromolecules*, *18*(12), 4121–4132.

Kubickova, A., Sanctis, J. B. De, & Hajduch, M. (2023). Isoform-Directed Control of c-Myc Functions: Understanding the Balance from Proliferation to Growth Arrest. *International Journal of Molecular Sciences 2023, Vol. 24, Page 17524*, *24*(24), 17524.

Kumar, A., Chowdhuri, A. R., Laha, D., Chandra, S., Karmakar, P., & Sahu, S. K. (2016). One-pot synthesis of carbon dot-entrenched chitosan-modified magnetic nanoparticles for fluorescence-based Cu2+ ion sensing and cell imaging. *RSC Advances*, *6*(64), 58979–58987.

Kumar, V., Qin, J., Jiang, Y., Duncan, R. G., Brigham, B., Fishman, S., Nair, J. K., Akinc, A., Barros, S. A., & Kasperkovitz, P. V. (2014). Shielding of Lipid Nanoparticles for siRNA Delivery: Impact on Physicochemical Properties, Cytokine Induction, and Efficacy. *Molecular Therapy - Nucleic Acids*, *3*(11), e210.

Kumari, S., Mg, S., & Mayor, S. (2010). Endocytosis unplugged: multiple ways to enter the cell. *Cell Research 2010 20:3*, *20*(3), 256–275.

Kurland, J. F., & Tansey, W. P. (2008). Myc-Mediated Transcriptional Repression by Recruitment of Histone Deacetylase. *Cancer Research*, *68*(10), 3624–3629.

Kwak, P. B., & Tomari, Y. (2012). The N domain of Argonaute drives duplex unwinding during RISC assembly. *Nature Structural and Molecular Biology*, *19*(2), 145–151.

Lai, K. C., Liu, C. J., Lin, T. J., Mar, A. C., Wang, H. H., Chen, C. W., Hong, Z. X., & Lee, T. C. (2016). Blocking TNF-α inhibits angiogenesis and growth of IFIT2-depleted metastatic oral squamous cell carcinoma cells. *Cancer Letters*, *370*(2), 207–215.

Lam, J. K. W., Chow, M. Y. T., Zhang, Y., & Leung, S. W. S. (2015). siRNA versus miRNA as therapeutics for gene silencing. *Molecular Therapy - Nucleic Acids*, *4*(9), e252.

Lang, I., Füllsack, S., Wyzgol, A., Fick, A., Trebing, J., Arana, J. A. C., Schäfer, V., Weisenberger, D., & Wajant, H. (2016). Binding studies of TNF receptor superfamily (TNFRSF) receptors on intact cells. *Journal of Biological Chemistry*, *291*(10), 5022–5037.

Langenhoven, L., Barnardt, P., Neugut, A. I., & Jacobson, J. S. (2016). Phenotype and Treatment of Breast Cancer in HIV-Positive and -Negative Women in Cape Town, South Africa. *Journal of Global Oncology*, *2*(5), 284–291.

Lara-Medina, F., Pérez-Sánchez, V., Saavedra-Pérez, D., Blake-Cerda, M., Arce, C., Motola-Kuba, D., Villarreal-Garza, C., González-Angulo, A. M., Bargalló, E., Aguilar, J. L., Mohar, A., & Arrieta, Ó. (2011). Triple-negative breast cancer in Hispanic patients: High prevalence, poor prognosis, and association with menopausal status, body mass index, and parity. *Cancer*, *117*(16), 3658–3669.

Layek, B., & Singh, J. (2017). Chitosan for DNA and gene therapy. *Chitosan Based Biomaterials*, *2*, 209–244.

Le Bohec, M., Bonchouo Kenzo, K., Piogé, S., Mura, S., Nicolas, J., Casse, N., Forcher, G., Fontaine, L., & Pascual, S. (2019). Structure-pDNA complexation and structure-cytotoxicity relationships of PEGylated, cationic aminoethyl-based polyacrylates with tunable topologies. *Polymer Chemistry*, *10*(15), 1968–1977.

Le Guével, X., Henry, M., Motto-Ros, V., Longo, E., Montañez, M. I., Pelascini, F., De La

Rochefoucauld, O., Zeitoun, P., Coll, J. L., Josserand, V., & Sancey, L. (2018). Elemental and optical imaging evaluation of zwitterionic gold nanoclusters in glioblastoma mouse models. *Nanoscale*, *10*(39), 18657–18664.

Le Guével, X., Prinz, E. M., Müller, R., Hempelmann, R., & Schneider, M. (2012). Synthesis and characterization of superparamagnetic nanoparticles coated with fluorescent gold nanoclusters. *Journal of Nanoparticle Research*, *14*(2), 1–10.

Le, W., Chen, B., Cui, Z., Liu, Z., & Shi, D. (2019). Detection of cancer cells based on glycolytic-regulated surface electrical charges. *Biophysics Reports*, *5*(1), 10–18.

Lechanteur, A., Furst, T., Evrard, B., Delvenne, P., Hubert, P., & Piel, G. (2016). PEGylation of lipoplexes: The right balance between cytotoxicity and siRNA effectiveness. *European Journal of Pharmaceutical Sciences*, *93*, 493–503.

Ledoux, A. C., & Perkins, N. D. (2014). NF-κB and the cell cycle. *Biochemical Society Transactions*, *42*(1), 76–81.

Lee, E., Ouzounova, M., Piranlioglu, R., Ma, M. T., Guzel, M., Marasco, D., Chadli, A., Gestwicki, J. E., Cowell, J. K., Wicha, M. S., Hassan, K. A., & Korkaya, H. (2019). The pleiotropic effects of TNFα in breast cancer subtypes is regulated by TNFAIP3/A20. *Oncogene*, *38*(4), 469–482.

Lee, H., Kim, I. K., & Park, T. G. (2010). Intracellular trafficking and unpacking of sirna/quantum dot-pei complexes modified with and without cell penetrating peptide: Confocal and flow cytometric fret analysis. *Bioconjugate Chemistry*, *21*(2), 289–295.

Lee, H. Y., Zhou, K., Smith, A. M., Noland, C. L., & Doudna, J. A. (2013). Differential roles of human Dicer-binding proteins TRBP and PACT in small RNA processing. *Nucleic Acids Research*, *41*(13), 6568–6576.

Lee, K. min, Giltnane, J. M., Balko, J. M., Schwarz, L. J., Guerrero-Zotano, A. L., Hutchinson, K. E., Nixon, M. J., Estrada, M. V., Sánchez, V., Sanders, M. E., Lee, T., Gómez, H., Lluch, A., Pérez-Fidalgo, J. A., Wolf, M. M., Andrejeva, G., Rathmell, J. C., Fesik, S. W., & Arteaga, C. L. (2017). MYC and MCL1 Cooperatively Promote Chemotherapy-Resistant Breast Cancer Stem Cells via Regulation of Mitochondrial Oxidative Phosphorylation. *Cell Metabolism*, *26*(4), 633–647.

Lee, P.-P. H., Hwang, J.-J., Murphy, G., & Ip, M. M. (2000). Functional Significance of MMP-9 in Tumor Necrosis Factor-Induced Proliferation and Branching Morphogenesis of Mammary Epithelial Cells. *Endocrinology*, *141*(10), 3764–3773.

Lee, S. J., Lee, A., Hwang, S. R., Park, J. S., Jang, J., Huh, M. S., Jo, D. G., Yoon, S. Y., Byun, Y., Kim, S. H., Kwon, I. C., Youn, I., & Kim, K. (2014). TNF-α gene silencing using polymerized siRNA/Thiolated glycol chitosan nanoparticles for rheumatoid arthritis. *Molecular Therapy*, *22*(2), 397–408.

Leek, R. D., Landers, R., Fox, S. B., Ng, F., Harris, A. L., & Lewis, C. E. (1998). Association of tumour necrosis factor alpha and its receptors with thymidine phosphorylase expression in invasive breast carcinoma. *British Journal of Cancer*, *77*(12), 2246–2251.

Lehmann, B. D., Bauer, J. A., Chen, X., Sanders, M. E., Chakravarthy, A. B., Shyr, Y., & Pietenpol, J. A. (2011). Identification of human triple-negative breast cancer subtypes and preclinical models for selection of targeted therapies. *Journal of Clinical Investigation*, *121*(7), 2750–2767.

Lehmann, B. D., Jovanović, B., Chen, X., Estrada, M. V., Johnson, K. N., Shyr, Y., Moses, H. L., Sanders, M. E., & Pietenpol, J. A. (2016). Refinement of Triple-Negative Breast Cancer Molecular Subtypes: Implications for Neoadjuvant Chemotherapy Selection. *PLOS ONE*, *11*(6), e0157368.

Lei, Y., Tang, L., Xie, Y., Xianyu, Y., Zhang, L., Wang, P., Hamada, Y., Jiang, K., Zheng, W., & Jiang, X. (2017). Gold nanoclusters-assisted delivery of NGF siRNA for effective treatment of pancreatic cancer. *Nature Communications*, *8*(1), 1–15.

Leibovich, S. J., Polverini, P. J., Shepard, H. M., Wiseman, D. M., Shively, V., & Nuseir, N. (1987). Macrophage-induced angiogenesis is mediated by tumour necrosis factor-α. *Nature*, *329*(6140), 630–632.

Lekshmi, A., Varadarajan, S. N., Lupitha, S. S., Indira, D., Ann Mathew, K., Nair, A. C., Nair, M., Prasad, T., Sekar, H., Gopalakrishnan, A. K., Murali, A., & Santhoshkumar, T. R. (2017). A quantitative real-time approach for discriminating apoptosis and necrosis. *Cell Death Discovery 2017 3:1*, *3*(1), 1–10.

Lemm, I., & Ross, J. (2002). Regulation of c-myc mRNA Decay by Translational Pausing in a Coding Region Instability Determinant. *Molecular and Cellular Biology*, *22*(12), 3959–3969.

Lentz, T. B., Gray, S. J., & Samulski, R. J. (2012). Viral vectors for gene delivery to the central nervous system. *Neurobiology of Disease*, *48*(2), 179–188.

Lewis, A. K., Valley, C. C., & Sachs, J. N. (2012). TNFR1 signaling is associated with backbone conformational changes of receptor dimers consistent with overactivation in the R92Q TRAPS mutant. *Biochemistry*, *51*(33), 6545–6555.

Li, B., Vincent, A., Cates, J., Brantley-Sieders, D. M., Polk, D. B., & Young, P. P. (2009). Low levels of tumor necrosis factor α increase tumor growth by inducing an endothelial phenotype of monocytes recruited to the tumor site. *Cancer Research*, *69*(1), 338–348.

Li, C. W., Xia, W., Huo, L., Lim, S. O., Wu, Y., Hsu, J. L., Chao, C. H., Yamaguchi, H., Yang, N. K., Ding, Q., Wang, Y., Lai, Y. J., LaBaff, A. M., Wu, T. J., Lin, B. R., Yang, M. H., Hortobagyi, G. N., & Hung, M. C. (2012). Epithelial-mesenchymal transition induced by TNF-α requires NF-κB-mediated transcriptional upregulation of Twist1. *Cancer Research*, *72*(5), 1290–1300.

Li, D., Chen, Z., & Mei, X. (2017). Fluorescence enhancement for noble metal nanoclusters. *Advances in Colloid and Interface Science*, *250*, 25–39.

Li, H. H., Zhu, H., Liu, L. S., Huang, Y., Guo, J., Li, J., Sun, X. P., Chang, C. X., Wang, Z. H., & Zhai, K. (2015). Tumour Necrosis Factor-α Gene Polymorphism Is Associated with Metastasis in Patients with Triple Negative Breast Cancer. *Scientific Reports*, *5*(1), 10244.

Li, L., Hu, X., Zhang, M., Ma, S., Yu, F., Zhao, S., Liu, N., Wang, Z., Wang, Y., Guan, H., Pan, X., Gao, Y., Zhang, Y., Liu, Y., Yang, Y., Tang, X., Li, M., Liu, C., Li, Z., & Mei, X. (2017). Dual Tumor-Targeting Nanocarrier System for siRNA Delivery Based on pRNA and Modified Chitosan. *Molecular Therapy. Nucleic Acids*, *8*, 169–183.

Li, L., Li, Z., Zhang, H., Zhang, S., Majeed, I., & Tan, B. (2013). Effect of polymer ligand structures on fluorescence of gold clusters prepared by photoreduction. *Nanoscale*, *5*(5), 1986–1992.

Li, N., Cusidó, M. T., Navarro, B., Tresserra, F., Baulies, S., Ara, C., & Fabregas, R. (2016). Breast sarcoma. A case report and review of literature. *International Journal of Surgery Case*

Reports, *24*, 203–205.

Li, N., Wang, J., Zhang, N., Zhuang, M., Zong, Z., Zou, J., Li, G., Wang, X., Zhou, H., Zhang, L., & Shi, Y. (2018). Cross-talk between TNF-α and IFN-γ signaling in induction of B7-H1 expression in hepatocellular carcinoma cells. *Cancer Immunology, Immunotherapy*, *67*(2), 271–283.

Li, Q., Liu, C. G., & Yu, Y. (2015). Separation of monodisperse alginate nanoparticles and effect of particle size on transport of vitamin E. *Carbohydrate Polymers*, *124*, 274–279.

Li, Q., Pan, Y., Chen, T., Du, Y., Ge, H., Zhang, B., Xie, J., Yu, H., & Zhu, M. (2018). Design and mechanistic study of a novel gold nanocluster-based drug delivery system. *Nanoscale*, *10*(21), 10166–10172.

Li, S., Jiang, C., Pan, J., Wang, X., Jin, J., Zhao, L., Pan, W., Liao, G., Cai, X., Li, X., Xiao, J., Jiang, J., & Wang, P. (2014). Regulation of c-Myc protein stability by proteasome activator REGγ. *Cell Death & Differentiation 2015 22:6*, *22*(6), 1000–1011.

Li, W., Liu, Q., Shi, J., Xu, X., & Xu, J. (2023). The role of TNF-α in the fate regulation and functional reprogramming of mesenchymal stem cells in an inflammatory microenvironment. *Frontiers in Immunology*, *14*, 1074863.

Li, X., Chen, M., Yang, W., Zhou, Z., Liu, L., & Zhang, Q. (2012). Interaction of bovine serum albumin with self-assembled nanoparticles of 6-O-cholesterol modified chitosan. *Colloids and Surfaces B: Biointerfaces*, *92*, 136–141.

Liang, H. F., Smith, C. T. G., Mills, C. A., & Silva, S. R. P. (2015). The band structure of graphene oxide examined using photoluminescence spectroscopy. *Journal of Materials Chemistry C*, *3*(48), 12484–12491.

Liang, M., Zhang, P., & Fu, J. (2007). Up-regulation of LOX-1 expression by TNF-α promotes trans-endothelial migration of MDA-MB-231 breast cancer cells. *Cancer Letters*, *258*(1), 31–37.

Lim, S. O., Li, C. W., Xia, W., Cha, J. H., Chan, L. C., Wu, Y., Chang, S. S., Lin, W. C., Hsu, J. M., Hsu, Y. H., Kim, T., Chang, W. C., Hsu, J. L., Yamaguchi, H., Ding, Q., Wang, Y., Yang, Y., Chen, C. H., Sahin, A. A., … Hung, M. C. (2016). Deubiquitination and Stabilization of PD-L1 by CSN5. *Cancer Cell*, *30*(6), 925–939.

Limbach, L. K., Li, Y., Grass, R. N., Brunner, T. J., Hintermann, M. A., Muller, M., Gunther, D., & Stark, W. J. (2005). Oxide nanoparticle uptake in human lung fibroblasts: Effects of particle size, agglomeration, and diffusion at low concentrations. *Environmental Science and Technology*, *39*(23), 9370–9376.

Lin, C.-A. J., Lee, C.-H., Hsieh, J.-T., Yu, W.-C., Yang, H.-Z., Li, J. K., Sperling, R., Wang, H.-H., Yeh, H.-I., Parak, W. J., & Chang, W. H. (2010). Synthesis and surface modification of highly fluorescent gold nanoclusters and their exploitation for cellular labeling. *Proc.S PIE*, *7575*.

Lin, C. Y., Lovén, J., Rahl, P. B., Paranal, R. M., Burge, C. B., Bradner, J. E., Lee, T. I., & Young, R. A. (2012). Transcriptional amplification in tumor cells with elevated c-Myc. *Cell*, *151*(1), 56–67.

Lin, R., Thompson, S., & Priess, J. R. (1995). pop-1 Encodes an HMG box protein required for the specification of a mesoderm precursor in Early C. elegans embryos. *Cell*, *83*(4), 599–609.

Lin, Y., Charchar, P., Christofferson, A. J., Thomas, M. R., Todorova, N., Mazo, M. M., Chen, Q., Doutch, J., Richardson, R., Yarovsky, I., & Stevens, M. M. (2018). Surface Dynamics and Ligand-Core Interactions of Quantum Sized Photoluminescent Gold Nanoclusters. *Journal of the American Chemical Society*, *140*(51), 18217–18226.

Littlewood, T. D., & Evan, G. I. (2023). Dimerization partners. In *Helix-Loop-Helix Transcription Factors* (pp. 37–41). Oxford University PressOxford.

Liu, G., Shao, Y., Wu, F., Xu, S., Peng, J., & Liu, L. (2013). DNA-hosted fluorescent gold nanoclusters: Sequence-dependent formation. *Nanotechnology*, *24*(1), 015503.

Liu, H., Zhao, Y., Cheng, S., Huang, N., & Leng, Y. (2012). Syntheses of novel chitosan derivative with excellent solubility, anticoagulation, and antibacterial property by chemical modification. *Journal of Applied Polymer Science*, *124*(4), 2641–2648.

Liu, J., Duchesne, P. N., Yu, M., Jiang, X., Ning, X., Vinluan, R. D., Zhang, P., & Zheng, J. (2016). Luminescent Gold Nanoparticles with Size-Independent Emission. *Angewandte Chemie - International Edition*, *55*(31), 8894–8898.

Liu, J., Liu, L., Li, S., Kang, Q., Zhang, R., & Zhu, Z. (2021). Self-assembled nanogels of luminescent thiolated silver nanoclusters and chitosan as bactericidal agent and bacterial sensor. *Materials Science and Engineering: C*, *118*, 111520.

Liu, J., Yu, M., Ning, X., Zhou, C., Yang, S., & Zheng, J. (2013). PEGylation and zwitterionization: Pros and cons in the renal clearance and tumor targeting of near-IR-emitting gold nanoparticles. *Angewandte Chemie - International Edition*, *52*(48), 12572–12576.

Liu, J., Zhang, Y., Zeng, Q., Zeng, H., Liu, X., Wu, P., Xie, H., He, L., Long, Z., Lu, X., Xiao, M., Zhu, Y., Bo, H., & Cao, K. (2019). Delivery of RIPK4 small interfering RNA for bladder cancer therapy using natural halloysite nanotubes. *Science Advances*, *5*(9), 6499–6524.

Liu, K., Liu, P., Liu, R., & Wu, X. (2015). Dual AO/EB staining to detect apoptosis in osteosarcoma cells compared with flow cytometry. *Medical Science Monitor Basic Research*, *21*, 15–20.

Liu, L., & Corma, A. (2018). Metal Catalysts for Heterogeneous Catalysis: From Single Atoms to Nanoclusters and Nanoparticles. In *Chemical Reviews* (Vol. 118, Issue 10, pp. 4981–5079). American Chemical Society.

Liu, M., Zhang, L., Zhao, Q., Jiang, X., Wu, L., & Hu, Y. (2018). Lower-Molecular-Weight Chitosan-Treated Polyethyleneimine: a Practical Strategy For Gene Delivery to Mesenchymal Stem Cells. *Cellular Physiology and Biochemistry*, *50*(4), 1255–1269.

Liu, T., Zhang, L., Joo, D., & Sun, S. C. (2017). NF-κB signaling in inflammation. *Signal Transduction and Targeted Therapy*, *2*(1), 1–9.

Liu, W., Lu, X., Shi, P., Yang, G., Zhou, Z., Li, W., Mao, X., Jiang, D., & Chen, C. (2020). TNF-α increases breast cancer stem-like cells through up-regulating TAZ expression via the non-canonical NF-κB pathway. *Scientific Reports*, *10*(1), 1–11.

Liu, W., Rudis, M. R., Cheplick, M. H., Millwood, R. J., Yang, J. P., Ondzighi-Assoume, C. A., Montgomery, G. A., Burris, K. P., Mazarei, M., Chesnut, J. D., & Stewart, C. N. (2020). Lipofection-mediated genome editing using DNA-free delivery of the Cas9/gRNA ribonucleoprotein into plant cells. *Plant Cell Reports*, *39*(2), 245–257.

Liu, X., Howard, K. A., Dong, M., Andersen, M., Rahbek, U. L., Johnsen, M. G., Hansen, O.

C., Besenbacher, F., & Kjems, J. (2007). The influence of polymeric properties on chitosan/siRNA nanoparticle formulation and gene silencing. *Biomaterials*, *28*(6), 1280–1288.

Liu, Y., Ai, K., Cheng, X., Huo, L., & Lu, L. (2010). Gold-Nanocluster-Based Fluorescent Sensors for Highly Sensitive and Selective Detection of Cyanide in Water. *Advanced Functional Materials*, *20*(6), 951–956.

Liu, Y., Ji, X., Kang, N., Zhou, J., Liang, X., Li, J., Han, T., Zhao, C., & Yang, T. (2020). Tumor necrosis factor α inhibition overcomes immunosuppressive M2b macrophage-induced bevacizumab resistance in triple-negative breast cancer. *Cell Death & Disease*, *11*(11), 993.

Liu, Y., Song, Z. M., Deng, X., Cui, Y., Yang, Y. F., Han, K., Jin, R., Wang, H., Liu, Y., & Cao, A. (2015). Chitosan-coated red fluorescent protein nanoparticle as a potential dual-functional siRNA carrier. *Nanomedicine*, *10*(13), 2005–2016.

Liu, Y., Zhu, Y. H., Mao, C. Q., Dou, S., Shen, S., Tan, Z. Bin, & Wang, J. (2014). Triple negative breast cancer therapy with CDK1 siRNA delivered by cationic lipid assisted PEG-PLA nanoparticles. *Journal of Controlled Release : Official Journal of the Controlled Release Society*, *192*, 114–121.

Liubomirski, Y., Lerrer, S., Meshel, T., Rubinstein-Achiasaf, L., Morein, D., Wiemann, S., Körner, C., & Ben-Baruch, A. (2019). Tumor-stroma-inflammation networks promote pro-metastatic chemokines and aggressiveness characteristics in triple-negative breast cancer. *Frontiers in Immunology*, *10*(757).

Livak, K. J., & Schmittgen, T. D. (2001). Analysis of relative gene expression data using real-time quantitative PCR and the 2(-Delta Delta C(T)) Method. *Methods (San Diego, Calif.)*, *25*(4), 402–408.

Llombart, V., & Mansour, M. R. (2022). Therapeutic targeting of "undruggable" MYC. *EBioMedicine*, *75*, 103756.

Lojk, J., Strojan, K., Miš, K., Bregar, B. V., Hafner Bratkovič, I., Bizjak, M., Pirkmajer, S., & Pavlin, M. (2017). Cell stress response to two different types of polymer coated cobalt ferrite nanoparticles. *Toxicology Letters*, *270*, 108–118.

Lokras, A., Thakur, A., Wadhwa, A., Thanki, K., Franzyk, H., & Foged, C. (2021). Optimizing the Intracellular Delivery of Therapeutic Anti-inflammatory TNF-α siRNA to Activated Macrophages Using Lipidoid-Polymer Hybrid Nanoparticles. *Frontiers in Bioengineering and Biotechnology*, *8*, 1538.

Londoño-Larrea, P., Vanegas, J. P., Cuaran-Acosta, D., Zaballos-García, E., & Pérez-Prieto, J. (2017). Water-Soluble Naked Gold Nanoclusters Are Not Luminescent. *Chemistry - A European Journal*, *23*(34), 8137–8141.

Lü, X., Zhang, H., Huang, Y., & Zhang, Y. (2018). A proteomics study to explore the role of adsorbed serum proteins for PC12 cell adhesion and growth on chitosan and collagen/chitosan surfaces. *Regenerative Biomaterials*, *5*(5), 261.

Luo, Z., Yuan, X., Yu, Y., Zhang, Q., Leong, D. T., Lee, J. Y., & Xie, J. (2012). From Aggregation-Induced Emission of Au(I)–Thiolate Complexes to Ultrabright Au(0)@Au(I)–Thiolate Core–Shell Nanoclusters. *Journal of the American Chemical Society*, *134*(40), 16662–16670.

Ma, P. L., Lavertu, M., Winnik, F. M., & Buschmann, M. D. (2017). Stability and binding affinity of DNA/chitosan complexes by polyanion competition. *Carbohydrate Polymers*, *176*,

167–176.

Ma, X., Zhai, Z. C., Zhang, M. L., Song, B. H., Zhu, Y. R., Yang, S. B., Dong, X. Q., Su, L. Y., Wang, C. F., Ma, H. X., & Luan, W. M. (2016). Molecular cloning and expression vector construction of bovine TRIM28. *Genetics and Molecular Research*, *15*(2).

Madden, S. K., de Araujo, A. D., Gerhardt, M., Fairlie, D. P., & Mason, J. M. (2021). Taking the Myc out of cancer: toward therapeutic strategies to directly inhibit c-Myc. *Molecular Cancer 2021 20:1*, *20*(1), 1–18.

Made, F., Wilson, K., Jina, R., Tlotleng, N., Jack, S., Ntlebi, V., & Kootbodien, T. (2017). Distribution of cancer mortality rates by province in South Africa. *Cancer Epidemiology*, *51*, 56–61.

Maguire, C. M., Rösslein, M., Wick, P., & Prina-Mello, A. (2018). Characterisation of particles in solution - a perspective on light scattering and comparative technologies. *Science and Technology of Advanced Materials*, *19*(1), 732–745.

Mahmoudian, R. A., Farshchian, M., & Abbaszadegan, M. R. (2020). Evaluation and Optimization of Lipofectamine 3000 Reagents for Transient Gene Expression in KYSE-30 Esophagus Cancer Cell Line. *Archives of Medical Laboratory Sciences*, *6*, 1-9 (e8).

Makki, J. (2015). Diversity of breast carcinoma: Histological subtypes and clinical relevance. *Clinical Medicine Insights: Pathology*, *8*(1), 23–31.

Malhotra, G. K., Zhao, X., Band, H., & Band, V. (2010). Histological, molecular and functional subtypes of breast cancers. *Cancer Biology & Therapy*, *10*(10), 955–960.

Malik, S. T. A., Griffin, D. B., Fiers, W., & Balkwill, F. R. (1989). Paradoxical effects of tumour necrosis factor in experimental ovarian cancer. *International Journal of Cancer*, *44*(5), 918–925.

Malik, S. T. A., Stuart Naylor, M., East, N., Oliff, A., & Balkwill, F. R. (1990). Cells secreting tumour necrosis factor show enhanced metastasis in nude mice. *European Journal of Cancer and Clinical Oncology*, *26*(10), 1031–1034.

Malorni, L., Shetty, P. B., De Angelis, C., Hilsenbeck, S., Rimawi, M. F., Elledge, R., Osborne, C. K., De Placido, S., & Arpino, G. (2012). Clinical and biologic features of triple-negative breast cancers in a large cohort of patients with long-term follow-up. *Breast Cancer Research and Treatment*, *136*(3), 795–804.

Mao, H. Q., Roy, K., Troung-Le, V. L., Janes, K. A., Lin, K. Y., Wang, Y., August, J. T., & Leong, K. W. (2001). Chitosan-DNA nanoparticles as gene carriers: Synthesis, characterization and transfection efficiency. *Journal of Controlled Release*, *70*(3), 399–421.

Mao, S., Neu, M., Germershaus, O., Merkel, O., Sitterberg, J., Bakowsky, U., & Kissel, T. (2006). Influence of polyethylene glycol chain length on the physicochemical and biological properties of poly(ethylene imine)-graft-poly(ethylene glycol) block copolymer/SiRNA polyplexes. *Bioconjugate Chemistry*, *17*(5), 1209–1218.

Marchetti, L., Klein, M., Schlett, K., Pfizenmaier, K., & Eisel, U. L. M. (2004). Tumor necrosis factor (TNF)-mediated neuroprotection against glutamate-induced excitotoxicity is enhanced by N-methyl-D-aspartate receptor activation: Essential role of a TNF receptor 2-mediated phosphatidylinositol 3-kinase-dependent NF-κB pathway. *Journal of Biological Chemistry*, *279*(31), 32869–32881.

Marconi, G. D., Fonticoli, L., Rajan, T. S., Pierdomenico, S. D., Trubiani, O., Pizzicannella, J., & Diomede, F. (2021). Epithelial-Mesenchymal Transition (EMT): The Type-2 EMT in Wound Healing, Tissue Regeneration and Organ Fibrosis. *Cells*, *10*(7), 1587.

Mark, K. S., Trickler, W. J., & Miller, D. W. (2001). Tumor Necrosis Factor-α Induces Cyclooxygenase-2 Expression and Prostaglandin Release in Brain Microvessel Endothelial Cells. *Journal of Pharmacology and Experimental Therapeutics*, *297*(3), 1051–1058.

Marquez, A. R., Madu, C. O., & Lu, Y. (2018). An Overview of Various Carriers for siRNA Delivery. *Oncomedicine*, *3*, 48–58.

Martino, E., Vuoso, D. C., D'Angelo, S., Mele, L., D'Onofrio, N., Porcelli, M., & Cacciapuoti, G. (2019). Annurca apple polyphenol extract selectively kills MDA-MB-231 cells through ROS generation, sustained JNK activation and cell growth and survival inhibition. *Scientific Reports 2019 9:1*, *9*(1), 1–15.

Massó-Vallés, D., & Soucek, L. (2020). Blocking Myc to Treat Cancer: Reflecting on Two Decades of Omomyc. *Cells 2020, Vol. 9, Page 883*, *9*(4), 883.

Matranga, C., Tomari, Y., Shin, C., Bartel, D. P., & Zamore, P. D. (2005). Passenger-strand cleavage facilitates assembly of siRNA into Ago2-containing RNAi enzyme complexes. *Cell*, *123*(4), 607–620.

Mattos, B. R., Bonacio, G. F., Vitorino, T. R., Garcia, V. T., Amaral, J. H., Dellalibera-Joviliano, R., Franca, S. C., Tanus-Santos, J. E., & Rizzi, E. (2020). TNF-α inhibition decreases MMP-2 activity, reactive oxygen species formation and improves hypertensive vascular hypertrophy independent of its effects on blood pressure. *Biochemical Pharmacology*, *180*, 114121.

McCann, K. E., & Hurvitz, S. A. (2018). Advances in the use of PARP inhibitor therapy for breast cancer. *Drugs in Context*, *7*(212540).

McCormack, V. A., Joffe, M., van den Berg, E., Broeze, N., dos Santos Silva, I., Romieu, I., Jacobson, J. S., Neugut, A. I., Schüz, J., & Cubasch, H. (2013). Breast cancer receptor status and stage at diagnosis in over 1,200 consecutive public hospital patients in Soweto, South Africa: A case series. *Breast Cancer Research*, *15*(5), R84.

McKinnon, K. M. (2018). Flow Cytometry: An Overview. *Current Protocols in Immunology*, *120*, 5.1.1-5.1.11.

McMahon, S. B. (2014). MYC and the control of apoptosis. *Cold Spring Harbor Perspectives in Medicine*, *4*(7), a014407.

Medler, J., & Wajant, H. (2019). Tumor necrosis factor receptor-2 (TNFR2): An overview of an emerging drug target. *Expert Opinion on Therapeutic Targets*, *23*(4), 295–307.

Meng, L., Zhou, J., Sasano, H., Suzuki, T., Zeitoun, K. M., & Bulun, S. E. (2001). Tumor necrosis factor α and interleukin 11 secreted by malignant breast epithelial cells inhibit adipocyte differentiation by selectively down-regulating CCAAT/enhancer binding protein α and peroxisome proliferator-activated receptor γ: Mechanism of desmoplastic reaction. *Cancer Research*, *61*(5), 2250–2255.

Meng, Z., & Lu, M. (2017). RNA Interference-Induced Innate Immunity, Off-Target Effect, or Immune Adjuvant? *Frontiers in Immunology*, *8*, 331.

Menon, C., Ghartey, A., Canter, R., Feldman, M., & Fraker, D. L. (2006). Tumor necrosis

factor-alpha damages tumor blood vessel integrity by targeting VE-cadherin. *Annals of Surgery*, *244*(5), 781–791.

Mercogliano, M. F., Bruni, S., Elizalde, P. V., & Schillaci, R. (2020). Tumor Necrosis Factor α Blockade: An Opportunity to Tackle Breast Cancer. *Frontiers in Oncology*, *10*(584).

Merkel, O. M., Beyerle, A., Librizzi, D., Pfestroff, A., Behr, T. M., Sproat, B., Barth, P. J., & Kissel, T. (2009). Nonviral siRNA delivery to the lung: investigation of PEG-PEI polyplexes and their in vivo performance. *Molecular Pharmaceutics*, *6*(4), 1246–1260.

Merkel, O. M., Germershaus, O., Wada, C. K., Tarcha, P. J., Merdan, T., & Kissel, T. (2009). Integrin αvβ3 Targeted Gene Delivery Using RGD Peptidomimetic Conjugates with Copolymers of PEGylated Poly(ethylene imine). *Bioconjugate Chemistry*, *20*(6), 1270–1280.

Mi, W., Tang, S., Guo, S., Li, H., & Shao, N. (2022). In situ synthesis of red fluorescent gold nanoclusters with enzyme-like activity for oxidative stress amplification in chemodynamic therapy. *Chinese Chemical Letters*, *33*(3), 1331–1336.

Mikheev, A. A., Shmendel, E. V., Zhestovskaya, E. S., Nazarov, G. V., & Maslov, M. A. (2020). Cationic Liposomes As Delivery Systems for Nucleic Acids. *Tonkie Khimicheskie Tekhnologii*, *15*(1), 7–27.

Mikulasova, A., Ashby, C., Tytarenko, R. G., Qu, P., Rosenthal, A., Dent, J. A., Ryan, K. R., Bauer, M. A., Wardell, C. P., Hoering, A., Mavrommatis, K., Trotter, M., Deshpande, S., Yaccoby, S., Tian, E., Keats, J., Auclair, D., Jackson, G. H., Davies, F. E., … Walker, B. A. (2020). Microhomology-mediated end joining drives complex rearrangements and overexpression of MYC and PVT1 in multiple myeloma. *Haematologica*, *105*(4), 1055–1066.

Miles, D. W., Happerfield, L. C., Naylor, M. S., Bobrow, L. G., Rubens, R. D., & Balkwwill, F. R. (1994). Expression of tumour necrosis factor (TNFα) and its receptors in benign and malignant breast tissue. *International Journal of Cancer*, *56*(6), 777–782.

Miller, D. M., Thomas, S. D., Islam, A., Muench, D., & Sedoris, K. (2012). c-Myc and Cancer Metabolism. *Clinical Cancer Research*, *18*(20), 5546–5553.

Miller, T. W., Balko, J. M., Ghazoui, Z., Dunbier, A., Anderson, H., Dowsett, M., González-Angulo, A. M., Mills, G. B., Miller, W. R., Wu, H., Shyr, Y., & Arteaga, C. L. (2011). A gene expression signature from human breast cancer cells with acquired hormone independence identifies MYC as a mediator of antiestrogen resistance. *Clinical Cancer Research*, *17*(7), 2024–2034.

Mirza, Z., & Karim, S. (2021). Nanoparticles-based drug delivery and gene therapy for breast cancer: Recent advancements and future challenges. *Seminars in Cancer Biology*, *69*, 226–237.

Mishra, S., Webster, P., & Davis, M. E. (2004). PEGylation significantly affects cellular uptake and intracellular trafficking of non-viral gene delivery particles. *European Journal of Cell Biology*, *83*(3), 97–111.

Miteva, M., Kirkbride, K. C., Kilchrist, K. V., Werfel, T. A., Li, H., Nelson, C. E., Gupta, M. K., Giorgio, T. D., & Duvall, C. L. (2015). Tuning PEGylation of mixed micelles to overcome intracellular and systemic siRNA delivery barriers. *Biomaterials*, *38*, 97–107.

Mitoma, H., Horiuchi, T., Tsukamoto, H., & Ueda, N. (2018). Molecular mechanisms of action of anti-TNF-α agents – Comparison among therapeutic TNF-α antagonists. *Cytokine*, *101*, 56–63.

Mocellin, S., Provenzano, M., Lise, M., Nitti, D., & Rossi, C. R. (2003). IncreasedTIA-1 gene expression in the tumor microenvironment after locoregional administration of tumor necrosis factor-? to patients with soft tissue limb sarcoma. *International Journal of Cancer*, *107*(2), 317–322.

Möckl, L. (2020). The Emerging Role of the Mammalian Glycocalyx in Functional Membrane Organization and Immune System Regulation. *Frontiers in Cell and Developmental Biology*, *8*, 253.

Molnár, I. A., Molnár, B. Á., Vízkeleti, L., Fekete, K., Tamás, J., Deák, P., Szundi, C., Székely, B., Moldvay, J., Vári-Kakas, S., Szász, M. A., Ács, B., Kulka, J., & Tőkés, A. M. (2017). Breast carcinoma subtypes show different patterns of metastatic behavior. *Virchows Archiv*, *470*(3), 275–283.

Montfort, A., Colacios, C., Levade, T., Andrieu-Abadie, N., Meyer, N., & Ségui, B. (2019). The TNF Paradox in Cancer Progression and Immunotherapy. *Frontiers in Immunology*, *10*(JULY), 1818.

Moon, H. J., Ku, M., Lee, H., Yoon, N., Yang, J., & Bong, K. W. (2018). Implantable Photothermal Agents based on Gold Nanorods-Encapsulated Microcube. *Scientific Reports*, *8*(1), 13683.

Moore, R. J., Owens, D. M., Stamp, G., Arnott, C., Burke, F., East, N., Holdsworth, H., Turner, L., Rollins, B., Pasparakis, M., Kollias, G., & Balkwill, F. (1999). Mice deficient in tumor necrosis factor-α are resistant to skin carcinogenesis. *Nature Medicine*, *5*(7), 828–831.

Moreno, A., Pitoc, G. A., Ganson, N. J., Layzer, J. M., Hershfield, M. S., Tarantal, A. F., & Sullenger, B. A. (2019). Anti-PEG Antibodies Inhibit the Anticoagulant Activity of PEGylated Aptamers. *Cell Chemical Biology*, *26*(5), 634-644.e3.

Morgan, M. J., & Liu, Z. G. (2010). Reactive Oxygen Species in TNFα-Induced Signaling and Cell Death. *Molecules and Cells*, *30*(1), 1.

Motoo, Y., Hill, N. O., Mahmoudi, M., & Osther, K. (1986). Antitumor effect of human necrosis factor on human hepatoma cells PLC/PRF/5. *The Japanese Journal of Experimental Medicine*, *56*(4), 151–154.

Mourdikoudis, S., Pallares, R. M., & Thanh, N. T. K. (2018). Characterization techniques for nanoparticles: comparison and complementarity upon studying nanoparticle properties. *Nanoscale*, *10*(27), 12871–12934.

Mueller, H., Flury, N., Liu, R., Scheidegger, S., & Eppenberger, U. (1996). Tumour necrosis factor and interferon are selectively cytostatic in vitro far hormone-dependent and hormone-independent human breast cancer cells. *European Journal of Cancer Part A*, *32*(13), 2312–2318.

Muhammed, M. A. H., Ramesh, S., Sinha, S. S., Pal, S. K., & Pradeep, T. (2008). Two distinct fluorescent quantum clusters of gold starting from metallic nanoparticles by pH-dependent ligand etching. *Nano Research*, *1*(4), 333–340.

Muhammed, M. A. H., Verma, P. K., Pal, S. K., Retnakumari, A., Koyakutty, M., Nair, S., & Pradeep, T. (2010). Luminescent quantum clusters of gold in bulk by albumin-induced core etching of nanoparticles: Metal ion sensing, metal-enhanced luminescence, and biolabeling. *Chemistry - A European Journal*, *16*(33), 10103–10112.

Mukhopadhyay, P., Chakraborty, S., Bhattacharya, S., Mishra, R., & Kundu, P. P. (2015). PH-

sensitive chitosan/alginate core-shell nanoparticles for efficient and safe oral insulin delivery. *International Journal of Biological Macromolecules*, *72*, 640–648.

Müller, M., Fazi, F., & Ciaudo, C. (2020). Argonaute Proteins: From Structure to Function in Development and Pathological Cell Fate Determination. *Frontiers in Cell and Developmental Biology*, *7*, 360.

Muraleetharan, V., Mantaj, J., Swedrowska, M., & Vllasaliu, D. (2019). Nanoparticle modification in biological media: implications for oral nanomedicines. *RSC Adv.*, *9*(69), 40487–40497.

Musgrove, E. A., Sergio, C. M., Loi, S., Inman, C. K., Anderson, L. R., Alles, M. C., Pinese, M., Caldon, C. E., Schütte, J., Gardiner-Garden, M., Ormandy, C. J., McArthur, G., Butt, A. J., & Sutherland, R. L. (2008). Identification of functional networks of estrogen- and c-Myc-responsive genes and their relationship to response to tamoxifen therapy in breast cancer. *PLoS ONE*, *3*(8), e2987.

Musnier, B., Wegner, K. D., Comby-Zerbino, C., Trouillet, V., Jourdan, M., Häusler, I., Antoine, R., Coll, J. L., Resch-Genger, U., & Le Guével, X. (2019). High photoluminescence of shortwave infrared-emitting anisotropic surface charged gold nanoclusters. *Nanoscale*, *11*(25), 12092–12096.

Mussbacher, M., Salzmann, M., Brostjan, C., Hoesel, B., Schoergenhofer, C., Datler, H., Hohensinner, P., Basílio, J., Petzelbauer, P., Assinger, A., & Schmid, J. A. (2019). Cell type specific roles of nf-kb linking inflamation and thrombosis. *Frontiers in Immunology*, *10*(FEB), 85.

Nabors, L. B., Suswam, E., Huang, Y., Yang, X., Johnson, M. J., & King, P. H. (2003). Tumor necrosis factor α induces angiogenic factor up-regulation in malignant glioma cells: A role for RNA stabilization and HuR. *Cancer Research*, *63*(14), 4181–4187.

Nair, J. K., Attarwala, H., Sehgal, A., Wang, Q., Aluri, K., Zhang, X., Gao, M., Liu, J., Indrakanti, R., Schofield, S., Kretschmer, P., Brown, C. R., Gupta, S., Willoughby, J. L. S., Boshar, J. A., Jadhav, V., Charisse, K., Zimmermann, T., Fitzgerald, K., … Maier, M. A. (2017). Impact of enhanced metabolic stability on pharmacokinetics and pharmacodynamics of GalNAc–siRNA conjugates. *Nucleic Acids Research*, *45*(19), 10969–10977.

Nair, S. K., & Burley, S. K. (2003). X-Ray Structures of Myc-Max and Mad-Max Recognizing DNA: Molecular Bases of Regulation by Proto-Oncogenic Transcription Factors. *Cell*, *112*(2), 193–205.

Nan, H., Chen, Z., Jiang, J., Li, J., Zhao, W., Ni, Z., Gu, X., & Xiao, S. (2018). The effect of graphene on surface plasmon resonance of metal nanoparticles. *Physical Chemistry Chemical Physics*, *20*(38), 25078–25084.

Napoli, C., Lemieux, C., & Jorgensen, R. (1990). Introduction of a Chimeric Chalcone Synthase Gene into Petunia Results in Reversible Co-Suppression of Homologous Genes in trans. *The Plant Cell*, *2*(4), 279–289.

Naruse, K., Matsuura-Suzuki, E., Watanabe, M., Iwasaki, S., & Tomari, Y. (2018). In vitro reconstitution of chaperone-mediated human RISC assembly. *RNA*, *24*(1), 6–11.

Naslavsky, N., & Caplan, S. (2018). The enigmatic endosome - sorting the ins and outs of endocytic trafficking. *Journal of Cell Science*, *131*(13), jcs216499.

Natal, R. de A., Paiva, G. R., Pelegati, V. B., Marenco, L., Alvarenga, C. A., Vargas, R. F.,

Derchain, S. F., Sarian, L. O., Franchet, C., Cesar, C. L., Schmitt, F. C., Weigelt, B., & Vassallo, J. (2019). Exploring Collagen Parameters in Pure Special Types of Invasive Breast Cancer. *Scientific Reports*, *9*(1), 7715.

National Cancer Registry. (2020). *National Cancer Registry 2017*.

Neamtu, I., Rusu, A. G., Diaconu, A., Nita, L. E., & Chiriac, A. P. (2017). Basic concepts and recent advances in nanogels as carriers for medical applications. *Drug Delivery*, *24*(1), 539–557.

Negishi, Y., Nobusada, K., & Tsukuda, T. (2005). Glutathione-protected gold clusters revisited: Bridging the gap between gold(I)-thiolate complexes and thiolate-protected gold nanocrystals. *Journal of the American Chemical Society*, *127*(14), 5261–5270.

Nel, C., Mannel, A., & Kruger, D. (2022). Triple-negative breast cancer - a retrospective audit of 151 cases seen at the Charlotte Maxeke Johannesburg Academic Hospital Breast Unit. *South African Journal of Surgery*, *60*(2), 115–118.

Neumeier, J., & Meister, G. (2021). siRNA Specificity: RNAi Mechanisms and Strategies to Reduce Off-Target Effects. *Frontiers in Plant Science*, *11*, 2196.

Neupane, K. P., & Pecoraro, V. L. (2011). Pb-207 NMR spectroscopy reveals that Pb(II) coordinates with glutathione (GSH) and tris cysteine zinc finger proteins in a PbS3 coordination environment. *Journal of Inorganic Biochemistry*, *105*(8), 1030–1034.

Nie, Z., Hu, G., Wei, G., Cui, K., Yamane, A., Resch, W., Wang, R., Green, D. R., Tessarollo, L., Casellas, R., Zhao, K., & Levens, D. (2012). c-Myc Is a Universal Amplifier of Expressed Genes in Lymphocytes and Embryonic Stem Cells. *Cell*, *151*(1), 68–79.

Nishimura, R., & Arima, N. (2008). Is triple negative a prognostic factor in breast cancer? *Breast Cancer*, *15*(4), 303–308.

Niu, Z., Samaridou, E., Jaumain, E., Coëne, J., Ullio, G., Shrestha, N., Garcia, J., Durán-Lobato, M., Tovar, S., Santander-Ortega, M. J., Lozano, M. V., Arroyo-Jimenez, M. M., Ramos-Membrive, R., Peñuelas, I., Mabondzo, A., Préat, V., Teixidó, M., Giralt, E., & Alonso, M. J. (2018). PEG-PGA enveloped octaarginine-peptide nanocomplexes: An oral peptide delivery strategy. *Journal of Controlled Release*, *276*, 125–139.

Noland, C. L., Ma, E., & Doudna, J. A. (2011). SiRNA Repositioning for Guide Strand Selection by Human Dicer Complexes. *Molecular Cell*, *43*(1), 110–121.

Noy, R., & Pollard, J. W. (2014). Tumor-Associated Macrophages: From Mechanisms to Therapy. *Immunity*, *41*(1), 49–61.

Ntekim, A. I., Folasire, A. M., & Ali-Gombe, M. (2019). *Pan African Medical Journal*, *34*(114).

Ogawa, N., Kawai, H., Terashima, T., Kojima, H., Oka, K., Chan, L., & Maegawa, H. (2014). Gene Therapy for Neuropathic Pain by Silencing of TNF-α Expression with Lentiviral Vectors Targeting the Dorsal Root Ganglion in Mice. *PLoS ONE*, *9*(3), e92073.

Ogawara, K. ichi, Furumoto, K., Takakura, Y., Hashida, M., Higaki, K., & Kimura, T. (2001). Surface hydrophobicity of particles is not necessarily the most important determinant in their in vivo disposition after intravenous administration in rats. *Journal of Controlled Release*, *77*(3), 191–198.

Olina, A. V., Kulbachinskiy, A. V., Aravin, A. A., & Esyunina, D. M. (2018). Argonaute Proteins and Mechanisms of RNA Interference in Eukaryotes and Prokaryotes. *Biochemistry*, *83*(5), 483–497.

Orosz, P., Echtenacher, B., Falk, W., Rüschoff, J., Weber, D., & Männel, D. N. (1993). Enhancement of experimental metastasis by tumor necrosis factor. *Journal of Experimental Medicine*, *177*(5), 1391–1398.

Otano, I., Alvarez, M., Minute, L., Ochoa, M. C., Migueliz, I., Molina, C., Azpilikueta, A., de Andrea, C. E., Etxeberria, I., Sanmamed, M. F., Teijeira, Á., Berraondo, P., & Melero, I. (2020). Human CD8 T cells are susceptible to TNF-mediated activation-induced cell death. *Theranostics*, *10*(10), 4481–4489.

Ou, J. N., Wiedeman, A. E., & Stevens, A. M. (2012). TNF-α and TGF-β counter-regulate PD-L1 expression on monocytes in systemic lupus erythematosus. *Scientific Reports*, *2*(295).

Page, M. J., Bester, J., & Pretorius, E. (2018). The inflammatory effects of TNF-α and complement component 3 on coagulation. *Scientific Reports*, *8*(1), 1–9.

Pagliarini, R., Shao, W., & Sellers, W. R. (2015). Oncogene addiction: pathways of therapeutic response, resistance, and road maps toward a cure. *EMBO Reports*, *16*(3), 280–296.

Pal-Bhadra, M., Bhadra, U., & Birchler, J. A. (1997). Cosuppression in Drosophila: Gene silencing of Alcohol dehydrogenase by white-Adh transgenes is Polycomb dependent. *Cell*, *90*(3), 479–490.

Pal, A., & Kundu, R. (2020). Human Papillomavirus E6 and E7: The Cervical Cancer Hallmarks and Targets for Therapy. *Frontiers in Microbiology*, *10*, 510168.

Pan, Y., Neuss, S., Leifert, A., Fischler, M., Wen, F., Simon, U., Schmid, G., Brandau, W., & Jahnen-Dechent, W. (2007). Size-Dependent Cytotoxicity of Gold Nanoparticles. *Small*, *3*(11), 1941–1949.

Parameswaran, N., & Patial, S. (2010). Tumor necrosis factor-a signaling in macrophages. *Critical Reviews in Eukaryotic Gene Expression*, *20*(2), 87–103.

Parveen, S., & Sahoo, S. K. (2011). Long circulating chitosan/PEG blended PLGA nanoparticle for tumor drug delivery. *European Journal of Pharmacology*, *670*(2–3), 372–383.

Patel, A., Unni, N., & Peng, Y. (2020). The Changing Paradigm for the Treatment of HER2-Positive Breast Cancer. *Cancers*, *12*(8), 2081.

Peñaloza, J. P., Márquez-Miranda, V., Cabaña-Brunod, M., Reyes-Ramírez, R., Llancalahuen, F. M., Vilos, C., Maldonado-Biermann, F., Velásquez, L. A., Fuentes, J. A., González-Nilo, F. D., Rodríguez-Díaz, M., & Otero, C. (2017). Intracellular trafficking and cellular uptake mechanism of PHBV nanoparticles for targeted delivery in epithelial cell lines. *Journal of Nanobiotechnology*, *15*(1), 1.

Pennica, D., Nedwin, G. E., Hayflick, J. S., Seeburg, P. H., Derynck, R., Palladino, M. A., Kohr, W. J., Aggarwal, B. B., & Goeddel, D. V. (1984). Human tumour necrosis factor: Precursor structure, expression and homology to lymphotoxin. *Nature*, *312*(5996), 724–729.

Pereira, P., Pedrosa, S. S., Wymant, J. M., Sayers, E., Correia, A., Vilanova, M., Jones, A. T., & Gama, F. M. (2015). siRNA Inhibition of Endocytic Pathways to Characterize the Cellular Uptake Mechanisms of Folate-Functionalized Glycol Chitosan Nanogels. *Molecular Pharmaceutics*, *12*(6), 1970–1979.

Perillo, B., Di Donato, M., Pezone, A., Di Zazzo, E., Giovannelli, P., Galasso, G., Castoria, G., & Migliaccio, A. (2020). ROS in cancer therapy: the bright side of the moon. *Experimental & Molecular Medicine 2020 52:2*, *52*(2), 192–203.

Perou, C. M., Sørlie, T., Eisen, M. B., van de Rijn, M., Jeffrey, S. S., Ress, C. A., Pollack, J. R., Ross, D. T., Johnsen, H., Akslen, L. A., Fluge, Ø., Pergammenschlkov, A., Williams, C., Zhu, S. X., Lønning, P. E., Børresen-Dale, A. L., Brown, P. O., & Botstein, D. (2000). Molecular portraits of human breast tumours. *Nature*, *406*(6797), 747–752.

Pileczki, V., Braicu, C., Gherman, C., & Berindan-Neagoe, I. (2012). TNF-α Gene Knockout in Triple Negative Breast Cancer Cell Line Induces Apoptosis. *International Journal of Molecular Sciences*, *14*(1), 411–420.

Pileczki, V., Pop, L., Braicu, C., Budisan, L., Morar, G. B., Monroig-Bosque, P. del C., Sandulescu, R. V., & Berindan-Neagoe, I. (2016). Double gene siRNA knockdown of mutant p53 and TNF induces apoptosis in triple-negative breast cancer cells. *OncoTargets and Therapy*, *9*, 6921–6933.

Pirianov, G., & Colston, K. W. (2001). Interactions of vitamin D analogue CB1093, TNFα and ceramide on breast cancer cell apoptosis. *Molecular and Cellular Endocrinology*, *172*(1–2), 69–78.

Pobezinskaya, Y. L., Kim, Y. S., Choksi, S., Morgan, M. J., Li, T., Liu, C., & Liu, Z. (2008). The function of TRADD in signaling through tumor necrosis factor receptor 1 and TRIF-dependent Toll-like receptors. *Nature Immunology*, *9*(9), 1047–1054.

Pomerantz, M. M., Ahmadiyeh, N., Jia, L., Herman, P., Verzi, M. P., Doddapaneni, H., Beckwith, C. A., Chan, J. A., Hills, A., Davis, M., Yao, K., Kehoe, S. M., Lenz, H. J., Haiman, C. A., Yan, C., Henderson, B. E., Frenkel, B., Barretina, J., Bass, A., … Freedman, M. L. (2009). The 8q24 cancer risk variant rs6983267 demonstrates long-range interaction with MYC in colorectal cancer. *Nature Genetics*, *41*(8), 882–884.

Poole, C. J., Zheng, W., Lee, H., Young, D., Lodh, A., Chadli, A., & van Riggelen, J. (2018). Targeting the MYC Oncogene in Burkitt Lymphoma through HSP90 Inhibition. *Cancers 2018, Vol. 10, Page 448*, *10*(11), 448.

Porret, E., Fleury, J. B., Sancey, L., Pezet, M., Coll, J. L., & Le Guével, X. (2020). Augmented interaction of multivalent arginine coated gold nanoclusters with lipid membranes and cells. *RSC Advances*, *10*(11), 6436–6443.

Portis, A. M., Carballo, G., Baker, G. L., Chan, C., & Walton, S. P. (2010). Confocal microscopy for the analysis of siRNA delivery by polymeric nanoparticles. *Microscopy Research and Technique*, *73*(9), 878.

Powell-Coffman, J. A., Knight, J., & Wood, W. B. (1996). Onset of C. elegans gastrulation is blocked by inhibition of embryonic transcription with an RNA polymerase antisense RNA. *Developmental Biology*, *178*(2), 472–483.

Präbst, K., Engelhardt, H., Ringgeler, S., & Hübner, H. (2017). Basic colorimetric proliferation assays: MTT, WST, and resazurin. In *Methods in Molecular Biology* (Vol. 1601, pp. 1–17). Humana Press Inc.

Prado-Vázquez, G., Gámez-Pozo, A., Trilla-Fuertes, L., Arevalillo, J. M., Zapater-Moros, A., Ferrer-Gómez, M., Díaz-Almirón, M., López-Vacas, R., Navarro, H., Maín, P., Feliú, J., Zamora, P., Espinosa, E., & Fresno Vara, J. Á. (2019). A novel approach to triple-negative

breast cancer molecular classification reveals a luminal immune-positive subgroup with good prognoses. *Scientific Reports*, *9*(1), 1–12.

Prencipe, G., Tabakman, S. M., Welsher, K., Liu, Z., Goodwin, A. P., Zhang, L., Henry, J., & Dai, H. (2009). PEG branched polymer for functionalization of nanomaterials with ultralong blood circulation. *Journal of the American Chemical Society*, *131*(13), 4783–4787.

Prieto, G. A., & Cotman, C. W. (2017). Cytokines and cytokine networks target neurons to modulate long-term potentiation. *Cytokine and Growth Factor Reviews*, *34*, 27–33.

Puimège, L., Libert, C., & Van Hauwermeiren, F. (2014). Regulation and dysregulation of tumor necrosis factor receptor-1. *Cytokine and Growth Factor Reviews*, *25*(3), 285–300.

Pusztai, L., Lewis, C. E., & McGee, J. O. D. (1993). Growth arrest of the breast cancer cell line, T47D, by TNFα cell cycle specificity and signal transduction. *British Journal of Cancer*, *67*(2), 290–296.

Pyo, K., Thanthirige, V. D., Kwak, K., Pandurangan, P., Ramakrishna, G., & Lee, D. (2015). Ultrabright Luminescence from Gold Nanoclusters: Rigidifying the Au(I)-Thiolate Shell. *Journal of the American Chemical Society*, *137*(25), 8244–8250.

Qian, H., Zhu, M., Wu, Z., & Jin, R. (2012). Quantum sized gold nanoclusters with atomic precision. *Accounts of Chemical Research*, *45*(9), 1470–1479.

Qiao, Y., He, H., Jonsson, P., Sinha, I., Zhao, C., & Dahlman-Wright, K. (2016). AP-1 is a key regulator of proinflammatory cytokine TNFα-mediated triple-negative breast cancer progression. *Journal of Biological Chemistry*, *291*(10), 5068–5079.

Qiao, Y., Shiue, C. N., Zhu, J., Zhuang, T., Jonsson, P., Wright, A. P. H., Zhao, C., & Dahlman-Wright, K. (2015). AP-1-mediated chromatin looping regulates ZEB2 transcription: New insights into TNFα-induced epithelial-mesenchymal transition in triple-negative breast cancer. *Oncotarget*, *6*(10), 7804–7814.

Qin, W., Hu, L., Zhang, X., Jiang, S., Li, J., Zhang, Z., & Wang, X. (2019). The Diverse Function of PD-1/PD-L Pathway Beyond Cancer. *Frontiers in Immunology*, *10*, 2298.

Qu, J., Zhao, X., Wang, J., Liu, X., Yan, Y., Liu, L., Cai, H., Qu, H., Lu, N., Sun, Y., Wang, F., Wang, J., & Zhang, J. (2017). MYC overexpression with its prognostic and clinicopathological significance in breast cancer. *Oncotarget*, *8*(55), 93998–94008.

Québatte, M., & Dehio, C. (2017). Systems-level interference strategies to decipher host factors involved in bacterial pathogen interaction: from RNAi to CRISPRi. *Current Opinion in Microbiology*, *39*, 34–41.

Queiroz, M. F., Melo, K., Sabry, D., Sassaki, G., & Rocha, H. (2014). Does the Use of Chitosan Contribute to Oxalate Kidney Stone Formation? *Marine Drugs*, *13*(1), 141–158.

Quintero-Fabián, S., Arreola, R., Becerril-Villanueva, E., Torres-Romero, J. C., Arana-Argáez, V., Lara-Riegos, J., Ramírez-Camacho, M. A., & Alvarez-Sánchez, M. E. (2019). Role of Matrix Metalloproteinases in Angiogenesis and Cancer. *Frontiers in Oncology*, *9*, 1370.

Quirke, V. M. (2017). Tamoxifen from Failed Contraceptive Pill to Best-Selling Breast Cancer Medicine: A Case-Study in Pharmaceutical Innovation. *Frontiers in Pharmacology*, *8*, 620.

Radnia, F., Mohajeri, N., Hashemi, F., Imani, M., & Zarghami, N. (2021). Design and development of folate-chitosan/CD nanogel: An efficient fluorescent platform for Cancer-

specific delivery of AntimiR-21. *Reactive and Functional Polymers*, *160*, 104814.

Radomska-Soukharev, A. (2007). Stability of lipid excipients in solid lipid nanoparticles. *Advanced Drug Delivery Reviews*, *59*(6), 411–418.

Rahl, P. B., & Young, R. A. (2014). MYC and Transcription Elongation. *Cold Spring Harbor Perspectives in Medicine*, *4*(1), a020990.

Rakha, E. A., Reis-Filho, J. S., Baehner, F., Dabbs, D. J., Decker, T., Eusebi, V., Fox, S. B., Ichihara, S., Jacquemier, J., Lakhani, S. R., Palacios, J., Richardson, A. L., Schnitt, S. J., Schmitt, F. C., Tan, P.-H., Tse, G. M., Badve, S., & Ellis, I. O. (2010). Breast cancer prognostic classification in the molecular era: the role of histological grade. *Breast Cancer Research*, *12*(4), 207.

Ramesh, G., & Reeves, W. B. (2003). TNFR2-mediated apoptosis and necrosis in cisplatin-induced acute renal failure. *American Journal of Physiology - Renal Physiology*, *285*(4), F610–F618.

Rao, M., & Sockanathan, S. (2005). Molecular mechanisms of RNAi: Implications for development and disease. *Birth Defects Research Part C: Embryo Today: Reviews*, *75*(1), 28–42.

Rauert, H., Wicovsky, A., Müller, N., Siegmund, D., Spindler, V., Waschke, J., Kneitz, C., & Wajant, H. (2010). Membrane Tumor Necrosis Factor (TNF) induces p100 processing via TNF receptor-2 (TNFR2). *Journal of Biological Chemistry*, *285*(10), 7394–7404.

Raveendran, S., Rochani, A., Maekawa, T., & Kumar, D. (2017). Smart Carriers and Nanohealers: A Nanomedical Insight on Natural Polymers. *Materials*, *10*(8), 929.

Reczek, C. R., & Chandel, N. S. (2017). The Two Faces of Reactive Oxygen Species in Cancer. *Annual Review of Cancer Biology*, *1*, 79–98.

Reczek, C. R., & Chandel, N. S. (2018). ROS Promotes Cancer Cell Survival through Calcium Signaling. *Cancer Cell*, *33*, 949–951.

Rehman, N., Khan, S., Manzoor, S., Abubakar, M., Sami, R., Alharthy, S. A., Baty, R. S., Jafri, I., Alsubhi, N. H., Qari, S. H., & Shahid, R. (2022). Estrogen Induces c-myc Transcription by Binding to Upstream ERE Element in Promoter. *Applied Sciences*, *12*(14), 6853.

Rehman, Z. U., Hoekstra, D., & Zuhorn, I. S. (2013). Mechanism of polyplex- and lipoplex-mediated delivery of nucleic acids: Real-time visualization of transient membrane destabilization without endosomal lysis. *ACS Nano*, *7*(5), 3767–3777.

Rejman, J., Oberle, V., Zuhorn, I. S., & Hoekstra, D. (2004). Size-dependent internalization of particles via the pathways of clathrin- and caveolae-mediated endocytosis. *The Biochemical Journal*, *377*(Pt 1), 159–169.

Ren, J., Jin, F., Yu, Z., Zhao, L., Wang, L., Bai, X., Zhao, H., Yao, W., Mi, X., Wang, E., Olopade, O. I., & Wei, M. (2013). MYC overexpression and poor prognosis in sporadic breast cancer with BRCA1 deficiency. *Tumor Biology*, *34*(6), 3945–3958.

Rennoll, S., & Yochum, G. (2015). Regulation of MYC gene expression by aberrant Wnt/β-catenin signaling in colorectal cancer. *World Journal of Biological Chemistry*, *6*(4), 290–300.

Reyes-González, J. M., & Vivas-Mejía, P. E. (2021). c-MYC and Epithelial Ovarian Cancer. *Frontiers in Oncology*, *11*, 601512.

Rheiner, S., & Bae, Y. (2016). Increased poly(ethylene glycol) density decreases transfection efficacy of siRNA/poly(ethylene imine) complexes. *AIMS Bioengineering*, *3*(4), 454–467.

Richard, I., Thibault, M., De Crescenzo, G., Buschmann, M. D., & Lavertu, M. (2013). Ionization Behavior of Chitosan and Chitosan–DNA Polyplexes Indicate That Chitosan Has a Similar Capability to Induce a Proton-Sponge Effect as PEI. *Biomacromolecules*, *14*(6), 1732–1740.

Ricobaraza, A., Gonzalez-Aparicio, M., Mora-Jimenez, L., Lumbreras, S., & Hernandez-Alcoceba, R. (2020). High-Capacity Adenoviral Vectors: Expanding the Scope of Gene Therapy. *International Journal of Molecular Sciences*, *21*(10), 3643.

Ríos-Navarro, C., De Pablo, C., Collado-Diaz, V., Orden, S., Blas-Garcia, A., Martínez-Cuesta, M. Á., Esplugues, J. V., & Alvarez, A. (2015). Differential effects of anti-TNF-α and anti-IL-12/23 agents on human leukocyte-endothelial cell interactions. *European Journal of Pharmacology*, *765*, 355–365.

Rivas, M. A., Carnevale, R. P., Proietti, C. J., Rosemblit, C., Beguelin, W., Salatino, M., Charreau, E. H., Frahm, I., Sapia, S., Brouckaert, P., Elizalde, P. V., & Schillaci, R. (2008). TNFα acting on TNFR1 promotes breast cancer growth via p42/P44 MAPK, JNK, Akt and NF-κB-dependent pathways. *Experimental Cell Research*, *314*(3), 509–529.

Roberts, N. J., Zhou, S., Diaz, L. A., & Holdhoff, M. (2011). Systemic use of tumor necrosis factor alpha as an anticancer agent. *Oncotarget*, *2*(10), 739–751.

Rocheleau, C. E., Downs, W. D., Lin, R., Wittmann, C., Bei, Y., Cha, Y. H., Ali, M., Priess, J. R., & Mello, C. C. (1997). Wnt signaling and an APC-related gene specify endoderm in early C. elegans embryos. *Cell*, *90*(4), 707–716.

Rodríguez, M., Cabal-Hierro, L., Carcedo, M. T., Iglesias, J. M., Artime, N., Darnay, B. G., & Lazo, P. S. (2011). NF-κB signal triggering and termination by tumor necrosis factor receptor 2. *Journal of Biological Chemistry*, *286*(26), 22814–22824.

Rodrik, V., Gomes, E., Hui, L., Rockwell, P., & Foster, D. A. (2006). Myc stabilization in response to estrogen and phospholipase D in MCF-7 breast cancer cells. *FEBS Letters*, *580*(24), 5647–5652.

Rogers, K. R., Navratilova, J., Stefaniak, A., Bowers, L., Knepp, A. K., Al-Abed, S. R., Potter, P., Gitipour, A., Radwan, I., Nelson, C., & Bradham, K. D. (2018). Characterization of engineered nanoparticles in commercially available spray disinfectant products advertised to contain colloidal silver. *Science of The Total Environment*, *619–620*, 1375–1384.

Romano, N., & Macino, G. (1992). Quelling: transient inactivation of gene expression in Neurospora crassa by transformation with homologous sequences. *Molecular Microbiology*, *6*(22), 3343–3353.

Rothstein, S. J., DiMaio, J., Strand, M., & Rice, D. (1987). Stable and heritable inhibition of the expression of nopaline synthase in tobacco expressing antisense RNA. *Proceedings of the National Academy of Sciences*, *84*(23), 8439–8443.

Rous, P. (1911). A Sarcoma Of The Fowl Transmissable By An Agent Seperable From The Tumor Cells. *The Journal of Experimental Medicine*, *13*(4), 397–411.

Rous, P., & Murphy, J. B. (1914). On The Causation By Filterable Agents Of Three Distinct Chicken Tumors. *The Journal of Experimental Medicine*, *19*(1), 52–68.

Rouzier, R., Perou, C. M., Symmans, W. F., Ibrahim, N., Cristofanilli, M., Anderson, K., Hess, K. R., Stec, J., Ayers, M., Wagner, P., Morandi, P., Fan, C., Rabiul, I., Ross, J. S., Hortobagyi, G. N., & Pusztai, L. (2005). Breast cancer molecular subtypes respond differently to preoperative chemotherapy. *Clinical Cancer Research*, *11*(16), 5678–5685.

Rozen, F., Zhang, J., & Pollak, M. (1998). Antiproliferative action of tumor necrosis factor-α on MCF-7 breast cancer cells is associated with increased insulin-like growth factor binding protein-3 accumulation. *International Journal of Oncology*, *13*(4), 865–869.

Rubio, M. F., Werbajh, S., Cafferata, E. G. A., Quaglino, A., Coló, G. P., Nojek, I. M., Kordon, E. C., Nahmod, V. E., & Costas, M. A. (2006). TNF-α enhances estrogen-induced cell proliferation of estrogen-dependent breast tumor cells through a complex containing nuclear factor-kappa B. *Oncogene*, *25*(9), 1367–1377.

Ruder, B., Atreya, R., & Becker, C. (2019). Tumour necrosis factor alpha in intestinal homeostasis and gut related diseases. *International Journal of Molecular Sciences*, *20*(8).

Rudzinski, W. E., Palacios, A., Ahmed, A., Lane, M. A., & Aminabhavi, T. M. (2016). Targeted delivery of small interfering RNA to colon cancer cells using chitosan and PEGylated chitosan nanoparticles. *Carbohydrate Polymers*, *147*, 323–332.

Rüegg, C., Yilmaz, A., Bieler, G., Bamat, J., Chaubert, P., & Lejeune, F. J. (1998). Evidence for the involvement of endothelial cell integrin αVβ3 in the disruption of the tumor vasculature induced by TNF and IFN-γ. *Nature Medicine*, *4*(4), 408–414.

Ruspi, G., Schmidt, E. M., McCann, F., Feldmann, M., Williams, R. O., Stoop, A. A., & Dean, J. L. E. (2014). TNFR2 increases the sensitivity of ligand-induced activation of the p38 MAPK and NF-κB pathways and signals TRAF2 protein degradation in macrophages. *Cellular Signalling*, *26*(4), 683–690.

Saatci, O., Huynh-Dam, K. T., & Sahin, O. (2021). Endocrine resistance in breast cancer: from molecular mechanisms to therapeutic strategies. *Journal of Molecular Medicine*, *99*(12), 1691–1710.

Sabuncu, A. C., Grubbs, J., Qian, S., Abdel-Fattah, T. M., Stacey, M. W., & Beskok, A. (2012). Probing nanoparticle interactions in cell culture media. *Colloids and Surfaces B: Biointerfaces*, *95*, 96–102.

Sajid, M. I., Moazzam, M., Kato, S., Yeseom Cho, K., & Tiwari, R. K. (2020). Overcoming Barriers for siRNA Therapeutics: From Bench to Bedside. *Pharmaceuticals (Basel, Switzerland)*, *13*(10), 294.

Sakurai, K., Amarzguioui, M., Kim, D. H., Alluin, J., Heale, B., Song, M. S., Gatignol, A., Behlke, M. A., & Rossi, J. J. (2011). A role for human Dicer in pre-RISC loading of siRNAs. *Nucleic Acids Research*, *39*(4), 1510–1525.

Salomon, B. L., Leclerc, M., Tosello, J., Ronin, E., Piaggio, E., & Cohen, J. L. (2018). Tumor Necrosis Factor α and Regulatory T Cells in Oncoimmunology. *Frontiers in Immunology*, *9*, 444.

Sami El-banna, F., Mahfouz, M. E., Leporatti, S., El-Kemary, M., & A. N. Hanafy, N. (2019). Chitosan as a Natural Copolymer with Unique Properties for the Development of Hydrogels. *Applied Sciences*, *9*(11), 2193.

Santander-Ortega, M. J., Peula-García, J. M., Goycoolea, F. M., & Ortega-Vinuesa, J. L. (2011). Chitosan nanocapsules: Effect of chitosan molecular weight and acetylation degree on

electrokinetic behaviour and colloidal stability. *Colloids and Surfaces B: Biointerfaces*, *82*(2), 571–580.

Santel, A., Aleku, M., Keil, O., Endruschat, J., Esche, V., Fisch, G., Dames, S., Lö, K., Fechtner, M., Arnold, W., Giese, K., Klippel, A., & Kaufmann, J. (2006). A novel siRNA-lipoplex technology for RNA interference in the mouse vascular endothelium. *Gene Therapy*, *13*(16), 1222–1234.

Santiago González, B., Rodríguez, M. J., Blanco, C., Rivas, J., López-Quintela, M. A., & Martinho, J. M. G. (2010). One step synthesis of the smallest photoluminescent and paramagnetic PVP-protected gold atomic clusters. *Nano Letters*, *10*(10), 4217–4221.

Santos-Carballal, B., Fernández, E. F., & Goycoolea, F. M. (2018). Chitosan in non-viral gene delivery: Role of structure, characterization methods, and insights in cancer and rare diseases therapies. *Polymers*, *10*(4), 444.

Sarisozen, C., Salzano, G., & Torchilin, V. P. (2015). Recent advances in siRNA delivery. *Biomolecular Concepts*, *6*(5–6), 321–341.

Scafuro, M., Capasso, L., Carafa, V., Altucci, L., & Nebbioso, A. (2021). Gene Transactivation and Transrepression in MYC-Driven Cancers. *International Journal of Molecular Sciences 2021, Vol. 22, Page 3458*, *22*(7), 3458.

Schaaff, G. T., Knight, G., Shafigullin, M. N., Borkman, R. F., & Whetten, R. L. (1998). Isolation and selected properties of a 10.4 kda gold:glutathione cluster compound. *Journal of Physical Chemistry B*, *102*(52), 10645–10646.

Schaub, F. X., Dhankani, V., Berger, A. C., Trivedi, M., Richardson, A. B., Shaw, R., Zhao, W., Zhang, X., Ventura, A., Liu, Y., Ayer, D. E., Hurlin, P. J., Cherniack, A. D., Eisenman, R. N., Bernard, B., Grandori, C., Caesar-Johnson, S. J., Demchok, J. A., Felau, I., … Mariamidze, A. (2018). Pan-cancer Alterations of the MYC Oncogene and Its Proximal Network across the Cancer Genome Atlas. *Cell Systems*, *6*(3), 282-300.e2.

Scheff, N. N., Ye, Y., Bhattacharya, A., MacRae, J., Hickman, D. N., Sharma, A. K., Dolan, J. C., & Schmidt, B. L. (2017). Tumor necrosis factor alpha secreted from oral squamous cell carcinoma contributes to cancer pain and associated inflammation. *Pain*, *158*(12), 2396–2409.

Schick, M., Habringer, S., Nilsson, J. A., & Keller, U. (2017). Pathogenesis and therapeutic targeting of aberrant MYC expression in haematological cancers. *British Journal of Haematology*, *179*(5), 724–738.

Schieber, M., & Chandel, N. S. (2014). ROS function in redox signaling and oxidative stress. *Current Biology*, *24*(10), R453–R462.

Schneider-Brachert, W., Tchikov, V., Neumeyer, J., Jakob, M., Winoto-Morbach, S., Held-Feindt, J., Heinrich, M., Merkel, O., Ehrenschwender, M., Adam, D., Mentlein, R., Kabelitz, D., & Schütze, S. (2004). Compartmentalization of TNF receptor 1 signaling: Internalized TNF receptosomes as death signaling vesicles. *Immunity*, *21*(3), 415–428.

Schütze, S., Machleidt, T., Adam, D., Schwandner, R., Wiegmann, K., Kruse, M. L., Heinrich, M., Wickel, M., & Krönke, M. (1999). Inhibition of receptor internalization by monodansylcadaverine selectively blocks p55 tumor necrosis factor receptor death domain signaling. *Journal of Biological Chemistry*, *274*(15), 10203–10212.

Scott, C. C., Vacca, F., & Gruenberg, J. (2014). Endosome maturation, transport and functions. *Seminars in Cell and Developmental Biology*, *31*, 2–10.

Sedger, L. M., & McDermott, M. F. (2014). TNF and TNF-receptors: From mediators of cell death and inflammation to therapeutic giants - past, present and future. *Cytokine and Growth Factor Reviews*, *25*(4), 453–472.

See, Y. X., Chen, K., & Fullwood, M. J. (2022). MYC overexpression leads to increased chromatin interactions at super-enhancers and MYC binding sites. *Genome Research*, *32*(4), 629–642.

Selvaprakash, K., & Chen, Y. C. (2014). Using protein-encapsulated gold nanoclusters as photoluminescent sensing probes for biomolecules. *Biosensors and Bioelectronics*, *61*, 88–94.

Semmler-Behnke, M., Kreyling, W. G., Lipka, J., Fertsch, S., Wenk, A., Takenaka, S., Schmid, G., & Brandau, W. (2008). Biodistribution of 1.4- and 18-nm gold particles in rats. *Small*, *4*(12), 2108–2111.

Setten, R. L., Rossi, J. J., & Han, S. ping. (2019). The current state and future directions of RNAi-based therapeutics. *Nature Reviews Drug Discovery*, *18*(6), 421–446.

Sgagias, M. K., Kasid, A., & Danforth, D. N. (1991). Interleukin-1α and tumor necrosis factor-α (TNFα) inhibit growth and induce TNF messenger RNA in MCF-7 human breast cancer cells. *Molecular Endocrinology*, *5*(11), 1740–1747.

Shajahan-Haq, A. N., Cook, K. L., Schwartz-Roberts, J. L., Eltayeb, A. E., Demas, D. M., Warri, A. M., Facey, C. O. B., Hilakivi-Clarke, L. A., & Clarke, R. (2014). MYC regulates the unfolded protein response and glucose and glutamine uptake in endocrine resistant breast cancer. *Molecular Cancer*, *13*(1), 239.

Shalgunov, V., Zaytseva-Zotova, D., Zintchenko, A., Levada, T., Shilov, Y., Andreyev, D., Dzhumashev, D., Metelkin, E., Urusova, A., Demin, O., McDonnell, K., Troiano, G., Zale, S., & Safarova, E. (2017). Comprehensive study of the drug delivery properties of poly(L-lactide)-poly(ethylene glycol) nanoparticles in rats and tumor-bearing mice. *Journal of Controlled Release*, *261*, 31–42.

Shang, G. S., Liu, L., & Qin, Y. W. (2017). IL-6 and TNF-α promote metastasis of lung cancer by inducing epithelial-mesenchymal transition. *Oncology Letters*, *13*(6), 4657–4660.

Shannahan, J. H., Lai, X., Ke, P. C., Podila, R., Brown, J. M., & Witzmann, F. A. (2013). Silver Nanoparticle Protein Corona Composition in Cell Culture Media. *PLOS ONE*, *8*(9), e74001.

Shea-Eaton, W. K., Lee, P. P. H., & Ip, M. M. (2001). Regulation of milk protein gene expression in normal mammary epithelial cells by tumor necrosis factor. *Endocrinology*, *142*(6), 2558–2568.

Sheiness, D., & Bishop, J. M. (1979). DNA and RNA from Uninfected Vertebrate Cells Contain Nucleotide Sequences Related to the Putative Transforming Gene of Avian Myelocytomatosis Virus. *Journal of Virology*, *31*(2), 514.

Shen, J., Xiao, Z., Zhao, Q., Li, M., Wu, X., Zhang, L., Hu, W., & Cho, C. H. (2018). Anti-cancer therapy with TNFα and IFNγ: A comprehensive review. *Cell Proliferation*, *51*(4), e12441.

Shen, L., O'Shea, J. M., Kaadige, M. R., Cunha, S., Wilde, B. R., Cohen, A. L., Welm, A. L., & Ayer, D. E. (2015). Metabolic reprogramming in triple-negative breast cancer through Myc suppression of TXNIP. *Proceedings of the National Academy of Sciences of the United States of America*, *112*(17), 5425–5430.

Shen, N., Liu, S., Cui, J., Li, Q., You, Y., Zhong, Z., Cheng, F., Guo, A. Y., Zou, P., Yuan, G., & Zhu, X. (2019). Tumor necrosis factor α knockout impaired tumorigenesis in chronic myeloid leukemia cells partly by metabolism modification and miRNA regulation. *OncoTargets and Therapy*, *12*, 2355–2364.

Shi, B., Zheng, M., Tao, W., Chung, R., Jin, D., Ghaffari, D., & Farokhzad, O. C. (2017). Challenges in DNA Delivery and Recent Advances in Multifunctional Polymeric DNA Delivery Systems. *Biomacromolecules*, *18*(8), 2231–2246.

Shi, J., Whyte, W. A., Zepeda-Mendoza, C. J., Milazzo, J. P., Shen, C., Roe, J. S., Minder, J. L., Mercan, F., Wang, E., Eckersley-Maslin, M. A., Campbell, A. E., Kawaoka, S., Shareef, S., Zhu, Z., Kendall, J., Muhar, M., Haslinger, C., Yu, M., Roeder, R. G., … Vakoc, C. R. (2013). Role of SWI/SNF in acute leukemia maintenance and enhancer-mediated Myc regulation. *Genes & Development*, *27*(24), 2648–2662.

Shi, J., Xu, Y., Xu, X., Zhu, X., Pridgen, E., Wu, J., Votruba, A. R., Swami, A., Zetter, B. R., & Farokhzad, O. C. (2014). Hybrid lipid–polymer nanoparticles for sustained siRNA delivery and gene silencing. *Nanomedicine: Nanotechnology, Biology and Medicine*, *10*(5), e897–e900.

Shim, M. S., Wang, X., Ragan, R., & Kwon, Y. J. (2010). Dynamics of Nucleic Acid/Cationic Polymer Complexation and Disassembly under Biologically Simulated Conditions Using In Situ Atomic Force Microscopy. *Microscopy Research and Technique*, *73*(9), 845.

Shin, H. R., Kwak, M., Lee, T. G., & Lee, J. Y. (2020). Quantifying the level of nanoparticle uptake in mammalian cells using flow cytometry. *Nanoscale*, *12*(29), 15743–15751.

Shirmohammadi, E., Ebrahimi, S. E. S., Farshchi, A., & Salimi, M. (2020). The efficacy of etanercept as anti-breast cancer treatment is attenuated by residing macrophages. *BMC Cancer*, *20*(1), 1–10.

Singh, A., Trivedi, P., & Jain, N. K. (2018). Advances in siRNA delivery in cancer therapy. *Artificial Cells, Nanomedicine, and Biotechnology*, *46*(2), 274–283.

Singh, P., Pandit, S., Mokkapati, V. R. S. S., Garg, A., Ravikumar, V., & Mijakovic, I. (2018). Gold Nanoparticles in Diagnostics and Therapeutics for Human Cancer. *International Journal of Molecular Sciences*, *19*(7), 1979–1994.

Smalheiser, N. R. (2012). The search for endogenous siRNAs in the mammalian brain. *Experimental Neurology*, *235*(2), 455–463.

Smith, H. G., Wilkinson, M. J., Smith, M. J. F., Strauss, D. C., & Hayes, A. J. (2018). The effect of age on outcomes after isolated limb perfusion for advanced extremity malignancies. *European Journal of Cancer*, *100*, 46–54.

Soares-Silva, M., Diniz, F. F., Gomes, G. N., & Bahia, D. (2016). The Mitogen-Activated Protein Kinase (MAPK) Pathway: Role in Immune Evasion by Trypanosomatids. *Frontiers in Microbiology*, *7*, 183.

Son, D. S., Kabir, S. M., Dong, Y., Lee, E., & Adunyah, S. E. (2013). Characteristics of chemokine signatures elicited by EGF and TNF in ovarian cancer cells. *Journal of Inflammation*, *10*(1), 25.

Sonawane, N. D., Szoka, F. C., & Verkman, A. S. (2003). Chloride accumulation and swelling in endosomes enhances DNA transfer by polyamine-DNA polyplexes. *The Journal of Biological Chemistry*, *278*(45), 44826–44831.

Song, Q., Meng, B., Xu, H., & Mao, Z. (2020). The emerging roles of vacuolar-type ATPase-dependent Lysosomal acidification in neurodegenerative diseases. *Translational Neurodegeneration*, *9*(1), 17.

Soria, G., Ofri-Shahak, M., Haas, I., Yaal-Hahoshen, N., Leider-Trejo, L., Leibovich-Rivkin, T., Weitzenfeld, P., Meshel, T., Shabtai, E., Gutman, M., & Ben-Baruch, A. (2011). Inflammatory mediators in breast cancer: Coordinated expression of TNFα & IL-1β with CCL2 & CCL5 and effects on epithelial-to-mesenchymal transition. *BMC Cancer*, *11*(1), 130.

Sørlie, T., Perou, C. M., Tibshirani, R., Aas, T., Geisler, S., Johnsen, H., Hastie, T., Eisen, M. B., Van De Rijn, M., Jeffrey, S. S., Thorsen, T., Quist, H., Matese, J. C., Brown, P. O., Botstein, D., Lønning, P. E., & Børresen-Dale, A. L. (2001). Gene expression patterns of breast carcinomas distinguish tumor subclasses with clinical implications. *Proceedings of the National Academy of Sciences of the United States of America*, *98*(19), 10869–10874.

Spotts, G. D., Patel, S. V., Xiao, Q., & Hann, S. R. (1997). Identification of Downstream-Initiated c-Myc Proteins Which Are Dominant-Negative Inhibitors of Transactivation by Full-Length c-Myc Proteins. *Molecular and Cellular Biology*, *17*(3), 1459–1468.

Srivastava, P., Wang, T., Clark, B. Z., Yu, J., Fine, J. L., Villatoro, T. M., Carter, G. J., Brufsky, A. M., Gorantla, V. C., Huggins-Puhalla, S. L., Emens, L. A., Basili, T., da Silva, E. M., Reis-Filho, J. S., & Bhargava, R. (2022). Clinical-pathologic characteristics and response to neoadjuvant chemotherapy in triple-negative low Ki-67 proliferation (TNLP) breast cancers. *Npj Breast Cancer*, *8*(1), 51.

Steinman, L. (2010). Modulation of postoperative cognitive decline via blockade of inflammatory cytokines outside the brain. *Proceedings of the National Academy of Sciences of the United States of America*, *107*(48), 20595–20596.

Stenken, J. A., & Poschenrieder, A. J. (2015). Bioanalytical chemistry of cytokines - A review. *Analytica Chimica Acta*, *853*(1), 95–115.

Stewart, R. L., Updike, K. L., Factor, R. E., Henry, N. L., Boucher, K. M., Bernard, P. S., & Varley, K. E. (2019). A multigene assay determines risk of recurrence in patients with triple-negative breast cancer. *Cancer Research*, *79*(13), 3466–3478.

Storci, G., Sansone, P., Mari, S., D'Uva, G., Tavolari, S., Guarnieri, T., Taffurelli, M., Ceccarelli, C., Santini, D., Chieco, P., Marcu, K. B., & Bonafè, M. (2010). TNFalpha up-regulates SLUG via the NF-kappaB/HIF1alpha axis, which imparts breast cancer cells with a stem cell-like phenotype. *Journal of Cellular Physiology*, *225*(3), 682–691.

Su, Y., Pelz, C., Huang, T., Torkenczy, K., Wang, X., Cherry, A., Daniel, C. J., Liang, J., Nan, X., Dai, M. S., Adey, A., Impey, S., & Sears, R. C. (2018). Post-translational modification localizes MYC to the nuclear pore basket to regulate a subset of target genes involved in cellular responses to environmental signals. *Genes and Development*, *32*(21–22), 1398–1419.

Subramoniam, A., Asha, V. V., Nair, S. A., Sasidharan, S. P., Sureshkumar, P. K., Rajendran, K. N., Karunagaran, D., & Ramalingam, K. (2012). Chlorophyll revisited: anti-inflammatory activities of chlorophyll a and inhibition of expression of TNF-α gene by the same. *Inflammation*, *35*(3), 959–966.

Suk, J. S., Xu, Q., Kim, N., Hanes, J., & Ensign, L. M. (2016). PEGylation as a strategy for improving nanoparticle-based drug and gene delivery. *Advanced Drug Delivery Reviews*, *99*(Pt A), 28–51.

Sun, S.-C. (2011). Non-canonical NF-κB signaling pathway. *Cell Research*, *21*(1), 71–85.

Sun, Y., Wang, D., Zhao, Y., Zhao, T., Sun, H., Li, X., Wang, C., Yang, B., & Lin, Q. (2018). Polycation-functionalized gold nanodots with tunable near-infrared fluorescence for simultaneous gene delivery and cell imaging. *Nano Research*, *11*(5), 2392–2404.

Sur, I. K., Hallikas, O., Vähärautio, A., Yan, J., Turunen, M., Enge, M., Taipale, M., Karhu, A., Aaltonen, L. A., & Taipale, J. (2012). Mice lacking a Myc enhancer that includes human SNP rs6983267 are resistant to intestinal tumors. *Science*, *338*(6112), 1360–1363.

Sutton, D., Kim, S., Shuai, X., Leskov, K., Marques, J. T., Williams, B. R. G., Boothman, D. A., & Gao, J. (2006). Efficient suppression of secretory clusterin levels by polymer-siRNA nanocomplexes enhances ionizing radiation lethality in human MCF-7 breast cancer cells in vitro. *International Journal of Nanomedicine*, *1*(2), 155.

Svobodova, E., Kubikova, J., & Svoboda, P. (2016). Production of small RNAs by mammalian Dicer. *Pflugers Archiv : European Journal of Physiology*, *468*(6), 1089–1102.

Szlosarek, P. W., Grimshaw, M. J., Kulbe, H., Wilson, J. L., Wilbanks, G. D., Burke, F., & Balkwill, F. R. (2006). Expression and regulation of tumor necrosis factor α in normal and malignant ovarian epithelium. *Molecular Cancer Therapeutics*, *5*(2), 382–390.

Tahara, K., Sakai, T., Yamamoto, H., Takeuchi, H., Hirashima, N., & Kawashima, Y. (2009). Improved cellular uptake of chitosan-modified PLGA nanospheres by A549 cells. *International Journal of Pharmaceutics*, *382*(1–2), 198–204.

Taishi, P., Churchill, L., Wang, M., Kay, D., Davis, C. J., Guan, X., De, A., Yasuda, T., Liao, F., & Krueger, J. M. (2007). TNFα siRNA reduces brain TNF and EEG delta wave activity in rats. *Brain Research*, *1156*(1), 125–132.

Tambe, P., Kumar, P., Gajbhiye, V., & Paknikar, K. (2016). SiRNA Mediated Gene Silencing: Hurdles, Strategies and Applications. *Pharmaceutical Nanotechnology*, *3*(4), 322–333.

Tamura, M., Ichinohe, S., Tamura, A., Ikeda, Y., & Nagasaki, Y. (2011). In vitro and in vivo characteristics of core-shell type nanogel particles: Optimization of core cross-linking density and surface poly(ethylene glycol) density in PEGylated nanogels. *Acta Biomaterialia*, *7*(9), 3354–3361.

Tanaka, K., Watanabe, M., Tanigaki, S., Iwashita, M., & Kobayashi, Y. (2018). Tumor necrosis factor-α regulates angiogenesis of BeWo cells via synergy of PlGF/VEGFR1 and VEGF-A/VEGFR2 axes. *Placenta*, *74*, 20–27.

Tang, M., O'Grady, S., Crown, J., & Duffy, M. J. (2022). MYC as a therapeutic target for the treatment of triple-negative breast cancer: preclinical investigations with the novel MYC inhibitor, MYCi975. *Breast Cancer Research and Treatment*, *195*(2), 105–115.

Tang, P., Hung, M. C., & Klostergaard, J. (1996). Human pro-tumor necrosis factor is a homotrimer. *Biochemistry*, *35*(25), 8216–8225.

Tangudu, N. K., Verma, V. K., Clemons, T. D., Beevi, S. S., Hay, T., Mahidhara, G., Raja, M., Nair, R. A., Alexander, L. E., Patel, A. B., Jose, J., Smith, N. M., Zdyrko, B., Bourdoncle, A., Luzinov, I., Iyer, K. S., Clarke, A. R., & Dinesh Kumar, L. (2015). RNA interference using c-Myc-conjugated nanoparticles suppresses breast and colorectal cancer models. *Molecular Cancer Therapeutics*, *14*(5), 1259–1269.

Tao, Y., Li, Z., Ju, E., Ren, J., & Qu, X. (2013). Polycations-functionalized water-soluble gold

nanoclusters: A potential platform for simultaneous enhanced gene delivery and cell imaging. *Nanoscale*, *5*(13), 6154–6160.

Taranejoo, S., Chandrasekaran, R., Cheng, W., & Hourigan, K. (2016). Bioreducible PEI-functionalized glycol chitosan: A novel gene vector with reduced cytotoxicity and improved transfection efficiency. *Carbohydrate Polymers*, *153*, 160–168.

Tartaglia, L. A., Pennica, D., & Goeddel, D. V. (1993). Ligand passing: the 75-kDa tumor necrosis factor (TNF) receptor recruits TNF for signaling by the 55-kDa TNF receptor. *The Journal of Biological Chemistry*, *268*(25), 18542–18548.

Tay, C. Y., Yu, Y., Setyawati, M. I., Xie, J., & Leong, D. T. (2014). Presentation matters: Identity of gold nanocluster capping agent governs intracellular uptake and cell metabolism. *Nano Research*, *7*(6), 805–815.

Tekie, F. S. M., Hajiramezanali, M., Geramifar, P., Raoufi, M., Dinarvand, R., Soleimani, M., & Atyabi, F. (2020). Controlling evolution of protein corona: a prosperous approach to improve chitosan-based nanoparticle biodistribution and half-life. *Scientific Reports 2020 10:1*, *10*(1), 1–14.

Thi, T. T. H., Pilkington, E. H., Nguyen, D. H., Lee, J. S., Park, K. D., & Truong, N. P. (2020). The importance of Poly(ethylene glycol) alternatives for overcoming PEG immunogenicity in drug delivery and bioconjugation. *Polymers*, *12*(2), 298.

Thibault, M., Astolfi, M., Tran-Khanh, N., Lavertu, M., Darras, V., Merzouki, A., & Buschmann, M. D. (2011). Excess polycation mediates efficient chitosan-based gene transfer by promoting lysosomal release of the polyplexes. *Biomaterials*, *32*(20), 4639–4646.

Thibault, M., Nimesh, S., Lavertu, M., & Buschmann, M. D. (2010). Intracellular trafficking and decondensation kinetics of chitosan-pDNA polyplexes. *Molecular Therapy*, *18*(10), 1787–1795.

Thomas, L. R., Adams, C. M., Wang, J., Weissmiller, A. M., Creighton, J., Lorey, S. L., Liu, Q., Fesik, S. W., Eischen, C. M., & Tansey, W. P. (2019). Interaction of the oncoprotein transcription factor MYC with its chromatin cofactor WDR5 is essential for tumor maintenance. *Proceedings of the National Academy of Sciences of the United States of America*, *116*(50), 25260–25268.

Thomas, L. R., Foshage, A. M., Weissmiller, A. M., Popay, T. M., Grieb, B. C., Qualls, S. J., Ng, V., Carboneau, B., Lorey, S., Eischen, C. M., & Tansey, W. P. (2016). Interaction of MYC with Host Cell Factor-1 is meditated by the evolutionarily-conserved Myc box IV motif. *Oncogene*, *35*(27), 3613–3618.

Thomas, R., Al-Khadairi, G., & Decock, J. (2021). Immune Checkpoint Inhibitors in Triple Negative Breast Cancer Treatment: Promising Future Prospects. *Frontiers in Oncology*, *10*, 3464.

Tian, T., Wang, M., & Ma, D. (2014). TNF-α, a good or bad factor in hematological diseases? *Stem Cell Investigation*, *1*, 12.

To, S. Q., Cheung, V., Lazarus, K. A., Knower, K. C., & Clyne, C. D. (2014). Estradiol regulates Tumor Necrosis Factor-α expression and secretion in Estrogen Receptor positive breast cancer cells. *Molecular and Cellular Endocrinology*, *394*(1–2), 21–28.

To, S. Q., Knower, K. C., & Clyne, C. D. (2013). Origins and Actions of Tumor Necrosis Factor α in Postmenopausal Breast Cancer. *Journal of Interferon & Cytokine Research*, *33*(7),

335–345.

Todoric, J., Antonucci, L., & Karin, M. (2016). Targeting inflammation in cancer prevention and therapy. *Cancer Prevention Research*, *9*(12), 895–905.

Tomita, Y., Ueda, T., Yoshimichi, D., Minamoto, T., & Kosaka, T. (2019). Expression of Coding Region Determinant-Binding Protein (CRD-BP) in Colorectal Cancer and Its Influence on Target Gene Expression and Clinical Characteristics. *Journal of Kanazawa Medical University*, *44*, 32–42.

Torrey, H., Khodadoust, M., Tran, L., Baum, D., Defusco, A., Kim, Y. H., & Faustman, D. L. (2019). Targeted killing of TNFR2-expressing tumor cells and Tregs by TNFR2 antagonistic antibodies in advanced Sézary syndrome. *Leukemia*, *33*(5), 1206–1218.

Trachootham, D., Alexandre, J., & Huang, P. (2009). Targeting cancer cells by ROS-mediated mechanisms: a radical therapeutic approach? *Nature Reviews. Drug Discovery*, *8*(7), 579–591.

Trevejo, J. M., Marino, M. W., Philpott, N., Josien, R., Richards, E. C., Elkon, K. B., & Falck-Pedersen, E. (2001). TNF-α-dependent maturation of local dendritic cells is critical for activating the adaptive immune response to virus infection. *Proceedings of the National Academy of Sciences of the United States of America*, *98*(21), 12162–12167.

Tsoli, M., Kuhn, H., Brandau, W., Esche, H., & Schmid, G. (2005). Cellular Uptake and Toxicity of Au55 Clusters. *Small*, *1*(8–9), 841–844.

Tu, W. B., Shiah, Y. J., Lourenco, C., Mullen, P. J., Dingar, D., Redel, C., Tamachi, A., Ba-Alawi, W., Aman, A., Al-awar, R., Cescon, D. W., Haibe-Kains, B., Arrowsmith, C. H., Raught, B., Boutros, P. C., & Penn, L. Z. (2018). MYC Interacts with the G9a Histone Methyltransferase to Drive Transcriptional Repression and Tumorigenesis. *Cancer Cell*, *34*(4), 579-595.e8.

Turkevich, J., Stevenson, P. C., & Hillier, J. (1951). A study of the nucleation and growth processes in the synthesis of colloidal gold. *Discussions of the Faraday Society*, *11*, 55.

Ude, A., Afi-Leslie, K., Okeke, K., Ogbodo, E., Ude, A., Afi-Leslie, K., Okeke, K., & Ogbodo, E. (2022). Trypan Blue Exclusion Assay, Neutral Red, Acridine Orange and Propidium Iodide. In A. Sukumaran & M. A. Mansour (Eds.), *Cytotoxicity - Understanding Cellular Damage and Response*. IntechOpen.

Umemura, S., Yoshida, S., Ohta, Y., Naito, K., Osamura, R. Y., & Tokuda, Y. (2007). Increased phosphorylation of Akt in triple-negative breast cancers. *Cancer Science*, *98*(12), 1889–1892.

Urbanek-Olejnik, K., Liszewska, M., Winczura, A., Hernik, A., Strucinski, P., & Ludwicki, J. K. (2018). Hypomethylation of the c-myc promoter region induced by phenobarbital in rat liver. *Roczniki Panstwowego Zakladu Higieny*, *69*(3), 307–314.

Urbiola, K., Blanco-Fernández, L., Ogris, M., Rödl, W., Wagner, E., & de Ilarduya, C. T. (2018). Novel PAMAM-PEG-Peptide Conjugates for siRNA Delivery Targeted to the Transferrin and Epidermal Growth Factor Receptors. *Journal of Personalized Medicine*, *8*(1), 4.

Urits, I., Swanson, D., Swett, M. C., Patel, A., Berardino, K., Amgalan, A., Berger, A. A., Kassem, H., Kaye, A., & Viswanath, O. (2020). A Review of Patisiran (ONPATTRO®) for the Treatment of Polyneuropathy in People with Hereditary Transthyretin Amyloidosis. *Neurology and Therapy*, *9*(2), 301–315.

Uversky, V. N., El-Baky, N. A., El-Fakharany, E. M., Sabry, A., Mattar, E. H., Uversky, A. V., & Redwan, E. M. (2017). Functionality of intrinsic disorder in tumor necrosis factor-α and its receptors. *FEBS Journal*, *284*(21), 3589–3618.

van de Looij, S. M., Hebels, E. R., Viola, M., Hembury, M., Oliveira, S., & Vermonden, T. (2022). Gold Nanoclusters: Imaging, Therapy, and Theranostic Roles in Biomedical Applications. *Bioconjugate Chemistry*, *33*(1), 4–23.

van Vlerken, L. E., Vyas, T. K., & Amiji, M. M. (2007). Poly(ethylene glycol)-modified Nanocarriers for Tumor-targeted and Intracellular Delivery. *Pharmaceutical Research*, *24*(8), 1405–1414.

Varley, A. J., & Desaulniers, J. P. (2021). Chemical strategies for strand selection in short-interfering RNAs. *RSC Advances*, *11*(4), 2415–2426.

Vennstrom, B., Sheiness, D., Zabielski, J., & Bishop, J. M. (1982). Isolation and characterization of c-myc, a cellular homolog of the oncogene (v-myc) of avian myelocytomatosis virus strain 29. *Journal of Virology*, *42*(3), 773–779.

Vermeulen, L. M. P., De Smedt, S. C., Remaut, K., & Braeckmans, K. (2018). The proton sponge hypothesis: Fable or fact? *European Journal of Pharmaceutics and Biopharmaceutics*, *129*, 184–190.

Wang, C., Mayer, J. A., Mazumdar, A., Fertuck, K., Kim, H., Brown, M., & Brown, P. H. (2011a). Estrogen induces c-myc gene expression via an upstream enhancer activated by the estrogen receptor and the AP-1 transcription factor. *Molecular Endocrinology*, *25*(9), 1527–1538.

Wang, C., Mayer, J. A., Mazumdar, A., Fertuck, K., Kim, H., Brown, M., & Brown, P. H. (2011b). Estrogen Induces c-myc Gene Expression via an Upstream Enhancer Activated by the Estrogen Receptor and the AP-1 Transcription Factor. *Molecular Endocrinology*, *25*(9), 1527–1538.

Wang, H. W., Noland, C., Siridechadilok, B., Taylor, D. W., Ma, E., Felderer, K., Doudna, J. A., & Nogales, E. (2009). Structural insights into RNA processing by the human RISC-loading complex. *Nature Structural and Molecular Biology*, *16*(11), 1148–1153.

Wang, H., Zhang, S., Lv, J., & Cheng, Y. (2021). Design of polymers for siRNA delivery: Recent progress and challenges. *VIEW*, *2*(3), 20200026.

Wang, J., Wang, Z. Y., Li, S. J., Zang, S. Q., & Mak, T. C. W. (2021). Carboranealkynyl-Protected Gold Nanoclusters: Size Conversion and UV/Vis–NIR Optical Properties. *Angewandte Chemie International Edition*, *60*(11), 5959–5964.

Wang, J. Y., Chen, J., Yang, J., Wang, H., Shen, X., Sun, Y. M., Guo, M., & Zhang, X. D. (2016). Effects of surface charges of gold nanoclusters on long-term in vivo biodistribution, toxicity, and cancer radiation therapy. *International Journal of Nanomedicine*, *11*, 3475–3485.

Wang, J., Zhang, G., Li, Q., Jiang, H., Liu, C., Amatore, C., & Wang, X. (2013). In vivo self-bio-imaging of tumors through in situ biosynthesized fluorescent gold nanoclusters. *Scientific Reports*, *3*(1), 1–6.

Wang, K., & Karin, M. (2015). Tumor-Elicited Inflammation and Colorectal Cancer. *Advances in Cancer Research*, *128*, 173–196.

Wang, Q., Zhang, H., Kajino, K., & Greene, M. I. (1998). BRCA1 binds c-Myc and inhibits its

transcriptional and transforming activity in cells. *Oncogene*, *17*(15), 1939–1948.

Wang, T., Larcher, L. M., Ma, L., & Veedu, R. N. (2018). Systematic Screening of Commonly Used Commercial Transfection Reagents towards Efficient Transfection of Single-Stranded Oligonucleotides. *Molecules 2018, Vol. 23, Page 2564*, *23*(10), 2564.

Wang, X., Yang, L., Huang, F., Zhang, Q., Liu, S., Ma, L., & You, Z. (2017). Inflammatory cytokines IL-17 and TNF-α up-regulate PD-L1 expression in human prostate and colon cancer cells. *Immunology Letters*, *184*, 7–14.

Wang, Y. F. W., & Kobayashi, M. (2013). Antibody detection: Principles and applications. In Y. Tang & C. Stratton (Eds.), *Advanced Techniques in Diagnostic Microbiology* (pp. 53–73). Springer US.

Wang, Y. hua, Liu, S., Zhang, G., Zhou, C. qi, Zhu, H. xia, Zhou, X. bo, Quan, L. ping, Bai, J. feng, & Xu, N. zhi. (2005). Knockdown of c-Myc expression by RNAi inhibits MCF-7 breast tumor cells growth in vitro and in vivo. *Breast Cancer Research*, *7*(2), R220–R228.

Wang, Y., Li, Q., Wei, X., Xu, J., Chen, Q., Song, S., Lu, Z., & Wang, Z. (2015). Targeted knockout of TNF-α by injection of lentivirus-mediated siRNA into the subacromial bursa for the treatment of subacromial bursitis in rats. *Molecular Medicine Reports*, *12*(3), 4389–4395.

Wang, Y., Wang, X., Ma, X., Chen, Q., He, H., Nau, W. M., & Huang, F. (2019). Coassembly of Gold Nanoclusters with Nucleic Acids: Sensing, Bioimaging, and Gene Transfection. *Particle & Particle Systems Characterization*, *36*(10), 1900281.

Wang, Y., Wang, X., Zhao, H., Liang, B., & Du, Q. (2012). Clusterin confers resistance to TNF-alphainduced apoptosis in breast cancer cells through NF-kappaB activation and Bcl-2 overexpression. *Journal of Chemotherapy*, *24*(6), 348–357.

Wei, Y., Resetca, D., Li, Z., Johansson-Åkhe, I., Ahlner, A., Helander, S., Wallenhammar, A., Morad, V., Raught, B., Wallner, B., Kokubo, T., Tong, Y., Penn, L. Z., & Sunnerhagen, M. (2019). Multiple direct interactions of TBP with the MYC oncoprotein. *Nature Structural & Molecular Biology*, *26*(11), 1035–1043.

Weichhaus, M., Broom, I., & Bermano, G. (2011). The molecular contribution of TNF-α in the link between obesity and breast cancer. *Oncology Reports*, *25*(2), 477–483.

Weigelt, B., Geyer, F. C., & Reis-Filho, J. S. (2010). Histological types of breast cancer: How special are they? *Molecular Oncology*, *4*(3), 192–208.

Weigelt, B., Mackay, A., A'hern, R., Natrajan, R., Tan, D. S. P., Dowsett, M., Ashworth, A., & Reis-Filho, J. S. (2010). Breast cancer molecular profiling with single sample predictors: A retrospective analysis. *The Lancet Oncology*, *11*(4), 339–349.

Weitzenfeld, P., Meron, N., Leibovich-Rivkin, T., Meshel, T., & Ben-Baruch, A. (2013). Progression of luminal breast tumors is promoted by ménage à trois between the inflammatory cytokine TNF α and the hormonal and growth-supporting arms of the tumor microenvironment. *Mediators of Inflammation*, *2013,*702536.

Westbrook, A. M., Wei, B., Hacke, K., Xia, M., Braun, J., & Schiestl, R. H. (2012). The role of tumour necrosis factor-α and tumour necrosis factor receptor signalling in inflammation-associated systemic genotoxicity. *Mutagenesis*, *27*(1), 77–86.

Wierstra, I., & Alves, J. (2008). The c-myc Promoter: Still MysterY and Challenge. *Advances in Cancer Research*, *99*, 113–333.

Wiese, K. E., Walz, S., Von Eyss, B., Wolf, E., Athineos, D., Sansom, O., & Eilers, M. (2013). The Role of MIZ-1 in MYC-Dependent Tumorigenesis. *Cold Spring Harbor Perspectives in Medicine*, *3*(12), a01429.

Wolczyk, D., Zaremba-Czogalla, M., Hryniewicz-Jankowska, A., Tabola, R., Grabowski, K., Sikorski, A. F., & Augoff, K. (2016). TNF-α promotes breast cancer cell migration and enhances the concentration of membrane-associated proteases in lipid rafts. *Cellular Oncology*, *39*(4), 353–363.

Wright, L., Joyce, P., Barnes, T. J., Lundmark, R., Bergström, C. A. S., Hubert, M., & Prestidge, C. A. (2021). A Comparison of Chitosan, Mesoporous Silica and Poly(lactic-co-glycolic) Acid Nanocarriers for Optimising Intestinal Uptake of Oral Protein Therapeutics. *Journal of Pharmaceutical Sciences*, *110*(1), 217–227.

Wu, X., Wu, M. Y., Jiang, M., Zhi, Q., Bian, X., Xu, M. D., Gong, F. R., Hou, J., Tao, M., Shou, L. M., Duan, W., Chen, K., Shen, M., & Li, W. (2017). TNF-α sensitizes chemotherapy and radiotherapy against breast cancer cells. *Cancer Cell International*, *17*(1), 1–12.

Wu, Z., & Jin, R. (2010). On the ligand's role in the fluorescence of gold nanoclusters. *Nano Letters*, *10*(7), 2568–2573.

Xanthoulea, S., Pasparakis, M., Kousteni, S., Brakebusch, C., Wallach, D., Bauer, J., Lassmann, H., & Kollias, G. (2004). Tumor necrosis factor (TNF) receptor shedding controls thresholds of innate immune activation that balance opposing TNF functions in infectious and inflammatory diseases. *Journal of Experimental Medicine*, *200*(3), 367–376.

Xia, J., Wang, X., Zhu, S., Liu, L., & Li, L. (2019). Gold Nanocluster-Decorated Nanocomposites with Enhanced Emission and Reactive Oxygen Species Generation. *ACS Applied Materials and Interfaces*, *11*(7), 7369–7378.

Xiao, Q., Ciaassen, G., Shi, J., Adachi, S., Sedivy, J., & Hann, S. R. (1998). Transactivation-defective c-MycS retains the ability to regulate proliferation and apoptosis. *Genes & Development*, *12*(24), 3803–3808.

Xie, X., Tan, F., Xu, A., Deng, K., Zeng, Y., & Huang, H. (2019). UV-induced peroxidase-like activity of gold nanoclusters for differentiating pathogenic bacteria and detection of enterotoxin with colorimetric readout. *Sensors and Actuators B: Chemical*, *279*, 289–297.

Xing, F., Sharma, S., Liu, Y., Mo, Y. Y., Wu, K., Zhang, Y. Y., Pochampally, R., Martinez, L. A., Lo, H. W., & Watabe, K. (2015). MiR-509 suppresses brain metastasis of breast cancer cells by modulating RhoC and TNF-α. *Oncogene*, *34*(37), 4890–4900.

Xu-Monette, Z. Y., Deng, Q., Manyam, G. C., Tzankov, A., Li, L., Xia, Y., Wang, X. X., Zou, D., Visco, C., Dybkær, K., Li, J., Zhang, L., Liang, H., Montes-Moreno, S., Chiu, A., Orazi, A., Zu, Y., Bhagat, G., Richards, K. L., … Young, K. H. (2016). MYC mutation profiling and prognostic significance in de novo diffuse large B-cell lymphoma. *Clinical Cancer Research : An Official Journal of the American Association for Cancer Research*, *22*(14), 3593–3605.

Xu, J., Chen, Y., & Olopade, O. I. (2010). MYC and Breast Cancer. *Genes & Cancer*, *1*(6), 629–640.

Yahia-Ammar, A., Sierra, D., Mérola, F., Hildebrandt, N., & Le Guével, X. (2016). Self-Assembled Gold Nanoclusters for Bright Fluorescence Imaging and Enhanced Drug Delivery. *ACS Nano*, *10*(2), 2591–2599.

Yamashita, T., Higashi, M., Momose, S., Adachi, A., Watanabe, T., Tanaka, Y., Tokuhira, M.,

Kizaki, M., & Tamaru, J. ichi. (2020). Decreased MYC-associated factor X (MAX) expression is a new potential biomarker for adverse prognosis in anaplastic large cell lymphoma. *Scientific Reports*, *10*(1), 1–10.

Yan, B., Wang, H., Rabbani, Z. N., Zhao, Y., Li, W., Yuan, Y., Li, F., Dewhirst, M. W., & Li, C. Y. (2006). Tumor necrosis factor-α is a potent endogenous mutagen that promotes cellular transformation. *Cancer Research*, *66*(24), 11565–11570.

Yan, C., Grimm, W. A., Garner, W. L., Qin, L., Travis, T., Tan, N., & Han, Y. P. (2010). Epithelial to mesenchymal transition in human skin wound healing is induced by tumor necrosis factor-α through bone morphogenic protein-2. *American Journal of Pathology*, *176*(5), 2247–2258.

Yan, D., Qin, N., Zhang, H., Liu, T., Yu, M., Jiang, X., Feng, W., Wang, J., Yin, B., Zhang, T., Zhou, M., & Li, Z. (2009). Expression of TNF-α leader sequence renders MCF-7 tumor cells resistant to the cytotoxicity of soluble TNF-α. *Breast Cancer Research and Treatment*, *116*(1), 91–102.

Yang, A., Qin, S., Schulte, B. A., Ethier, S. P., Tew, K. D., & Wang, G. Y. (2017). MYC inhibition depletes cancer stem-like cells in triple-negative breast cancer. *Cancer Research*, *77*(23), 6641–6650.

Yang, C., Gao, S., Dagnæs-Hansen, F., Jakobsen, M., & Kjems, J. (2017). Impact of PEG Chain Length on the Physical Properties and Bioactivity of PEGylated Chitosan/siRNA Nanoparticles in Vitro and in Vivo. *ACS Applied Materials and Interfaces*, *9*(14), 12203–12216.

Yang, J. P., & Huang, L. (1998). Time-dependent maturation of cationic liposome–DNA complex for serum resistance. *Gene Therapy*, *5*(3), 380–387.

Yang, Q., Jones, S. W., Parker, C. L., Zamboni, W. C., Bear, J. E., & Lai, S. K. (2014). Evading immune cell uptake and clearance requires PEG grafting at densities substantially exceeding the minimum for brush conformation. *Molecular Pharmaceutics*, *11*(4), 1250–1258.

Yang, T.-Q., Peng, B., Shan, B.-Q., Zong, Y.-X., Jiang, J.-G., Wu, P., & Zhang, K. (2020). Origin of the Photoluminescence of Metal Nanoclusters: From Metal-Centered Emission to Ligand-Centered Emission. *Nanomaterials (Basel, Switzerland)*, *10*(2), 261.

Yang, Y., Nan, J., Hou, J., Yu, B., Zhao, T., Xu, S., Lv, S., & Zhang, H. (2014). Cytotoxicity of gold nanoclusters in human liver cancer cells. *International Journal of Nanomedicine*, *9*(1), 5441–5448.

Yang, Y., Xie, X., Xu, X., Xia, X., Wang, H., Li, L., Dong, W., Ma, P., Yang, Y., Liu, Y., & Mei, X. (2016). Thermal and magnetic dual-responsive liposomes with a cell-penetrating peptide-siRNA conjugate for enhanced and targeted cancer therapy. *Colloids and Surfaces B: Biointerfaces*, *146*, 607–615.

Yau, S. H., Varnavski, O., & Goodson, T. (2013). An ultrafast look at Au nanoclusters. *Accounts of Chemical Research*, *46*(7), 1506–1516.

Ye, L.-L., Wei, X.-S., Zhang, M., Niu, Y.-R., & Zhou, Q. (2018). The Significance of Tumor Necrosis Factor Receptor Type II in CD8(+) Regulatory T Cells and CD8(+) Effector T Cells. *Frontiers in Immunology*, *9*, 583.

Yee, D., Shah, K. M., Coles, M. C., Sharp, T. V., & Lagos, D. (2017). MicroRNA-155 induction via TNF-α and IFN-γ suppresses expression of programmed death ligand-1 (PD-L1)

in human primary cells. *Journal of Biological Chemistry*, *292*(50), 20683–20693.

Yi, T. (2018). Identifying RISC Components Using Ago2 Immunoprecipitation and Mass Spectrometry BT - mRNA Decay: Methods and Protocols. In S. R. Lamandé (Ed.), *Methods in Molecular Biology* (pp. 149–159). Springer New York.

Yin, S., Cheryan, V. T., Xu, L., Rishi, A. K., & Reddy, K. B. (2017). Myc mediates cancer stem-like cells and EMT changes in triple negative breast cancers cells. *PLOS ONE*, *12*(8), e0183578.

Yu, M., Zhou, X., Niu, L., Lin, G., Huang, J., Zhou, W., Gan, H., Wang, J., Jiang, X., Yin, B., & Li, Z. (2013). Targeting transmembrane TNF-α suppresses breast cancer growth. *Cancer Research*, *73*(13), 4061–4074.

Yu, S., Li, F., Huang, X., Dong, C., & Ren, J. (2020). In Situ Study of Interactions between Endogenous c- myc mRNA with CRDBP in a Single Living Cell by Combining Fluorescence Cross-Correlation Spectroscopy with Molecular Beacons. *Analytical Chemistry*, *92*(4), 2988–2996.

Yuan, X., Goswami, N., Chen, W., Yao, Q., & Xie, J. (2016). Insights into the effect of surface ligands on the optical properties of thiolated Au25 nanoclusters. *Chemical Communications*, *52*(30), 5234–5237.

Zanganeh, S., Jafari, T., Khakpash, N., Erfanzadeh, M., & Ho, J. Q. (2016). Nanoparticles in Circulation: Blood Stability. In P. Stroeve & M. Mahmoudi (Eds.), *Drug Delivery Systems* (pp. 53–87). World Scientific Publishing Co.

Zhang, C., Li, C., Liu, Y., Zhang, J., Bao, C., Liang, S., Wang, Q., Yang, Y., Fu, H., Wang, K., & Cui, D. (2015). Gold Nanoclusters-Based Nanoprobes for Simultaneous Fluorescence Imaging and Targeted Photodynamic Therapy with Superior Penetration and Retention Behavior in Tumors. *Advanced Functional Materials*, *25*(8), 1314–1325.

Zhang, C., Shu, W., Zhou, G., Lin, J., Chu, F., Wu, H., & Liu, Z. (2018). Anti-TNF-α Therapy Suppresses Proinflammatory Activities of Mucosal Neutrophils in Inflammatory Bowel Disease. *Mediators of Inflammation*, *2018*, 3021863.

Zhang, C., Tang, N., Liu, X. J., Liang, W., Xu, W., & Torchilin, V. P. (2006). siRNA-containing liposomes modified with polyarginine effectively silence the targeted gene. *Journal of Controlled Release*, *112*(2), 229.

Zhang, C., Yuan, W., Wu, Y., Wan, X., & Gong, Y. (2021). Co-delivery of EGFR and BRD4 siRNA by cell-penetrating peptides-modified redox-responsive complex in triple negative breast cancer cells. *Life Sciences*, *266*, 118886.

Zhang, G., Liu, Z., Han, Y., Wang, X., & Yang, Z. (2016). Overexpression of miR-509 increases apoptosis and inhibits invasion via suppression of tumor necrosis factor-α in triple-negative breast cancer Hs578T cells. *Oncology Research*, *24*(4), 233–238.

Zhang, H., Huang, X., Li, L., Zhang, G., Hussain, I., Li, Z., & Tan, B. (2012). Photoreductive synthesis of water-soluble fluorescent metal nanoclusters. *Chemical Communications*, *48*(4), 567–569.

Zhang, H., Liu, Q., Wang, T., Yun, Z., Li, G., Liu, J., & Jiang, G. (2013). Facile preparation of glutathione-stabilized gold nanoclusters for selective determination of chromium (III) and chromium (VI) in environmental water samples. *Analytica Chimica Acta*, *770*, 140–146.

Zhang, L., & Wang, E. (2014). Metal nanoclusters: New fluorescent probes for sensors and bioimaging. *Nano Today*, *9*(1), 132–157.

Zhang, M. M., Bahal, R., Rasmussen, T. P., Manautou, J. E., & Zhong, X. bo. (2021). The growth of siRNA-based therapeutics: updated clinical studies. *Biochemical Pharmacology*, *189*, 114432.

Zhang, Q., West-Osterfield, K., Spears, E., Li, Z., Panaccione, A., & Hann, S. R. (2017). MB0 and MBI Are Independent and Distinct Transactivation Domains in MYC that Are Essential for Transformation. *Genes*, *8*(5), 134.

Zhang, W., Zhou, Y., Li, X., Xu, X., Chen, Y., Zhu, R., & Yin, L. (2018). Macrophage-targeting and reactive oxygen species (ROS)-responsive nanopolyplexes mediate anti-inflammatory siRNA delivery against acute liver failure (ALF). *Biomaterials Science*, *6*(7), 1986–1993.

Zhang, X., Choi, P. S., Francis, J. M., Imielinski, M., Watanabe, H., Cherniack, A. D., & Meyerson, M. (2016). Identification of focally amplified lineage-specific super-enhancers in human epithelial cancers. *Nature Genetics*, *48*(2), 176.

Zhang, X. D., Luo, Z., Chen, J., Wang, H., Song, S. S., Shen, X., Long, W., Sun, Y. M., Fan, S., Zheng, K., Leong, D. T., & Xie, J. (2015). Storage of gold nanoclusters in muscle leads to their biphasic in vivo clearance. *Small*, *11*(14), 1683–1690.

Zhang, X. D., Wu, D., Shen, X., Liu, P. X., Fan, F. Y., & Fan, S. J. (2012). In vivo renal clearance, biodistribution, toxicity of gold nanoclusters. *Biomaterials*, *33*(18), 4628–4638.

Zhang, X., Wang, X., Wu, T., Li, B., Liu, T., Wang, R., Liu, Q., Liu, Z., Gong, Y., & Shao, C. (2015). Isoliensinine induces apoptosis in triple-negative human breast cancer cells through ROS generation and p38 MAPK/JNK activation. *Scientific Reports 2015 5:1*, *5*(1), 1–13.

Zhang, Y., Sun, C., Wang, C., Jankovic, K. E., & Dong, Y. (2021). Lipids and Lipid Derivatives for RNA Delivery. *Chemical Reviews*, *121*(20), 12181.

Zhang, Z., Lin, G., Yan, Y., Li, X., Hu, Y., Wang, J., Yin, B., Wu, Y., Li, Z., & Yang, X. P. (2018). Transmembrane TNF-alpha promotes chemoresistance in breast cancer cells. *Oncogene*, *37*(25), 3456–3470.

Zhao, J. Y., Cui, R., Zhang, Z. L., Zhang, M., Xie, Z. X., & Pang, D. W. (2014). Cytotoxicity of nucleus-targeting fluorescent gold nanoclusters. *Nanoscale*, *6*(21), 13126–13134.

Zhao, L., Yang, G., Shi, Y., Su, C., & Chang, J. (2015). Co-delivery of Gefitinib and chloroquine by chitosan nanoparticles for overcoming the drug acquired resistance. *Journal of Nanobiotechnology*, *13*(1), 57.

Zhao, R.-X., Liu, A. Y., Wen, Q. L., Wu, B. C., Wang, J., Hu, Y. L., Pu, Z. F., Ling, J., & Cao, Q. (2021). Glutathione stabilized green-emission gold nanoclusters for selective detection of cobalt ion. *Spectrochimica Acta Part A: Molecular and Biomolecular Spectroscopy*, *254*, 119628.

Zheng, J., Nicovich, P. R., & Dickson, R. M. (2007). Highly fluorescent noble-metal quantum dots. *Annual Review of Physical Chemistry*, *58*, 409–431.

Zheng, J., Zhang, C., & Dickson, R. M. (2004). Highly fluorescent, water-soluble, size-tunable gold quantum dots. *Physical Review Letters*, *93*(7), 077402.

Zheng, Y., Lai, L., Liu, W., Jiang, H., & Wang, X. (2017). Recent advances in biomedical applications of fluorescent gold nanoclusters. *Advances in Colloid and Interface Science*, *242*, 1–16.

Zhi, D., Zhang, S., Cui, S., Zhao, Y., Wang, Y., & Zhao, D. (2013). The headgroup evolution of cationic lipids for gene delivery. *Bioconjugate Chemistry*, *24*(4), 487–519.

Zhitomirsky, B., Farber, H., & Assaraf, Y. G. (2018). LysoTracker and MitoTracker Red are transport substrates of P-glycoprotein: implications for anticancer drug design evading multidrug resistance. *Journal of Cellular and Molecular Medicine*, *22*(4), 2131–2141.

Zhou, C., Hao, G., Thomas, P., Liu, J., Yu, M., Sun, S., Öz, O. K., Sun, X., & Zheng, J. (2012). Near-infrared emitting radioactive gold nanoparticles with molecular pharmacokinetics. *Angewandte Chemie - International Edition*, *51*(40), 10118–10122.

Zhou, C., Long, M., Qin, Y., Sun, X., & Zheng, J. (2011). Luminescent gold nanoparticles with efficient renal clearance. *Angewandte Chemie - International Edition*, *50*(14), 3168–3172.

Zhu, J., He, K., Dai, Z., Gong, L., Zhou, T., Liang, H., & Liu, J. (2019). Self-Assembly of Luminescent Gold Nanoparticles with Sensitive pH-Stimulated Structure Transformation and Emission Response toward Lysosome Escape and Intracellular Imaging. *Analytical Chemistry*, *91*(13), 8237–8243.

Zhu, K., Liu, Q., Zhou, Y., Tao, C., Zhao, Z., Sun, J., & Xu, H. (2015). Oncogenes and tumor suppressor genes: Comparative genomics and network perspectives. *BMC Genomics*, *16*(7), 1–11.

Zhu, L., Yang, Y., Li, X., Zheng, Y., Li, Z., Chen, H., & Gao, Y. (2022). Facile preparation of indocyanine green and tiny gold nanoclusters co-loaded nanocapsules for targeted synergistic sono-/photo-therapy. *Journal of Colloid and Interface Science*, *627*, 596–609.

Zhu, T., Qian, J., Shen, Z., Shao, H., Qian, K., Jin, W., & Qin, A. (2023). Vector-delivered artificial miRNA effectively inhibits Porcine epidemic diarrhea virus replication. *Virology Journal*, *20*(1), 164.

Zhu, X., Chen, L., Huang, B., Wang, Y., Ji, L., Wu, J., Di, G., Liu, G., Yu, K., Shao, Z., & Wang, Z. (2020). The prognostic and predictive potential of Ki-67 in triple-negative breast cancer. *Scientific Reports*, *10*(1), 225.

Zhuang, Q., Jia, H., Du, L., Li, Y., Chen, Z., Huang, S., & Liu, Y. (2014). Targeted surface-functionalized gold nanoclusters for mitochondrial imaging. *Biosensors and Bioelectronics*, *55*, 76–82.

Ziebarth, J. D., & Wang, Y. (2010). Understanding the protonation behavior of linear polyethylenimine in solutions through Monte Carlo simulations. *Biomacromolecules*, *11*(1), 29–38.

Zimmerli, D., Brambillasca, C. S., Talens, F., Bhin, J., Linstra, R., Romanens, L., Bhattacharya, A., Joosten, S. E. P., Da Silva, A. M., Padrao, N., Wellenstein, M. D., Kersten, K., de Boo, M., Roorda, M., Henneman, L., de Bruijn, R., Annunziato, S., van der Burg, E., Drenth, A. P., … Jonkers, J. (2022). MYC promotes immune-suppression in triple-negative breast cancer via inhibition of interferon signaling. *Nature Communications*, *13*(1), 1–18.

Zimmermann, M., & Meyer, N. (2011). Annexin V/7-AAD Staining in Keratinocytes BT - Mammalian Cell Viability: Methods and Protocols. In M. J. Stoddart (Ed.), *Mammalian Cell Viability* (pp. 57–63). Humana Press.

Zingler, P., Särchen, V., Glatter, T., Caning, L., Saggau, C., Kathayat, R. S., Dickinson, B. C., Adam, D., Schneider-Brachert, W., Schütze, S., & Fritsch, J. (2019). Palmitoylation is required for TNF-R1 signaling. *Cell Communication and Signaling*, *17*(1).

Zins, K., Abraham, D., Sioud, M., & Aharinejad, S. (2007). Colon cancer cell-derived tumor necrosis factor-α mediates the tumor growth-promoting response in macrophages by up-regulating the colony-stimulating factor-1 pathway. *Cancer Research*, *67*(3), 1038–1045.

Zong, Y., & Pegram, M. (2021). Research advances and new challenges in overcoming triple-negative breast cancer. *Cancer Drug Resistance*, *4*(3), 517–542.

APPENDIX

Appendix A: Published paper

Invited Review Article NANOBIOMEDICINE

Nanobiomedicine
Volume 7: 1–15

DOI: 10.1177/1849543520983196
journals.sagepub.com/home/nab
SAGE

Therapeutic applications of CRISPR/Cas9 in breast cancer and delivery potential of gold nanomaterials

Jananee Padayachee and Moganavelli Singh

Abstract

Globally, approximately 1 in 4 cancers in women are diagnosed as breast cancer (BC). Despite significant advances in the diagnosis and therapy BCs, many patients develop metastases or relapses. Hence, novel therapeutic strategies are required, that can selectively and efficiently kill malignant cells. Direct targeting of the genetic and epigenetic aberrations that occur in BC development is a promising strategy to overcome the limitations of current therapies, which target the tumour phenotype. The clustered regularly interspaced short palindromic repeats (CRISPR)/Cas system, composed of only an easily modifiable single guide RNA (sgRNA) sequence bound to a Cas9 nuclease, has revolutionised genome editing due to its simplicity and efficiency compared to earlier systems. CRISPR/Cas9 and its associated catalytically inactivated dCas9 variants facilitate the knockout of overexpressed genes, correction of mutations in inactivated genes, and reprogramming of the epigenetic landscape to impair BC growth. To achieve efficient genome editing *in vivo*, a vector is required to deliver the components to target cells. Gold nanomaterials, including gold nanoparticles and nanoclusters, display many advantageous characteristics that have facilitated their widespread use in theranostics, as delivery vehicles, and imaging and photothermal agents. This review highlights the therapeutic applications of CRISPR/Cas9 in treating BCs, and briefly describes gold nanomaterials and their potential in CRISPR/Cas9 delivery.

Keywords

Breast cancer, genome editing, CRISPR/Cas9, gold nanoparticles, gold nanoclusters

Date received: 16 April 2020; accepted: 3 December 2020

Introduction

Advances in the treatment of breast cancers (BCs) have led to significant improvements in the overall survival of patients. Local therapies, including surgery and radiotherapy, in conjunction with adjuvant targeted therapies and chemotherapy are mainstays of BC treatment.[1] Based on immunohistochemical staining of hormone receptors (HR), human epidermal growth factor receptor-2 (HER2), and ki67, a marker of cell proliferation, BCs can be divided into four subtypes which respond to different therapies. The majority of BCs are HR+ luminal tumours, which can be further subdivided into luminal A (HR+, HER2-, low ki67) and B (HR+, HER2+/high ki67) subtypes.[2] These cancers generally respond well to endocrine therapies targeting the estrogen receptor (ER) and display relatively good prognoses.[3] HER2+ BCs, which are HR- and HER2+, are treated using anti-HER2 drugs. Triple negative breast cancers (TNBC) are HR- and HER2-, with chemotherapy and

Nano-Gene and Drug Delivery Laboratory, Discipline of Biochemistry, School of Life Sciences, College of Agriculture, Engineering and Science, University of KwaZulu-Natal (Westville Campus), Durban, South Africa

Corresponding author:
Moganavelli Singh, Nano-Gene and Drug Delivery Laboratory, Discipline of Biochemistry, School of Life Sciences, College of Agriculture, Engineering and Science, University of KwaZulu-Natal (Westville Campus), Private Bag X54001, Durban 4000, South Africa.
Email: singhm1@ukzn.ac.za

Appendix B: Similarity report